

A STUDY ON THE CATALYTIC PYROLYSIS AND COMBUSTION  
CHARACTERISTICS OF TURKISH LIGNITE AND CO-PROCESSING  
EFFECTS WITH BIOMASS UNDER VARIOUS AMBIENT CONDITIONS

A THESIS SUBMITTED TO  
THE GRADUATE SCHOOL OF APPLIED AND NATURAL SCIENCES  
OF  
MIDDLE EAST TECHNICAL UNIVERSITY

BY

EHSAN ABBASI ATIBEH

IN PARTIAL FULFILLMENT OF THE REQUIREMENTS  
FOR  
THE DEGREE OF MASTER OF SCIENCE  
IN  
MECHANICAL ENGINEERING

JULY 2012

Approval of the thesis:

**A STUDY ON THE CATALYTIC PYROLYSIS AND COMBUSTION  
CHARACTERISTICS OF TURKISH LIGNITE AND CO-PROCESSING  
EFFECTS WITH BIOMASS UNDER VARIOUS AMBIENT  
CONDITIONS**

Submitted by **EHSAN ABBASI ATIBEH** in partial fulfillment of the requirements for the degree of **Master of Science in Mechanical Engineering Department, Middle East Technical University** by,

Prof. Dr. Canan Özgen  
Dean, Graduate School of **Natural and Applied Sciences**

\_\_\_\_\_

Prof. Dr. Suha Oral  
Head of Department, **Mechanical Engineering**

\_\_\_\_\_

Asst. Prof. Dr. Ahmet Yozgatlıgil  
Supervisor, **Mechanical Engineering Dept., METU**

\_\_\_\_\_

**Examining Committee Members:**

Assoc. Prof. Dr. Cemil Yamalı  
Mechanical Engineering Dept., METU

\_\_\_\_\_

Asst. Prof. Dr. Ahmet Yozgatlıgil  
Mechanical Engineering Dept., METU

\_\_\_\_\_

Assoc. Prof. Dr. Almıla Güvenç Yazıcıoğlu  
Mechanical Engineering Dept., METU

\_\_\_\_\_

Asst. Prof. Dr. Cüneyt Sert  
Mechanical Engineering Dept., METU

\_\_\_\_\_

Assoc. Prof. Dr. Murat Aktaş  
Mechanical Engineering Dept., TOBB-ETU

\_\_\_\_\_

**Date:**

**02.07.2012**

**I hereby declare that all information in this document has been obtained and presented in accordance with academic rules and ethical conduct. I also declare that, as required by these rules and conduct, I have fully cited and referenced all material and results that are not original to this work.**

Name, Last name: Ehsan Abbasi Atibeh

Signature :

## **ABSTRACT**

### **A STUDY ON THE CATALYTIC PYROLYSIS AND COMBUSTION CHARACTERISTICS OF TURKISH LIGNITE AND CO-PROCESSING EFFECTS WITH BIOMASS UNDER VARIOUS AMBIENT CONDITIONS**

Abbasi Atibeh, Ehsan

M.Sc., Department of Mechanical Engineering

Supervisor: Asst. Prof. Dr. Ahmet Yozgatlıgil

July 2012, 223 pages

In this study the catalytic pyrolysis and combustion characteristics of Turkish coal samples in  $O_2/N_2$  and  $O_2/CO_2$  (oxy-fuel conditions) ambient conditions were explored and the evolution of emissions during these tests was investigated using non-isothermal Thermo-gravimetric Analysis (TGA) technique combined with Fourier Transform Infrared (FTIR) spectroscopy. Potassium carbonate ( $K_2CO_3$ ), calcium hydroxide ( $Ca(OH)_2$ ), iron (III) oxide ( $Fe_2O_3$ ) and iron (III) chloride ( $FeCl_3$ ) were employed as precursors of catalysts to investigate the effects of potassium (K), calcium (Ca) and iron (Fe). Furthermore the effects of these catalysts on calorimetric tests of Turkish coal samples were investigated.

TGA-FTIR pyrolysis tests were carried out in 100 % N<sub>2</sub> and 100 % CO<sub>2</sub> ambient conditions which are the main diluting gases in air and oxy-fuel conditions. Lignite pyrolysis tests revealed that the major difference between pyrolysis in these two ambient conditions was observed beyond 720 °C and Derivative Thermogravimetric (DTG) profiles experienced sharp peaks at 785 °C in pure CO<sub>2</sub> cases which can be attributed to char-CO<sub>2</sub> gasification reaction. Furthermore K<sub>2</sub>CO<sub>3</sub> found to be the most effective catalyst in lignite char gasification reaction during pyrolysis tests in 100 % CO<sub>2</sub>. Combustion experiments were carried out in various oxygen concentrations from 21 % to 35 % in N<sub>2</sub> and CO<sub>2</sub> ambient conditions. Lignite combustion tests carried out in CO<sub>2</sub> ambient revealed that in 30 % and 35 % oxygen concentrations, the relative active sequence of catalysts to the reaction rates of devolatilization can be described as Fe>> K> Ca> Raw-form and Fe> Ca> Raw-form>> K respectively. Furthermore K-based catalyst showed the best char reactivity due to its much higher reaction rates in all the oxygen concentrations. Emission profiles of CO<sub>2</sub>, CO, H<sub>2</sub>O, CH<sub>4</sub>, SO<sub>x</sub>, COS, NH<sub>3</sub>, NO and HCl evolved species were analyzed using Fourier Transform Infrared spectroscopy (FTIR) method for pyrolysis and combustion tests in both N<sub>2</sub> and CO<sub>2</sub> ambient conditions. A good correlation was seen in most of the combustion tests between the T<sub>2max</sub> (temperature of the maximum rate of weight loss in the devolatilization region of combustion) and T<sub>FG-max</sub> (temperature of the maximum flue gas emission) and also between |(dm/dt)<sub>2max</sub>| (the maximum rate of weight loss in the devolatilization region) and maximum spectral absorbance at a given wavenumber in both N<sub>2</sub> and CO<sub>2</sub> ambient conditions.

Finally the possible way of using biomass as a potential source of inexpensive catalysts in the co-processing of coal and biomass was investigated through co-processing combustion tests of lignite and biomass ash contents in O<sub>2</sub>/N<sub>2</sub> and O<sub>2</sub>/CO<sub>2</sub> ambient conditions. These experiments revealed that the hazelnut shell and walnut shell ash contents were significantly effective in increasing the char reactivity of Kangal lignite due to high concentration of potassium based oxides in the ash. Furthermore the catalytic reactivity of wheat straw, cattle manure and saw dust ash

contents were observed in the devolatilization region due to high concentrations of alkali and alkaline earth metals existed in the ash. In conclusion, these results revealed that the ash contents of the evolved biomass fuels can be used as a potential source of inexpensive alkali and alkaline earth metal catalysts and develop a step forward in economic aspects of catalytic coal combustion.

**Keywords:** Oxy-fuel combustion, Catalyst, Lignite, Biomass, TGA-FTIR

## ÖZ

# TÜRK LİNYİTLERİNİN VE BİYORYAKIT KARIŞIMLARININ ÇEŞİTLİ ATMOSFER KOŞULLARINDA PİROLİZ VE YANMA ÖZELLİKLERİ HAKKINDA BİR ÇALIŞMA

Abbasi Atibeh, Ehsan

Y. Lisans, Makina Mühendisliği Bölümü

Tez Yöneticisi: Yrd. Doç. Dr. Ahmet Yozgatlıgil

Temmuz 2012, 223 sayfa

Bu çalışmada Türk linyitlerinin,  $O_2/N_2$  ve  $O_2/CO_2$  (oksi-yakıt) ortamlarında katalitik piroliz ve yanma özellikleri incelenmiştir. Ayrıca testler esnasında salınım değişimleri eş ısıllı olmayan Thermo-gravimetric Analiz (TGA) ve Fourier Transform Infrared (FTIR) spektroskopi methodları ile gözlemlenmiştir. Potasyum karbonat ( $K_2CO_3$ ), kalsiyum hidroksit ( $Ca(OH)_2$ ), demir (III) oksit ( $Fe_2O_3$ ) ve demir (III) klorit ( $FeCl_3$ ), bileşikleri potasyum (K), kalsiyum (Ca) ve demir (Fe) elementlerinin katalitik etkilerinin gözlemlenmesi için kullanılmıştır. Katalizörlerin Türk linyitlerinin kalorimetri testlerine etkileri de incelenmiştir.

TGA-FTIR piroliz deneyleri hava ve oksijen ortamlarının ana seyreltik bileşenleri

olan N<sub>2</sub> ve CO<sub>2</sub> % 100 olduđu atmosfer içinde yapılmıştır. Linyit piroliz testleri sonucunda bu iki ortam arasında 720 °C'den sonra önemli farklılaşmalar görülmüştür. Örneğin 785 °C' de % 100 CO<sub>2</sub> ortamında karbon- CO<sub>2</sub> gazlaşma reaksiyonlarına bađlı olabilecek keskin tepe noktaları görülmüştür. Ayrıca % 100 CO<sub>2</sub> içeren ortamda yapılan testlerde, K<sub>2</sub>CO<sub>3</sub> bileşiminin linyit karbon- CO<sub>2</sub> gazlaşma reaksiyonlarında en etkili katalizör olduđu gözlemlenmiştir. Yanma deneyleri % 21 ve % 35 arasında deđişen oksijen oranlarında, N<sub>2</sub> ve CO<sub>2</sub> ortamlarında yapılmıştır. Linyitin % 30 ve % 35 oksijen içeren oksijen yakıt ortamında devolatilizasyon hızına katalizörlerin etkisi Fe >> K > Ca > katkısız linyit ve Fe > Ca > katkısız linyit >> K olarak görülmüştür. Ayrıca, potasyum bileşeni katalizörlerin bütün oksijen oranlarında en etkin karbon-CO<sub>2</sub> gazlaşma reaksiyonlarına sebep olduđu görülmüştür. N<sub>2</sub> ve CO<sub>2</sub> ortamlarının her ikisinde de, piroliz ve yanma sırasında CO<sub>2</sub>, CO, H<sub>2</sub>O, CH<sub>4</sub>, SO<sub>x</sub>, COS, NH<sub>3</sub>, NO ve HCl salınımları FTIR yöntemi kullanılarak izlenmiştir. Bütün yanma deneylerinde T<sub>2max</sub> (yanma devolatilizasyonu sırasında maksimum ađırlık kaybı oranına karşılık gelen sıcaklık) ve T<sub>FG-max</sub> (maksimum emisyonla karşılık gelen sıcaklık) ve ayrıca |(dm/dt)<sub>2max</sub>| (yanma devolatilizasyonu sırasında maksimum ađırlık kaybı oranı) ve belirli bir dalga boyunda maksimum spektral tutunum arasında anlamlı bađıntılara rastlanmıştır.

Son olarak hava ve oksijen-yakıt ortamlarında biokütlenin kömürün eş işlenmesinde ucuz bir katalizör olarak kullanılmasına yönelik olanaklar incelenmiştir. Bu deneylerde, fındık ve ceviz kabuklarının küllerinin Kangal linyitinin karbon dönüşüm reaksiyonları üzerindeki müspet etkileri gözlemlenmiştir. Bu etki fındık ve kestane kabuđu küllerinin yüksek oranlarda potasyum içermesinden kaynaklanmaktadır. Ayrıca, buđday samanı, inek gübresi ve odun talaşının içerdii yüksek oranlardaki alkali ve toprak alkalilere bađlı olarak devolatilizasyon esnasında katalitik reaksiyonlara rastlanmıştır. Özetlemek gerekirse, gözlemlenen sonuçlar ışığında gelecekte, biokütlenin işlenmesi ile elde edilecek küller, içerdikleri yüksek oranlardaki alkali ve toprak alkaliler nedeniyle, ucuz birer katalizör olarak kullanılabileceđi ortaya çıkmaktadır.

**Anahtar kelimeler:** Oksijen-yakıt yanma, Katalizör, Linyit, Biyokütle, TGA-FTIR

*To My Wife and My Parents*

## ACKNOWLEDGEMENTS

This dissertation would not have been possible without the support from mentors, family, friends and Mechanical and Mining Engineering Departments.

I would like to express my deepest and sincere thankfulness to my thesis supervisor Asst. Prof. Dr. Ahmet Yozgatlıgil for his guidance, endurance, criticism, encouragement, support and precious insight throughout my thesis work.

Financial support of BAP (Eng. Scientific Research Projects) through BAP-03-02-2011-002 project is gratefully acknowledged. I also wish to greatly appreciate Central Laboratory of the Middle East Technical University for the support provided during these experiments, Prof. Dr. Necati Özkan for his expert advice and Ebru Deniz and Ayşe Nur Özkan for their help during my TGA-FTIR experiments.

I also would like to specifically thank Agah Köker (Mineral Research and Exploration (MTA)), Prof. Dr. Ali Ihsan Arol and Prof. Dr. M. Ümit Atalay (Mining Eng. Dep.) for their comprehensive support of this study.

Many thanks to my dear friends Mohsen Atabaki, Salar Vayghannezhad and Emrah Çamlı due to their endless support, encouragement and hopeful point of view in all situations.

I warmly thank Tahsin Işıksal, Aytekin Arslan and Levent Şahin for their help during laboratory works.

Finally I would like to express my deepest pleasure to my mother Susan Gharavi, my father Hassan Abbasi Atibeh and my brothers Peyman and Erfan Abbasi Atibeh for their never ending support, trust love and encouragement and with all my heart, I wish to express my greatest thanks to my wife Aysan Molaei who always was supportive, kind and so patient during my thesis work. She is my luck and this study would have been simply impossible without her.

## TABLE OF CONTENTS

ABSTRACT .....	iv
ÖZ.....	vii
ACKNOWLEDGEMENTS .....	x
TABLE OF CONTENTS .....	xi
LIST OF TABLES .....	xvi
LIST OF FIGURES.....	xx
LIST OF SYMBOLS AND ABBREVIATIONS.....	xxviii
CHAPTERS	
1. INTRODUCTION.....	1
2. LITERATURE SURVEY .....	5
2.1 Coal.....	5
2.2 Greenhouse Gas (GHG) Emissions and Other Pollutants.....	8
2.3 Carbon Capture and Storage (CCS) .....	10
2.4 Oxy-fuel Combustion Technology.....	13
2.5 TGA-FTIR Experiments .....	18
3. SAMPLES AND EXPERIMENTAL METHODS.....	26
3.1 Samples .....	26
3.1.1 Addition of the Catalysts (Impregnation).....	32
3.2 Experimental Set-Up and Procedure.....	35

3.2.1 TGA-FTIR Tests .....	35
3.2.1.1 TGA-FTIR Experimental Matrix .....	44
3.2.1.2 Combustion Regions in TGA-FTIR Studies .....	49
3.2.1.3 Characteristic Parameters in TGA-FTIR Studies.....	50
3.2.2 Ash Analysis with XRF Method .....	52
3.2.2.1 Repeatability Tests .....	57
3.2.3 Calorimetric Tests .....	58
3.2.3.1 Catalytic Effects on Calorimetric Tests .....	62
3.2.3.2 Sources of Errors in Calorimetric Tests .....	64
<b>4. TGA-FTIR EXPERIMENTS OF KANGAL LIGNITE PYROLYSIS .....</b>	<b>65</b>
4.1 Effects of N <sub>2</sub> and CO <sub>2</sub> Ambient Conditions.....	66
4.2 Effects of Catalysts .....	69
4.3 FTIR Results .....	71
4.3.1 Effects of N <sub>2</sub> and CO <sub>2</sub> Ambient Conditions.....	71
4.3.2 Effects of Catalysts in CO <sub>2</sub> Pyrolysis.....	73
<b>5. TGA-FTIR COMBUSTION TESTS.....</b>	<b>76</b>
5.1 TGA/DTG Profiles of Kangal Lignite and Tunçbilek Sub-Bituminous Samples (Combustion Tests).....	77
5.2 Combustion Tests of Kangal Lignite .....	79
5.2.1 Effects of N <sub>2</sub> and CO <sub>2</sub> Diluting Gases in Different Oxygen Mole Fractions (TGA/DTG Results).....	79
5.2.2 Effects of N <sub>2</sub> and CO <sub>2</sub> Ambient Conditions (FTIR Results).....	84
5.2.3 Effects of Different Oxygen Mole Fractions (TGA/DTG Results).....	89
5.2.4 Effects of Different Oxygen Mole Fractions (FTIR Results in N <sub>2</sub>	

ambient) .....	93
5.2.5 Effects of Different Oxygen Mole Fractions (FTIR Results in CO <sub>2</sub> ambient) .....	98
5.2.6 Effects of Catalysts on Combustion Tests of Kangal Lignite in O <sub>2</sub> /N <sub>2</sub> Ambient (TGA/DTG Results).....	101
5.2.7 Effects of Catalysts on Combustion Tests of Kangal Lignite in N <sub>2</sub> Ambient (FTIR Results).....	106
5.2.8 Effects of Catalysts on Combustion Tests of Kangal Lignite in CO <sub>2</sub> Ambient (TGA/DTG Results).....	111
5.2.8.1 Kangal Lignite Combustion in 21 % O <sub>2</sub> in CO <sub>2</sub> Ambient.....	111
5.2.8.2 Kangal Lignite Combustion in 25 % O <sub>2</sub> in CO <sub>2</sub> Ambient.....	115
5.2.8.3 Kangal Lignite Combustion in 30 % O <sub>2</sub> in CO <sub>2</sub> Ambient.....	117
5.2.8.4 Kangal Lignite Combustion in 35 % O <sub>2</sub> in CO <sub>2</sub> Ambient.....	119
5.2.9 Effects of Catalysts on Reaction Rates of Kangal Lignite Combustion....	121
5.2.9.1 Effects of Catalysts in the Devolatalization Region.....	121
5.2.9.2 Effects of Catalysts in the Char Combustion Region.....	122
5.2.10 Effects of Catalysts on Combustion Tests of Kangal Lignite in CO <sub>2</sub> Ambient (FTIR Results).....	124
5.2.11 Effects of Ambient on Catalytic Reactivity in Kangal Lignite Combustion Tests.....	131
5.2.11.1 Fe-based Catalyst .....	131
5.2.11.2 K-based Catalyst .....	133
5.3 Combustion Tests of Tunçbilek Sub-Bituminous Coal Sample .....	135
5.3.1 Effects of N <sub>2</sub> and CO <sub>2</sub> Ambient Conditions (TGA/DTG Results).....	135
5.3.2 Effects of N <sub>2</sub> and CO <sub>2</sub> Ambient Conditions (FTIR Results).....	136

5.3.3 Effects of Different Oxygen Mole Fractions (TGA/DTG Results).....	138
5.3.4 Effects of Different Oxygen Mole Fractions (FTIR Results) .....	138
5.3.5 Effects of Catalysts on Combustion Tests of Tunçbilek Sub-Bituminous Coal Sample in N <sub>2</sub> Ambient (TGA/DTG Results).....	140
5.3.6 Effects of Catalysts on Combustion Tests of Tunçbilek Sub-Bituminous Coal Sample in N <sub>2</sub> Ambient (FTIR Results).....	141
5.3.7 Effects of Catalysts on Combustion Tests of Tunçbilek Sub-Bituminous Coal Sample in CO <sub>2</sub> Ambient (TGA/DTG Results) .....	142
5.3.8 Effects of Catalysts on Combustion Tests of Tunçbilek Sub-Bituminous Coal Sample in CO <sub>2</sub> Ambient (FTIR Results) .....	144
5.4 Co-processing Combustion Tests of Lignite and the Ash Contents of Turkish Biomass Fuels .....	145
5.4.1 Biomass Ash Analyses .....	146
5.4.2 Combustion Test Results.....	149
5.4.2.1 Combustion Tests Carried Out in Air .....	149
5.4.2.2 Combustion Tests Carried Out in 30 % O <sub>2</sub> in CO <sub>2</sub> Ambient .....	154
6. CONCLUSIONS .....	161
6.1 Calorimetric Tests .....	161
6.2 TGA-FTIR Tests .....	162
6.2.1 Pyrolysis Tests of Kangal Lignite .....	162
6.2.2 Combustion Tests.....	163
6.3 Future Work.....	167
REFERENCES .....	169
APPENDICES	
A. MATERIALS AND EXPERIMENTAL .....	177

B. CALORIMETRIC TEST RESULTS.....	195
C. TGA-FTIR (EXPERIMENTAL).....	206
D. TGA-FTIR (RESULTS).....	208
E. CURRICULUM VITAE .....	222

## LIST OF TABLES

### TABLES

Table 2.1 Composition of ash forming oxides [46].....	24
Table 3.1 Proximate analyses of Turkish coal samples.....	28
Table 3.2 Ultimate analysis of Kangal lignite and Tunçbilek sub-bituminous used in TGA-FTIR tests.....	29
Table 3.3 Moisture content of the coal samples.....	31
Table 3.4 IR wavenumbers of the evolved gases.....	43
Table 3.5 TGA-FTIR experimental matrix of original and impregnated Kangal lignite and Tunçbilek sub-bituminous coal samples.....	45
Table 3.6 TGA-FTIR experimental matrix of original and impregnated Kangal lignite and Tunçbilek sub-bituminous coal samples (continued).....	46
Table 3.7 TGA-FTIR experimental matrix of original and impregnated Kangal lignite and Tunçbilek sub-bituminous coal samples (continued).....	47
Table 3.8 TGA-FTIR experimental matrix of original Kangal lignite and the impregnated samples with biomass ash contents.....	48
Table 3.9 Ash analyses of the original and impregnated Kangal lignite samples.....	55
Table 3.10 Ash analyses of the original and impregnated Seyitömer lignite samples.....	55
Table 3.11 Ash analyses of the original and impregnated Tunçbilek sub-bituminous samples.....	56
Table 3.12 Ash analyses of the original and impregnated Zonguldak bituminous	

samples .....	56
Table 3.13 Repeatability tests in XRF analyses .....	57
Table 4.1 N <sub>2</sub> and CO <sub>2</sub> pyrolysis characteristics.....	68
Table 4.2 Effects of catalysts in CO <sub>2</sub> pyrolysis .....	69
Table 5.1 Characteristic parameters of Kangal lignite combustion in 21 % O <sub>2</sub> .....	81
Table 5.2 Characteristic parameters of evolved gases during combustion tests in 21 % O <sub>2</sub> .....	85
Table 5.3. Characteristic parameters of evolved gases during combustion tests in 30 % O <sub>2</sub> .....	88
Table 5.4 Characteristic parameters of Kangal lignite combustion in N <sub>2</sub> ambient ....	90
Table 5.5 Characteristic parameters of Kangal lignite combustion in CO <sub>2</sub> ambient..	90
Table 5.6 Effects of catalysts in air combustion tests of Kangal lignite .....	102
Table 5.7 Characteristic parameters of Kangal lignite combustion tests in 21 % O <sub>2</sub> in CO <sub>2</sub> ambient .....	112
Table 5.8 Combustion characteristics of raw and impregnated Kangal lignite samples in different O <sub>2</sub> / CO <sub>2</sub> mixtures .....	114
Table 5.9 Characteristic parameters of Kangal lignite combustion tests in 25 % O <sub>2</sub> in CO <sub>2</sub> ambient .....	115
Table 5.10 Characteristic parameters of Kangal lignite combustion tests in 30 % O <sub>2</sub> in CO <sub>2</sub> ambient .....	117
Table 5.11 Characteristic parameters of Kangal lignite combustion tests in 35 % O <sub>2</sub> in CO <sub>2</sub> ambient .....	119
Table 5.12 Ash analyses of the Turkish biomass fuels.....	147
Table 5.13 Characteristic temperatures and parameters of original and impregnated Kangal lignite combustion tests in air .....	150
Table 5.14 Concentrations of K-based oxides in the ash contents of impregnated	

Kangal lignite .....	154
Table 5.15 Characteristic temperatures and parameters of original and impregnated Kangal lignite combustion tests in 30 % O <sub>2</sub> in CO <sub>2</sub> ambient.....	156
Table 5.16 Concentrations of Ca-based oxides in the ash contents of impregnated Kangal lignite .....	160
Table A.1 Original humidity content analyses of Kangal and Seyitömer lignite samples (as received) (%).....	177
Table A.2 Original humidity content analyses of Tunçbilek and Zonguldak coal samples (as received) (%).....	178
Table A.3 Humidity content analyses of Kangal and Seyitömer lignite samples as used in the tests (after milling) (%) .....	179
Table A.4 Humidity content analyses of Tunçbilek and Zonguldak coal samples as used in the tests (after milling) (%) .....	180
Table A.5 Humidity content analyses of the impregnated coal samples.....	180
Table A.6 Production of crop residues in Turkey [80].....	181
Table A.7 Specifications of the Perkin Elmer Pyris STA 6000 TGA.....	182
Table A.8 Specifications of the Perkin Elmer Spectrum 1 FTIR spectrometer .....	184
Table A.9 Specifications of Cole-Parmer EW-03229-03 variable area flow meter.....	186
Table A.10 Flow meter calibration data for different gases .....	188
Table A.11 XRF ash analyses of Kangal lignite and impregnated lignite samples..	189
Table A.12 XRF ash analysis of hazelnut shell (HSh) biomass.....	194
Table B.1 Calorimetric test results of Tunçbilek sub- bituminous samples .....	196
Table B.2 Calorimetric test results of Seyitömer lignite samples .....	197
Table B. 3 Calorimetric test results of Kangal lignite samples .....	198
Table B. 4 Calorimetric test results of Zonguldak bituminous samples.....	199

Table B.5 Sample weight definition (Tunçbilek sub-bituminous) .....	200
Table B.6 Sample weight definition (Kangal lignite).....	201
Table B.7 Sample weight definition (Seyitömer lignite).....	202
Table B.8 Sample weight definition (Zonguldak bituminous) .....	203
Table B.9 Repeatability in calorific value tests of impregnated Kangal lignite with $K_2CO_3$ catalyst.....	204
Table B.10 Repeatability in calorific value tests of Tunçbilek sub-bituminous samples impregnated with 5 % catalysts .....	205
Table C.1 Flow fluctuations during TGA-FTIR combustion tests.....	206
Table C.2 Flow fluctuations during TGA-FTIR pyrolysis tests.....	207
Table D.1 Characteristic temperatures and parameters of Fe-form Kangal lignite combustion in $O_2/N_2$ ambient.....	219
Table D.2 Characteristic temperatures and parameters of Fe-form Kangal lignite combustion in $O_2/CO_2$ ambient .....	219
Table D.3 Characteristic temperatures and parameters of K-form Kangal lignite combustion in $O_2/N_2$ ambient.....	220
Table D.4 Characteristic temperatures and parameters of K-form Kangal lignite combustion in $O_2/CO_2$ ambient .....	220

## LIST OF FIGURES

### FIGURES

Fig. 2.1 Different coal types and their applications [47] .....	7
Fig. 2.2 The Greenhouse Effect [47] .....	9
Fig. 2.3 Overall plants configurations for the three main CCS technologies [12] .....	12
Fig. 2.4 Flow sheet of oxy-fuel technology for power generation with CO <sub>2</sub> capture and storage, showing the major components.....	14
Fig. 2.5 The O <sub>2</sub> mole fractions required at burner inlet (to achieve similar AFT as in air-fired case) for oxy-wet and oxy-dry conditions [10] .....	17
Fig. 3.1 Turkish biomass fuels: hazelnut shell (left) and walnut shell (right) .....	27
Fig. 3.2 Jaw (left) and roll (right) crushers.....	30
Fig. 3.3 Ceramic ball mill.....	31
Fig. 3.4 Impregnated Kangal lignite samples with biomass ash used in TGA-FTIR tests .....	34
Fig. 3.5 Schematic view of the IR spectroscopy .....	38
Fig 3.6 Schematic diagram of the experimental setup.....	39
Fig. 3.7 Experimental setup.....	40
Fig. 3.8 Perkin Elmer Pyris STA 6000 TGA (left), Spectrum 1 FTIR spectrometer (right).....	41
Fig. 3.9 Internal view of the TGA at METU Central Laboratory (Perkin Elmer Pyris STA 6000) .....	41
Fig. 3.10 TGA system coupled with FTIR spectrometer and the heated line between	

two devices .....	42
Fig. 3.11 TGA and DTG profiles of Kangal lignite combustion during 21 % O <sub>2</sub> in CO <sub>2</sub> ambient .....	50
Fig. 3.12 Ignition temperature (T <sub>i</sub> ) definition sketch [56].....	52
Fig. 3.13 XRF test tablets .....	54
Fig. 3.14 X-ray Fluorescence SPECTRO iQ (left) and the hydraulic press (right)....	54
Fig. 3.15 Oxygen bomb .....	58
Fig. 3.16 Oxygen bomb calorimeter (left) and schematic view (right) .....	59
Fig. 3.17 Oxygen bomb calorimeter set up .....	60
Fig. 3.18 Calorific values of Kangal lignite samples with catalysts.....	63
Fig. 3.19 Calorific values of Tunçbilek sub-bituminous samples with catalysts .....	63
Fig. 4.1 TGA profiles of N <sub>2</sub> and CO <sub>2</sub> pyrolysis tests .....	67
Fig. 4.2 DTG profiles of N <sub>2</sub> and CO <sub>2</sub> pyrolysis tests .....	68
Fig. 4.3 DTG profiles of CO <sub>2</sub> pyrolysis tests with catalysts.....	70
Fig. 4.4 TGA profiles of CO <sub>2</sub> pyrolysis tests with catalysts.....	70
Fig. 4.5 Formation profile of CO <sub>2</sub> during N <sub>2</sub> pyrolysis test .....	72
Fig. 4.6 Formation profiles of evolved gases during N <sub>2</sub> and CO <sub>2</sub> pyrolysis tests .....	73
Fig. 4.7 Formation profiles of CO and COS evolved gases during CO <sub>2</sub> pyrolysis tests with catalysts .....	75
Fig. 5.1 Combustion profiles of Kangal and Tunçbilek samples in air .....	78
Fig. 5.2 Combustion profiles of Kangal and Tunçbilek samples in 30 % O <sub>2</sub> in CO <sub>2</sub> ambient .....	78
Fig. 5.3 TGA and DTG profiles of Kangal lignite combustion during 21 % O <sub>2</sub> in N <sub>2</sub> and 21 % O <sub>2</sub> in CO <sub>2</sub> ambient conditions .....	80
Fig. 5.4 TGA and DTG profiles of Kangal lignite combustion during 25 % O <sub>2</sub> in N <sub>2</sub>	

and 25 % O <sub>2</sub> in CO <sub>2</sub> ambient conditions .....	81
Fig. 5.5 TGA and DTG profiles of Kangal lignite combustion during 30 % O <sub>2</sub> in N <sub>2</sub> and 30 % O <sub>2</sub> in CO <sub>2</sub> ambient conditions .....	82
Fig. 5.6 TGA and DTG profiles of Kangal lignite combustion during 35 % O <sub>2</sub> in N <sub>2</sub> and 35 % O <sub>2</sub> in CO <sub>2</sub> ambient conditions .....	82
Fig. 5.7 Maximum reaction rates in the second region and characteristic temperatures of lignite combustion tests in various oxygen mole fractions in both N <sub>2</sub> and CO <sub>2</sub> ambient conditions.....	83
Fig. 5.8 Formation profiles of evolved gases during combustion tests in air and in 21 % O <sub>2</sub> in CO <sub>2</sub> ambient .....	85
Fig. 5.9 Formation profiles of evolved gases during combustion tests in 30 % O <sub>2</sub> in N <sub>2</sub> and 30 % O <sub>2</sub> in CO <sub>2</sub> ambient conditions .....	87
Fig. 5.10 DTG profiles of Kangal lignite under various oxygen mole fractions in N <sub>2</sub> ambient .....	91
Fig. 5.11 TGA profiles of Kangal lignite under various oxygen mole fractions in N <sub>2</sub> ambient .....	91
Fig. 5.12 DTG profiles of Kangal lignite under various oxygen mole fractions in CO <sub>2</sub> ambient .....	92
Fig. 5.13 TGA profiles of Kangal lignite under various oxygen mole fractions in CO <sub>2</sub> ambient .....	92
Fig. 5.14 Formation profiles of CO <sub>2</sub> during combustion tests of Kangal lignite in N <sub>2</sub> ambient .....	93
Fig. 5.15 Formation profiles of evolved gases during combustion tests of Kangal lignite in N <sub>2</sub> ambient.....	94
Fig. 5.16 Characteristics parameters of combustion tests of Kangal lignite in N <sub>2</sub> ambient: correlations between: a) T <sub>2max</sub> and T <sub>FG-max</sub> , b)  (dm/dt) <sub>2max</sub>   and maximum absorbance of the evolved gases in FTIR spectra.....	96

Fig. 5.17 Formation profiles of NH <sub>3</sub> and NO during combustion tests of Kangal lignite in N <sub>2</sub> ambient.....	97
Fig. 5.18 Formation profiles of evolved gases during combustion tests of Kangal lignite in CO <sub>2</sub> ambient .....	99
Fig. 5.19 Characteristics parameters of combustion tests of Kangal lignite in CO <sub>2</sub> ambient: correlations between: a) T <sub>2max</sub> and T <sub>FG-max</sub> , b)  (dm/dt) <sub>2max</sub>   and maximum absorbance of the evolved gases in FTIR spectra.....	100
Fig. 5.20 DTG profiles of catalytic combustion tests of Kangal lignite in air .....	103
Fig. 5.21 TGA profiles of catalytic combustion tests of Kangal lignite in air .....	103
Fig. 5.22 TGA profiles of catalytic combustion tests of Kangal lignite in 30 % O <sub>2</sub> in N <sub>2</sub> ambient.....	104
Fig. 5.23 DTG profiles of catalytic combustion tests of Kangal lignite in 30 % O <sub>2</sub> in N <sub>2</sub> ambient.....	104
Fig. 5.24 Maximum reaction rates in the second and third regions during Kangal lignite catalytic combustion under various oxygen mole fractions in N <sub>2</sub> ambient...	105
Fig. 5.25 Formation profiles of CO <sub>2</sub> during catalytic combustion tests of Kangal lignite in air.....	106
Fig. 5.26 Formation profiles of evolved gases during catalytic combustion tests of Kangal lignite in air .....	107
Fig. 5.27 Formation profiles of CO <sub>2</sub> during catalytic combustion tests of Kangal lignite in 30 % O <sub>2</sub> in N <sub>2</sub> ambient .....	108
Fig. 5.28 Formation profiles of evolved gases during catalytic combustion tests of Kangal lignite in 30 % O <sub>2</sub> in N <sub>2</sub> ambient.....	109
Fig. 5.29 Formation profiles of nitrogen containing species during catalytic combustion tests of Kangal lignite in 30 % O <sub>2</sub> in N <sub>2</sub> ambient .....	110
Fig. 5.30 DTG profiles of catalytic combustion tests of Kangal lignite in 21 % O <sub>2</sub> in CO <sub>2</sub> ambient .....	113

Fig. 5.31 TGA profiles of catalytic combustion tests of Kangal lignite in 21 % O <sub>2</sub> in CO <sub>2</sub> ambient .....	113
Fig. 5.32 DTG profiles of catalytic combustion tests of Kangal lignite in 25 % O <sub>2</sub> in CO <sub>2</sub> ambient .....	116
Fig. 5.33 TGA profiles of catalytic combustion tests of Kangal lignite in 25 % O <sub>2</sub> in CO <sub>2</sub> ambient .....	116
Fig. 5.34 DTG profiles of combustion tests of Kangal lignite in 30 % O <sub>2</sub> in CO <sub>2</sub> ambient .....	118
Fig. 5.35 TGA profiles of combustion tests of Kangal lignite in 30 % O <sub>2</sub> in CO <sub>2</sub> ambient .....	118
Fig. 5.36 DTG profiles of catalytic combustion tests of Kangal lignite in 35 % O <sub>2</sub> in CO <sub>2</sub> ambient- second region.....	120
Fig. 5.37 DTG profiles of catalytic combustion tests of Kangal lignite in 35 % O <sub>2</sub> in CO <sub>2</sub> ambient- third region .....	120
Fig. 5.38 TGA profiles of catalytic combustion tests of Kangal lignite in 35 % O <sub>2</sub> in CO <sub>2</sub> ambient .....	121
Fig. 5.39 Maximum reaction rates in the second and third regions of combustion during Kangal lignite catalytic combustion under various oxygen mole fractions in CO <sub>2</sub> ambient .....	123
Fig. 5.40 Formation profiles of evolved gases during catalytic combustion tests in 21 % O <sub>2</sub> in CO <sub>2</sub> ambient.....	124
Fig. 5.41 Formation profiles of evolved gases during catalytic combustion tests in 30 % O <sub>2</sub> in CO <sub>2</sub> ambient.....	126
Fig. 5.42 Formation profiles of CH <sub>4</sub> during K-form sample combustion test in 30 % O <sub>2</sub> in CO <sub>2</sub> ambient .....	127
Fig. 5.43 Formation profiles of NH <sub>3</sub> and NO during catalytic combustion tests in 30 % O <sub>2</sub> in CO <sub>2</sub> ambient.....	128

Fig. 5.44 Characteristics parameters of the catalytic combustion tests in 30 % O <sub>2</sub> in CO <sub>2</sub> ambient: correlations between: a) T <sub>2max</sub> and T <sub>FG-max</sub> , b)  (dm/dt) <sub>2max</sub>   and maximum absorbance of the evolved gases in FTIR spectra .....	130
Fig. 5.45 DTG profiles of Fe-form Kangal lignite combustion in 25 % O <sub>2</sub> .....	131
Fig. 5.46 DTG profiles of Fe-form Kangal lignite combustion in 30 % O <sub>2</sub> .....	132
Fig. 5.47 DTG profiles of Fe-form Kangal lignite combustion in 35 % O <sub>2</sub> .....	133
Fig. 5.48 DTG profiles of K-form Kangal lignite combustion in 25 % O <sub>2</sub> .....	134
Fig. 5.49 DTG profiles of K-form Kangal lignite combustion in 30 % O <sub>2</sub> .....	134
Fig. 5.50 DTG profiles of K-form Kangal lignite combustion in 35 % O <sub>2</sub> .....	135
Fig. 5.51 TGA and DTG profiles of Tunçbilek coal combustion during 30 % O <sub>2</sub> in N <sub>2</sub> and 30 % O <sub>2</sub> in CO <sub>2</sub> ambient conditions .....	136
Fig. 5.52 Formation profiles of evolved gases during combustion tests under 30 % O <sub>2</sub> in N <sub>2</sub> and 30 % O <sub>2</sub> in CO <sub>2</sub> ambient conditions .....	137
Fig. 5.53 Combustion profiles of Tunçbilek sample under 21 % O <sub>2</sub> in N <sub>2</sub> and 30 % O <sub>2</sub> in N <sub>2</sub> ambient conditions .....	138
Fig. 5.54 Formation profiles of CO <sub>2</sub> during Tunçbilek combustion tests in N <sub>2</sub> ambient.....	139
Fig. 5.55 Formation profiles of evolved gases during Tunçbilek combustion tests in N <sub>2</sub> ambient.....	140
Fig. 5.56 Combustion profiles of catalytic Tunçbilek combustion tests in 30 % O <sub>2</sub> in N <sub>2</sub> ambient.....	141
Fig. 5.57 Formation profiles of evolved gases during catalytic Tunçbilek combustion tests in 30 % O <sub>2</sub> in N <sub>2</sub> ambient .....	142
Fig. 5.58 TGA profiles of catalytic Tunçbilek combustion tests in 30 % O <sub>2</sub> in CO <sub>2</sub> ambient.....	143
Fig. 5.59 DTG profiles of Tunçbilek catalytic combustion tests in 30 % O <sub>2</sub> in CO <sub>2</sub>	

ambient .....	144
Fig. 5.60 Formation profiles of evolved gases during catalytic Tunçbilek combustion tests in 30 % O <sub>2</sub> in CO <sub>2</sub> ambient.....	145
Fig. 5.61 Major contributions of alkali and alkaline earth metals in the ash contents of Turkish biomass fuels .....	148
Fig. 5.62 DTG combustion curves of original and impregnated Kangal lignite with biomass ash contents in air .....	151
Fig. 5.63 DTG profile comparisons of K-form lignite and the catalytic effects of HSh and WSh ash contents in air .....	153
Fig. 5.64 DTG combustion curves of original and impregnated Kangal lignite with biomass ash contents in 30 % O <sub>2</sub> in CO <sub>2</sub> ambient .....	157
Fig. 5.65 DTG profile comparisons of K-form lignite and the catalytic effects of HSh and WSh ash contents in 30 % O <sub>2</sub> in CO <sub>2</sub> ambient .....	158
Fig. 5.66 DTG profile comparisons of Ca-form lignite and the catalytic effect of SD ash content in 30 % O <sub>2</sub> in CO <sub>2</sub> ambient.....	160
Fig. A.1 Typical FTIR spectra of important species for being used in identification and calibration [62].....	183
Fig. A.2 EW-03229-03 Cole-Parmer variable area flow meter drawing sketch .....	187
Fig. D.1 Formation profiles of evolved gases during combustion tests in 25 % O <sub>2</sub> in N <sub>2</sub> and 25 % O <sub>2</sub> in CO <sub>2</sub> ambient conditions .....	208
Fig. D.2 Formation profiles of NO during combustion tests in 25 % O <sub>2</sub> in N <sub>2</sub> and 25 % O <sub>2</sub> in CO <sub>2</sub> ambient conditions .....	209
Fig. D.3 Formation profiles of evolved gases during combustion tests in 35 % O <sub>2</sub> in N <sub>2</sub> and 35 % O <sub>2</sub> in CO <sub>2</sub> ambient conditions .....	210
Fig. D.4 Formation profiles of NO during combustion tests in 35 % O <sub>2</sub> in N <sub>2</sub> and 35 % O <sub>2</sub> in CO <sub>2</sub> ambient conditions .....	211
Fig. D.5 Formation profiles of CO <sub>2</sub> during catalytic combustion tests in 25 % O <sub>2</sub> in	

N <sub>2</sub> ambient .....	211
Fig. D.6 Formation profiles of evolved gases during catalytic combustion tests in 25 % O <sub>2</sub> in N <sub>2</sub> ambient .....	212
Fig. D.7 Formation profiles of nitrogen containing species during catalytic combustion tests in 25 % O <sub>2</sub> in N <sub>2</sub> ambient.....	213
Fig. D.8 Formation profiles of CO <sub>2</sub> during catalytic combustion tests in 35 % O <sub>2</sub> in N <sub>2</sub> ambient .....	214
Fig. D.9 Formation profiles of evolved gases during catalytic combustion tests in 35 % O <sub>2</sub> in N <sub>2</sub> ambient .....	215
Fig. D.10 Formation profiles of nitrogen containing species during catalytic combustion tests in 35 % O <sub>2</sub> in N <sub>2</sub> ambient.....	216
Fig. D.11 Formation profiles of evolved gases during catalytic combustion tests in 25 % O <sub>2</sub> in CO <sub>2</sub> ambient.....	217
Fig. D.12 Formation profiles of evolved gases during catalytic combustion tests in 35 % O <sub>2</sub> in CO <sub>2</sub> ambient.....	218
Fig. D.13 Formation profile of HCN during combustion test of Tunçbilek coal sample in air .....	221

## LIST OF SYMBOLS AND ABBREVIATIONS

$T_{in}$ (°C)	Initial decomposition temperature
$T_{ig}$ (°C)	Ignition temperature
$T_{2max}$ (°C)	Peak temperature in the devolatilization region (second region of combustion)
$T_{3max}$ (°C)	Peak temperature in the char gasification and oxidation region (third region of combustion)
$T_b$ (°C)	Burnout temperature
$T_{FG-max}$ (°C)	Temperature of the maximum flue gas emission
$ (dm/dt)_{2max} $ (%/min)	The absolute value of the maximum rate of weight loss in the devolatilization region (second region of combustion)
$ (dm/dt)_{3max} $ (%/min)	The absolute value of the maximum rate of weight loss in the char gasification and oxidation region (third region of combustion)
$dm/dt$ (%/min) (specific reactivity)	Rate of weight loss at any time during pyrolysis or combustion processes
TGA	Thermogravimetric Analysis
DTG	Derivative Thermogravimetric Analysis
DSC	Differential Scanning Calorimeter
FTIR	Fourier Transform Infrared spectroscopy
EGA	Evolved Gas Analysis

<b>XRF</b>	X-ray Fluorescence spectroscopy
<b>MFM</b>	Mass Flow Meter
<b>GHG</b>	Greenhouse Gas
<b>CCS</b>	Carbon Dioxide Capture and Storage
<b>AFT</b>	Adiabatic Flame Temperature
<b>FBC</b>	Fluidized Bed Combustion
<b>IGCC</b>	Integrated Gasification Combined Cycle

## CHAPTER 1

### INTRODUCTION

Energy sources are the need of modern civilization. The increasing world population and the continuous improvement in living standards, technological and economic developments have led to drastic increases in the demand for energy. According to *The World Energy Outlook* projects, world energy supply will rise 40 % up to 2030 [1]. About 85 % of the world's commercial energy needs are currently supplied by fossil fuels [2] and among the mix of this energy supply; coal is the source of about 27 % of the world primary energy consumption and it accounts for about 34 % of all the electricity generated in the world, while much of this occurs by means of the combustion of pulverized coal [3]. Although other alternative fuels are being researched recently to reduce the reliance on fossil fuels, they will be in the center of the energy scene in far future. Therefore in the foreseeable future, with the 826 billion tons of proved reserves [4], coal is believed to be a major energy source in many parts of the world. However, the utilization of coal was also related to the increasing environmental concern because of greenhouse gas (GHG) emissions and especially CO<sub>2</sub>, as the major contributor to the greenhouse effect and a main cause for global warming. Emissions of the greenhouse gas carbon dioxide from coal-fired power plants are very high, accounting for 40 % of total global emissions [5]. Therefore the abatement of GHG emissions and mitigation of the negative consequences derived from the climate change are now an urgent challenge [6, 7]. On the other hand the risks of pollutants emitted during coal combustion are being raised due to the contribution of these pollutants to rain acidification,

global warming and depletion of stratospheric ozone layer [8, 9].

Reduction of greenhouse gas emissions from fossil fuel-fired power generation can be achieved by efficiency improvement, switching to lower carbon fuels and CO<sub>2</sub> capture and storage (CCS) [10]. Carbon dioxide capture and storage (CCS) has been suggested as a step change method to reduce CO<sub>2</sub> emissions from coal combustion and would enable the world to continue to use fossil fuels but with much reduced emissions of CO<sub>2</sub> [2]. There are several options for capture and storage of CO<sub>2</sub> from coal combustion and gasification. These CCS methods are profoundly discussed elsewhere [11-13] and a brief description can be found in Chapter 2.3. However the major problem is that the combustion of fossil fuels in air typically leads to a dilute CO<sub>2</sub> concentration in the flue gas stream (typically 15 % by volume), rendering it unsuitable for direct sequestration in a supercritical state from compression which requires a high CO<sub>2</sub> concentration [7, 14, 15].

Oxy-fuel combustion technology is an emerging approach toward CCS methods. Oxy-fuel combustion is not technically a capture technology but rather a process during which a combination of oxygen, typically of greater than 95 % purity, and recycled flue gas as the main heat carrier through the boiler (nitrogen free combustion ambient) is used for the combustion of a fuel. Thereby, combustion of fossil fuels occurs in O<sub>2</sub>/CO<sub>2</sub> (oxy-fuel condition) rather than in O<sub>2</sub>/N<sub>2</sub> ambient as in conventional air fired systems. Therefore, this technology is one of several promising new technologies for enrichment of CO<sub>2</sub> in the flue gas to levels as high as 95 % in the flue gas stream [16]. Oxy-fuel combustion technology for coal fired power generation along with laboratory and pilot scale studies have been described and reviewed in detail recently [10, 12, 17, 18]. However, switching from conventional to oxy-fuel pulverized coal combustion technology brings a number of technical challenges. Previous results have shown that the replacement of N<sub>2</sub> by CO<sub>2</sub> can cause significant differences in combustion furnace operation parameters such as flame ignition, burning stability, char burnout, heat and mass transfer, gas temperature profiles, emissions and ash properties mostly due to differences in gas properties between CO<sub>2</sub> and N<sub>2</sub> [17, 19-25]. Furthermore previous studies on oxy-fuel

combustion mainly revealed that the overall O<sub>2</sub> concentration at the inlet to the boiler should be between 27 % and 35 vol % in order to yield comparable adiabatic flame temperatures and heat transfer profiles as seen for conventional combustion in air [12]. This need for higher oxygen concentration can be explained by higher heat capacity of CO<sub>2</sub> which causes lower adiabatic flame temperature (AFT) and delay in combustion process [10,12, 17, 22, 25, 26].

On the other hand for improving coal combustion efficiency, many methods were applied to coal conversion process, including advanced reactor (Circulating Fluidized Bed), oxygen enriched technology and catalytic combustion. Catalysts were added into pulverized coal by physical mixing or impregnation which can improve coal combustion characteristics. At present, catalytic combustion of pulverized coal is mainly applied in power plant boiler, entrained-flow reactor and coal injection for blast furnace iron making [27]. Previous studies have revealed that constituents of coal mineral matter significantly affect other types of coal conversion reactions [28-30]. Besides that, according to the wide variety of literature, using different types of catalysts have been recognized as a potential way for improvement of the emissions and therefore clean and efficient utilization of coal. Alkali, alkaline earth metals and transition metallic species are accounted as effective catalysts for the combustion, pyrolysis and gasification of a wide variety of carbonaceous materials [8, 28, 31-37]. Moreover, the study on the pollutants emitted during coal combustion is still of significant interest. According to the literature, using different types of catalysts have been recognized as a potential way for the clean and efficient utilization of coal and improvement of the emissions [8, 31, 38-44].

However, most of researches were focused on the effects of catalysts on pyrolysis and combustion behavior of coal samples in O<sub>2</sub>/N<sub>2</sub> ambient, whereas effects of catalysts on oxy-fuel (O<sub>2</sub>/CO<sub>2</sub> ambient) combustion characteristics of indigenous coal samples using Thermogravimetric Analyzer coupled with Fourier Transform Infrared Spectrometer (TGA-FTIR) are not available to date. Therefore, the main objective in this thesis study was to profoundly explore the effects of three inorganic materials, potassium (K) which is an alkali metal, calcium (Ca) which is an alkaline

earth metal and iron (Fe) which is a transition metal, on oxy-fuel ( $O_2/CO_2$  ambient) combustion, pyrolysis and emission characteristics of Turkish lignite and sub-bituminous samples using TGA-FTIR. These catalysts are environment-friendly compounds with lower toxicity which have shown significant catalytic activities in pyrolysis, combustion and emission control of coal samples worldwide [8, 28, 31-37].

As a preliminary approach to the experimental part of this study, an attempt was done to investigate the possible influences of these three inorganic materials of potassium (K), calcium (Ca) and iron (Fe) on calorific values of four different indigenous coal samples including lignite, sub-bituminous and bituminous types using Oxygen bomb calorimeter.

Finally the possible way of using Turkish biomass as a potential source of inexpensive catalysts in the co-processing of coal and biomass ash under oxy-fuel conditions was examined. Alkali metal salts, especially potassium salts, are considered as effective catalysts by steam and  $CO_2$ , while too expensive for industry application [45]. On the other hand considerable amounts of these alkali metal oxides, especially potassium oxides, were traced in the ash of biomass fuels like wheat straw, olive bagasse and hazelnut shell [46]. Therefore various types of biomass including walnut shell, hazelnut shell, wheat straw, Limba wood saw dust and cattle manure from the domestic sources were used in these experiments and the results compared with the results obtained from the utilization of potassium (K), calcium (Ca) and iron (Fe) inorganic catalysts.

In this thesis study, the summary of the literature survey including oxy-fuel combustion and TGA-FTIR catalytic tests are reported in Chapter 2. The samples used throughout this study and the experimental methods and sample analyses are described in Chapter 3. The results and discussion part including pyrolysis and combustion tests are embodied in the Chapters 4 and 5 respectively. Finally the conclusion part can be reviewed in Chapter 6.

## CHAPTER 2

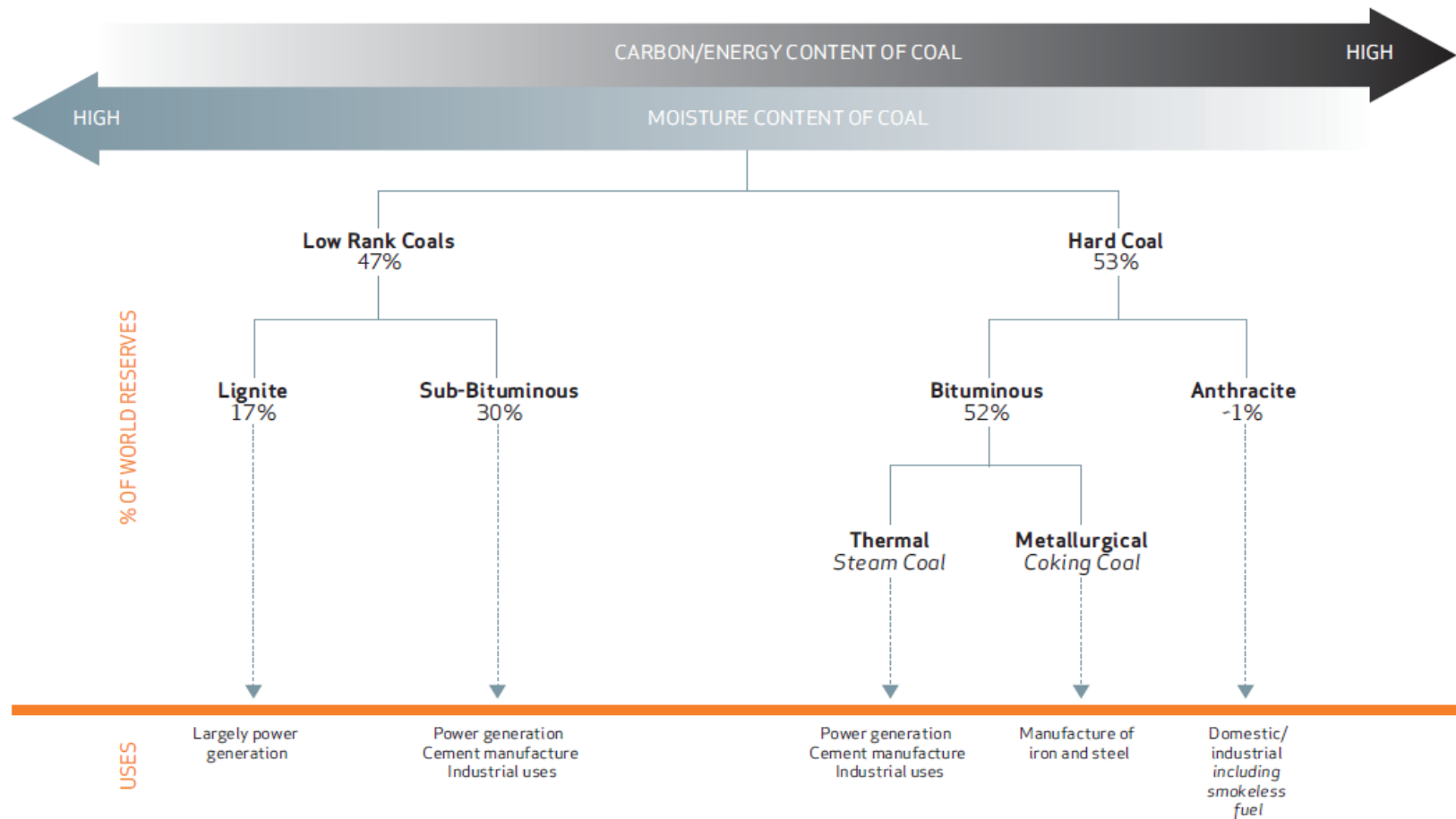
### LITERATURE SURVEY

#### 2.1 Coal

Coal is one of the most vital energy sources in meeting the rapidly growing energy needs of the world. Today almost 40 % of the electricity production worldwide is relied on coal and it is expected to remain constant during the next 30 years. Furthermore this contribution in many countries, like Poland, South Africa, Australia and China is much higher, about 94 %, 92 %, 76 % and 77 % respectively [47, 48]. The main part of coal production in Turkey is also used for electricity production. So the important role of coal not only in electricity production, but also in many other industrial activities like steel and cement production is obviously undeniable. Pulverized Coal-Firing technology is the most common power generation technology worldwide which is supported by decades of experience and is being used in many parts of the world.

Coal is originally the remains of prehistoric vegetation aggregated in swamps and peat bogs which altered over time. The coal quality is specified by the formation time period, temperature and pressure which is called *organic maturity*. This gradual change applied on coal deposits - known as coalification- would alter the physical and chemical properties of coal which is referred to as *coal rank*. At the first step the peat is converted into lignite which is also referred to as *brown coal*. Continuing effects of pressure and temperature will impose further change in lignite over millions of years and increase its rank into the range known as *sub-bituminous*. These low rank coals are characterized by their high humidity and low carbon and

energy content. Moreover, these physical and chemical alternations as a result of pressure and temperature will continue further and make the coals become harder and blacker forming the *bituminous* or *hard coals* and finally *anthracite*. These types of coal contain lower humidity, higher carbon content and therefore higher energy content. Fig. 2.1 shows the different coal types and their applications.



7

Fig. 2.1 Different coal types and their applications [47]

Although coal reserves are expected to last longer (over 190 years) than other types of the fossil fuels (for example for oil the expected period is 42 years) [47], all the resources of fossil fuel will eventually run out on the earth. Therefore, an efficient use of these fuel reserves is an essential concern worldwide and significant improvement should continue to utilize coal and other types of fossil fuels more efficiently and clean. With 38 % increase in coal production over the past 20 years, currently 4030 million tons of coal is produced worldwide and is expected to reach 7000 million tons by 2030 [47]. Therefore coal will continue to play an important role in the world's energy mix. The top five coal producers can be named as: China, the USA, India, Australia and South Africa.

## **2.2 Greenhouse Gas (GHG) Emissions and Other Pollutants**

Production and utilization of energy has considerable impacts on the environment. Therefore, minimizing these negative impacts of human activities on the nature and mitigating the environmental concern of energy utilization is of great importance worldwide. Naturally occurring gases in the atmosphere help to regulate the earth's temperature by trapping other radiation which is known as *the Greenhouse Effect* (Fig. 2.2). The major greenhouse gases are carbon dioxide (CO<sub>2</sub>), nitrous oxide (N<sub>2</sub>O), methane (CH<sub>4</sub>), water vapor (H<sub>2</sub>O), sulphur hexafluoride, hydrofluorocarbons and perfluorocarbons among which the first three are associated with different coal utilizations worldwide.

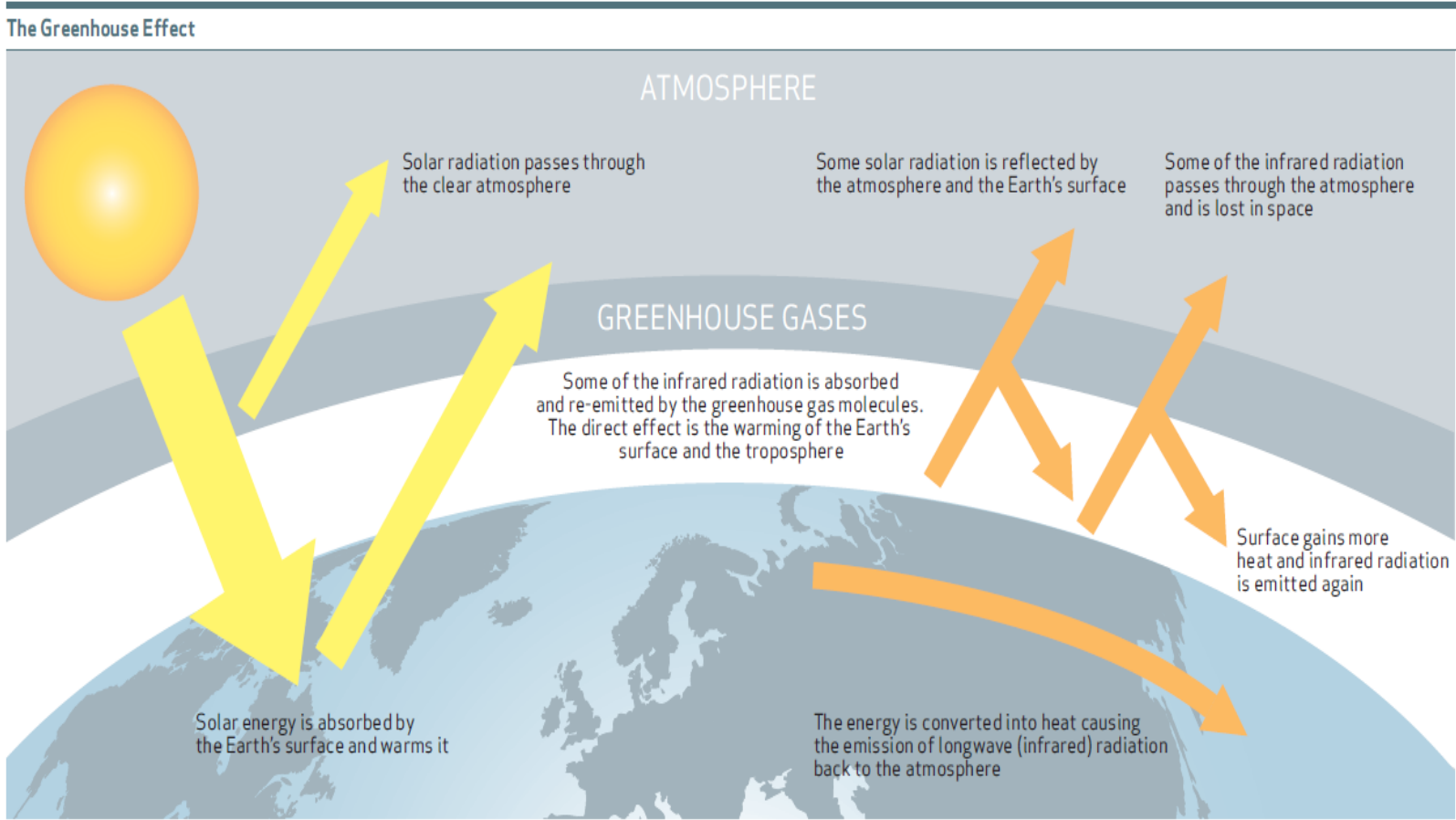


Fig. 2.2 The Greenhouse Effect [47]

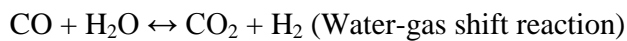
Considerable amount of sulphur exists in the coal as an impurity which will form  $\text{SO}_x$  during combustion.  $\text{NO}_x$  is also a product during any fossil fuel combustion and burning.  $\text{SO}_x$  (sulphur oxides) and  $\text{NO}_x$  (nitrogen oxides) emitted from combustion of fossil fuels and especially coal, react chemically with water vapor in the atmosphere and form acids which will then be showered during rainfall.  $\text{NO}_x$  can also cause the development of smog as well as acid rain. Considerable amount of research is being performed in order to reduce the emissions of  $\text{SO}_x$  and  $\text{NO}_x$  from fossil fuel combustion and more important from coal-fired power plants. An alternative way of reducing  $\text{SO}_x$  emissions rather than using low sulphur content coal is flue gas desulphurisation (FGD) system which is developed for use in coal-fired power plants. These systems, known as *scrubbers*, can remove up to 99 % of sulphur oxide emissions. Fluidized bed combustion (FBC) as an advanced technological approach is an efficient alternative in reducing both sulphur and nitrogen oxides up to 90 % or more. In such a system, pulverized coal particles are burned while suspended in flowing air at high velocities. The bed would cause the rapid blending of the particles which would allow the system to reach complete coal combustion in lower temperatures.

### **2.3 Carbon Capture and Storage (CCS)**

The greenhouse gas emissions, especially carbon dioxide as a major contributor from coal-fired power plants, are very high, accounting for 40 % of total global emissions [5]. As such anthropogenic emissions are the main causes of global climate change leading global warming, the reduction of these emissions and the negative effects of global warming problem are now an urgent challenge. The abatement of GHG emissions from fossil fuel-fired power generation can be achieved by efficiency improvement, switching to lower carbon fuels and  $\text{CO}_2$  capture and storage (CCS) [10]. Carbon dioxide capture and storage (CCS) has been suggested as a step change method to reduce  $\text{CO}_2$  emissions from coal combustion and would enable the world to continue to use fossil fuels but with much reduced emissions of  $\text{CO}_2$ . There are several technologies for capture and storage of  $\text{CO}_2$

from coal combustion and gasification which are shown in Fig. 2.3 [11, 12].

*Pre-combustion capture:* In this CO<sub>2</sub> capture method, coal gasification is applied to produce a synthesis gas mixture (syngas) which contains mainly CO, CO<sub>2</sub> and H<sub>2</sub>. Carbon dioxide is a direct product of the carbon-oxygen reaction. In the production of synthesis gas, carbon gasification via the reaction with CO<sub>2</sub> is greatly encouraged. The CO conversion to CO<sub>2</sub> is then performed through the water-gas shift reaction:



The CO<sub>2</sub> from this reaction can be separated from the syngas mixture and leave a hydrogen-rich stream of flue gas which will be combusted in the gas turbine. Pre-combustion CO<sub>2</sub> capture also referred to as *fuel decarburization* is more beneficial to be used in connection with Integrated Gasification Combined Cycle (IGCC) power plants.

*Post-combustion capture:* In this CO<sub>2</sub> capture method, CO<sub>2</sub> is separated from the flue gas mixture of conventional pulverized-coal-fired power plants just before they are emitted to the atmosphere. This is done by applying a new final processing stage of wet scrubbing with aqueous amine solutions. The CO<sub>2</sub> removed from the solvent during the regeneration process is dried, compressed and transported to safe geological storage.

*Oxy-fuel combustion technology:* Oxy-fuel combustion technology is an emerging approach toward CCS methods which will be discussed in Chapter 2.4.

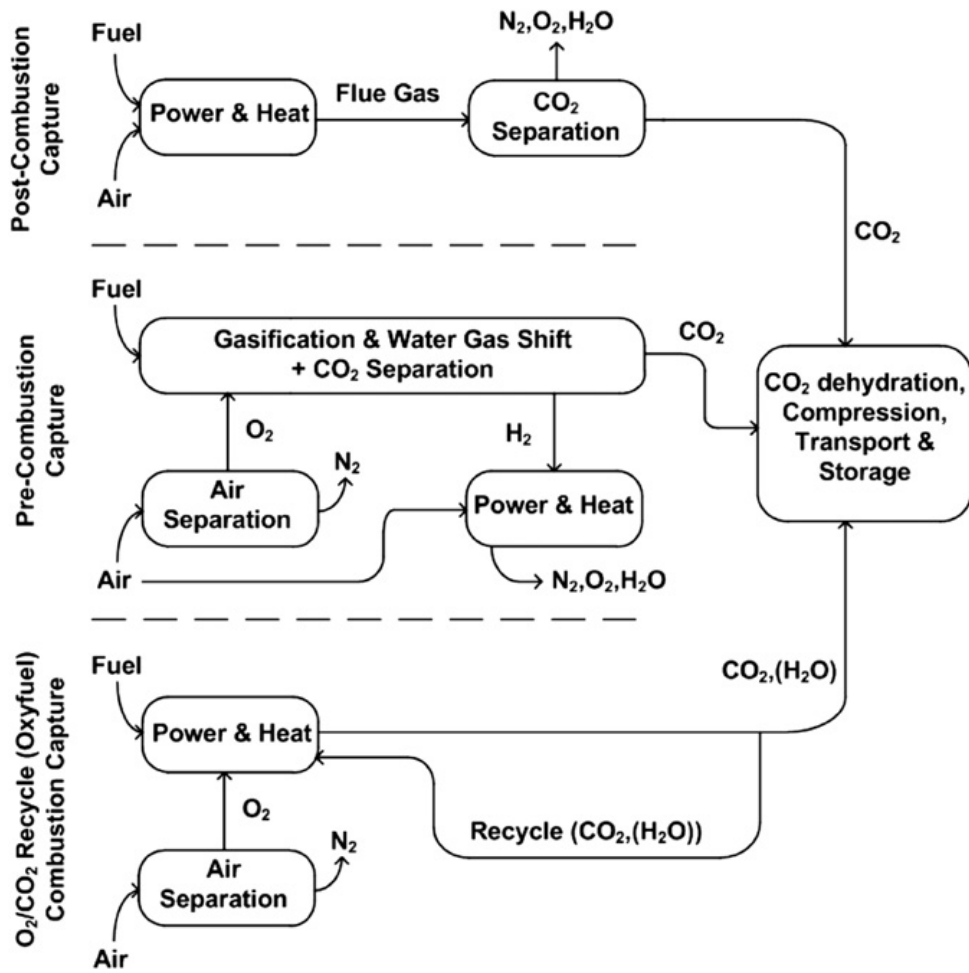


Fig. 2.3 Overall plants configurations for the three main CCS technologies [12]

## 2.4 Oxy-fuel Combustion Technology

CO<sub>2</sub> capture and sequestration can be achieved more readily from a concentrated CO<sub>2</sub> stream, which can be generated by firing fossil fuels with oxygen and drying the combustion effluent. This technique is called *oxy-fuel combustion*. In 1982, the technology was proposed for coal-fired processes by Abraham to generate CO<sub>2</sub> for Enhanced Oil Recovery [10]. After initial introduction in 1982, oxy-fuel technology for pulverized coal combustion was researched as a means to produce relatively pure CO<sub>2</sub> for Enhanced Oil Recovery. Despite these research efforts, the technology did not pick up on a large scale for this application. However, the increase in the awareness of greenhouse gas emissions into the atmosphere has renewed the interest in this technology, with a two-fold focus:

- The generation of a relatively pure CO<sub>2</sub> for sequestration,
- The potential to reduce pollutant emissions, in particular NO<sub>x</sub>

The oxy-fuel technology can produce a sequestration ready high-CO<sub>2</sub> concentration effluent gas. In this technology, oxygen (95-97 % by volume) from an air separation unit (ASU) is used as a fuel oxidant instead of conventional air. By eliminating N<sub>2</sub> from the input oxidant, the flue gas volume considerably decreases consisting largely of CO<sub>2</sub> and condensable water vapor which will make it quiet suitable for cost effective sequestration of CO<sub>2</sub>. To moderate the combustion temperatures in the furnace, the input oxygen stream is mixed with dry recycled flue gas (containing mostly CO<sub>2</sub>). Mixing recycled flue gas with oxygen at the inlet of the burner is necessary since the available construction materials, currently are not able to withstand the high temperature resulted from combustion carried out in pure oxygen. Thus, the combustion takes place in an O<sub>2</sub>/CO<sub>2</sub>, instead of an O<sub>2</sub>/N<sub>2</sub> ambient. Previous studies on oxy-fuel combustion mainly revealed that the overall O<sub>2</sub> concentration at the inlet to the boiler should be between 27 and 35 vol % in order to yield comparable adiabatic flame temperatures and heat transfer profiles as seen for conventional combustion in air. A general flow sheet of oxy-fuel technology is provided in Fig. 2.4.

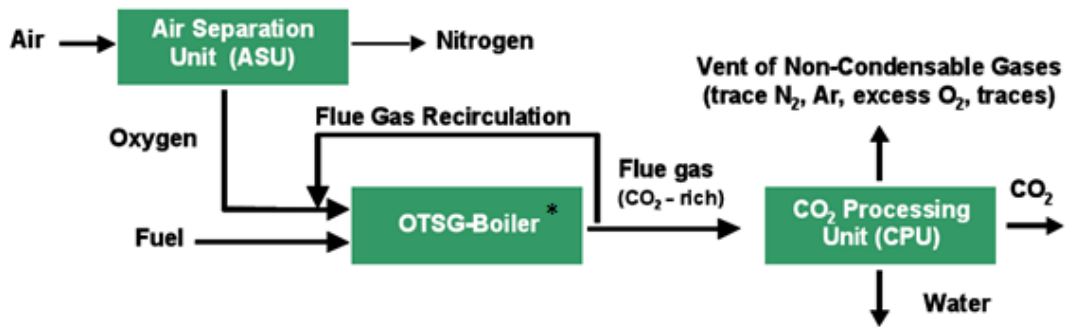


Fig. 2.4 Flow sheet of oxy-fuel technology for power generation with CO<sub>2</sub> capture and storage, showing the major components

\* Once-through Steam Generators

Performing combustion in O<sub>2</sub>/CO<sub>2</sub> rather than O<sub>2</sub>/N<sub>2</sub> ambient (substitution of CO<sub>2</sub> for N<sub>2</sub>), however, affects the ignition and combustion characteristics of pulverized coal, burner stability, flame propagation, gas temperature, char burnout, radiating properties of the flame, efficiency of the boiler and evolution of pollutants [5, 10, 17, 49]. Such issues may be partly attributed to the replacement of nitrogen with higher-heat-capacity carbon dioxide gas which would cause lower combustion temperatures. Furthermore the requirement of an Air Separation Unit (ASU) in oxy-fuel technology will cause a significant reduction in efficiency compared to currently used technology.

Previous studies on oxy-fuel combustion mainly revealed that the burnout is improved in this technology. The emission rate of CO is reported to be similar in air and oxy-fuel combustion even though significantly increased CO levels are seen within the flame zone in O<sub>2</sub>/CO<sub>2</sub> ambient. SO<sub>2</sub> emissions are likewise reported to be of similar magnitude regardless of flue gas composition. The NO<sub>x</sub> emissions is, however, significantly reduced during oxy-fuel compared to air-firing systems due to a near-elimination of thermal NO formation and to reburning of NO<sub>x</sub> passed through

the burners with the recirculated flue gas. Reduction of the emission rates by 70- 80 % have been reported [25, 50-52]. However, the oxy- fuel environment is expected to lead to a significant increase in the SO<sub>3</sub> concentration within the boiler, increasing the risk of both high and low-temperature corrosion as well as increased retention of sulphur in the fly ash [12].

The CCS methods are profoundly discussed through an extensive research studies worldwide with an especial focus on oxy-fuel combustion technology.

Strube and Manfrida [53] carried out a study on the effects of different CO<sub>2</sub> capture methods on plant performance and all the processes were simulated with Aspen Plus. It was indicated that post-combustion capture showed the highest impact on plant performance while capturing of CO<sub>2</sub> in oxy fuel technology was observed to have the lowest specific energy penalty of all the explored options.

Gibbins and Chalmers [11] studied on technologies that are being developed to prevent the carbon dioxide emissions vented in to the atmosphere. Different possibilities of CCS method were investigated closely and critical aspects of CO<sub>2</sub> geological storage activities have also been identified and discussed in this study.

Irfan et al. [7] made an overview on coal gasification in CO<sub>2</sub> ambient since 1948. In this study the effects of some inorganic catalysts including Na, K, Ca and Ni were also investigated. Furthermore, oxy-fuel combustion technology and its effects over the coal combustion along with the effects of particle size, heating rate and usage of different reactors were reported and overviewed.

Oxy-fuel combustion technology was profoundly explored by Buhre et al. [17]. This technology was reported to be a near-zero emission technology, also referred to as *zero- emission technology (CCS)*, that can be used in both existing pulverized coal-fired power stations or as a new technology in implementation of new plants. Furthermore, studies from the techno-economic point of view revealed that oxy-fuel combustion is a cost effective method of CO<sub>2</sub> capture and is technically feasible with current technologies. Furthermore, in this study, the following issues are reported for oxy-fuel combustion technology in comparison with air combustion:

- The lower heat transfer in the convective section of the boiler
- The lower flame propagation speed and delayed ignition due to the higher heat capacity of CO<sub>2</sub> compared to that of N<sub>2</sub>
- Improvement in the reactivity of char with increasing oxygen mole fraction in both O<sub>2</sub>/N<sub>2</sub> and O<sub>2</sub>/CO<sub>2</sub> ambient conditions
- Reduction in NO<sub>x</sub> emission due to the reduction in thermal NO<sub>x</sub> and reburning
- Decreased SO<sub>2</sub> emissions and significant increase of sulphur in the furnace deposits which leads to an increase in furnace corrosion

In the research presented by Bejarano and Levendis [18], single coal particle combustion characteristics in both O<sub>2</sub>/N<sub>2</sub> and O<sub>2</sub>/CO<sub>2</sub> ambient conditions were investigated. A drop-tube furnace facility operated at temperatures of 1400 K and 1600 K was used to perform these experiments. Experimental results revealed that the combustion of coal particles experienced higher mean temperatures and shorter times in O<sub>2</sub>/N<sub>2</sub> than in oxy-fuel conditions at similar oxygen mole fractions which were caused by replacing N<sub>2</sub> with higher-heat-capacity CO<sub>2</sub> gas and also by thermal radiation enhancements. However, the corresponding burnout times were shorter. Furthermore, as the oxygen concentration in the mixture was enhanced, the particle temperatures increased and the burnout times decreased. During the tests performed in oxy-fuel conditions, it was observed that coal-N to NO<sub>x</sub> conversion was decreased; a better char burnout, lower CO emission and lower unburned carbon amounts were also achieved. Another important result reported in this study was the equivalent oxygen concentration in oxy-fuel condition to have the same volatile and char temperature as in air combustion which was reported to be 26 and 30 % for the evolved lignite and bituminous coal samples respectively.

The adiabatic flame temperature in air and oxy-retrofit combustion was compared in the study carried out by Terry Wall et al. [10]. The adiabatic flame temperature (AFT) for air combustion case under 20 % excess air is indicated in Fig. 2.5. The two oxy-retrofit combustion cases of oxy-wet and oxy-dry are included in the figure. In

the case of oxy-wet recycle, the recycled flue gas included water vapor while in oxy-dry recycle water vapor was removed from the recycled flue gas. As illustrated in Fig. 2.5, the overall O<sub>2</sub> concentration was around 27 and 35 vol % in oxy-wet and oxy-dry conditions in order to yield comparable adiabatic flame temperatures as seen for conventional combustion in air. These oxygen mole fractions were used as a reference in experimental parts of this study.

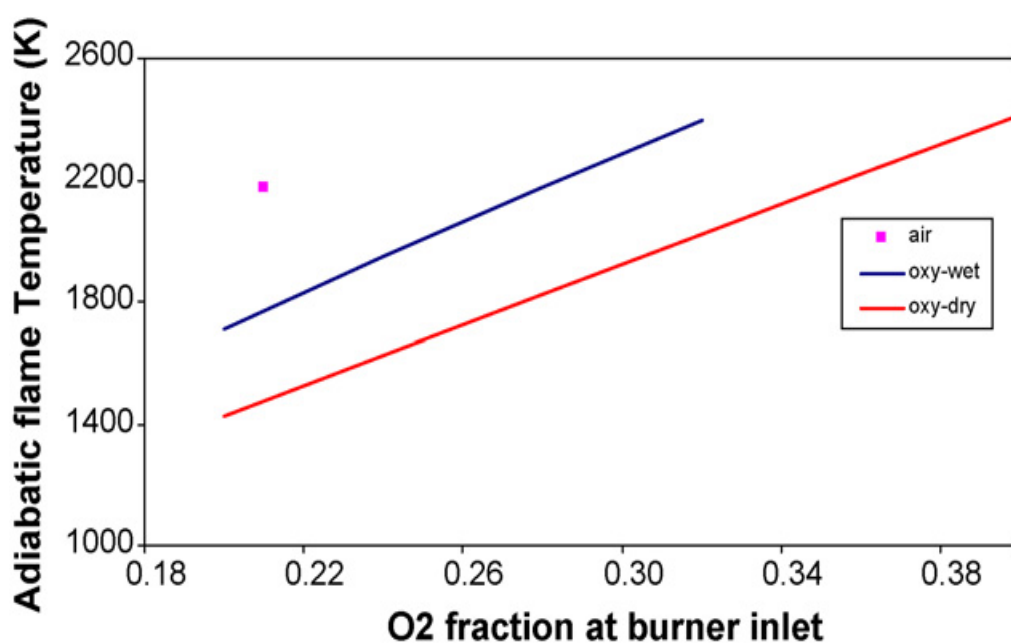


Fig. 2.5 The O<sub>2</sub> mole fractions required at burner inlet (to achieve similar AFT as in air-fired case) for oxy-wet and oxy-dry conditions [10]

As a result, a need has been identified for successful implementation of oxy-fuel combustion which requires a detailed understanding of changes associated with replacing N<sub>2</sub> with CO<sub>2</sub>. This means that a further research is needed to obtain a fundamental understanding of the changes between oxy-fuel combustion (O<sub>2</sub>/CO<sub>2</sub>

ambient) and conventional air-fired combustion. Furthermore, a detailed modeling of the different coal combustion processes under oxy-fuel conditions are required for accurate performance predictions. A main part of this study is focused on the science underpinning oxy-fuel combustion technology during which the effects of two diluting gases  $N_2$  and  $CO_2$  and various oxygen mole fractions (21-35 %) are investigated.

## **2.5 TGA-FTIR Experiments**

Thermogravimetric Analysis (TGA) has been found as a useful method to study the combustion and pyrolysis behavior and kinetics of samples in the coal science field and biomass studies. This system coupled with Fourier Transform Infrared spectrometer (FTIR) is used for determination of evolved gases during such tests. These methods are profoundly used in research studies regarding coal and biomass combustion and pyrolysis characteristics worldwide. During this literature survey a special focus was devoted to the effects of different catalysts on coal combustion and pyrolysis behavior of pulverized coal.

Sis [3] carried out a study on the effects of particle size on combustion kinetics and properties using TGA (Thermogravimetric Analysis) and DTA (Differential Thermal Analysis) techniques. 14 different size ranges of Turkish lignite (Elbistan region) from 38  $\mu m$  to more than 2 mm were used in these experiments. Some differences in proximate analyses of lignite samples were observed due to change in particle size. During the TGA tests, 10 mg of each sample was exposed to air flow rate of 50 ml/min and underwent heating rate of 10  $^{\circ}C/ min$  from room temperature to 900  $^{\circ}C$ . It was reported that the activation energies were higher for finer particles. Furthermore, the main peaks in the devolatilization region shifted slightly to lower temperatures as the particle size decreased and a slight rise was reported in the char oxidation region for fine particles.

In the study carried out by Öztaş and Yürüm [28], the effects of mineral matter on pyrolysis characteristics of Turkish Zonguldak bituminous (300-500  $^{\circ}C$ ) were

investigated and the acid washed lignite samples were used to make comparisons. It was concluded that the inorganic matters of calcium (Ca), iron (Fe) and magnesium (Mg) had some positive catalytic effects on pyrolysis process. However silicates reduce the conversion rate in pyrolysis tests.

Yang and Cai [31] investigated the effects of inorganic catalysts of potassium (K), calcium (Ca), nickel (Ni) and iron (Fe) on pyrolysis of bituminous and lignite samples using TG-FTIR. The catalysts were added to the raw coals with the particle size range of 50-150  $\mu\text{m}$ . 20 mg of the sample was used in each test under 100 %  $\text{N}_2$  and two heating rates of 20  $^\circ\text{C}/\text{min}$  and 40  $^\circ\text{C}/\text{min}$  were used. It was indicated that the  $\text{K}_2\text{CO}_3$  precursor was not active in coal pyrolysis while Ca, Fe and Ni catalysts showed considerable catalytic effects. Moreover, it was reported that the maximum rate of weight loss shifted to higher temperature zone at high heating rate, since the coal samples experienced shorter residence time.

Liu et al. [8] studied the effects of  $\text{NaCl}$ ,  $\text{CaCl}_2$ ,  $\text{FeCl}_3$ ,  $\text{FeCl}_2$  and  $\text{Fe}_2\text{O}_3$  catalysts on combustion characteristics and  $\text{SO}_2$  emissions of Chinese coal samples. TGA was used during these experiments under constant heating rate of 20  $^\circ\text{C}/\text{min}$  and 30  $^\circ\text{C}/\text{min}$  and total air flow rate of 60 ml/min. 20 mg of each sample was used in the tests from room temperature to 1000  $^\circ\text{C}$ . The addition of catalysts was performed through physically dry mixing method and corresponded 6 % by weight. It was demonstrated that the  $\text{CaCl}_2$  showed the best catalytic reactivity in  $\text{SO}_2$  reduction. Furthermore,  $\text{FeCl}_3$  and  $\text{FeCl}_2$  were effective catalysts in improving combustion characteristics although they increased the  $\text{SO}_2$  concentration in the flu gas.

Liu et al. [33] carried out a study on the effects of mineral matter on the reactivity of coal samples and kinetic behaviors of some low rank Chinese coals during pyrolysis tests using TGA method. The raw and demineralized samples added with doping agents  $\text{CaO}$ ,  $\text{K}_2\text{CO}_3$  and  $\text{Al}_2\text{O}_3$  were used as samples. The particles were ground to below 125  $\mu\text{m}$  (120 Mesh) and were impregnated by the evolved catalysts corresponded 10 % by weight. 20 mg of the sample was tested under 30 ml/min  $\text{N}_2$  flow at heating rate of 10  $^\circ\text{C}/\text{min}$  from 110  $^\circ\text{C}$  to 800  $^\circ\text{C}$  during each run. It was indicated that the lower rank coals were more sensitive to these catalytic activities.

Furthermore, it was demonstrated that the inorganic catalysts of CaO, K<sub>2</sub>CO<sub>3</sub> and Al<sub>2</sub>O<sub>3</sub> improved the reactivity of coal pyrolysis which was also affected by temperature and coal types. A decrease in activation energy was also observed during the catalytic pyrolysis runs.

The effects of alkaline metal (AM) matters, Na and K, on the pyrolysis and gasification processes of coal conversion were studied by Shenqi et al. [34]. A high rank Chinese coal (particle size < 75 μm) used as a sample and the aqueous solution impregnation method was used to add the catalysts to the acid washed samples in order to better investigate the effects of the evolved catalysts. 5 %, 10 % and 20 % (by mass) of the catalysts concentration were used. The pyrolysis tests performed in a pressurized thermobalance under constant N<sub>2</sub> flow and the heating rate of 10 °C/min. In the gasification tests, N<sub>2</sub> flow was replaced with CO<sub>2</sub> (1000 ml/min) when desired temperature achieved and continued until a constant weight was reached. It was reported that acid washed coal samples showed the highest reactivity in the pyrolysis region while they had a relatively low gasification rate. On the other hand, it was indicated that, although the impregnated samples demonstrated relatively low pyrolysis rate, the corresponding chars had high gasification reactivity. Furthermore, one can see the effects of pyrolysis temperature and the contents of alkaline metals in char samples in this study.

Steam gasification of coal char and the effects of potassium carbonate (K<sub>2</sub>CO<sub>3</sub>) as a catalyst were explored on a laboratory fixed bed reactor by Wang et al. [35]. It was observed that the steam gasification of coal char using 10-17.5 % K<sub>2</sub>CO<sub>3</sub> (by mass), as a catalyst, occurred remarkably in the temperature range of 700-750 °C. Furthermore, it was confirmed that the catalytic steam gasification of coal char produced high yield of hydrogen in comparison with the non-catalytic gasification.

In the study carried out by Yu et al. [36], a considerable enhancement in hydrogen production during the steam gasification of Victorian brown coal using iron as a catalyst was shown. Ferric chloride (FeCl<sub>3</sub>) was used for iron loading (~3 % by mass) into the acid-washed Loy Yang brown coal using aqueous solution. Gasification experiments were carried out using a quartz reactor at a fast particle

heating rate. It was revealed that the overall gasification rate of a char increased greatly in the presence of iron. Moreover, the impregnated coal samples with iron catalyst greatly increased the production of hydrogen and carbon dioxide during the gasification of chars.

The effects of five metal catalysts, K, Na, Ca, Mg, and Fe, were studied on CO<sub>2</sub> gasification reactivity of softwood char by Huang et al. [37]. TGA method was used in these experiments and the impregnation of the catalysts performed using aqueous solution of the evolved catalysts precursors. During each test about 10 mg of the generated char heated at a rate of 10 °C/min up to a final temperature of 1150 °C under a continuous CO<sub>2</sub> flow of 400 ml/min. It was reported that the gasification reactivity of biomass char can be improved by metal catalysts in the order of K > Na > Ca > Fe > Mg.

The emission characteristics during the co-combustion process of wheat straw and coal was examined by Wang et al. [39] using TGA-FTIR and the evolved gases of HCl, SO<sub>2</sub>, CO<sub>2</sub> and NO<sub>x</sub> were monitored. Blends of typical anthracite coal and wheat straw with (40 %, 60 %, 85 %, 90 % and 100 % of wheat straw by mass) were used as samples. During these experiments the sample weight, total air flow rate, heating rate and final temperature were 5.5 mg (< 200 μm), 50 ml/min, 20 °C/min and 900 °C respectively. The results in this study revealed that the HCl peak occurred at 310 °C for all blends. Furthermore, the analysis showed that the optimum straw to coal mass ratio in order to generate the lowest levels of HCl, NO<sub>x</sub> and SO<sub>2</sub> pollutants was 60:40.

TGA analysis has been used to explore the ignition and burnout characteristics of a raw and catalysts added samples by Ma et al. [54]. MnO<sub>2</sub>, Fe<sub>2</sub>O<sub>3</sub> and BaCO<sub>3</sub> were used as catalysts. The air total flow rate was 20 ml/min and the samples heated from the ambient temperature to 1000 °C at the heating rate of 20 °C/min. The ignition index and burn out index were used to characterize the ignition and burnout characteristics of the samples and the results indicated that the relative active sequence of catalysts to the ignition performance and burnout performance was described as MnO<sub>2</sub> > BaCO<sub>3</sub> > Fe<sub>2</sub>O<sub>3</sub> and Fe<sub>2</sub>O<sub>3</sub> > BaCO<sub>3</sub> > MnO<sub>2</sub> respectively.

Furthermore, it was revealed that the enhancement in emission of volatile matters was the most important issue reducing the ignition temperature.

Fang et al. [55] performed a study on the effects of various oxygen concentrations on pyrolysis and combustion of wood using TGA-FTIR. In this study, the activation energy during pyrolysis and combustion processes was observed to be a linear function of oxygen concentration. Furthermore, the maximum values of DTG curves shifted to lower temperature zone as oxygen concentration increased. As illustrated in this study, the process of wood combustion can be divided into four steps of moisture release, volatile matter combustion, semi-coke combustion and finally remaining semi-coke reaction with CO<sub>2</sub>.

In the work reported by Zhu et al. [45], co-pyrolysis of coal and wheat straw was studied. In this study, the aim was investigating the wheat straw characteristics during co-pyrolysis with coal as an inexpensive source of potassium-based catalyst using TGA. These experiments were carried out with various concentrations of wheat straw in the blend: 0 %, 20 %, 30 %, 50 % and 100 % by mass. 9 mg of the sample (< 120 μm) was purged under 50 ml/min of nitrogen and heated at the heating rate of 40 °C/min. When the desired temperature was reached, the isothermal gasification reaction of the char sample was initiated by switching on a flow of 70 ml/min of CO<sub>2</sub>. As a result the gasification reactivity of chars improved as the concentration of wheat straw in the blend was increased. Furthermore, as the char prepared from acid washed wheat straw/coal blend showed a similar reactivity to the coal char, it was concluded that the high reactivity of wheat straw/coal blend was due to the high content of alkali components especially potassium (K) in the biomass ash.

The effects of calcium-based catalysts on the removal of sulfur containing species of coal samples during pyrolysis tests were studied by Guan et al. [42] using a fixed-bed reactor. Bituminous coal was used in these experiments (150-250 μm) and CaCO<sub>3</sub>, CaO and Ca(OH)<sub>2</sub> were used as precursors of calcium catalyst. Different catalyst addition methods of mechanically dry mixing, wet impregnation and ultrasonic irradiation in the Ca(OH)<sub>2</sub> solution were used to add the calcium to the coal samples. This study revealed that Ca(OH)<sub>2</sub> and CaO were effective catalysts in

reducing the sulfur containing gases and resulted in retention of sulphur evolved from untreated coal in the char up to 95 %. However, impregnation and ultrasonic treatment showed better improvements in sulphur retention capacity. Moreover, in the same catalyst addition method  $\text{Ca}(\text{OH})_2$  was more effective than  $\text{CaO}$ , while  $\text{CaCO}_3$  showed a little effect at high temperature.

Selcuk and Yuzbasi [19] investigated the pyrolysis and combustion characteristics of Turkish lignite under air and oxy-fuel conditions using TGA-FTIR and the evolved gases of  $\text{CO}_2$ ,  $\text{CO}$ ,  $\text{H}_2\text{O}$ ,  $\text{CH}_4$ ,  $\text{SO}_2$  and  $\text{COS}$  were monitored. During these tests carried out in a TGA system coupled with FTIR, 12 mg of lignite sample ( $< 100 \mu\text{m}$ ) heated at the heating rate of  $40 \text{ }^\circ\text{C}/\text{min}$  from room temperature up to  $950 \text{ }^\circ\text{C}$ . The total gas flow rate through the system was adjusted to  $70 \text{ ml}/\text{min}$  and  $45 \text{ ml}/\text{min}$  for pyrolysis and combustion tests respectively. Pyrolysis tests carried out under 100 %  $\text{N}_2$  and 100 %  $\text{CO}_2$  ambient conditions. The combustion tests performed under 21 % and 30 %  $\text{O}_2$  in both  $\text{N}_2$  and  $\text{CO}_2$  ambient conditions. In this study similar trends were observed up to  $720 \text{ }^\circ\text{C}$  during the pyrolysis tests in both ambient conditions. However, beyond this temperature range, further weight loss was occurred in the  $\text{CO}_2$  ambient which was thought to be a result of  $\text{CO}_2$ -char gasification reaction. Furthermore, a delayed combustion process was observed during the combustion tests under oxy-fuel conditions. Moreover, the effects of oxygen mole fraction was considerably higher than that of diluting ambient and shifted the DTG curves to lower temperature zone and much higher reaction rates. FTIR results revealed that  $\text{CO}$  formation increased significantly due to char- $\text{CO}_2$  gasification reaction and consecutively  $\text{COS}$  formation experienced considerable peak in 100 %  $\text{CO}_2$  ambient.

In the work reported by Li et al. [56], the effects of oxygen mole fraction, combustion ambient, heating rate and different particle sizes on combustion characteristics of pulverized coal under different oxy-fuel conditions were investigated using TGA-FTIR technique. A Chinese bituminous coal was used in these tests during which around 10 mg of the coal sample was heated up to  $1000 \text{ }^\circ\text{C}$  at the heating rate of  $30 \text{ }^\circ\text{C}/\text{min}$  in both  $\text{O}_2/\text{N}_2$  and  $\text{O}_2/\text{CO}_2$  ambient conditions. The total gas flow rate was adjusted to  $80 \text{ ml}/\text{min}$ . Various oxygen mole fractions (21 %,

30 %, 40 % and 80 %), particle sizes (< 48  $\mu\text{m}$ , 48-74  $\mu\text{m}$  and 74-90  $\mu\text{m}$ ) and heating rates (10  $^{\circ}\text{C}/\text{min}$ , 20  $^{\circ}\text{C}/\text{min}$  and 30  $^{\circ}\text{C}/\text{min}$ ) were used to monitor the related effects. The results indicated that during the combustion tests, three stages of weight loss were recognized in the TGA/DTG curves: moisture release, devolatilization and char gasification. Combustion of coal particles was delayed in  $\text{O}_2/\text{CO}_2$  compared with that in  $\text{O}_2/\text{N}_2$  ambient at the same  $\text{O}_2$  mole fraction. As the oxygen concentration in the mixture was enhanced, the DTG curves of pulverized coal combustion shifted to lower temperature zone, the process reaction rate increased and the burnout time was shortened. Moreover, it was indicated that the refinement of pulverized coal particles will result in improvements of combustion process.

In the study reported by Bakisgan et al. [46], a detailed ash analysis of Turkish biomass fuels was performed. The biomass fuels under study were wheat straw, olive bagasse and hazelnut shell for which the ash concentration corresponded 7.9 % 3.9 % and 1.2 % respectively. In the ash content of these biomass fuels Si, Ca, K, Mg and P were the most abundant species. The ashing process for determination of the ash amount as well as obtaining required ash for further analyses were carried out at oxidation temperature  $575 \pm 25$   $^{\circ}\text{C}$ . The compositions of ash forming oxides, reported in this study are listed in Table 2.1.

Table 2.1 Composition of ash forming oxides [46]

Oxide	%, By weight		
	Wheat straw	Hazelnut shells	Olive bagasse
$\text{K}_2\text{O}$	24.6	38.7	51.6
$\text{CaO}$	19.1	27.6	23.3
$\text{SiO}_2$	35.6	1.3	7.1
$\text{MgO}$	5.2	7.4	2.3
$\text{Al}_2\text{O}_3$	–	0.7	1.9
$\text{P}_2\text{O}_5$	6.4	4.8	7.5
Others	9.1	19.5	6.3

As illustrated in this table, considerable amount of  $K_2O$  was traced in the ash contents regarding wheat straw, hazelnut shell and olive bagasse which were 24.6 %, 38.7 % and 51.6 % respectively. The ash analyses also revealed that there was high amount of  $CaO$  in the ash contents of the biomass fuels tested. Furthermore, significant amount of  $SiO_2$  was seen in wheat straw ash which was not traced in the ash contents of hazelnut shell and olive bagasse.

As a result, a need has been identified for a detailed understanding of the effects of various inorganic catalysts on combustion and pyrolysis characteristics of Turkish coal samples in both  $O_2/N_2$  and  $O_2/CO_2$  ambient conditions. Furthermore, the possible use of the ash contents of Turkish biomass fuels, as precursors of catalysts during combustion tests, was also investigated.

## CHAPTER 3

### SAMPLES AND EXPERIMENTAL METHODS

#### 3.1 Samples

Most of the Turkish coal reserves are low-grade lignite usually containing high sulfur contents and low calorific values. Lignite is the second most important potential source of energy in Turkey. 2 % of the world's lignite reserves are located in Turkey. Turkey is ranked as seventh in the world from the aspect of lignite reserves and sixth in production [57]. In this study, four types of Turkish coal samples and five common Turkish biomass fuels were studied. Turkish coal samples were selected from the feeders of Kangal, Seyitömer, Tunçbilek and Zonguldak power plants and are named as their resource regions. The Kangal, Seyitömer, Tunçbilek and Zonguldak coal samples are also illustrated with K, S, T and Z abbreviations respectively throughout this study. Kangal and Seyitömer low rank coals are classified as lignite while Tunçbilek and Zonguldak are categorized as sub-bituminous and bituminous respectively. Therefore, a wide variety of coal ranks were covered in these experiments. The coal samples were directly selected from the feeding lines of the power plants and were used in the experiments in order to match the quality being used in electricity production. Common biomass fuels of Turkey namely walnut shell (WSh), hazelnut shell (HSh), wheat straw (WS), Limba wood saw dust (SD) and cattle manure (CM) were also used in the tests regarding coal and biomass co-processing. Examples of Turkish biomass fuels are shown in Fig. 3.1.



Fig. 3.1 Turkish biomass fuels: hazelnut shell (left) and walnut shell (right)

Potassium carbonate ( $K_2CO_3$ ) which is an alkali metal salt, calcium hydroxide ( $Ca(OH)_2$ ) which is an alkaline earth metal hydroxide, iron (III) oxide or ferric oxide ( $Fe_2O_3$ ) which is a transition metal oxide and iron(III) chloride, also called ferric chloride ( $FeCl_3$ ) were employed as precursors of potassium (K), calcium (Ca) and iron (Fe) catalysts. These metallic compounds were all commercially available with high purity.

In calorimetric tests, Kangal, Seyitömer, Tunçbilek and Zonguldak coal samples were used while Kangal and Tunçbilek samples were selected for TGA-FTIR. Co-processing tests of biomass and lignite were performed with Kangal lignite.

Proximate and ultimate analyses of the coal samples were carried out in MTA (General Directorate of Mineral Research and Exploration) according to ASTM standards with the same particle size as used throughout this study ( $< 106 \mu m$  or 140 Mesh). The particle size of the sample might have slight influences on proximate analysis results according to several references [3, 58, 59]. Calorific values of the fuels were measured by using oxygen bomb calorimeter. Proximate and ultimate analyses of coal samples together with their calorific values are summarized in Tables 3.1 and 3.2. Kangal and Seyitömer lignite samples can be characterized by

their low calorific values, high moisture contents (~41 % and 23 % respectively) and high ash contents (~31 % and 36 % respectively). Furthermore, Kangal lignite contains very low fixed carbon content (around 3.3 %).

Table 3.1 Proximate analyses of Turkish coal samples

<b>Proximate analysis (as received, %by wt.)</b>				
	Kangal	Seyitömer	Tunçbilek	Zonguldak
<b>Moisture</b>	40.85	22.55	7.67	11.54
<b>Ash</b>	31.21	35.85	43.24	8.32
<b>Volatile matter</b>	24.64	26.52	26.38	27.44
<b>Fixed carbon</b>	3.30	15.08	22.71	52.70
<b>Proximate analysis (Dry basis, %by wt.)</b>				
	Kangal	Seyitömer	Tunçbilek	Zonguldak
<b>Moisture</b>	-	-	-	-
<b>Ash</b>	52.77	46.29	46.83	9.40
<b>Volatile matter</b>	41.66	34.24	28.57	31.02
<b>Fixed carbon</b>	5.57	19.47	24.60	59.58
<b>HHV (MJ/Kg)</b>	9.943	9.179	14.377	17.695
<b>HHV (Kcal/Kg)</b>	2374.8	2192.5	3433.8	4226.4

Table 3.2 Ultimate analysis of Kangal lignite and Tunçbilek sub-bituminous used in TGA-FTIR tests

Ultimate analysis (as received, %by wt.)		
	Kangal Lignite	Tunçbilek sub-bituminous
<b>C</b>	28.30	42.05
<b>H</b>	2.00	2.72
<b>O*</b>	11.37	3.63
<b>N</b>	0.82	1.44
<b>S<sub>Combustible</sub></b>	1.31	0.91
<b>S in ash</b>	2.46	0.81
<b>S<sub>Total</sub></b>	3.77	1.72
* By difference		

All the stages of sample preparation and catalyst impregnation were performed in the Mineral Processing laboratory of Mining Engineering Department at Middle East Technical University. The samples were first used to perform the moisture content tests as received basis. 10 g of each sample (sufficiently fine particles) was dried at  $107 \pm 4$  °C in the low temperature furnace and was weighed consecutively over the time increments of 15 minutes until it reaches constant weight. A slight increase observed at the end of some of the time increments was due to moisture absorbance of hot coal particles during the weighing procedure. After performing the humidity content tests, the process of sample preparation, continued with crushing by first jaw and then roll crushers (Fig. 3.2). Then 2 kg of each sample was selected for milling and sieving to desired particle size of  $< 106 \mu\text{m}$  (140 Mesh). The milling process was done with ceramic ball mill as illustrated in Fig. 3.3. However the original samples could not be milled as they were received due to formation of a sticky cake over the walls of the mill as a result of moisture content. So step by step drying and milling processes were carried out during which the drying period was different in the case of each coal sample. A 2 hour milling process was done

consecutively and a 140 Mesh sieve was used to screen the particles below 106  $\mu\text{m}$ . The moisture content of this particle size range after milling (used in further experiments) was measured through a series of tests similar to the tests performed for original samples. The original humidity results along with humidity as tested results are listed in Table 3.3. A detailed procedure of humidity analyses can be found in Appendix A.



Fig. 3.2 Jaw (left) and roll (right) crushers



Fig. 3.3 Ceramic ball mill

Table 3.3 Moisture content of the coal samples

<b>Coal Type</b>	<b>Original Humidity (as received) (%)</b>	<b>Humidity as tested (after milling) (%)</b>
<b>Kangal</b>	40.85	27.63
<b>Seyitömer</b>	22.55	16.00
<b>Tunçbilek</b>	7.67	4.37
<b>Zonguldak</b>	11.54	2.60

### 3.1.1 Addition of the Catalysts (Impregnation)

Potassium carbonate ( $K_2CO_3$ ), calcium hydroxide ( $Ca(OH)_2$ ), iron (III) oxide or ferric oxide ( $Fe_2O_3$ ) and iron(III) chloride, also called ferric chloride ( $FeCl_3$ ) were employed as precursors of potassium (K), calcium (Ca) and iron (Fe) catalysts. All of the precursors used were commercially available reagents with high purity of greater than 99 %. As was reported in the literature [42], the addition of additives by impregnation and ultrasonic treatment showed much better reactivity than mechanical mixing in pyrolysis and combustion processes. Impregnation method would allow the aqueous solution of the catalysts to be absorbed by porous nature coal particles and the inside surfaces of the particles would also be exposed to the catalytic effects. Therefore, the impregnation method was used for the addition of water soluble catalysts ( $K_2CO_3$ ,  $Ca(OH)_2$  and  $FeCl_3$ ). However in order to provide fully comparable samples in the cases of water soluble catalysts and the water insoluble one ( $Fe_2O_3$ ), the same procedure of catalyst addition was applied.

Kangal lignite and Tunçbilek sub-bituminous coal were selected to be used in TGA-FTIR studies. Since coal is a heterogeneous substance, it is important to ensure that the prepared samples are representative of the coal types. For this purpose, 30 g of Kangal lignite or Tunçbilek sub-bituminous coal samples was taken from the sample pool randomly and was mechanically mixed at 80 rpm for 2 hours to have a homogeneous mixture. After that 5×5.5 g of each coal sample was weighed out of this homogeneous sample pool into five separate petri plates (glass containers). These samples were dried at 100 °C for 90 minutes, and then collected into five capped containers quickly and placed in a dessicator to be cooled without absorbing any moisture from the environment. These dry samples were used in the following steps of catalysts addition (impregnation).

The impregnated K-form, Ca-form, and two Fe-forms ( $Fe_2O_3$  and  $FeCl_3$  precursors) samples were obtained by mixing the raw coal ( $< 106 \mu m$ ) with a saturated aqueous solution of  $K_2CO_3$ ,  $Ca(OH)_2$  and  $FeCl_3$  and an insoluble mixture of deionized water and  $Fe_2O_3$  respectively to form a slurry. The Raw-form samples were also used to form slurry without any additives. The amount of deionized water

and coal samples during the impregnation processes were adjusted to 30 ml and 4g respectively. The catalysts addition to the raw Kangal lignite and Tunçbilek sub-bituminous coal by impregnation corresponded 5 % in terms of mass ratio of catalysts precursors to coal (dry basis). The slurries in the capped containers were then continuously stirred by using magnetic mixers at room temperature for 24 hours followed by evaporation of water at 60 °C for sufficient time (around 48 hours). The resulting mixtures were pounded and mechanically stirred for 2 hours at the speed of 80 rpm in order to have completely homogeneous mixtures (since TGA experiments are performed with a very small amount of sample and therefore the prepared impregnated samples must be completely homogenous in order to get accurate results). These impregnated Kangal lignite and Tunçbilek sub-bituminous coal samples were used in TGA-FTIR tests.

In co-processing experiments of biomass and lignite, Kangal lignite and five Turkish biomass fuels were used and the biomass ash contents were used as the precursors of catalysts, since considerable amount of metallic compounds are reported in the ash deposits of biomass. The same impregnation method and procedure was used as described in this chapter and these samples were used in the TGA-FTIR tests. The biomass ash addition to the raw Kangal lignite by impregnation corresponded 15 % in terms of mass ratio of biomass ash to coal (dry basis). Fig. 3.4 shows the impregnated samples with biomass ash contents used in TGA-FTIR tests.



Fig. 3.4 Impregnated Kangal lignite samples with biomass ash used in TGA-FTIR tests

In calorimetric tests, catalyst additions to the raw coal by impregnation, corresponded 2 %, 5 % and 10 % in terms of mass ratio of catalyst precursors to coal. In these tests both  $\text{FeCl}_3$  and  $\text{Fe}_2\text{O}_3$  were applied as precursors of Fe-based catalyst. In sample preparation methods regarding the calorimetric tests, the amount of deionized water and coal samples during the impregnation processes were adjusted to 30 ml, 75 ml and 30 ml and 6 g, 30 g and 6 g for 2 %, 5 % and 10 % of catalyst concentration respectively. The 5 % catalyst impregnation was prepared in higher quantity since these samples were used to do the ash analysis carried out using XRF (X-ray Fluorescence spectroscopy) method. Preparation of the samples for calorimetric tests was similar to the TGA-FTIR sample preparation method. The drying step of the coal samples before adjusting the concentration of catalysts in coal (in terms of mass ratio) was not performed and partly wet coal samples (after milling basis (Table 3.3)) were used. A correction factor was used in these tests as will be described in Chapter 3.2.3.2.

The impregnated coal samples used in the calorimetric tests are labeled according

to the following method:

Coal sample abbreviations (K, S, T or Z) + Percentage of catalyst addition (2 %, 5 % or 10 %) name of the catalyst precursor ( $\text{Fe}_2\text{O}_3$ ,  $\text{FeCl}_3$ ,  $\text{K}_2\text{CO}_3$  or  $\text{Ca}(\text{OH})_2$ )

During the calorimetric tests, samples should be used as dry basis in order to eliminate the mass of inherent water from calorimetric calculations. Therefore, as a final step, the prepared samples were dried at 100 °C for an additional 60 minutes to ensure that completely dry samples were prepared for the calorimetric tests and were packed and kept in the dessicator. This time period was determined from a series of preliminary tests which confirmed that this time of drying is enough to obtain completely dry samples (Appendix A). In order to provide sufficient ash amount for XRF tests from the samples with 5 % catalyst addition, after being dried at 60 °C, the samples are divided into two parts (around 5 g and 25 g). In order to do this selection, the papered blend should first be pounded and mechanically mixed and then around 5 g of each sample should be separated for calorimetric tests. This procedure will help providing samples as homogeneous as possible. The rest parts of these samples were used in ash preparation processes. The original form of the samples were dried at 100 °C and used in the tests.

## **3.2 Experimental Set-Up and Procedure**

### **3.2.1 TGA-FTIR Tests**

Thermogravimetric Analysis (TGA), Differential Scanning Calorimetry (DSC), and Differential Thermal Analysis (DTA) techniques are useful tools to study the combustion and pyrolysis behavior and kinetics of coal samples. Thermogravimetric Analysis is a technique in which the sample mass is monitored as a function of temperature or time as it undergoes a controlled heating or cooling process in a controlled atmosphere. A Thermogravimetric Analyzer (TGA) is a laboratory tool

used for material characterization during dehydration, decomposition, and oxidation of a sample using this technique.

A Thermogravimetric Analyzer (TGA) consists of a sample pan in a furnace which is supported by a precision balance. Sample purge gas, which may be inert or an oxidative gas, flows over the sample and determines the process environment. A built in mass flow controller is used to control the sample purge gas. Balance purge gas enters the device through a separate port and maintains a constant environment for the balance. The furnace cool-down is done with the chiller and integral forced air features. Sample and reference temperatures are measured directly with embodied sensors.

Thermogravimetric Analysis (TGA) thermal curves are displayed so that the X-axis indicates the weight of the sample (mg or %) and the Y-axis can be displayed as time or temperature. The Derivative Thermogravimetric (DTG) curves can also be extracted from TGA curves which illustrates the rate of weight loss (mg/min or %/min) over the X-axis and is a very useful method in exploring the reaction rates during TGA tests.

In order to explore the evolution of product gases from a TGA system, several techniques are used in which two or more devices are combined. This approach is referred to as evolved gas analysis (EGA). Thermogravimetric Analyzer (TGA) coupled with Fourier Transform Infrared spectroscopy (FTIR) is the most common type of Evolved Gas Analyzing (TGA – EGA) systems which is known as *TGA-FTIR technique*.

The electromagnetic spectrum between the visible and microwave regions is known as *infrared (IR) region*. The IR part of electromagnetic spectrum is divided into three regions of near, mid and IR regions. The mid IR region is the region in which the wavelengths varies from  $3 \times 10^{-4}$  to  $3 \times 10^{-3}$  cm (in wavenumbers, the mid IR range is  $4000-400 \text{ cm}^{-1}$ ) and is being used quite often in the practical aspects of organic chemistry. A rise in wavenumber will lead to an increase in energy content. The infrared radiation is converted into the energy regarding molecular vibration as this radiation is absorbed by organic molecules. Radiation at the mid-IR regions

demonstrates extensive information about chemical bonds of the evolved species. One of the most valuable data that can be extracted by measuring the transmittance, radiance, and reflectance of the stream in mid-IR regions, is recognizing the evolved species concentration. Infrared spectroscopy has been a common and widely used method of material analysis for over seventy years. In this method an organic molecule is exposed to infrared radiation. The absorption of IR radiation takes place when the radiant energy matches the energy related with specific molecular vibration and some of it is passed through (transmitted). Furthermore molecular compounds are a unique combination of atoms with different infrared spectrum and as a result the vibrational spectrum of a molecule is considered to be a unique physical property. Therefore the infrared spectrum can be used as a fingerprint for identification of the evolved molecules. Moreover the magnitude of the peaks in the spectrum can be used to quantify the amount of material present. A schematic view of the IR spectroscopy is illustrated in Fig. 3.5.

Fourier Transform Infrared spectrometry (FTIR) is a preferred method of IR spectroscopy which was developed to overcome the limitations of dispersive instruments. In dispersive methods the main problem was the slow scanning process which is solved in FTIR through simultaneous measurements of infrared frequencies. The other FTIR advantages over the dispersive technique can be mentioned as follow: Sensitivity, mechanical simplicity, internally calibrated and etc. So these specifications has made the FTIR method more suitable for wide variety of analyses including identifying unknown materials, determination of the sample quality and the amount of components in a mixture.

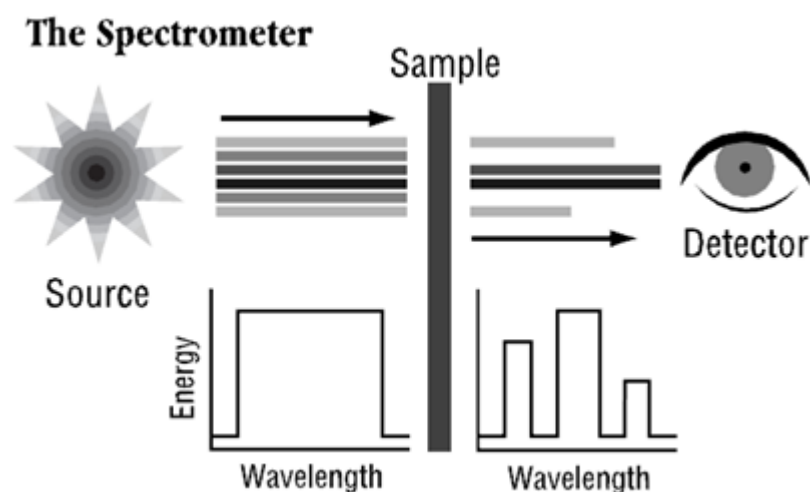


Fig. 3.5 Schematic view of the IR spectroscopy

Fourier Transform Infrared spectroscopy (FTIR) coupled with TGA to study the evolved gas analysis (EGA) in coal science research appears to be more and more common. Fig. 3.6 shows a schematic diagram of the experimental setup. The setup is indicated in Fig. 3.7. The experimental setup consists of Perkin Elmer Pyris STA 6000 TGA (Fig. 3.8 and the components Fig. 3.9), Spectrum 1 FTIR spectrometer (from PerkinElmer Company) (Fig. 3.8), a set of two stage regulators to better damp the flow fluctuations and two variable area mass flow meters (MFM) to monitor and adjust the flow of the gaseous species. The Perkin Elmer Pyris STA 6000 TGA and Spectrum 1 FTIR spectrometer were controlled by Pyris Software (Version 11.0.0.0449) and Spectrum TimeBase software (Application Version: 3.1.2.0041) respectively. In the present work TGA (Thermogravimetry) and DTG (Derivative Thermogravimetry) profiles were used to determine pyrolysis and combustion characteristics of the original and impregnated coal samples in both  $O_2/N_2$  and  $O_2/CO_2$  ambient conditions. The TGA/DTG profiles are derived with 3800 process points in Pyris Software from PerkinElmer Company.

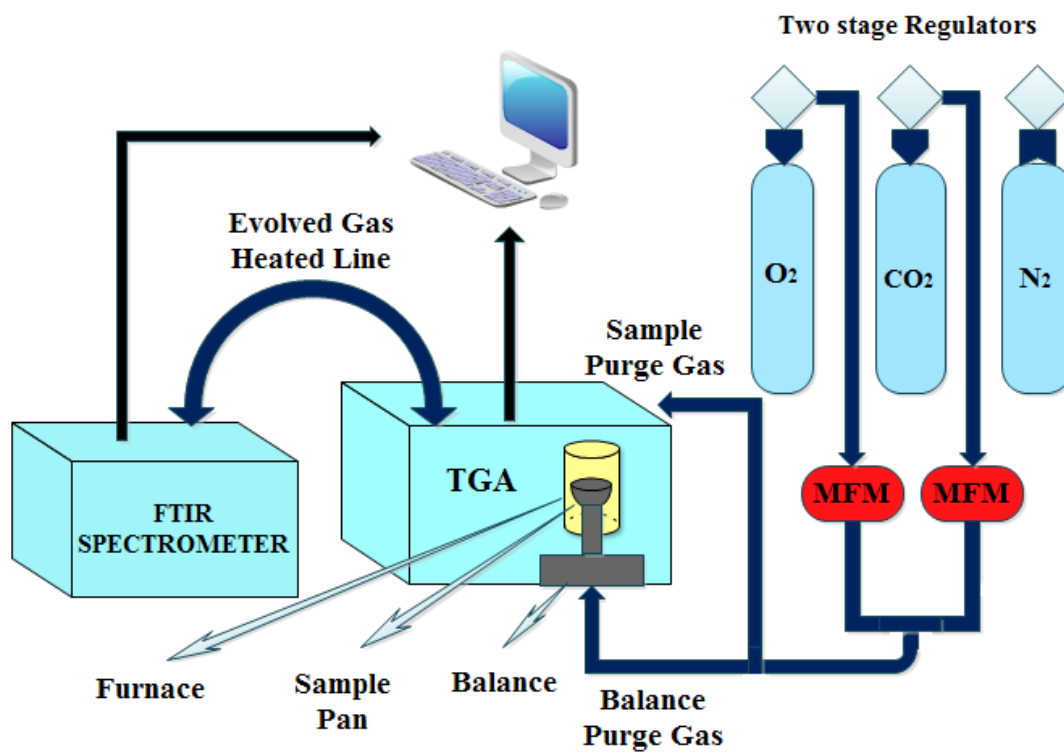


Fig 3.6 Schematic diagram of the experimental setup



Fig. 3.7 Experimental setup

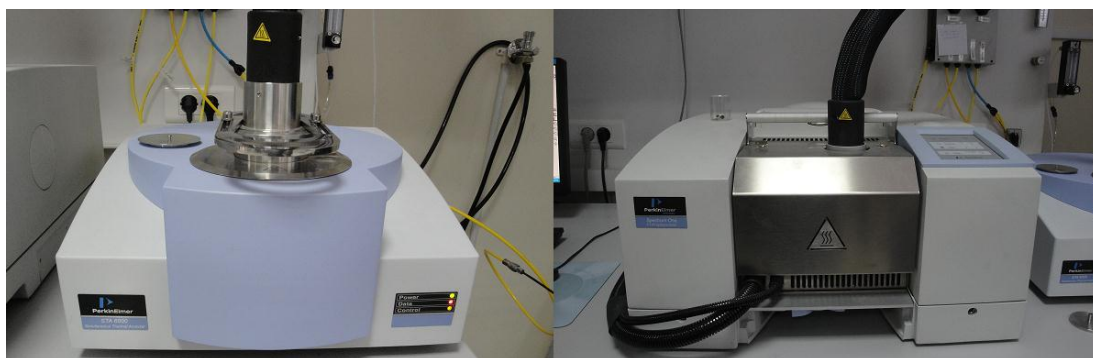


Fig. 3.8 Perkin Elmer Pyris STA 6000 TGA (left), Spectrum 1 FTIR spectrometer (right)

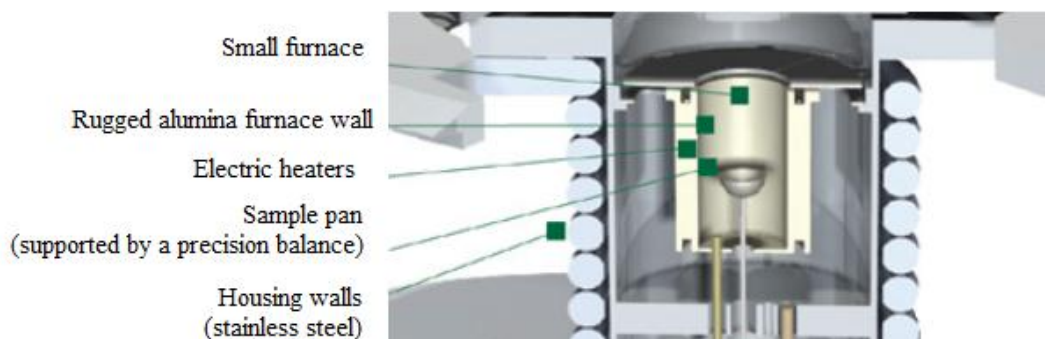


Fig. 3.9 Internal view of the TGA at METU Central Laboratory (Perkin Elmer Pyris STA 6000)

The TGA system was coupled with FTIR spectrometer for determination of evolved gases during pyrolysis and combustion experiments. TGA and FTIR were connected by a heated line at the temperature of 270 °C in order to prevent the condensation of gases (Fig. 3.10).

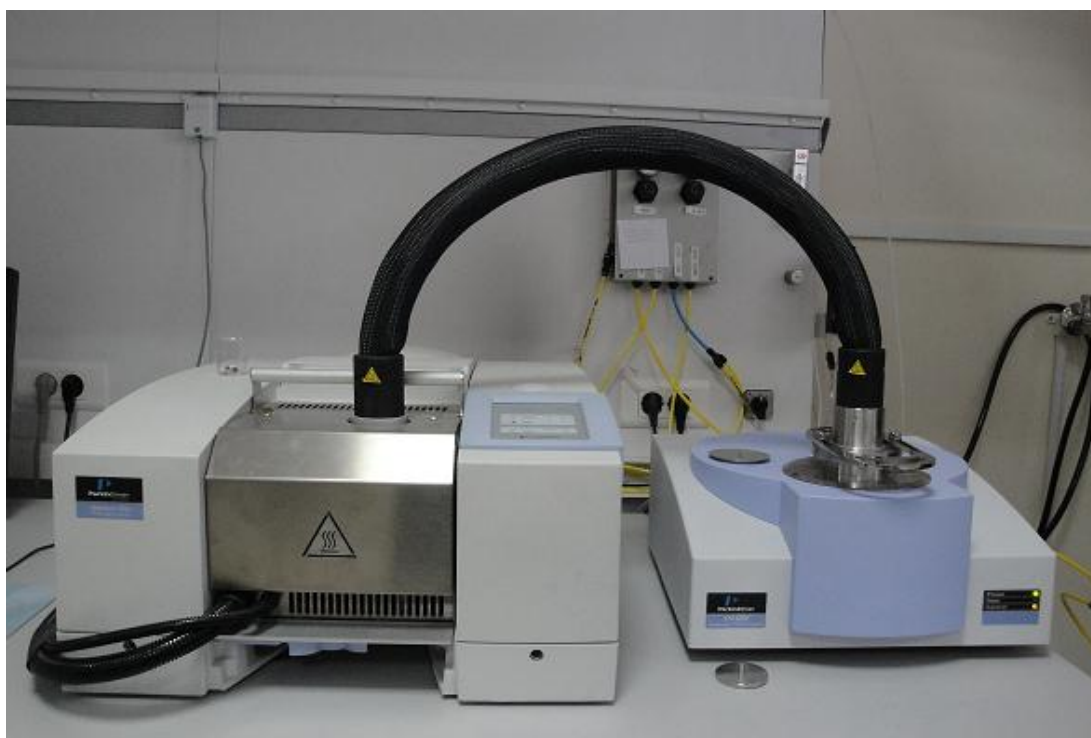


Fig. 3.10 TGA system coupled with FTIR spectrometer and the heated line between two devices

FTIR is highly sensitive to  $\text{H}_2\text{O}$  and  $\text{CO}_2$ , thus in order to minimize the environment effect and ensure the stability of TGA-FTIR, before each test the whole system was purged for at least 15 minutes. Then the background gas profile from the FTIR device was checked and if required the system was left to operate for enough time with a flow of oxygen rich gas and the elevated line temperature of around  $310^\circ\text{C}$  in order to burn and clean the possible contaminations inside the connecting line. The experiment started only when the system was stable. FTIR spectra were collected with  $4\text{ cm}^{-1}$  resolution, in the range of  $700\text{-}4000\text{ cm}^{-1}$  IR absorption band. The FTIR gas vacuum flow was adjusted to  $50\text{ ml}_n/\text{min}$  in both combustion and pyrolysis tests. A linear relation between spectral absorbance at a given wavenumber

and concentration of gaseous components is given by Beer's Law [60]. In this study, the points of absorbance (arbitrary unit) at a certain wavenumber are plotted against temperature in order to obtain a formation profile for each evolved gas observed in the spectra during experiments. The IR wavenumbers of CO<sub>2</sub>, CO, H<sub>2</sub>O, CH<sub>4</sub>, SO<sub>x</sub>, COS, NH<sub>3</sub>, NO, NO<sub>2</sub>, N<sub>2</sub>O, HCN and HCl are listed in Table 3.4. These wavenumbers are selected between the strong absorption bands of these gases so that, an attempt was done to avoid any overlap between the desired absorption bands [31, 39, 60-65]. However, due to interference problems, it was not possible to distinguish between the SO<sub>2</sub> and SO<sub>3</sub> species, and both of them can contribute to the wavenumber of 1374 cm<sup>-1</sup>. Thus, SO<sub>x</sub> was assumed to be due to both species. Furthermore, formation profiles of NO<sub>x</sub> related species such as NO and NO<sub>2</sub> are not reported in some cases due to overlap of their absorption bands with the characteristic absorption bands of water.

Table 3.4 IR wavenumbers of the evolved gases

Main volatile products	CO <sub>2</sub>	CO	H <sub>2</sub> O	CH <sub>4</sub>	SO <sub>x</sub>	COS	NH <sub>3</sub>	NO	NO <sub>2</sub>	N <sub>2</sub> O	HCN	HCl
Wavenumber (cm <sup>-1</sup> )	2360	2182	1510	3016	1374	2042	962	1903	1640	2563	3290	2798

About 25 mg of the original and impregnated coal samples with particle size less than 106 μm was heated with a relatively low heating rate of 15 °C/ min from room temperature up to 980 °C during each experiment to fully monitor the pyrolysis and combustion processes. The required combustion ambient was formed by mixing the desired ratio of the two gases by using two different mass flow meters. The total gas flow during the combustion tests was around 80 ml<sub>n</sub>/min. 30ml<sub>n</sub>/min of this mixture was used as a system purge gas and the remaining 50 ml<sub>n</sub>/min was sent through the

balance as a balance purge gas. It is always important to have the balance purge higher than the sample purge. This balance gas positive purge differential prevents volatile gases from back streaming into the balance area which may contaminate the ultra-precision balance. In the case of pyrolysis tests, the system purge gas was adjusted to 40 ml<sub>n</sub>/min and the total gas flow was set to 140 ml<sub>n</sub>/min. This higher total flow ensures an inert atmosphere on the sample during the run and there will be enough N<sub>2</sub> or CO<sub>2</sub> flow during pyrolysis tests provided for FTIR vacuum and there would be no leakage from the environment. The working pressure of O<sub>2</sub>, N<sub>2</sub> and CO<sub>2</sub> gases were adjusted to 2.2 bar, 2.5 bar and 2.45 bar respectively.

The combustion experiments were performed in oxygen mole fractions of 21 % (oxygen concentration equivalent to normal air combustion), 25 %, 30 % and 35 % in order to explore the effects of elevated oxygen mole fractions in both N<sub>2</sub> and CO<sub>2</sub> ambient conditions. Pyrolysis tests were carried out in 100 % N<sub>2</sub> and 100 % CO<sub>2</sub> ambient conditions which are the main diluting gases in air and oxy-fuel conditions respectively.

### **3.2.1.1 TGA-FTIR Experimental Matrix**

The experimental matrix of TGA-FTIR tests throughout this study is listed in Tables 3.5- 3.8.

Table 3. 5 TGA-FTIR experimental matrix of original and impregnated Kangal lignite and Tunçbilek sub- bituminous coal samples

Run Number	Coal Sample	Catalyst	Oxygen Mole Fraction	Environment	Combustion/ Pyrolysis
1	Kangal lignite	-	21 %	O <sub>2</sub> / N <sub>2</sub>	combustion
2	Kangal lignite	-	25 %	O <sub>2</sub> / N <sub>2</sub>	combustion
3	Kangal lignite	-	30 %	O <sub>2</sub> / N <sub>2</sub>	combustion
4	Kangal lignite	-	35 %	O <sub>2</sub> / N <sub>2</sub>	combustion
5	Kangal lignite	-	0 %	N <sub>2</sub>	pyrolysis
6	Kangal lignite	-	21 %	O <sub>2</sub> /CO <sub>2</sub>	combustion
7	Kangal lignite	-	25 %	O <sub>2</sub> /CO <sub>2</sub>	combustion
8	Kangal lignite	-	30 %	O <sub>2</sub> /CO <sub>2</sub>	combustion
9	Kangal lignite	-	35 %	O <sub>2</sub> /CO <sub>2</sub>	combustion
10	Kangal lignite	-	0 %	CO <sub>2</sub>	pyrolysis

Table 3. 6 TGA-FTIR experimental matrix of original and impregnated Kangal lignite and Tunçbilek sub- bituminous coal samples (continued)

Run Number	Coal Sample	Catalyst	Oxygen Mole Fraction	Environment	Combustion/Pyrolysis
11	Kangal lignite	Fe <sub>2</sub> O <sub>3</sub>	21 %	O <sub>2</sub> /CO <sub>2</sub>	Combustion
12	Kangal lignite	Fe <sub>2</sub> O <sub>3</sub>	25 %	O <sub>2</sub> /CO <sub>2</sub>	Combustion
13	Kangal lignite	Fe <sub>2</sub> O <sub>3</sub>	30 %	O <sub>2</sub> /CO <sub>2</sub>	Combustion
14	Kangal lignite	Fe <sub>2</sub> O <sub>3</sub>	35 %	O <sub>2</sub> /CO <sub>2</sub>	Combustion
15	Kangal lignite	Fe <sub>2</sub> O <sub>3</sub>	0 %	CO <sub>2</sub>	Pyrolysis
16	Kangal lignite	Ca(OH) <sub>2</sub>	21 %	O <sub>2</sub> /CO <sub>2</sub>	Combustion
17	Kangal lignite	Ca(OH) <sub>2</sub>	25 %	O <sub>2</sub> /CO <sub>2</sub>	Combustion
18	Kangal lignite	Ca(OH) <sub>2</sub>	30 %	O <sub>2</sub> /CO <sub>2</sub>	Combustion
19	Kangal lignite	Ca(OH) <sub>2</sub>	35 %	O <sub>2</sub> /CO <sub>2</sub>	Combustion
20	Kangal lignite	Ca(OH) <sub>2</sub>	0 %	CO <sub>2</sub>	Pyrolysis
21	Kangal lignite	K <sub>2</sub> CO <sub>3</sub>	21 %	O <sub>2</sub> /CO <sub>2</sub>	combustion
22	Kangal lignite	K <sub>2</sub> CO <sub>3</sub>	25 %	O <sub>2</sub> /CO <sub>2</sub>	combustion
23	Kangal lignite	K <sub>2</sub> CO <sub>3</sub>	30 %	O <sub>2</sub> /CO <sub>2</sub>	combustion
24	Kangal lignite	K <sub>2</sub> CO <sub>3</sub>	35 %	O <sub>2</sub> /CO <sub>2</sub>	combustion
25	Kangal lignite	K <sub>2</sub> CO <sub>3</sub>	0 %	CO <sub>2</sub>	pyrolysis

Table 3.7 TGA-FTIR experimental matrix of original and impregnated Kangal lignite and Tunçbilek sub-bituminous coal samples (continued)

Run Number	Coal Sample	Catalyst	Oxygen Mole Fraction	Environment	Combustion/Pyrolysis
26	Tunçbilek sub-bituminous	-	21 %	O <sub>2</sub> / N <sub>2</sub>	combustion
27	Tunçbilek sub-bituminous	-	30 %	O <sub>2</sub> /CO <sub>2</sub>	combustion
28	Tunçbilek sub-bituminous	Fe <sub>2</sub> O <sub>3</sub>	30 %	O <sub>2</sub> /CO <sub>2</sub>	combustion
29	Tunçbilek sub-bituminous	Ca(OH) <sub>2</sub>	30 %	O <sub>2</sub> /CO <sub>2</sub>	combustion
30	Tunçbilek sub-bituminous	K <sub>2</sub> CO <sub>3</sub>	30 %	O <sub>2</sub> /CO <sub>2</sub>	combustion
38	Kangal lignite	K <sub>2</sub> CO <sub>3</sub>	21 %	O <sub>2</sub> / N <sub>2</sub>	combustion
39	Kangal lignite	K <sub>2</sub> CO <sub>3</sub>	25 %	O <sub>2</sub> / N <sub>2</sub>	combustion
40	Kangal lignite	K <sub>2</sub> CO <sub>3</sub>	30 %	O <sub>2</sub> / N <sub>2</sub>	combustion
41	Kangal lignite	K <sub>2</sub> CO <sub>3</sub>	35 %	O <sub>2</sub> / N <sub>2</sub>	combustion

Table 3. 8 TGA-FTIR experimental matrix of original Kangal lignite and the impregnated samples with biomass ash contents

Run Number	Coal Sample	Catalyst	Oxygen Mole Fraction	Environment
1	Kangal lignite	HSh	21 %	O <sub>2</sub> /N <sub>2</sub>
2	Kangal lignite	HSh	30 %	O <sub>2</sub> /N <sub>2</sub>
3	Kangal lignite	HSh	21 %	O <sub>2</sub> /CO <sub>2</sub>
4	Kangal lignite	HSh	30 %	O <sub>2</sub> /CO <sub>2</sub>
5	Kangal lignite	WSh	21 %	O <sub>2</sub> /N <sub>2</sub>
6	Kangal lignite	WSh	30 %	O <sub>2</sub> /N <sub>2</sub>
7	Kangal lignite	WSh	21 %	O <sub>2</sub> /CO <sub>2</sub>
8	Kangal lignite	WSh	30 %	O <sub>2</sub> /CO <sub>2</sub>
9	Kangal lignite	WS	21 %	O <sub>2</sub> /N <sub>2</sub>
10	Kangal lignite	WS	30 %	O <sub>2</sub> /N <sub>2</sub>
11	Kangal lignite	WS	21 %	O <sub>2</sub> /CO <sub>2</sub>
11	Kangal lignite	WS	30 %	O <sub>2</sub> /CO <sub>2</sub>
13	Kangal lignite	CM	21 %	O <sub>2</sub> /N <sub>2</sub>
14	Kangal lignite	CM	30 %	O <sub>2</sub> /N <sub>2</sub>
15	Kangal lignite	CM	21 %	O <sub>2</sub> /CO <sub>2</sub>
16	Kangal lignite	CM	30 %	O <sub>2</sub> /CO <sub>2</sub>
17	Kangal lignite	SD	21 %	O <sub>2</sub> /N <sub>2</sub>
18	Kangal lignite	SD	30 %	O <sub>2</sub> /N <sub>2</sub>
19	Kangal lignite	SD	21 %	O <sub>2</sub> /CO <sub>2</sub>
20	Kangal lignite	SD	30 %	O <sub>2</sub> /CO <sub>2</sub>
21	Kangal lignite	-	21 %	O <sub>2</sub> /N <sub>2</sub>
22	Kangal lignite	-	30 %	O <sub>2</sub> /CO <sub>2</sub>

### 3.2.1.2 Combustion Regions in TGA-FTIR Studies

When the pulverized coal first enters the hot environment, particles rapidly undergo a process called *devolatilization* yielding a mixture of primary volatiles or tars consisting mainly of high molecular weight carbon species plus a mixture of combustible gases containing CO, H<sub>2</sub>, CH<sub>4</sub> and small amounts of other hydrocarbons. The remaining char consists of highly polymeric aromatics, unsaturated hydrocarbons and the ash. The amount of volatiles, their composition and the rate at which they are released are all strongly dependent on many physical and chemical properties of the original coal.

In combustion tests, the TGA/ DTG plots clearly suggested that there were three stages of weight loss (Fig. 3.11). These regions were determined according to the approximate starting and end points of DTG curves which shows thermal breakdown of organic matters and volatiles in the samples. The first region on the DTG curve was due to the moisture and low boiling point organic matters in the sample. The second region where the main weight loss occurred was due to oxidation and removal of volatile matters from the sample. Furthermore, complicated chemical reactions, such as formation of liquid and gaseous products, occur in this interval. The third region was due to oxidation of the char remaining after the volatiles were removed from the samples and oxygen diffuses gradually to the surface of the fixed carbon. During the combustion tests in O<sub>2</sub>/N<sub>2</sub> ambient and equivalent oxygen mole fractions in CO<sub>2</sub> ambient, these three regions were seen approximately in 28-200 °C, 200-520 °C and beyond 520 °C temperature intervals respectively.

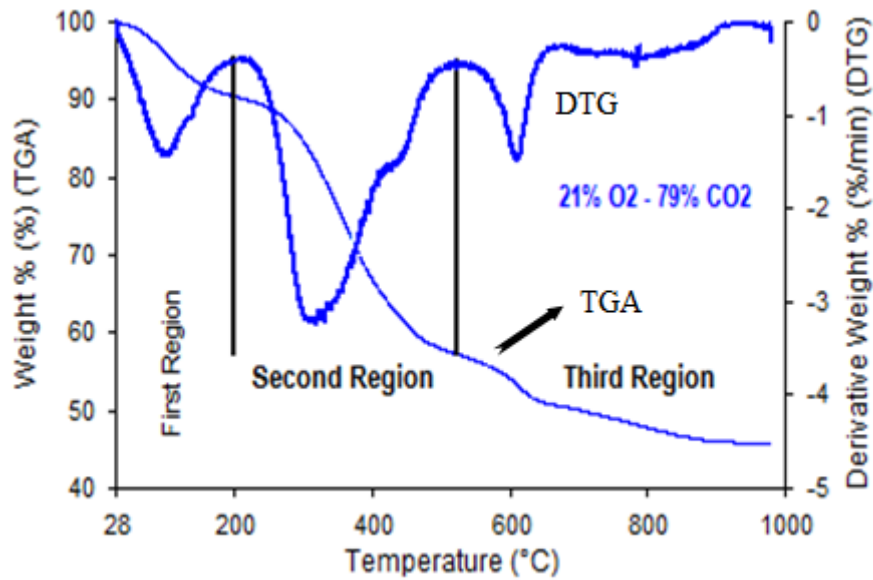


Fig. 3.11 TGA and DTG profiles of Kangal lignite combustion during 21 % O<sub>2</sub> in CO<sub>2</sub> ambient

### 3.2.1.3 Characteristic Parameters in TGA-FTIR Studies

TGA/DTG and FTIR profiles obtained during pyrolysis and combustion experiments were used to determine the characteristic parameters such as initial decomposition temperature ( $T_{in}$ ), peak temperature in the second region due to devolatilization ( $T_{2max}$ ), ignition temperature ( $T_{ig}$ ), burnout temperature ( $T_b$ ), temperature of the maximum flue gas emission ( $T_{FG-max}$ ) and the absolute value of the maximum rate of weight loss in the second region ( $|(dm/dt)_{2max}|$  (%/min)). Furthermore,  $|(dm/dt)_{3max}|$  and ( $T_{3max}$ ) were also defined as the absolute value of the maximum weight loss rate occurred in the third region of combustion due to char gasification and oxidation and the corresponding temperature respectively. The specific reactivity ( $dm/dt$ ) (%/min) can also be defined as the rate of weight loss of the sample at any time during pyrolysis or combustion processes.  $T_{in}$  represents the initiation of weight loss and was defined as the temperature at which the rate of

weight loss reaches 0.5 %/min after initial moisture loss peak in DTG profiles.  $T_{2max}$  is the point at which the maximum reaction rate  $|(dm/dt_{2max})|$  occurs in the second region of combustion due to devolatilization and is related to fuel structure. This peak temperature is the measure of combustibility. Lower the peak temperature, easier is the ignition of the fuel. Different from initial decomposition temperature, ignition temperature ( $T_{ig}$ ) is defined as the temperature at which coal starts burning. It was taken as the temperature at which the weight loss curves in the oxidation and pyrolysis experiments diverge and a sudden decrease is seen in the DTG curve [66]. The procedure for determining the ignition temperature was defined as following: firstly, a vertical line passing through the DTG peak point was drawn upward to meet the TG curve at point A; secondly, a tangent line was made to the TG curve at point A, which met the extended TG initial level line at point C; thirdly, another vertical line was made downwards from point C, which intersected with the abscissa at one point, the corresponding temperature of this point was defined as the ignition temperature (Fig. 3.12) [54, 56]. The last characteristic temperature considered in TGA/DTG curves was the burnout temperature ( $T_b$ ) which represents the temperature where sample oxidation is completed and reflects the thermal behavior of coal organic matter during combustion and pyrolysis. It was taken as the point immediately before reaction ceased when the rate of weight loss was 0.5%/min. The initial and final decomposition temperatures are related to the difficulty with which the reaction proceeds. Moreover,  $T_{FG-max}$  (FTIR profiles) was the temperature at which the maximum flue gas emission (absorbance at the certain wavenumber) occurred in the second region.

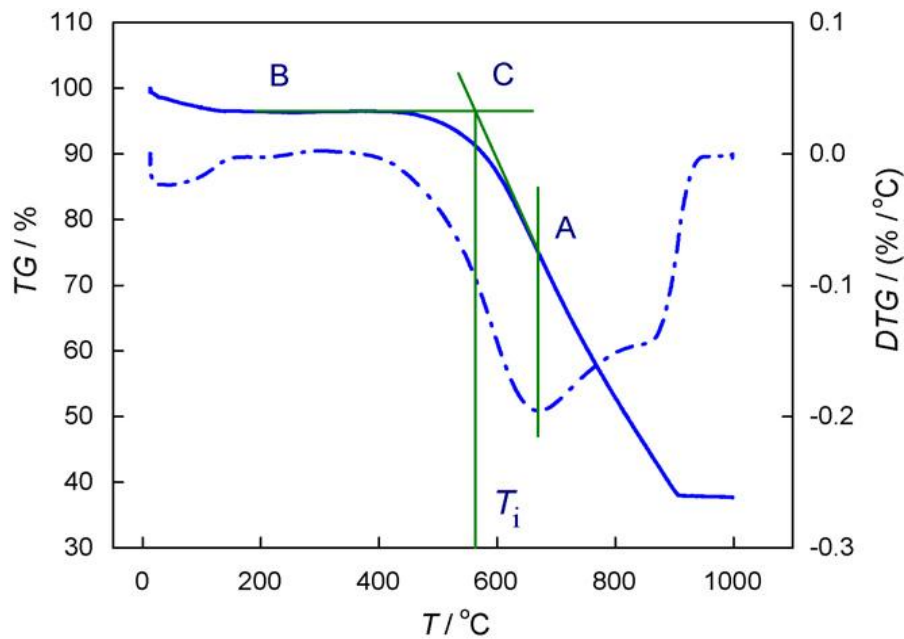


Fig. 3.12 Ignition temperature ( $T_i$ ) definition sketch [56]

### 3.2.2 Ash Analysis with XRF Method

X-ray Fluorescence (XRF) spectrometer is used for routine and relatively non-destructive chemical analyses of minerals, rocks, fluids and sediments. XRF works on wavelength-dispersive spectroscopic principles and uses relatively large amount of sample. The stability and ease of use of XRF devices along with low cost and relative ease of sample preparation of this method make the utilization of these X-ray spectrometers one of the most common methods in chemical analyses and tracing elements in wide variety of substances.

Responses of atoms exposed to radiation in XRF method have made it possible to chemically analyze and trace elements in geological materials. When materials are exposed to a short wavelength radiation (with high energy), the atoms become ionized. If the energy of the radiation is sufficient to dislodge a tightly-held inner electron, the atom becomes unstable and an outer electron replaces the missing inner

electron. When this happens, energy is released due to the decreased binding energy of the inner electron orbital compared with an outer one. The emitted radiation is of lower energy than the primary incident X-rays and is termed fluorescent radiation. Because the energy of the emitted photon is characteristic of a transition between specific electron orbitals in a particular element, the resulting fluorescent X-rays can be used to detect the abundances of elements that are present in the sample. XRF analyses would provide data in the form of element oxides and separating different types of one element's oxides is not possible in these analyses.

In the preparation of ash samples for analysis, slow burning of the coal samples is necessary to prevent the retention of sulfur as sulfate in the ash. In selected test methods (ASTM D-3682; ASTM D-4326), the ash from original lignite and impregnated samples (catalyst concentrations of 5 %) was prepared by placing a weighed amount of sample (around 20 g and < 106  $\mu\text{m}$  in size) in a cold muffle furnace. The temperature was gradually raised to 500 °C (932 °F) in 1 hour and to 750 °C (1382 °F) in 2 hours [67]. The resulted ash was then cooled in the dessicator to prevent moisture absorption from the environment. Then, a blend of 6.25 g ash and 1.4 g diluent was pressed under the pressure of 300 bar for around 5 minutes to make the XRF (X-ray Fluorescence spectrometer) test tablets (Fig. 3.13). The X-ray Fluorescence, SPECTRO iQ (Fig. 3.14) was utilized for determination of ash composition. Prior to the ash analysis tests, three types of calibration tests were run. The results of ash analyses are listed in Tables 3.9-3.12. In these tables one can see the effects of impregnation on ash composition of the coal samples. These tables are illustrated in element-based oxides since XRF analysis would provide data in the form of element oxides and separating different types of one element's oxides is not possible in these analyses. It should be noticed that considerable amounts of silicium and aluminum oxides were observed in the ash contents of the coal samples used. Furthermore, it was revealed that the Kangal lignite used in TGA-FTIR tests, originally had high amount of calcium oxide in the ash.



Fig. 3.13 XRF test tablets



Fig. 3.14 X-ray Fluorescence SPECTRO iQ (left) and the hydraulic press (right)

Table 3.9 Ash analyses of the original and impregnated Kangal lignite samples

<b>Element-based Oxides</b> (% By weight)	<b>Si</b>	<b>Al</b>	<b>Ca</b>	<b>Mg</b>	<b>K</b>	<b>Na</b>	<b>Fe</b>	<b>Ti</b>	<b>P</b>	<b>S</b>
<b>Kangal lignite</b>	34.00	15.96	24.40	4.107	1.120	<0.11	6.037	0.6774	0.1361	14.84
<b>Fe<sub>2</sub>O<sub>3</sub>-form</b>	29.84	14.03	21.58	3.707	<0.0012	<0.11	16.70	0.4486	0.1145	13.49
<b>FeCl<sub>3</sub>-form</b>	29.18	13.10	21.12	3.413	0.905	<0.11	11.55	0.5042	<0.001	12.34
<b>Ca(OH)<sub>2</sub>-form</b>	31.64	14.73	30.71	3.864	0.986	<0.11	5.391	0.5784	0.0955	13.88
<b>K<sub>2</sub>CO<sub>3</sub>-form</b>	30.60	12.85	23.53	3.155	8.574	<0.11	5.775	0.6116	0.1392	15.06

Table 3.10 Ash analyses of the original and impregnated Seyitömer lignite samples

<b>Element-based Oxides</b> (% By weight)	<b>Si</b>	<b>Al</b>	<b>Ca</b>	<b>Mg</b>	<b>K</b>	<b>Na</b>	<b>Fe</b>	<b>Ti</b>	<b>P</b>	<b>S</b>
<b>Seyitömer lignite</b>	52.98	21.82	2.923	5.434	1.899	<0.11	10.86	0.7133	<0.001	5.338
<b>Fe<sub>2</sub>O<sub>3</sub>-form</b>	50.39	21.85	2.349	4.175	2.153	<0.11	16.62	0.7003	<0.001	3.964
<b>FeCl<sub>3</sub>-form</b>	52.87	21.82	2.276	4.468	2.219	<0.11	14.86	0.6345	<0.001	2.797
<b>Ca(OH)<sub>2</sub>-form</b>	NA	NA	NA	NA	NA	NA	NA	NA	NA	NA
<b>K<sub>2</sub>CO<sub>3</sub>-form</b>	51.10	21.37	2.321	4.363	8.079	<0.11	9.251	0.6951	<0.001	5.049

Table 3.11 Ash analyses of the original and impregnated Tunçbilek sub-bituminous samples

<b>Element-based Oxides (% By weight)</b>	<b>Si</b>	<b>Al</b>	<b>Ca</b>	<b>Mg</b>	<b>K</b>	<b>Na</b>	<b>Fe</b>	<b>Ti</b>	<b>P</b>	<b>S</b>
<b>Tunçbilek sub-bituminous</b>	57.85	21.51	3.095	5.095	1.398	<0.11	8.721	0.7888	0.0854	3.454
<b>Fe<sub>2</sub>O<sub>3</sub>-form</b>	52.52	19.73	2.965	4.758	1.279	<0.11	16.55	0.7334	<0.001	3.372
<b>FeCl<sub>3</sub>-form</b>	53.04	19.35	3.236	5.824	1.485	<0.11	13.82	0.7495	<0.001	4.394
<b>Ca(OH)<sub>2</sub>-form</b>	50.90	19.04	10.26	5.014	1.345	<0.11	7.880	0.6782	<0.001	6.994
<b>K<sub>2</sub>CO<sub>3</sub>-form</b>	52.90	19.68	2.926	4.869	7.545	<0.11	8.074	0.7064	<0.001	5.425

Table 3.12 Ash analyses of the original and impregnated Zonguldak bituminous samples

<b>Element-based Oxides (% By weight)</b>	<b>Si</b>	<b>Al</b>	<b>Ca</b>	<b>Mg</b>	<b>K</b>	<b>Na</b>	<b>Fe</b>	<b>Ti</b>	<b>P</b>	<b>S</b>
<b>Zonguldak bituminous</b>	54.50	30.42	2.038	2.752	4.266	<0.11	5.835	1.165	<0.001	1.524
<b>Fe<sub>2</sub>O<sub>3</sub>-form</b>	49.14	27.82	1.903	2.585	3.791	<0.11	14.81	1.052	<0.001	1.348
<b>FeCl<sub>3</sub>-form</b>	NA	NA	NA	NA	NA	NA	NA	NA	NA	NA
<b>Ca(OH)<sub>2</sub>-form</b>	48.03	26.53	10.64	2.588	3.851	<0.11	5.697	1.130	<0.001	3.613
<b>K<sub>2</sub>CO<sub>3</sub>-form</b>	48.96	26.69	2.046	2.443	10.93	<0.11	5.675	1.113	<0.001	2.429

### 3.2.2.1 Repeatability Tests

In order to test the repeatability of XRF analysis, a set of experiments were performed using S + 5 % FeCl<sub>3</sub> and T + 5 % FeCl<sub>3</sub> samples. In the case of each sample, three XRF runs were performed and the results are listed in Table 3.13.

Table 3.13 Repeatability tests in XRF analyses

Element-based Oxides (% By weight)	Si	Al	Ca	Mg	K	Na	Fe	S	Av. Error (%)
S + 5 % FeCl <sub>3</sub> (run # 1)	52.89	21.86	2.292	4,406	2.267	< 0,11	14.88	2.711	
S + 5 % FeCl <sub>3</sub> (run # 2)	52.82	21.85	2.278	4.416	2.267	< 0,11	14.92	2.713	
S + 5 % FeCl <sub>3</sub> (run # 3)	52.81	21.81	2.276	4.460	2.277	< 0,11	14.91	2.717	
Max Elemental Error (%)	0.15	0.23	0.70	1.23	0.44	0	0.27	0.22	0.46
T + 5 % FeCl <sub>3</sub> (run # 1)	52.27	19.49	3.200	5.813	1.248	< 0,11	13.80	4.313	
T + 5 % FeCl <sub>3</sub> (run # 2)	53.14	19.40	3.233	5.797	1.416	< 0,11	13.85	4.296	
T + 5 % FeCl <sub>3</sub> (run # 3)	53.34	19.48	3.180	5.899	1.330	< 0,11	13.81	4.316	
Max Elemental Error (%)	2.05	0.46	1.67	1.76	13.46	0	0.36	0.47	2.53

### 3.2.3 Calorimetric Tests

A bomb- or combustion calorimeter is a device used to measure the amount of heat created by a sample which is combusted under controlled conditions. This combustion takes place in a closed vessel (Fig. 3.15) which is sank in water and embedded under relatively high oxygen pressure. A weighed amount of sample (1-2 g) is placed in the crucible located in to the stainless steel bomb filled with oxygen up to the pressure of 25-30 bar (in a typical calorimeter). Then an ignition wire is used to ignite the sample. During the burning process, the heat created is transferred into the surrounding water. The inner vessel is finely isolated using an outer vessel in order to ensure that the created heat does not get out of the system or the system is not affected by the environment while the room temperature changes. This rise in water temperature is monitored using a precision thermometer and is used in the calculations. Oxygen bomb calorimeter and the schematic view of the components are indicated in Fig. 3.16. There are various types of calorimeters among which Differential Scanning Calorimeter (DSC) is known as a common method in calorimetric analysis.



Fig. 3.15 Oxygen bomb

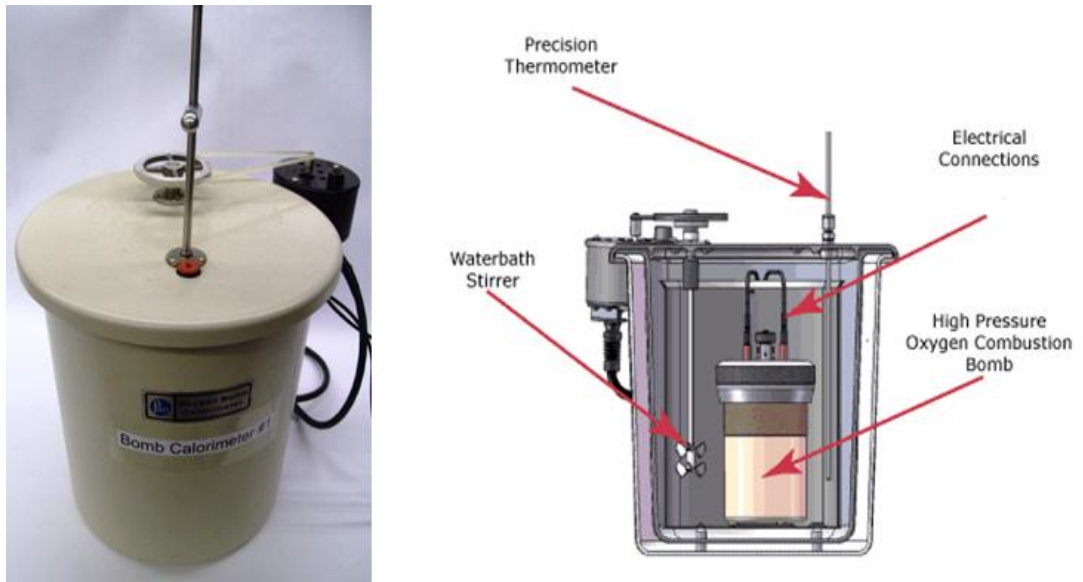


Fig. 3.16 Oxygen bomb calorimeter (left) and schematic view (right)

The calorimetric tests were carried out using oxygen bomb calorimeter for K, S, T and Z coal samples in the Mineral Processing laboratory of Mining Engineering Department at Middle East Technical University (Fig. 3.17).



Fig. 3.17 Oxygen bomb calorimeter set up

Around 1.5 g of the raw or impregnated coal samples (completely dry) were weighed using a digital scale with high balance resolution. The sample container was put in the embedded place inside the bomb with a fine wire passing through the sample. The standard wire length of 10 cm was used in all the experiments. The bomb was closed and filled with oxygen up to 25 bar pressure. The removable water container was filled with specified amount of distilled water and was placed in the isolated tank during each experiment. The stainless steel bomb containing the sample and oxygen under high pressure was placed in the water inside the isolated tank and electrical connections were plugged in to their embodied sockets for igniting the sample. A precision thermometer was used to monitor the temperature before sample

ignition ( $T_1$ ) and the maximum temperature reached ( $T_2$ ). This thermometer was working within the temperature interval of 27-35 °C. A magnifier was used to better monitor the temperature. A water bath stirrer was used to generate internal flow around the bomb to help the system become thermally stable. During each experiment and prior to ignition, the whole system was left for enough time (around 10 min) to become thermally stable while the water was being stirred.  $T_1$  was recorded just before igniting the sample and  $T_2$  was the maximum temperature reached just before its fall-off. The higher heating values (HHV) of the samples were then derived using the following formula:

$$\text{Calorific Value (HHV) (Kcal/Kg)} = \frac{2416 \times (T_2 - T_1)}{m} \quad (3.1)$$

$T_2$  (°C): Maximum temperature

$T_1$  (°C): Temperature before ignition

$m$  (g): Modified sample mass

Each experiment was carried out at least twice in order to check the repeatability and the average was considered as the calorific value of the sample. At the end of each test the ash amount of the sample was measured. Ambient temperature might also be considered as a variable during these kinds of experiments. In the case of all our experiments, ambient temperature varied within the temperature interval of 17-20 °C and therefore this effect was considered negligible in our calorimetric tests.

In order to make sure that the added catalysts were directly ineffective during calorimetric tests, four runs were carried out with the pure catalysts. In these experiments, it was observed that no temperature increase was traced for all the pure catalysts used, confirming that these additions did not have any direct influence in creating temperature difference.

### 3.2.3.1 Catalytic Effects on Calorimetric Tests

In this part of the study, an attempt was done to profoundly explore the possible influences of three inorganic materials, potassium (K), calcium (Ca) and iron (Fe), on calorific values of four different indigenous coal samples using oxygen bomb calorimeter. Potassium carbonate ( $K_2CO_3$ ), calcium hydroxide ( $Ca(OH)_2$ ), iron (III) oxide ( $Fe_2O_3$ ) and iron (III) chloride ( $FeCl_3$ ) were employed as precursors of the mentioned catalysts. In calorimetric tests, catalyst additions to the raw coal by impregnation, corresponded 2 %, 5 % and 10 % in terms of mass ratio of catalyst precursors to coal. Sample preparation and tests methodology can be reviewed in Chapter 3.1. Detailed results of calorimetric tests for different coal samples are listed in Appendix B. The calorific values of the original coal samples (dry basis) used in these tests were 2375 Kcal/Kg, 2192 Kcal/Kg, 3434 Kcal/Kg and 4226 Kcal/Kg for Kangal, Seyitömer, Tunçbilek and Zonguldak samples respectively.

Results obtained from the calorimetric tests of Kangal lignite and Tunçbilek sub-bituminous samples are illustrated in Figs. 3.18 and 3.19. As illustrated in these figures, no significant effects of catalysts were seen in the calorific values of Kangal and Tunçbilek samples. Although there were some slight differences in the calorific values of the impregnated samples, these fluctuations can be a result of the experimental and impregnation errors. Therefore, within the experimental uncertainty, calorific values were almost the same and no significant catalytic effects were observed in the calorimetric tests.

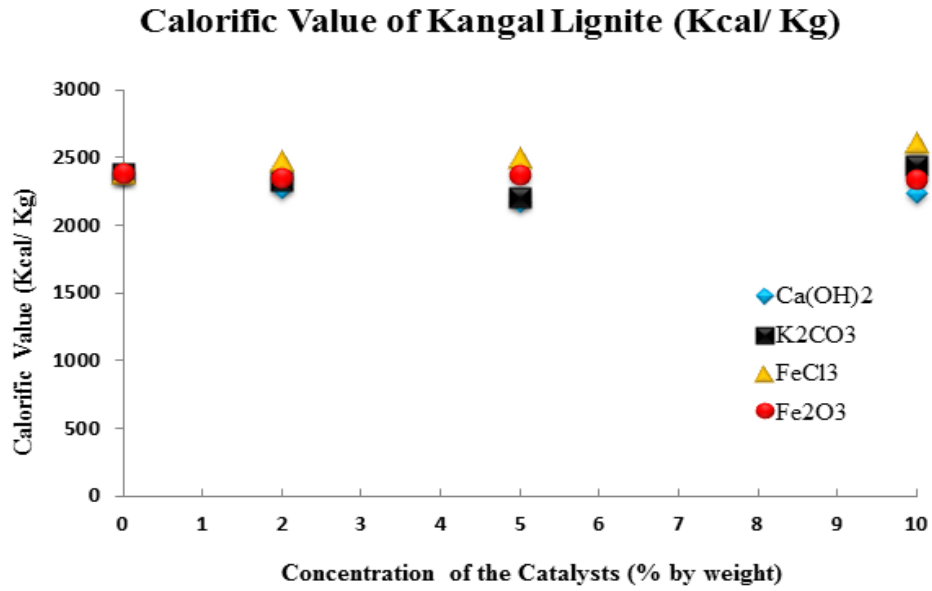


Fig. 3.18 Calorific values of Kangal lignite samples with catalysts

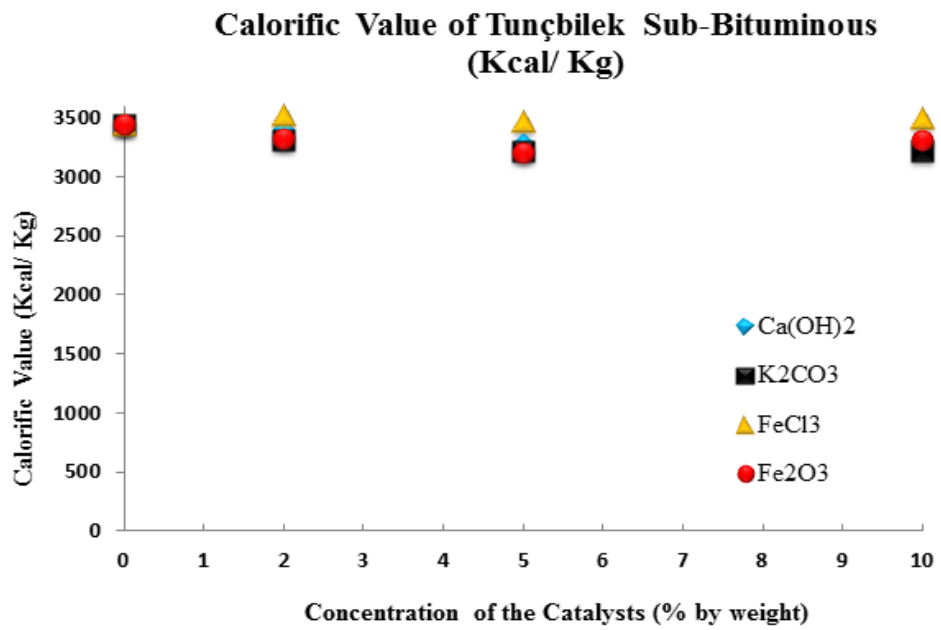


Fig. 3.19 Calorific values of Tunçbilek sub-bituminous samples with catalysts

### 3.2.3.2 Sources of Errors in Calorimetric Tests

1) The  $m$  in the denominator of the equation for deriving higher heating value (HHV) (Chapter 3.2.3) should be related to the effective mass of the coal samples used in these experiments. Therefore, the mass of the added catalyst used for impregnation of the coal samples should be subtracted from the total weight of the sample in each experiment. This should be done as long as it was confirmed that these catalysts did not show any direct influence in calorimetric tests, thus having only the mass of the effective part in the denominator of HHV equation. On the other hand, addition of the catalysts with the percentages of 2 %, 5 % and 10% was carried out in terms of mass ratio of catalyst precursors to the coal samples as tested (after milling and not the completely dry samples) (Table 3.3). However, completely dried samples should have been utilized in formation of these mixtures, since after the final dehumidifying process and eliminating the mass of remaining water from the samples, the contribution of the catalysts would no longer be 2 %, 5 % and 10 % but higher than these percentages which was related to the humidity contents of each sample at the time of adding into catalyst slurries. Therefore, the sample effective mass was modified as illustrated in Appendix B. The humidity content of the samples used in the process of impregnation was extracted from Table 3.3 which was 27.63 %, 16.00 %, 4.37 % and 2.60 % for K, S, T and Z coal samples respectively.

2) The time interval between  $T_1$  and  $T_2$  recording points were reported to be within 400-450 seconds for 10 arbitrary selected runs. On the other hand, the system temperature would drop 0.11-0.18 °C during such a period even after becoming thermally stable before sample ignition which could be due to the weakness of system isolation. Therefore, this temperature drop (and even more since the system temperature is rising during these tests) should be added to the temperature difference between  $T_1$  and  $T_2$ . However, this effect was not considered in calorimetric tests performed in this study, since this would not affect the comparative nature of this study.

3) Although the wire used for igniting the sample would contribute in producing heat, this effect is not embodied in the HHV equation suggested by the producer.

## CHAPTER 4

### TGA-FTIR EXPERIMENTS OF KANGAL LIGNITE PYROLYSIS

The coal pyrolysis reaction is the first stage of coal thermal treatment. Pyrolysis can be defined as decomposition caused by exposure to high temperature in an oxygen free atmosphere which is the most important aspect of coal behavior because it occurs in all major coal conversion processes, like combustion, gasification, carbonization and liquefaction. The process of coal pyrolysis can be divided in to two steps:

- (1) Coal  $\rightarrow$  primary product + gas (H, CH and so on) + char;
- (2) Primary product  $\rightarrow$  secondary product + gas [68].

Pyrolysis as the preliminary process of coal combustion plays a crucial role in determining flame stability, ignition, and product distributions [69]. The ignition temperature of lignite is determined by volatile combustion. Therefore, lignite pyrolysis rate is a very important factor affecting the ignition temperature. Pyrolysis tests of Kangal lignite carried out in both 100 % N<sub>2</sub> and 100 % CO<sub>2</sub> ambient conditions.

DTG profiles throughout the analysis of pyrolysis tests were smoothed using 10 points window and standard smoothing algorithm (Pyris Software).

#### 4.1 Effects of N<sub>2</sub> and CO<sub>2</sub> Ambient Conditions

In this study the effects of the ambient conditions on pyrolysis behavior of Kangal lignite was investigated in 100 % N<sub>2</sub> and 100 % CO<sub>2</sub> ambient conditions. TGA and DTG profiles of pyrolysis tests are shown in Figs. 4.1 and 4.2 and the results are listed in Table 4.1. It was observed that pyrolysis behavior of the lignite sample in 100 % N<sub>2</sub> and 100 % CO<sub>2</sub> ambient conditions was very similar to each other up to 720 °C. This indicates that CO<sub>2</sub> also behaves as an inert gas until this temperature. After the moisture release in the first 220 °C temperature zone, pyrolysis continued with the release of volatile matter content. The primary pyrolysis took place between 220-445 °C temperature interval which included the release of larger fraction of volatiles, mainly light species and gases, CO<sub>2</sub>, light aliphatic gases, CH<sub>4</sub> and H<sub>2</sub>O. Tar and hydrocarbons evolved between 445-550 °C during which additional gas formation such as CH<sub>4</sub>, CO and H<sub>2</sub> from ring condensation was mainly observed [69, 70]. Pyrolysis opens up some dead pores and enlarges sizes of already existing pores. Therefore, in the initial stages of gasification at around 650 °C, disorganized carbon from tars are removed which results in opening of inaccessible porosity and then an increase in all sizes of pores which enhance reactivity until up to a certain conversion. With further increase in conversion, the most active sites decrease leading a loss in active surface area and as a consequence reactivity decreases [71]. The major difference in pyrolysis of lignite samples in these two different atmospheres was observed after 720 °C with the separation of TGA profiles. In 700-980 °C temperature range, additional peaks were displayed in both DTG profiles as shown in Fig. 4.2. As illustrated in Table 4.1, in 100 % CO<sub>2</sub> ambient, the maximum weight loss rate in this temperature range was found to be considerably higher with higher corresponding temperature (T<sub>3max</sub>). In 100 % N<sub>2</sub>, a peak appearing at 727 °C is attributed to partial burning of combustible matter at high temperatures by using inherent oxygen which is about 11 % in Kangal lignite. On the other hand, the sharp peak observed at 785 °C in DTG profile of pyrolysis tests in 100 % CO<sub>2</sub> (Fig. 4.2) can be attributed to char-CO<sub>2</sub> gasification reaction:



Char-CO<sub>2</sub> gasification reaction may increase the reactivity of char in O<sub>2</sub>/CO<sub>2</sub> conditions due to the high concentrations of CO<sub>2</sub>. This sharp peak observed in the temperature range beyond 720 °C was in a good agreement with Kwon et al. [72]. This also can be confirmed by higher total weight loss in 100 % CO<sub>2</sub> (59.9 %) with respect to 100 % N<sub>2</sub> (43.6 %) and by other studies [56, 14].

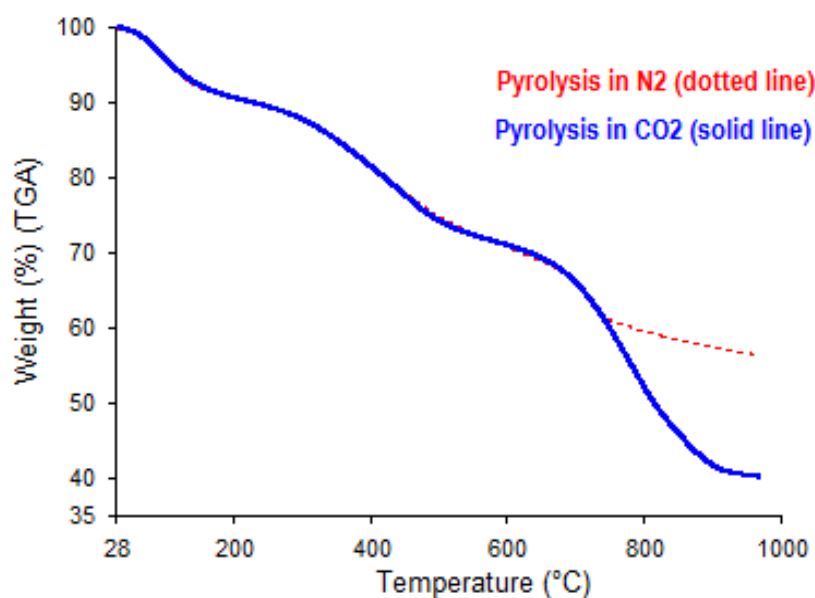


Fig. 4.1 TGA profiles of N<sub>2</sub> and CO<sub>2</sub> pyrolysis tests

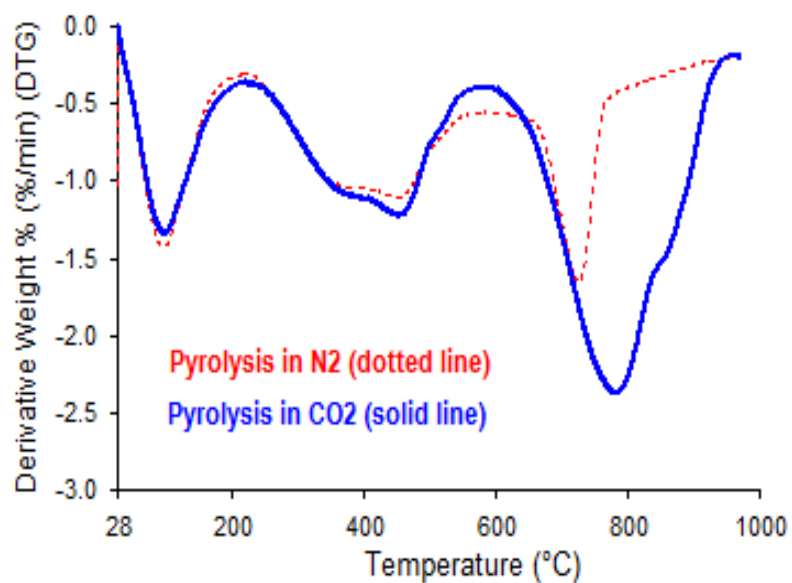


Fig. 4.2 DTG profiles of N<sub>2</sub> and CO<sub>2</sub> pyrolysis tests

Table 4.1 N<sub>2</sub> and CO<sub>2</sub> pyrolysis characteristics

	Pyrolysis in 100 % N <sub>2</sub>	Pyrolysis in 100 % CO <sub>2</sub>
<b>T<sub>in</sub> (°C)</b>	270	269
<b>T<sub>3max</sub> (°C)</b>	727	785
<b> <math>(\frac{dm}{dt})_{3max}</math> (%/min)</b>	1.74	2.44
<b>Total weight loss up to 980 °C (%)</b>	43.6	59.9

## 4.2 Effects of Catalysts

The possible impacts of different catalysts on pyrolysis of Kangal lignite in 100 % CO<sub>2</sub> ambient were investigated and the results are illustrated in Figs. 4.3 and 4.4 and listed in Table 4.2.  $T_{3\max}$  and  $|(dm/dt)_{3\max}|$  were related to the gasification of char. As illustrated in Table 4.2, although there was no considerable change in  $T_{3\max}$  during the char-CO<sub>2</sub> gasification reaction, the maximum weight loss rate of this process was influenced by the evolved catalysts. The K-based catalyst increased the maximum rate to 2.78 %/min, while the Ca- and Fe-based catalysts decreased this rate to 2.2 %/min and 2.35 %/min respectively in comparison with Raw-form pyrolysis rate, 2.44 %/min. Therefore, K<sub>2</sub>CO<sub>3</sub> found to be the most effective catalyst in char gasification in 100 % CO<sub>2</sub>. The catalytic gasification mechanism of K<sub>2</sub>CO<sub>3</sub> can be found elsewhere [35]. The total weight loss of the impregnated lignite samples was slightly higher than in Raw-form case which might be due to the direct influence of catalysts remained in the ash.

Table 4.2 Effects of catalysts in CO<sub>2</sub> pyrolysis

	Raw-form	Fe-form	Ca-form	K-form
$T_{3\max}$ (°C)	785	783	783	789
$ (dm/dt)_{3\max} $ (%/min)	2.44	2.35	2.20	2.78
Total weight loss up to 980 °C (%)	59.9	56.9	57.7	57.4

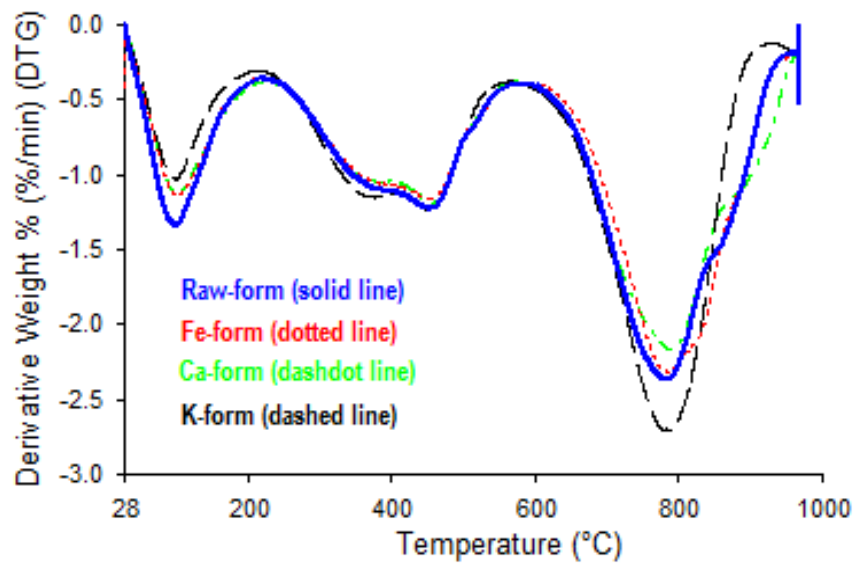


Fig. 4.3 DTG profiles of CO<sub>2</sub> pyrolysis tests with catalysts

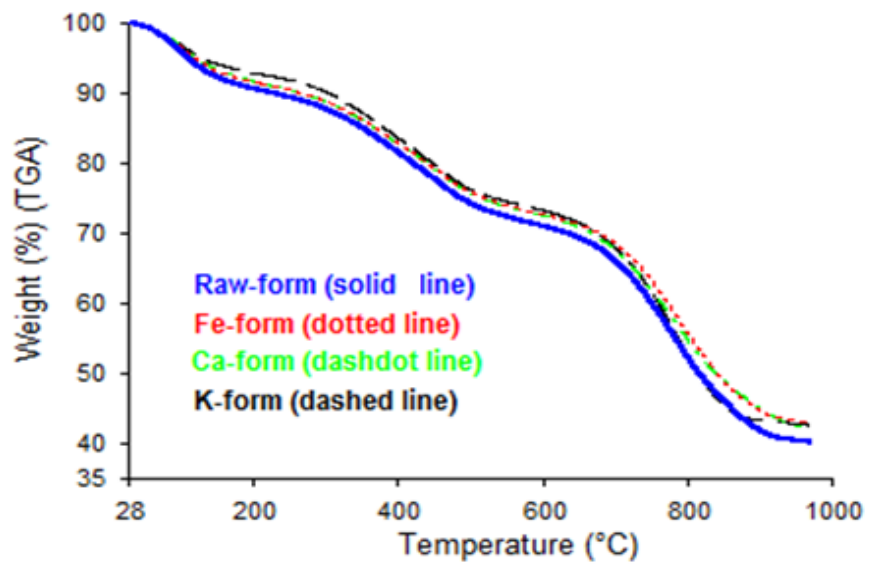


Fig. 4.4 TGA profiles of CO<sub>2</sub> pyrolysis tests with catalysts

### 4.3 FTIR Results

#### 4.3.1 Effects of N<sub>2</sub> and CO<sub>2</sub> Ambient Conditions

Formation profiles of evolved gases including CO<sub>2</sub>, CO, H<sub>2</sub>O, SO<sub>x</sub> and COS during pyrolysis tests in 100 % N<sub>2</sub> and 100 % CO<sub>2</sub> ambient conditions are reported and shown in Figs. 4.5 and 4.6. The evolved species of CH<sub>4</sub>, HCN, NO, N<sub>2</sub>O and HCl were not considered because these concentrations were below the sensible limits of FTIR during pyrolysis tests. In both ambient conditions, H<sub>2</sub>O peak was detected at around 100 °C due to moisture release and also in the temperature range of 200-750 °C with small peaks at 400 °C and 525 °C in 100 % N<sub>2</sub> and 100 % CO<sub>2</sub> ambient conditions respectively. In 100 % N<sub>2</sub>, CO<sub>2</sub> release started after 180 °C and continues until 780 °C with two strong peaks at 360 °C and 730 °C. In the case of low rank coals, CO<sub>2</sub> is formed from aliphatic and aromatic carboxyl and carboxylate groups at low temperatures. At high temperatures, however, CO<sub>2</sub> derive from thermally more stable ether structures, quinones and oxygen-bearing heterocycles [73]. In pyrolysis tests under 100 % CO<sub>2</sub> ambient, the evolution of CO started at 400 °C and reached a main peak at 800 °C. This peak zone was in a good agreement with the temperature at which the maximum reaction rates occurred in pyrolysis tests and confirms that in 100 % CO<sub>2</sub>, significant amount of CO was evolved from char-CO<sub>2</sub> gasification reaction ( $C(s) + CO_2(g) \leftrightarrow 2CO$ ). Therefore, formation of CO was found to be the major contributor to the evolved gases in CO<sub>2</sub> ambient with its highest absorbance intensity at high temperature zone. On the other hand, in 100 % N<sub>2</sub>, negligible amount of CO was formed due to partial burning of combustible matter which experienced a peak at 735 °C. In pyrolysis tests of high sulphur content lignite, SO<sub>2</sub> and COS releases were also noted. As indicated in Fig. 4.6, pyrolysis in 100 % CO<sub>2</sub> revealed that the evolution of SO<sub>x</sub> took place in high temperature zone, as the emission started at 900 °C and reached the maximum at 950 °C. In the case of 100 % N<sub>2</sub>, the SO<sub>x</sub> evolution occurred between 250 °C and 600 °C during which the corresponding absorbance intensity was much lower than the peak in 100 % CO<sub>2</sub> and this was in good agreement with Liu the literature. Liu et al. [8] reported that in 100 % N<sub>2</sub>, SO<sub>2</sub> would easily be formed and released at a lower temperature level and

more than half of the  $\text{SO}_2$  yield was observed at lower than  $600\text{ }^\circ\text{C}$ . Several studies have reported that the oxy-fuel process using recycled flue gas resulted in a higher concentration of  $\text{SO}_2$  which might be associated with higher amounts of secondary sulphur species ( $\text{SO}_3$ ,  $\text{H}_2\text{S}$ ,  $\text{COS}$ ) during the process. The other sulphur containing gas,  $\text{COS}$ , is formed by reaction of pyrite or sulphur formed during pyrite decomposition with  $\text{CO}$  [19].  $\text{COS}$  formation increased significantly with the initiation of gasification reaction in  $\text{CO}_2$  ambient and experienced three peaks at  $530\text{ }^\circ\text{C}$ ,  $780\text{ }^\circ\text{C}$  and  $910\text{ }^\circ\text{C}$ . Higher  $\text{CO}$  concentration in pyrolysis environment led to the higher formation of  $\text{COS}$  in  $100\% \text{CO}_2$ , in contrast to  $100\% \text{N}_2$  [19].

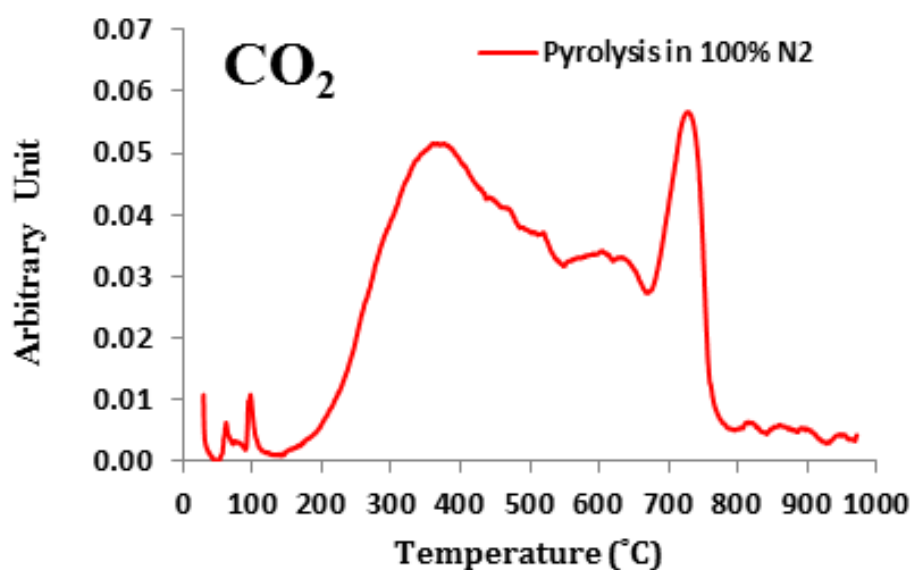


Fig. 4.5 Formation profile of  $\text{CO}_2$  during  $\text{N}_2$  pyrolysis test

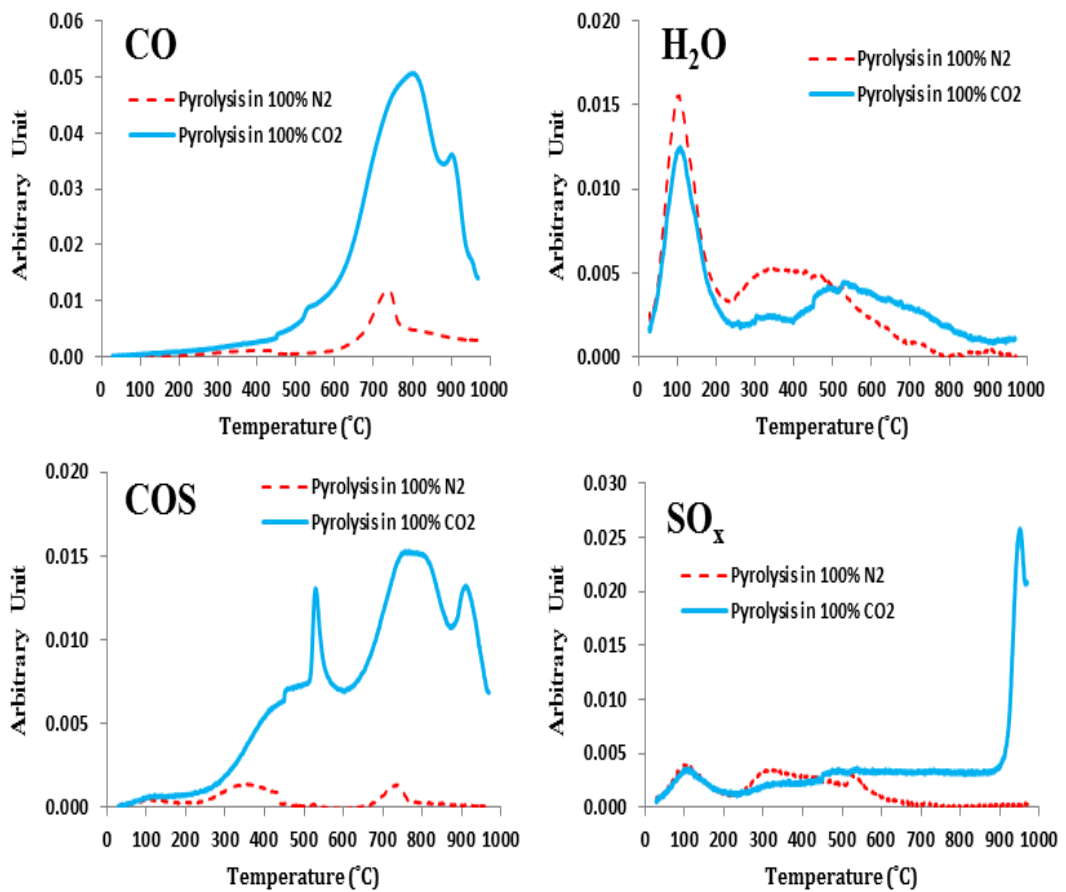


Fig. 4.6 Formation profiles of evolved gases during N<sub>2</sub> and CO<sub>2</sub> pyrolysis tests

### 4.3.2 Effects of Catalysts in CO<sub>2</sub> Pyrolysis

In the catalytic pyrolysis tests, Fe<sub>2</sub>O<sub>3</sub>, Ca(OH)<sub>2</sub> and K<sub>2</sub>CO<sub>3</sub> compounds were used as precursors of Fe, Ca and K catalysts respectively to form Fe-form, Ca-form and K-form samples. The effects of these catalysts on the formation profiles of evolved gases including CO and COS were investigated in 100 % CO<sub>2</sub> which is the main diluting gas in oxy-fuel condition and the results are shown in Fig. 4.7. The formation profiles of CO decreased in the cases of all the catalysts with an extra peak at 900 °C for Fe<sub>2</sub>O<sub>3</sub>. However, the Ca-based catalyst was the most effective, since

$\text{Ca(OH)}_2$  catalyzed the water-gas shift reaction, resulting in the decrease of CO [31]. Sulphur containing gases, COS, appeared in the FTIR spectra. COS is formed by reaction of pyrite or sulphur formed during pyrite decomposition with CO [19]. COS formation increased significantly with the initiation of gasification reaction at 720 °C in 100 %  $\text{CO}_2$ . Higher CO concentration in pyrolysis environment led to the formation of COS in 100 %  $\text{CO}_2$ , in contrast to 100 %  $\text{N}_2$ . The evolution of COS decreased in the case of all the catalysts and maximum release was observed at 780 °C.  $\text{Ca(OH)}_2$  and CaO were reported to be quite effective in capturing the sulfur-containing gases by Guan et al. [42]. COS evolution profiles experienced three peaks in the cases of Raw- and Fe- form samples at 530 °C, 780 °C and 910 °C. Two main peaks were observed in the cases of Ca- and K-based catalyst. The effects of the evolved catalysts on  $\text{SO}_x$  formation were not reported since  $\text{SO}_x$  evolution mainly occurs in the temperature regions beyond the limitations of our TGA-FTIR system.

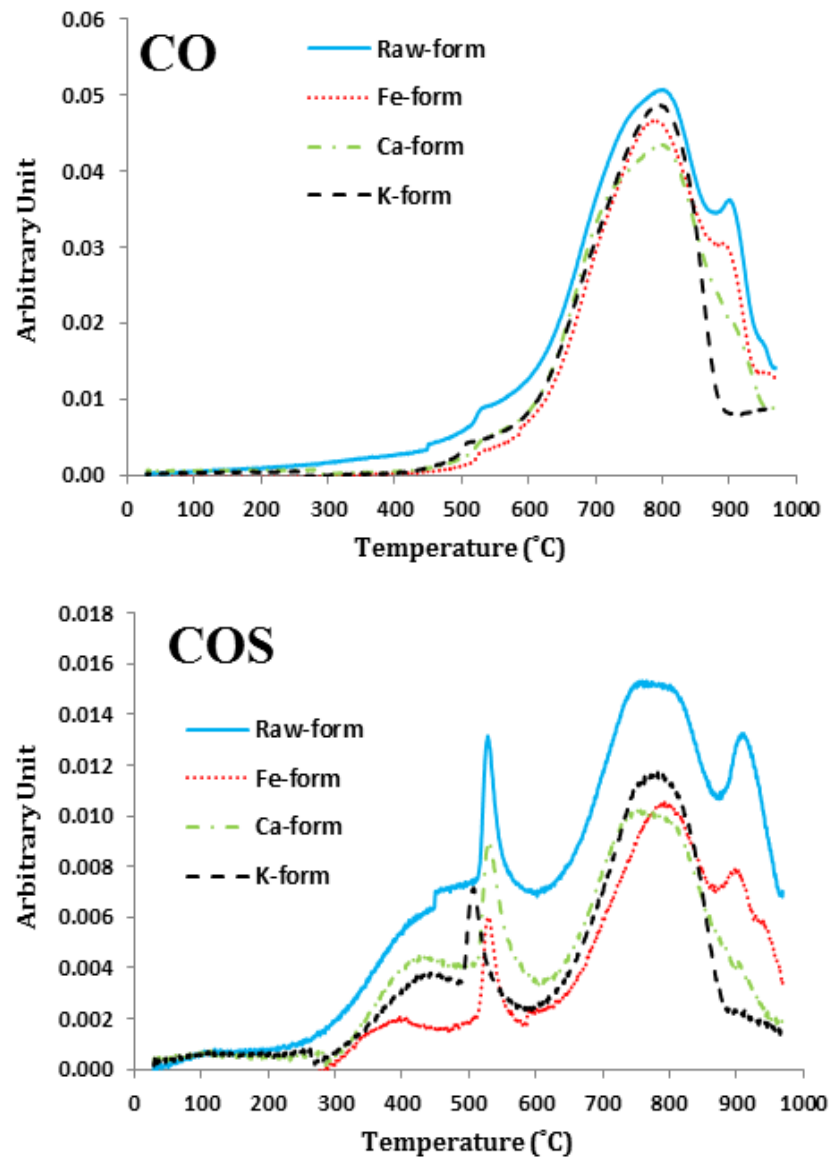


Fig. 4.7 Formation profiles of CO and COS evolved gases during CO<sub>2</sub> pyrolysis tests with catalysts

## CHAPTER 5

### TGA-FTIR COMBUSTION TESTS

Kangal lignite and Tunçbilek sub-bituminous samples were selected to be used in TGA-FTIR studies of combustion tests. In catalytic combustion tests,  $\text{Fe}_2\text{O}_3$ ,  $\text{Ca}(\text{OH})_2$  and  $\text{K}_2\text{CO}_3$  compounds were used as precursors of Fe, Ca and K catalysts respectively to form Fe-form, Ca-form and K-form samples. Combustion tests of raw and impregnated coal samples were carried out in air (21 %  $\text{O}_2$  in  $\text{N}_2$ ), oxygen-enriched air (25 %  $\text{O}_2$  in  $\text{N}_2$ , 30 %  $\text{O}_2$  in  $\text{N}_2$ , 35 %  $\text{O}_2$  in  $\text{N}_2$ ), oxy-fuel environment with equivalent oxygen concentration as in air (21 %  $\text{O}_2$  in  $\text{CO}_2$ ) and oxygen-enriched oxy-fuel environments (25 %  $\text{O}_2$  in  $\text{CO}_2$ , 30 %  $\text{O}_2$  in  $\text{CO}_2$ , 35 %  $\text{O}_2$  in  $\text{CO}_2$ ). Previous studies on oxy-fuel combustion mainly revealed that the overall  $\text{O}_2$  concentration at the inlet to the boiler should be between 27 and 35 vol % in order to yield comparable adiabatic flame temperatures (AFT) and heat transfer profiles as seen for conventional combustion in air [12]. This oxygen mole fraction range was used as a main reference in comparative analyses.

DTG profiles throughout the analysis of combustion tests were smoothed using 10 points window and *standard smoothing algorithm* (Pyris Software). Furthermore, FTIR profiles are illustrated while smoothed using *exponential smoothing* method under damping factor of 0.5 in order to have optimum view of the profiles without underestimating the values.

The characteristic temperatures of  $T_{\text{ig}}$ ,  $T_{2\text{max}}$ ,  $T_{\text{b}}$ ,  $T_{\text{FG-max}}$  along with  $|(\text{dm}/\text{dt})_{2\text{max}}|$  (%/min) (absolute value of the maximum rate of weight loss in the second region) and maximum absorbance (arbitrary unit) of the evolved gases are investigated to

explore the effects of N<sub>2</sub> and CO<sub>2</sub> diluting gases, oxygen mole fractions and catalysts on combustion characteristics and evolution of the evolved gases during combustion tests.

### **5.1 TGA/DTG Profiles of Kangal Lignite and Tunçbilek Sub-Bituminous Samples (Combustion Tests)**

TGA and DTG profiles of combustion tests performed by Kangal lignite and Tunçbilek sub-bituminous samples in air and 30 % O<sub>2</sub> in CO<sub>2</sub> are illustrated in Figs. 5.1 and 5.2 respectively. In air combustion case, as illustrated in Fig. 5.1, three stages of weight loss were observed separately in Kangal lignite DTG curve. Since the higher volatile matter content of Kangal lignite (41.66 % dry basis) with respect to Tunçbilek sub-bituminous sample (28.57 % dry basis) led to oxidation and removal of volatile matters in lower temperature zone (200-500 °C) and prior to the sufficient temperature required for starting the char combustion. However, in Tunçbilek sub-bituminous combustion tests, the main weight loss occurred during the temperature interval of 200-550 °C and devolatilization and char burning steps are not discretely separated. The maximum rate of weight loss in the second region ( $|(dm/dt)_{2max}|$ ) and the corresponding temperature ( $T_{2max}$ ) was observed to be much higher in the case of Tunçbilek providing higher temperature medium for char combustion which was thought to be the reason of continuous devolatilization and char oxidation regions. However, a slight peak at around 590 °C might be due to the char combustion remaining after the first stage of volatile and char combustion.  $T_b$  was observed to be considerably lower in Tunçbilek combustion in air with respect to Kangal lignite combustion. The total weight loss was reported to be almost the same in both samples.

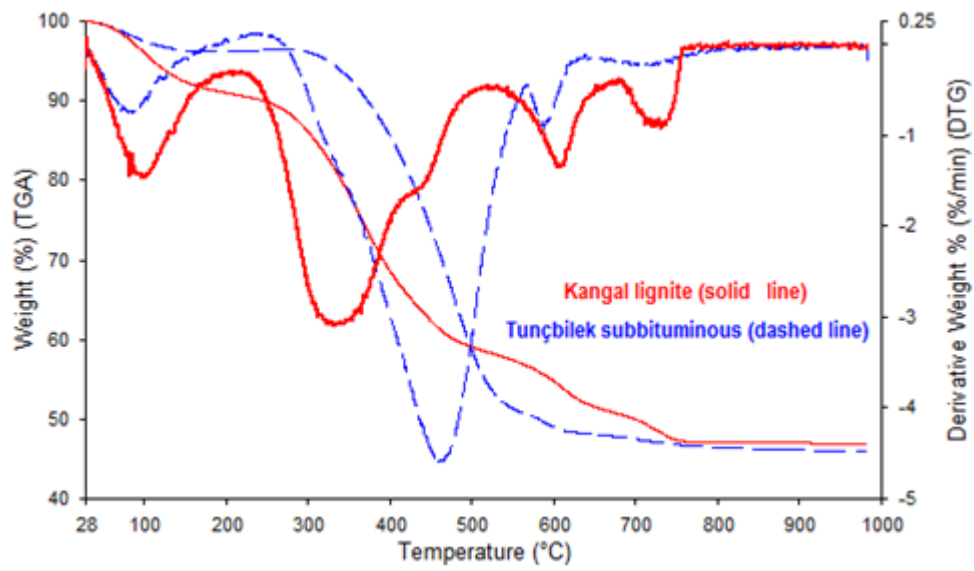


Fig. 5.1 Combustion profiles of Kangal and Tunçbilek samples in air

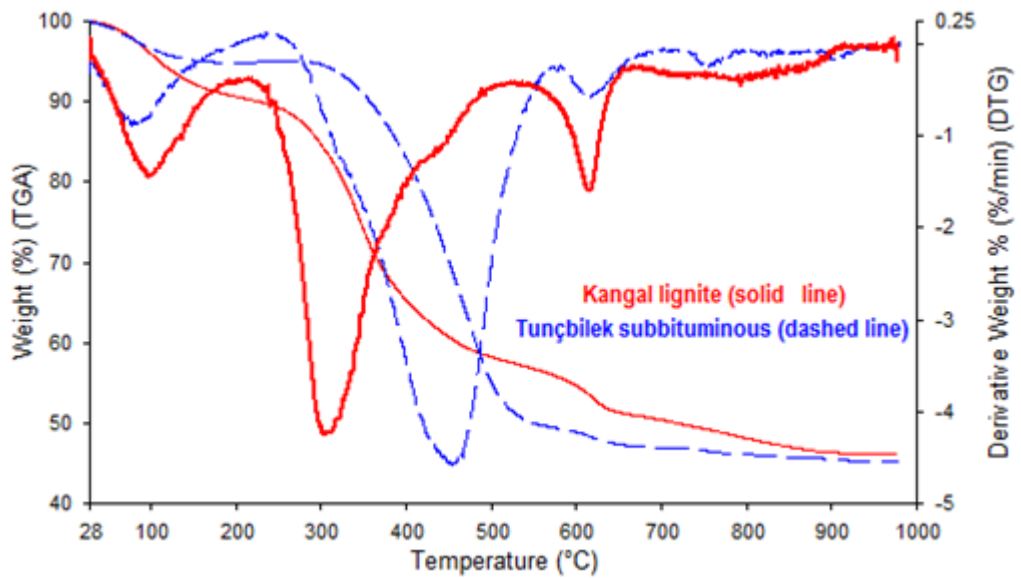


Fig. 5.2 Combustion profiles of Kangal and Tunçbilek samples in 30% O<sub>2</sub> in CO<sub>2</sub> ambient

In the combustion tests carried out in 30 % O<sub>2</sub> in CO<sub>2</sub>, T<sub>2max</sub> was considerably lower in lignite than in sub-bituminous (304 °C versus 457 °C). However a slight change in |(dm/dt)<sub>2max</sub>| was observed in DTG curves of these two samples.

## 5.2 Combustion Tests of Kangal Lignite

### 5.2.1 Effects of N<sub>2</sub> and CO<sub>2</sub> Diluting Gases in Different Oxygen Mole Fractions (TGA/DTG Results)

The TGA/DTG curves indicated in Figs. 5.3 to 5.6 are profiles to analyze the effects of the diluting gas on combustion characteristics of lignite in various oxygen concentrations. Ignition temperature, combustion rate and burnout behavior were determined for evaluation of combustion reactivity in both second and third regions. The lower the ignition temperature and the higher the maximum combustion rate, the better the reactivity. The similarity in TGA/DTG profiles obtained at the same oxygen concentration levels but with different ambient conditions was an expected result. During the combustion tests in O<sub>2</sub>/N<sub>2</sub> and O<sub>2</sub>/CO<sub>2</sub> mixtures, the mass losses of around 9 %, 33 % and 11 % took place in the first, second and third regions respectively. Therefore, the second region is the most important region to examine since the major mass loss and complicated chemical reactions, such as formation of liquid and gaseous products, occur in this interval.

T<sub>ig</sub> and T<sub>2max</sub> were higher in all the oxygen mole fractions (except for 30 % O<sub>2</sub>) during combustion tests in N<sub>2</sub> with respect to CO<sub>2</sub> ambient. These differences were more significant in 21 % O<sub>2</sub> (Table 5.1) during which 11 °C and 13 °C of temperature difference was experienced in the cases of T<sub>ig</sub> and T<sub>2max</sub> respectively. However, these results are not supported by previous studies, since they do not agree with the expected delay in oxy-fuel combustion in most of the oxygen concentrations. In TGA technique combustion temperature of the sample is controlled by electrical heating and sample temperature is not affected by combustion environment effectively. Therefore, different heat capacities of diluting gases in combustion environment has no significant effect on combustion in contrast to practical tests as also confirmed by

Rathnam et al. [14]. As illustrated in Fig. 5.7 and with regard to each oxygen concentration, although the maximum reaction rate ( $|(dm/dt)_{2max}|$  (%/min)) was slightly higher in 21 % O<sub>2</sub> in CO<sub>2</sub> than in air combustion, in elevated oxygen cases (25 %, 30 % and 35 %),  $|(dm/dt)_{2max}|$  were higher in O<sub>2</sub>/N<sub>2</sub> ambient. The maximum reaction rates in O<sub>2</sub>/N<sub>2</sub> corresponded 3.72 %/min, 6.72 %/min and 11.34 %/min with increasing oxygen concentration from 25 % to 35 % respectively. Therefore, the higher reactivity of the sample in 21 % O<sub>2</sub> in CO<sub>2</sub> ambient was confirmed by the lower T<sub>ig</sub> and T<sub>2max</sub> in addition with higher  $|(dm/dt)_{2max}|$ . Accordingly, the higher reactivity of the sample in 30 % O<sub>2</sub> in N<sub>2</sub> ambient was confirmed by the lower T<sub>ig</sub> and T<sub>2max</sub> in addition with higher  $|(dm/dt)_{2max}|$ . T<sub>b</sub> was independent from oxygen concentration and showed to be 640 °C and 750 °C in O<sub>2</sub>/CO<sub>2</sub> and O<sub>2</sub>/N<sub>2</sub> ambient conditions respectively. This result was in agreement with Rathnam et al. [14] in which two coal types showed significant improvements in burnout during oxy-fuel conditions compared to air conditions. In O<sub>2</sub>/N<sub>2</sub> case, the third region of DTG profiles differed from the oxy-fuel case. In this region, the DTG profile of N<sub>2</sub> diluting combustion case experienced another peak that was not seen in oxy-fuel case.

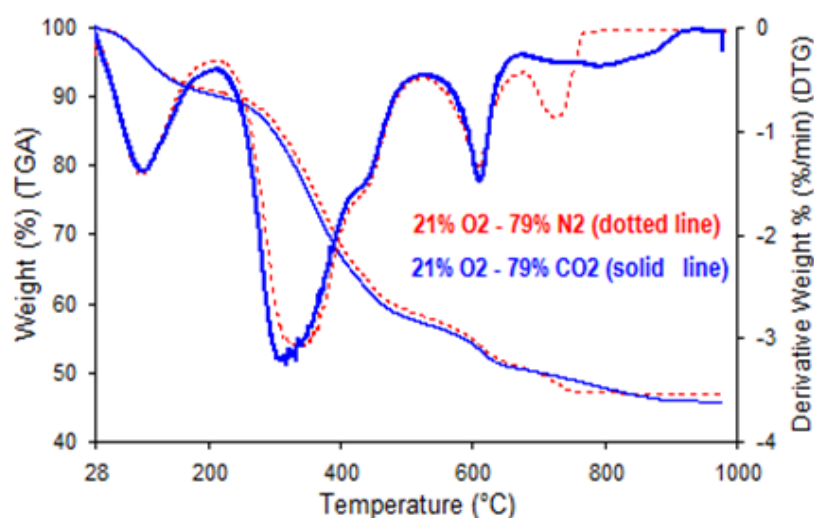


Fig. 5.3 TGA and DTG profiles of Kangal lignite combustion during 21 % O<sub>2</sub> in N<sub>2</sub> and 21 % O<sub>2</sub> in CO<sub>2</sub> ambient conditions

Table 5.1 Characteristic parameters of Kangal lignite combustion in 21 % O<sub>2</sub>

	21 % O <sub>2</sub> -79 % N <sub>2</sub>	21 % O <sub>2</sub> -79 % CO <sub>2</sub>
T <sub>in</sub> (°C)	243	234
T <sub>ig</sub> (°C)	287	276
T <sub>2max</sub> (°C)	332	319
T <sub>b</sub> (°C)	751	639
(dm/dt) <sub>2max</sub>  (%/min)	3.01	3.28

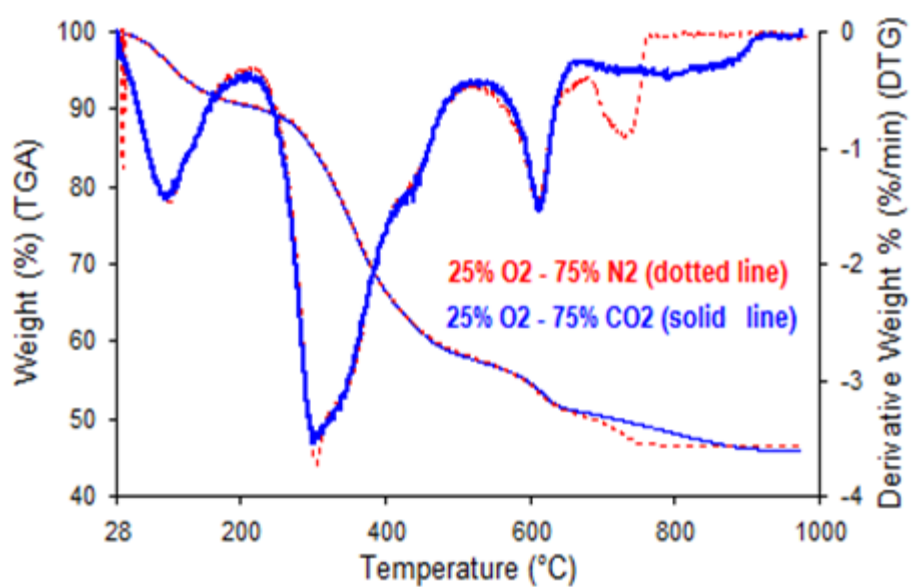


Fig. 5.4 TGA and DTG profiles of Kangal lignite combustion during 25 % O<sub>2</sub> in N<sub>2</sub> and 25 % O<sub>2</sub> in CO<sub>2</sub> ambient conditions

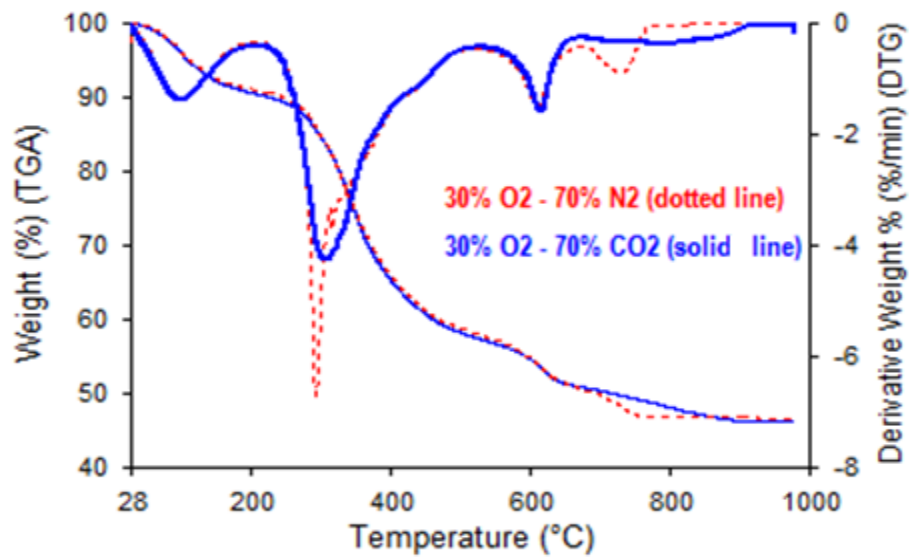


Fig. 5.5 TGA and DTG profiles of Kangal lignite combustion during 30 % O<sub>2</sub> in N<sub>2</sub> and 30 % O<sub>2</sub> in CO<sub>2</sub> ambient conditions

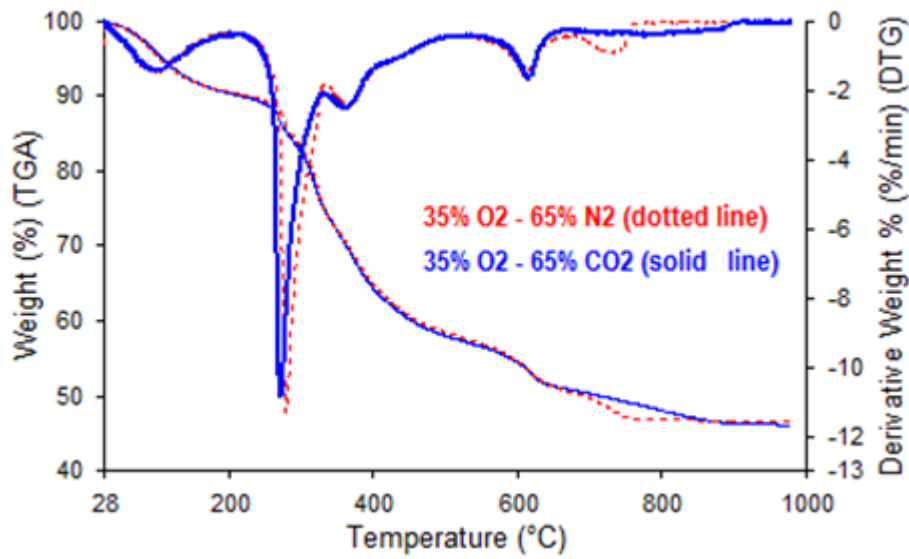


Fig. 5.6 TGA and DTG profiles of Kangal lignite combustion during 35 % O<sub>2</sub> in N<sub>2</sub> and 35 % O<sub>2</sub> in CO<sub>2</sub> ambient conditions

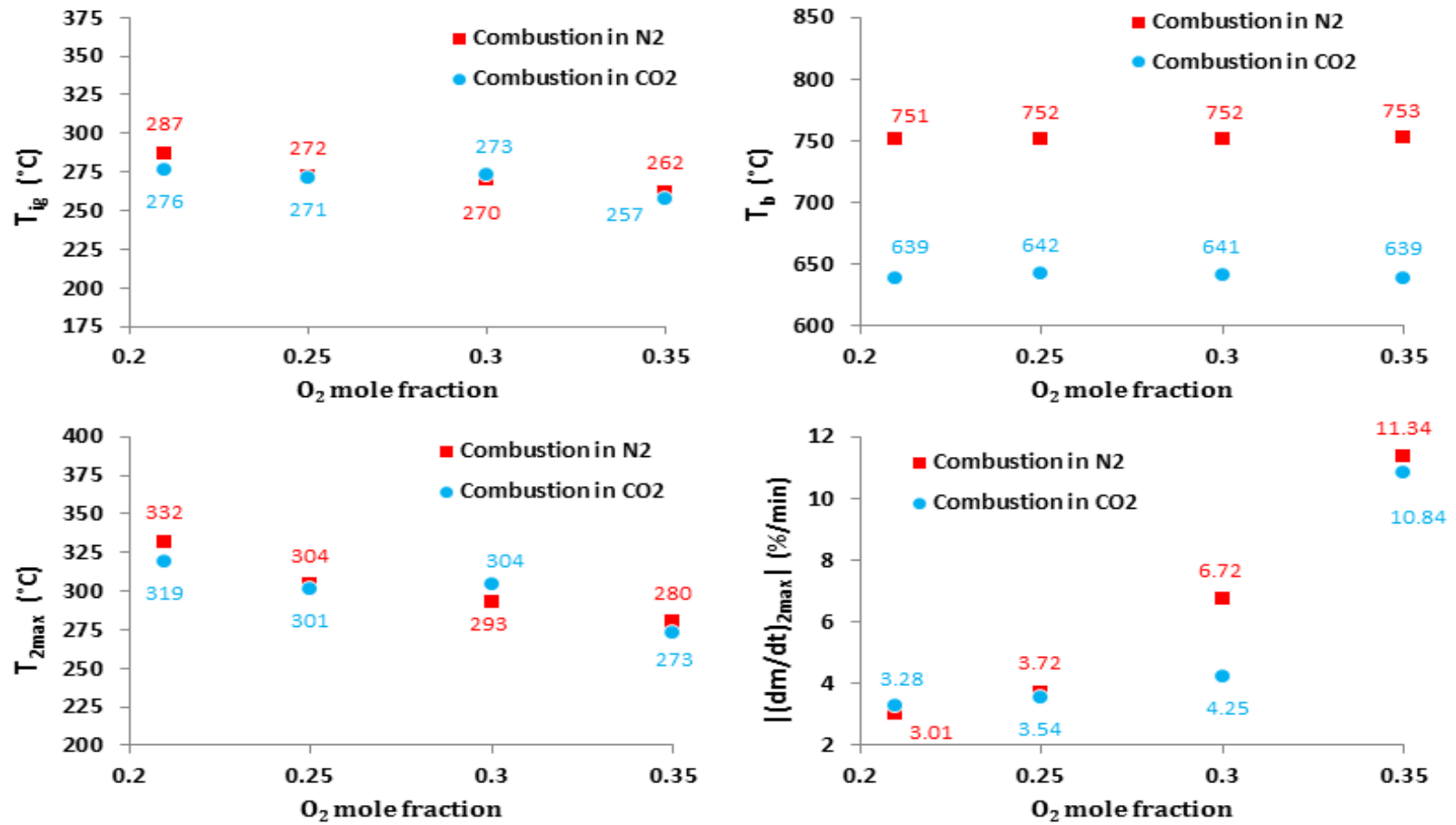


Fig. 5.7 Maximum reaction rates in the second region and characteristic temperatures of lignite combustion tests in various oxygen mole fractions in both  $N_2$  and  $CO_2$  ambient conditions

### 5.2.2 Effects of N<sub>2</sub> and CO<sub>2</sub> Ambient Conditions (FTIR Results)

In this section, the possible impacts of different ambient conditions on evolution of combustion gases are investigated through FTIR tests. Formation profiles of evolved gases including CO, H<sub>2</sub>O, SO<sub>x</sub> and COS during combustion tests in air and 21 % O<sub>2</sub> in CO<sub>2</sub> ambient are illustrated in Fig. 5.8 and the results are listed in Table 5.2. In both ambient conditions, two peaks were detected at 350 °C and 610 °C in CO evolution profiles for which the first peak occurred with 24 °C and 30 °C delay in N<sub>2</sub> and CO<sub>2</sub> ambient conditions respectively in comparison with T<sub>2max</sub> in the second region. Actually, required time for the transfer of combustion gases from the Thermogravimetric Analyzer to the gas cell of FTIR spectrometer caused a delay between the TGA result and the corresponding IR spectra. However, a good agreement was observed between the second peak and the maximum rate of weight loss due to char combustion in the third region. H<sub>2</sub>O evolution profiles have two peaks at 100 °C and 325 °C in both ambient conditions for which the first peak was due to the primary moisture release. These two peaks were in good agreement with DTG curves. Sulphur containing emissions are mainly related to the sulphur content of the sample which was relatively high (~ 4 %) in Kangal lignite. SO<sub>x</sub> and COS profiles had their single peaks at 315 °C and 325 °C respectively with an extra shoulder at 400 °C in the case of SO<sub>x</sub>. The first slight peak at 100 °C in SO<sub>x</sub> formation profiles was more likely to be related to the water vapor emissions. In the general case, the emission of CO, H<sub>2</sub>O, SO<sub>x</sub> and COS gases in this oxygen concentration was slightly higher in oxy-fuel conditions with respect to normal air combustion as |(dm/dt)<sub>2max</sub>| increased from 3.01 %/min to 3.28 %/min. During the test conditions, no considerable emissions were detected in temperatures above 700 °C as CH<sub>4</sub> and HCl concentrations were too low to be traced in this oxygen mole fraction.

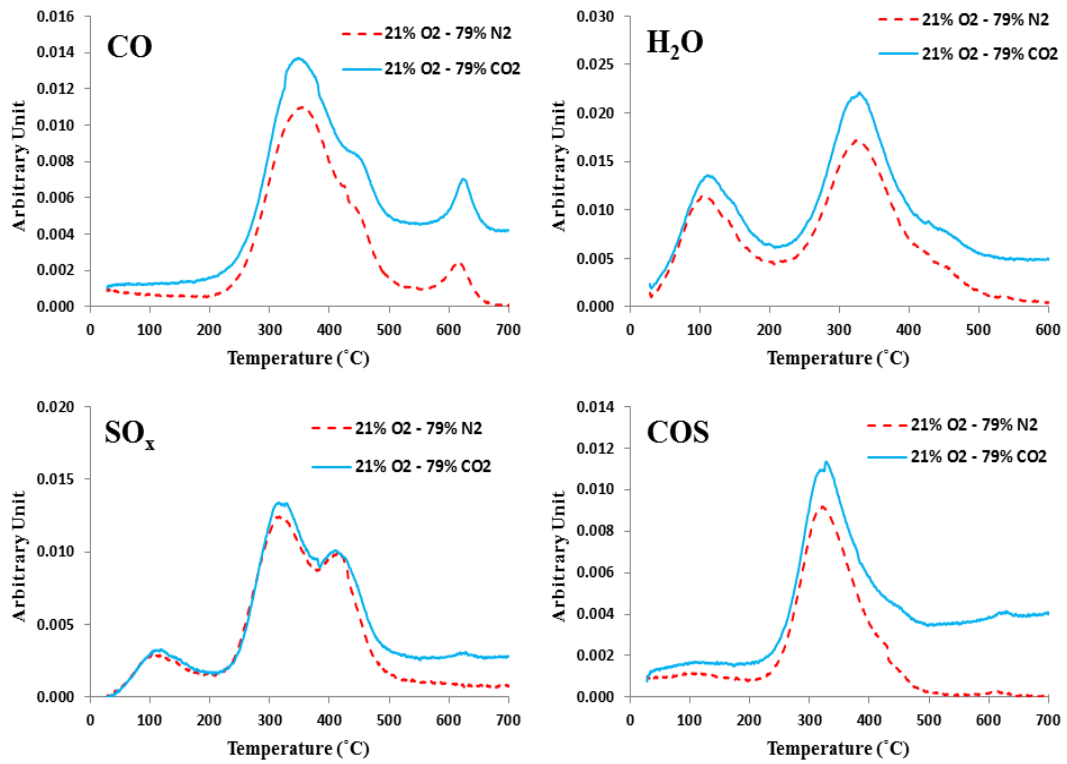


Fig. 5.8 Formation profiles of evolved gases during combustion tests in air and in 21 % O<sub>2</sub> in CO<sub>2</sub> ambient

Table 5.2 Characteristic parameters of evolved gases during combustion tests in 21 % O<sub>2</sub>

Flue Gases	21 % O <sub>2</sub> -79 % N <sub>2</sub>		21 % O <sub>2</sub> -79 % CO <sub>2</sub>	
	T <sub>FG-max</sub> (°C)	Max. Absorbance (Arbitrary Unit)	T <sub>FG-max</sub> (°C)	Max. Absorbance (Arbitrary Unit)
<b>CO</b>	356	1.10E-2	349	1.37E-2
<b>H<sub>2</sub>O</b>	324	1.72E-2	329	2.21E-2
<b>SO<sub>x</sub></b>	316	1.27E-2	315	1.41E-2
<b>COS</b>	321	9.18E-3	329	1.13E-2
T <sub>2max</sub> (°C) = 332		(dm/dt) <sub>2max</sub>  (%/min) = 3.01	T <sub>2max</sub> (°C) = 319	
			(dm/dt) <sub>2max</sub>  (%/min) = 3.28	

Formation profiles of gases during combustion tests in elevated oxygen mole fraction in N<sub>2</sub> and in CO<sub>2</sub> ambient conditions (30 % O<sub>2</sub>) are illustrated in Fig. 5.9 and the results are listed in Table 5.3. In these elevated oxygen tests, the CO peak and T<sub>FG-max</sub> were higher in O<sub>2</sub>/CO<sub>2</sub>. On the contrary, the evolution profiles of H<sub>2</sub>O, SO<sub>x</sub> and COS experienced sharper peaks with higher maximum absorbance and lower corresponding temperatures in N<sub>2</sub> rather than CO<sub>2</sub> ambient conditions. Therefore, a good agreement was seen with T<sub>2max</sub> and |(dm/dt)<sub>2max</sub>| where the maximum reaction rate due to the devolatilization was remarkably higher (6.72 %/min ) and T<sub>2max</sub> was lower (293 °C) in O<sub>2</sub>/N<sub>2</sub> with respect to O<sub>2</sub>/CO<sub>2</sub> which was 4.25 %/min and 304 °C respectively. In the general case, a delay was reported for T<sub>FG-max</sub> which was higher for T<sub>2max</sub> in the case of all the evolved gases in 30 % O<sub>2</sub> in both N<sub>2</sub> and CO<sub>2</sub> ambient conditions.

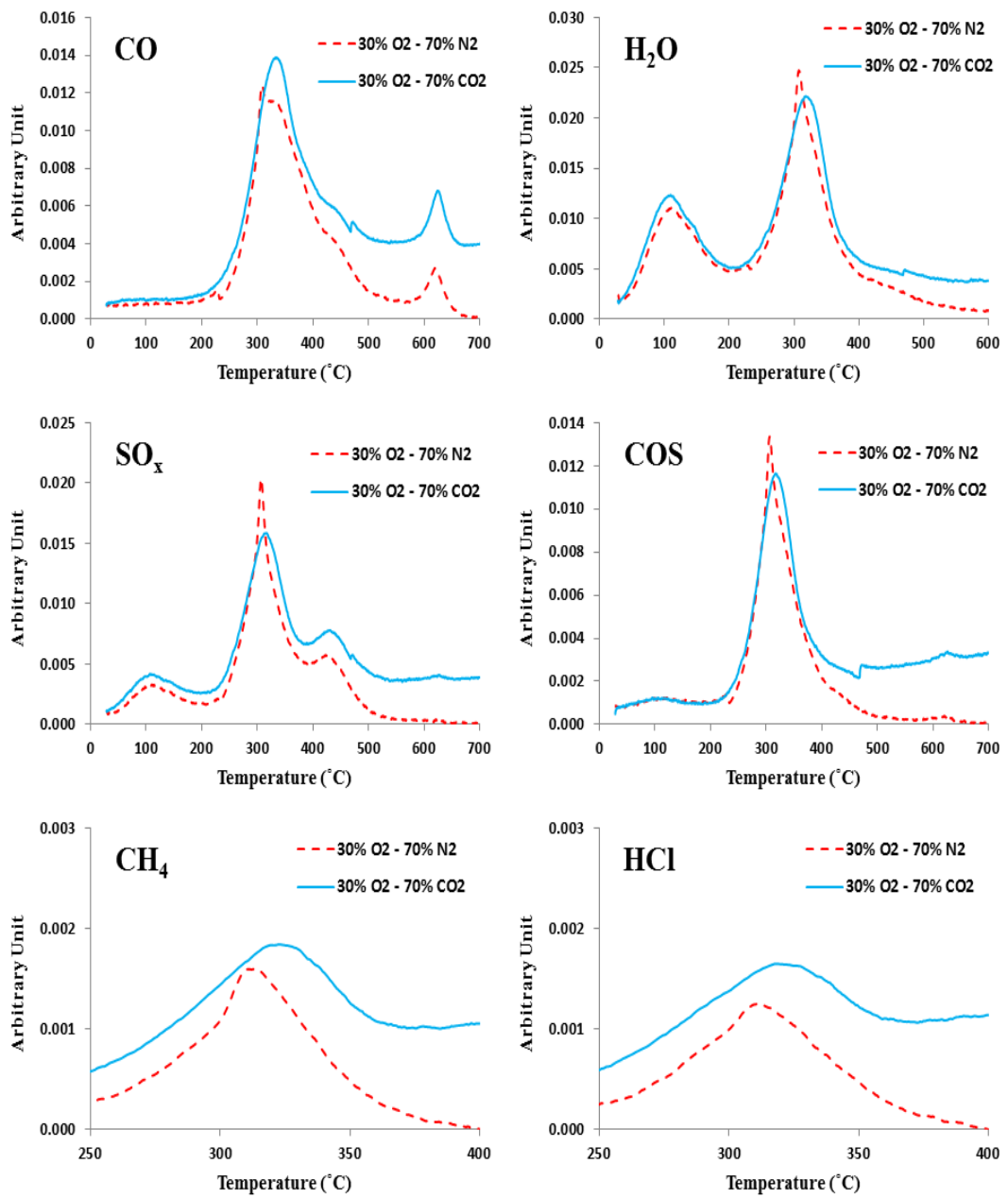


Fig. 5.9 Formation profiles of evolved gases during combustion tests in 30 % O<sub>2</sub> in N<sub>2</sub> and 30 % O<sub>2</sub> in CO<sub>2</sub> ambient conditions

The evolutions of CH<sub>4</sub> and HCl were also examined. HCl formation during combustion tests is mainly contributed to the Cl content and one possibility is that the water vapor decomposes into H<sup>+</sup> and OH<sup>-</sup> ions, with OH<sup>-</sup> substituting for the Cl<sup>-</sup> in the inorganic compounds, and the substituted Cl<sup>-</sup> combines with H<sup>+</sup> to produce HCl [39]. During these experiments, the higher maximum absorbance at the higher corresponding temperatures was observed for both CH<sub>4</sub> and HCl in oxy-fuel conditions. However, weak peaks were observed for CH<sub>4</sub> for which the main reason might be lower aliphatic chains to produce light hydrocarbons.

Table 5.3. Characteristic parameters of evolved gases during combustion tests in 30 % O<sub>2</sub>

Flue Gases	30 % O <sub>2</sub> -70 % N <sub>2</sub>		30 % O <sub>2</sub> -70 % CO <sub>2</sub>				
	T <sub>FG-max</sub> (°C)	Max. Absorbance (Arbitrary Unit)	T <sub>FG-max</sub> (°C)	Max. Absorbance (Arbitrary Unit)			
<b>CO</b>	309	1.24E-2	334	1.39E-2			
<b>H<sub>2</sub>O</b>	307	2.47E-2	319	2.22E-2			
<b>SO<sub>x</sub></b>	307	2.04E-2	315	1.63E-2			
<b>COS</b>	306	1.34E-2	317	1.16E-2			
<b>CH<sub>4</sub></b>	313	1.06E-3	322	1.84E-3			
<b>HCl</b>	311	1.25E-3	319	1.65E-3			
T <sub>2max</sub> (°C) = 293		(dm/dt) <sub>2max</sub>  (%/min) = 6.72		T <sub>2max</sub> (°C) = 304		(dm/dt) <sub>2max</sub>  (%/min) = 4.25	

### 5.2.3 Effects of Different Oxygen Mole Fractions (TGA/DTG Results)

DTG and TGA curves indicated in Figs. 5.10- 5.13 are derived to explore the effects of oxygen mole fractions of 21 %, 25 %, 30 % and 35% on the combustion characteristics of Kangal lignite in both N<sub>2</sub> and CO<sub>2</sub> ambient conditions and the results are also listed in Tables 5.4 and 5.5. Comparison of DTG curves in Figs. 5.10 and 5.12 indicated that the effect of oxygen concentration was more significant than that of the diluting gas (N<sub>2</sub> or CO<sub>2</sub>) on the combustion profiles. While combustion in O<sub>2</sub>/N<sub>2</sub> and O<sub>2</sub>/CO<sub>2</sub> mixtures with identical oxygen concentrations resulted in only slight differences in combustion characteristics of lignite, elevated oxygen levels in combustion ambient shifted the weight loss curves to lower temperature zone accompanied with much higher reaction rates. In some studies, it was demonstrated that the force of the fusion layer around solid particles is reduced by the presence of oxygen [55, 74]. This situation also results in the faster release of volatiles depending on the nature of solid particles and experimental conditions. High volatile matter content of lignite and the ease with which it is released, result in the formation of a sharper preliminary peak previously observed in low rank coals [75]. As illustrated in Figs. 5.10 and 5.12, similar trends in the early stage of the process (up to 250 °C) in both ambient conditions revealed that the initiation of the combustion process is not affected by oxygen concentration level. But at higher temperatures and in the second region (200 -520 °C), more significant differences were displayed in DTG curves and these profiles were clearly different in this region of combustion. Furthermore, it was observed that when the oxygen concentration increased, the process of combustion of samples varied from a single stage to double stages in this temperature interval. No difference was observed in the third region of combustion at the elevated oxygen concentration. Total weight loss of the lignite samples was found to be almost the same in all combustion cases. Effects of oxygen concentration on characteristic temperatures are very clear. T<sub>ig</sub> decreased from 287 °C to 262 °C and from 276 °C to 257 °C as the oxygen concentration was increased from 21 % to 35 % in O<sub>2</sub>/N<sub>2</sub> and O<sub>2</sub>/CO<sub>2</sub> respectively. Furthermore, T<sub>2max</sub> dropped considerably from 332 °C to 280 °C and from 319 °C to 273 °C and the maximum reaction rates increased

significantly from 3.01 %/min to 11.34 %/min and from 3.28 %/min to 10.84 %/min as the oxygen concentration was increased from 21 % to 35 % in O<sub>2</sub>/N<sub>2</sub> and O<sub>2</sub>/CO<sub>2</sub> ambient conditions respectively. Therefore, the reactivity of the sample increased by increasing the oxygen mole fraction from 21 % to 35 % and complete combustion was achieved at lower temperatures and shorter times. T<sub>b</sub> did not change considerably during these tests.

Table 5.4 Characteristic parameters of Kangal lignite combustion in N<sub>2</sub> ambient

	21 % O <sub>2</sub> -79 % N <sub>2</sub>	25 % O <sub>2</sub> -75 % N <sub>2</sub>	30 % O <sub>2</sub> -70 % N <sub>2</sub>	35 % O <sub>2</sub> -65 % N <sub>2</sub>
T <sub>in</sub> (°C)	243	242	239	237
T <sub>ig</sub> (°C)	287	272	270	262
T <sub>2max</sub> (°C)	332	304	293	280
T <sub>b</sub> (°C)	751	752	752	753
<b>(dm/dt)<sub>2max</sub></b>  (%/min)	3.01	3.72	6.72	11.34
T <sub>3max</sub> (°C)	608	610	612	614
<b>(dm/dt)<sub>3max</sub></b>  (%/min)	1.35	1.47	1.52	1.51

Table 5.5 Characteristic parameters of Kangal lignite combustion in CO<sub>2</sub> ambient

	21 % O <sub>2</sub> -79 % CO <sub>2</sub>	25 % O <sub>2</sub> -75 % CO <sub>2</sub>	30 % O <sub>2</sub> -70 % CO <sub>2</sub>	35 % O <sub>2</sub> -65 % CO <sub>2</sub>
T <sub>in</sub> (°C)	234	235	239	233
T <sub>ig</sub> (°C)	276	271	273	257
T <sub>2max</sub> (°C)	319	301	304	273
T <sub>b</sub> (°C)	639	642	641	639
<b>(dm/dt)<sub>2max</sub></b>  (%/min)	3.28	3.54	4.25	10.84
T <sub>3max</sub> (°C)	611	613	617	615
<b>(dm/dt)<sub>3max</sub></b>  (%/min)	1.49	1.55	1.60	1.65

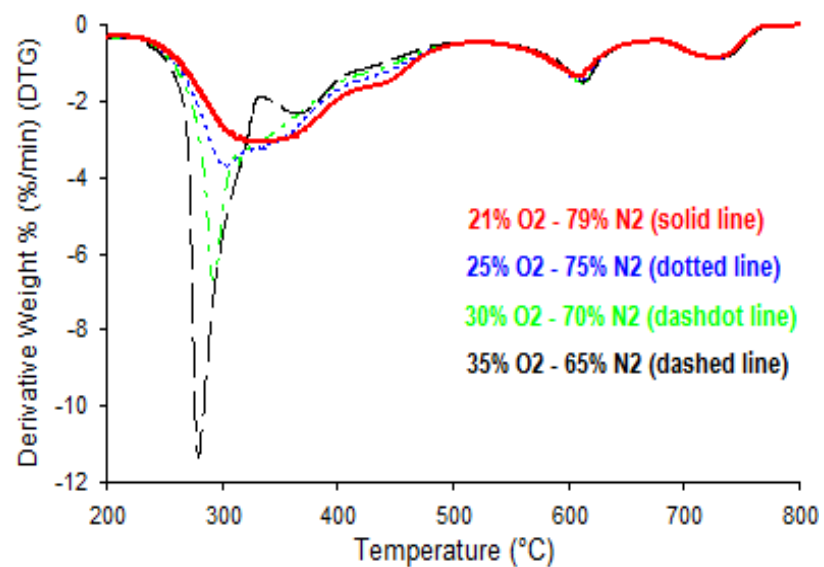


Fig. 5.10 DTG profiles of Kangal lignite under various oxygen mole fractions in N<sub>2</sub> ambient

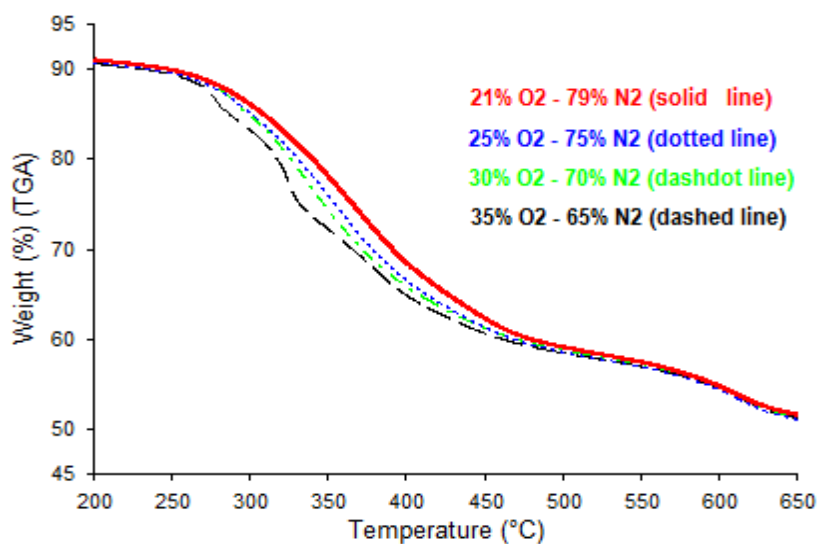


Fig. 5.11 TGA profiles of Kangal lignite under various oxygen mole fractions in N<sub>2</sub> ambient

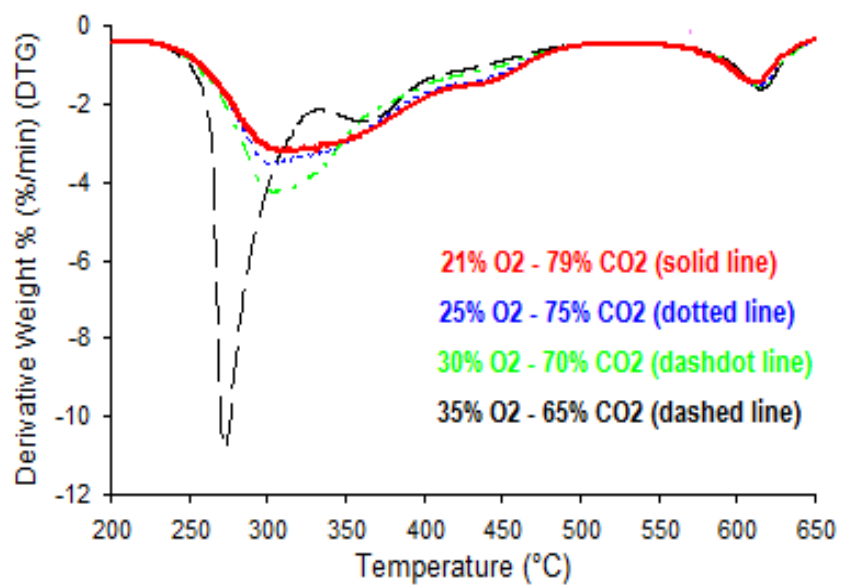


Fig. 5.12 DTG profiles of Kangal lignite under various oxygen mole fractions in CO<sub>2</sub> ambient

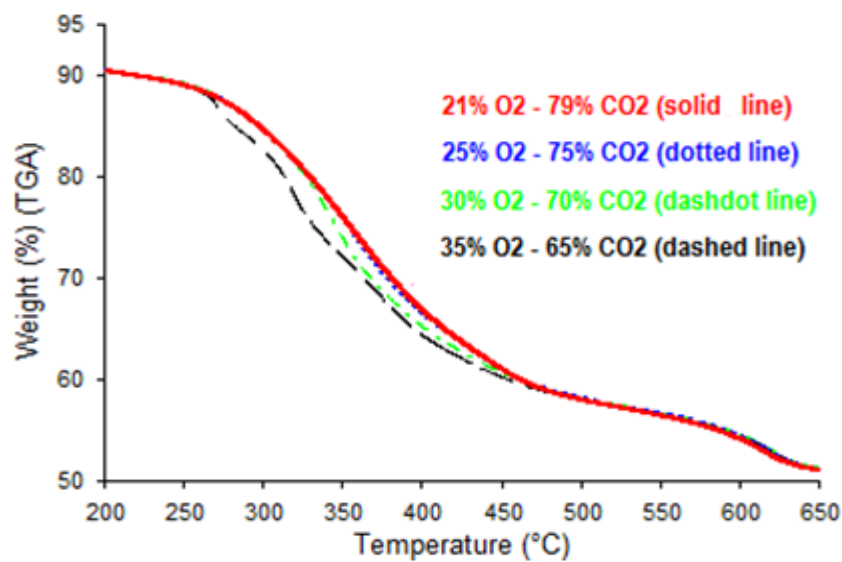


Fig. 5.13 TGA profiles of Kangal lignite under various oxygen mole fractions in CO<sub>2</sub> ambient

#### 5.2.4 Effects of Different Oxygen Mole Fractions (FTIR Results in N<sub>2</sub> ambient)

The evolution of CO<sub>2</sub> as a main combustion emission during combustion tests under various oxygen mole fractions in N<sub>2</sub> ambient is illustrated in Fig. 5.14. Low rank coals have high content of oxygen-containing functional groups such as carboxyl, hydroxyl, ether and carbonyl groups leading to higher peaks of CO<sub>2</sub> and CO in comparison with high rank coals [31]. Three main peaks were observed for CO<sub>2</sub>, the most remarkable at the second region and two other at 610 °C and 730 °C. The first peak was due to the oxidation and removal of volatile matter which shifted to lower temperatures and higher absorbance as oxygen concentration increased to 35 %. At 35 % O<sub>2</sub> in N<sub>2</sub> ambient, CO<sub>2</sub> profile had a shoulder at 370 °C which was due to the fact that the process of combustion in this region varied from a single stage to double stages as oxygen concentration increased. As illustrated in Figs. 5.10 and 5.14, these three CO<sub>2</sub> peaks were greatly consistent with the peaks of reaction rates in DTG curves.

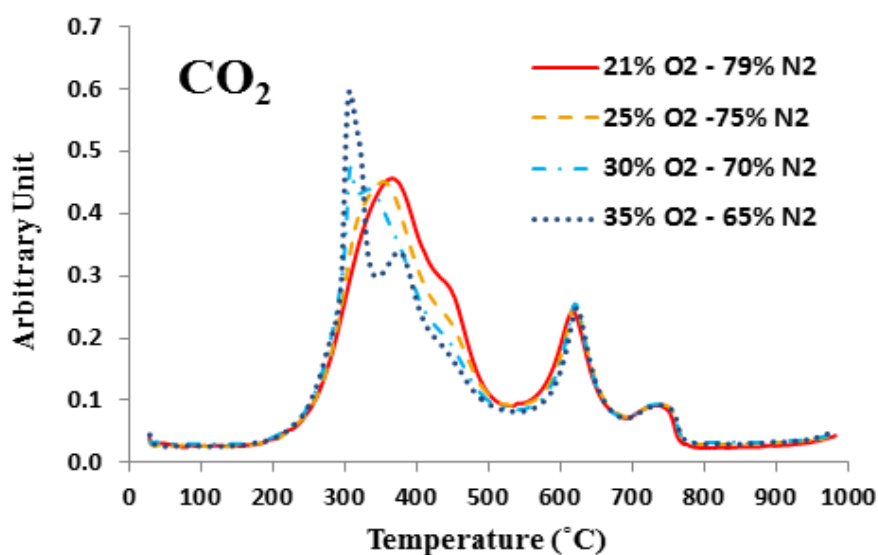


Fig. 5.14 Formation profiles of CO<sub>2</sub> during combustion tests of Kangal lignite in N<sub>2</sub> ambient

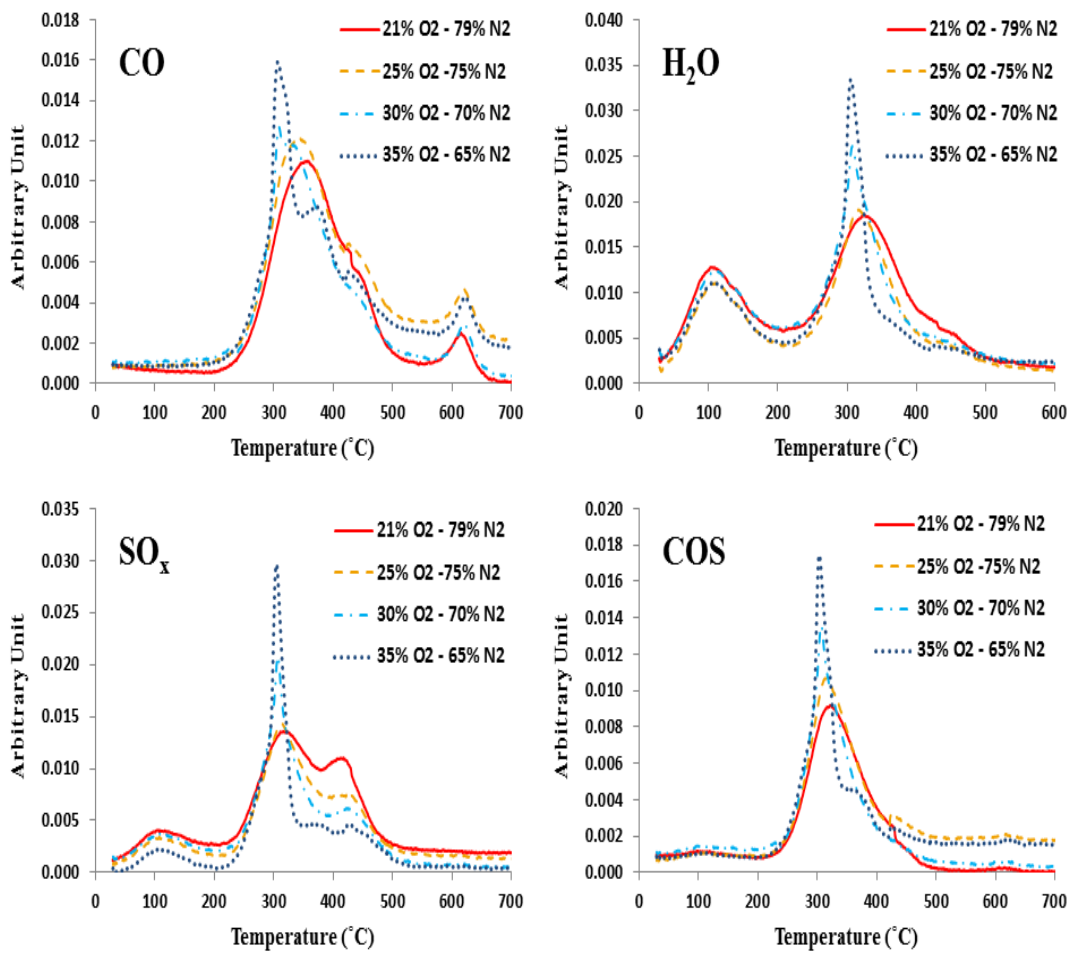


Fig. 5.15 Formation profiles of evolved gases during combustion tests of Kangal lignite in N<sub>2</sub> ambient

Fig. 5.15 demonstrates the evolution profiles of CO, H<sub>2</sub>O, SO<sub>x</sub> and COS under various oxygen mole fractions in N<sub>2</sub> ambient. A large fraction of these emissions mainly occurred during the temperature interval of 200-500 °C due to volatile combustion and sharper peaks were observed as we switched to higher oxygen concentrations. It was reported that SO<sub>x</sub> absorbance also experienced distinct peaks within the temperature range of 400-450 °C which suggested that SO<sub>x</sub> originates from different sources. Shoulders at 370 °C were more obvious during tests in 35 %

O<sub>2</sub> in N<sub>2</sub> for CO and COS profiles.

In order to clearly investigate the effects of oxygen mole fraction and correlations between the maximum rate of weight loss in DTG curves ( $|(dm/dt)_{2max}|$ ) and the peak absorbance of the emissions and also between T<sub>2max</sub> and T<sub>FG-max</sub>, these results are plotted in Fig. 5.16.

These comparisons (Fig. 5.16 (a)) indicated that the decreasing trend was observed in both T<sub>FG-max</sub> and T<sub>2max</sub> as the oxygen mole fraction had increasing trend from 21 % to 35 %. T<sub>FG-max</sub> for CO<sub>2</sub> and CO was 366 °C and 356 °C in 21 % O<sub>2</sub> and 354 °C and 343 °C in 25 % O<sub>2</sub> respectively which was much higher in comparison with T<sub>2max</sub> in 21 % and 25 % O<sub>2</sub> (332 °C and 304 °C respectively). T<sub>FG-max</sub> for water vapor and sulphur containing species, SO<sub>x</sub> and COS, decreased with lower slope with respect to T<sub>2max</sub> and a great agreement was observed in T<sub>FG-max</sub> of the evolved gases in 30 % and 35 % oxygen concentrations.

As illustrated in Fig. 5.16 (b), the maximum reaction rate increased as we switched to higher oxygen concentrations. Maximum absorbance of the evolved gases also had this increasing trend during the tests performed in elevated oxygen concentrations. However, these results indicated that switching to higher oxygen concentrations was more effective in increasing sulphur containing species, especially SO<sub>x</sub>, for which the maximum absorbance grew more than twice in 35 % O<sub>2</sub> with respect to 21 % O<sub>2</sub>.

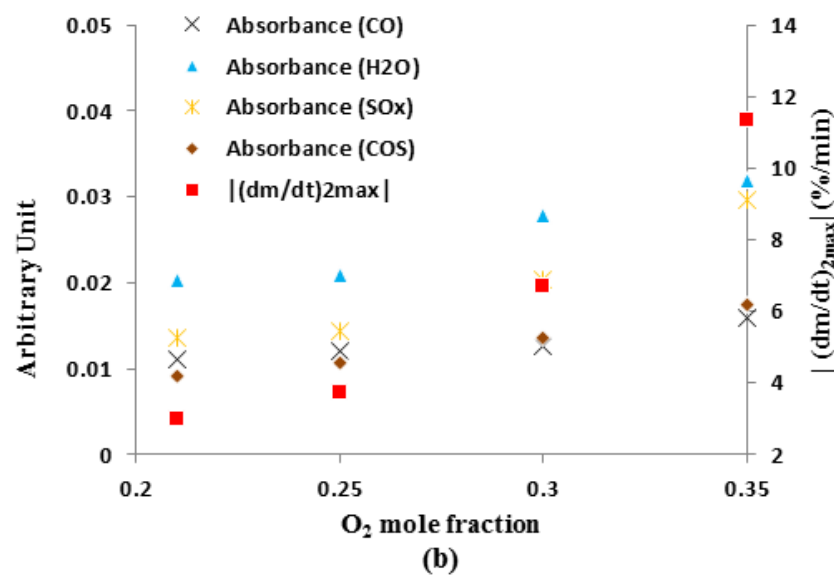
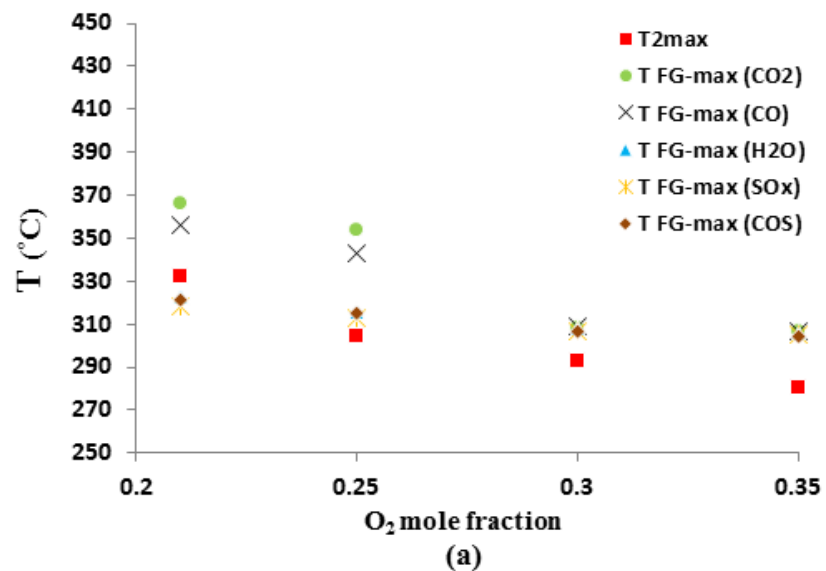


Fig. 5.16 Characteristic parameters of combustion tests of Kangal lignite in N<sub>2</sub> ambient: correlations between: a)  $T_{2max}$  and  $T_{FG-max}$ , b)  $|(dm/dt)_{2max}|$  and maximum absorbance of the evolved gases in FTIR spectra

It is well known that ammonia ( $\text{NH}_3$ ), hydrogen cyanide (HCN) and isocyanic acid (HNCO) are the precursors of nitrogen oxides ( $\text{NO}_x$  and  $\text{N}_2\text{O}$ ) [41]. In this study, formation profiles of  $\text{NO}_x$  related species such as NO and  $\text{NO}_2$  are not reported due to overlapping of their absorption bands with the characteristic absorption bands of water. No appreciable amounts of HCN and  $\text{N}_2\text{O}$  were detectable by the FTIR method. The effect of oxygen mole fraction in  $\text{N}_2$  ambient was also examined for  $\text{NH}_3$  (Fig. 5.17). Two peaks were observed within the temperature ranges of 300-400 °C and 600-700 °C for which the former was due to volatile matter combustion and the latter due to char oxidation. Furthermore, while the evolution of  $\text{NH}_3$  was observed to be slightly higher in the second region, it had lower absorbance in the third region. No considerable emissions were detected above 700 °C.

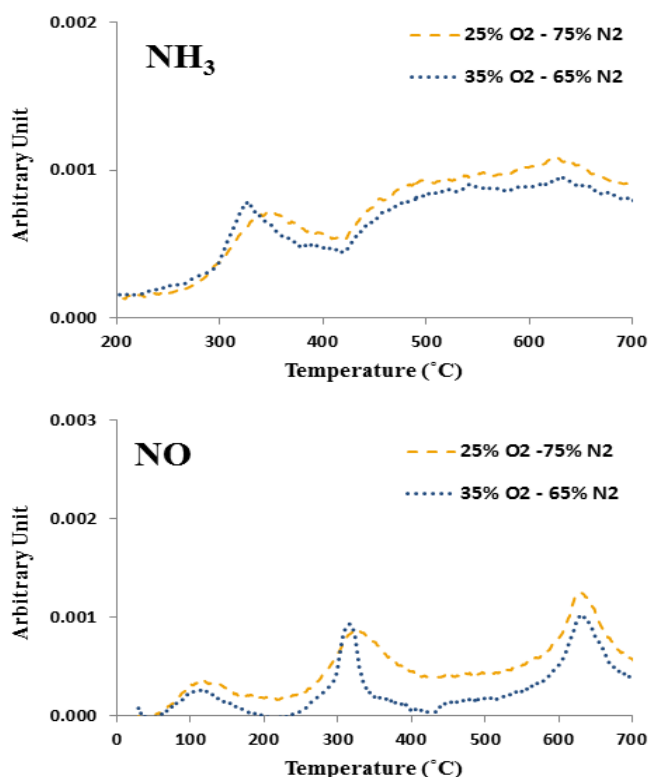


Fig. 5.17 Formation profiles of  $\text{NH}_3$  and NO during combustion tests of Kangal lignite in  $\text{N}_2$  ambient

### 5.2.5 Effects of Different Oxygen Mole Fractions (FTIR Results in CO<sub>2</sub> Ambient)

Fig. 5.18 demonstrates the evolution profiles of CO, H<sub>2</sub>O, SO<sub>x</sub> and COS under various oxygen mole fractions in CO<sub>2</sub> ambient and T<sub>FG-max</sub> and the maximum absorbance of the evolved gases are reported in Fig. 5.19. As illustrated in Fig. 5.19 (a), T<sub>FG-max</sub> was reduced from 349 °C to 299 °C, 315 °C to 296 °C and 328 °C to 294 °C in the cases of CO, SO<sub>x</sub> and COS respectively as T<sub>2max</sub> decreased from 319 °C to 273 °C while oxygen mole fraction increased from 21 % to 35 %. Therefore, T<sub>FG-max</sub> occurred with a considerable delay with respect to T<sub>2max</sub> which was more considerable in CO emissions. A part of this delay might be due to the required time for the transportation of combustion gases from the Thermogravimetric Analyzer to the gas cell of FTIR spectrometer.

Fig. 5.19 (b) indicates that the maximum rate of weight loss ( $|(dm/dt)_{2max}|$ ) increased moderately as we switched from 21 % to 30 % O<sub>2</sub> and it continued to increase drastically up to 35 % O<sub>2</sub>. This considerable increase was also observed in SO<sub>x</sub> and COS. Lower CO concentration in 25 % O<sub>2</sub> ambient led to the lower formation of COS in this oxygen mole fraction.

Formation profiles of CH<sub>4</sub> and HCl were also examined in 25 % and 35 % O<sub>2</sub> in CO<sub>2</sub> ambient conditions (Fig. 5.18). The evolutions of CH<sub>4</sub> and HCl were higher and T<sub>FG-max</sub> was lower in 35 % O<sub>2</sub>. CH<sub>4</sub> emission peaked at 322 °C and 303 °C and HCl emission peaked at 318 °C and 304 °C in 25 % O<sub>2</sub> in CO<sub>2</sub> and 35 % O<sub>2</sub> in CO<sub>2</sub> ambient conditions respectively. No considerable emissions were detected for CH<sub>4</sub> and HCl above 400 °C.

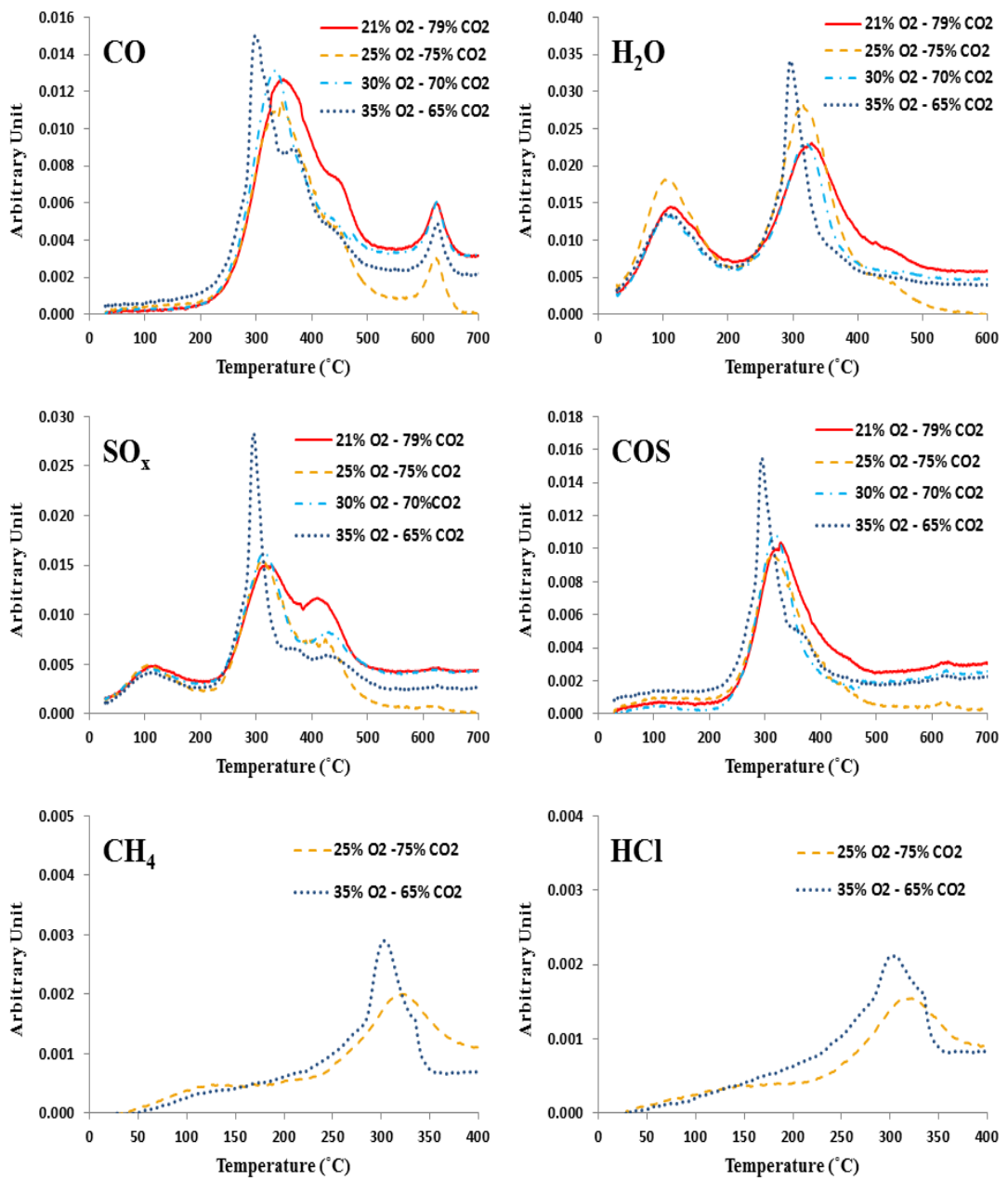


Fig. 5.18 Formation profiles of evolved gases during combustion tests of Kangal lignite in CO<sub>2</sub> ambient

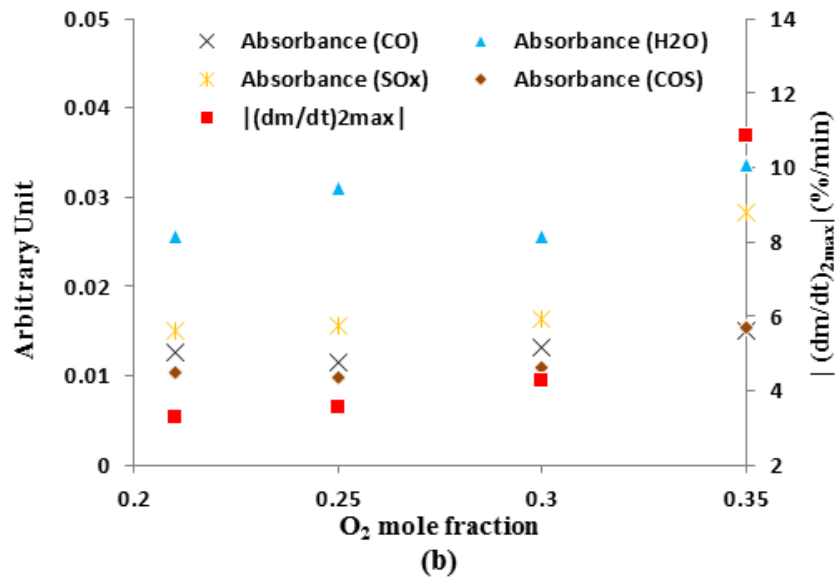
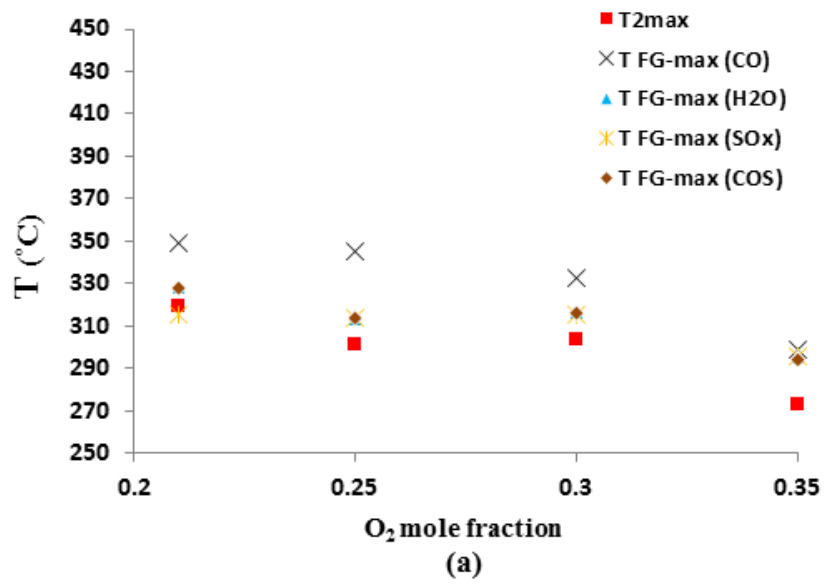


Fig. 5.19 Characteristic parameters of combustion tests of Kangal lignite in CO<sub>2</sub> ambient: correlations between: a)  $T_{2max}$  and  $T_{FG-max}$ , b)  $|(dm/dt)_{2max}|$  and maximum absorbance of the evolved gases in FTIR spectra

### 5.2.6 Effects of Catalysts on Combustion Tests of Kangal Lignite in O<sub>2</sub>/N<sub>2</sub> Ambient (TGA/DTG Results)

In order to investigate the effects of catalysts in O<sub>2</sub>/N<sub>2</sub> ambient, the combustion tests were performed in air and elevated oxygen concentrations in N<sub>2</sub> with the raw, Fe-form and K-form lignite samples. The TGA and DTG profiles of catalytic combustion tests in air are illustrated in Figs. 5.20 and 5.21 and the results are listed in Table 5.6. The profiles of catalytic combustion tests under 30 % O<sub>2</sub> in N<sub>2</sub> ambient are also demonstrated in Figs. 5.22 and 5.23. Moreover, one can see the effects of catalysts on combustion tests under 25 % O<sub>2</sub> in N<sub>2</sub> and 35 % O<sub>2</sub> in N<sub>2</sub> ambient conditions in Appendix D.

During combustion tests in air and in the case of K-based sample, it was illustrated that although the T<sub>in</sub> was almost the same as in original lignite combustion in air, the T<sub>ig</sub> and T<sub>2max</sub> dropped by 13 °C and 24 °C from 287 °C and 332 °C in Raw-form tests respectively. Furthermore, considerable peaks were observed at 490 °C in both 21 % and 30 % O<sub>2</sub> which were not observed in Raw- and Fe-form samples. These peaks regarding char combustion in the third region indicated that char reactivity was much higher in the case of K-based catalyst and this peak was improved in oxygen enriched experiments. In 30 % O<sub>2</sub> tests, |(dm/dt)<sub>2max</sub>| was observed to be much higher in the case of all the samples and occurred in lower corresponding temperatures. Fe-based lignite sample did not show any considerable catalytic effect in air combustion. However, an improved reactivity of Fe-form sample in the second region was confirmed by higher maximum reaction rate with respect to Raw-form combustion in 30 % O<sub>2</sub>.

The effects of catalysts on maximum reaction rates during combustion processes in the second and third regions under various O<sub>2</sub> mole fractions in N<sub>2</sub> ambient were investigated and the results are indicated in Fig. 5.24. As illustrated in Fig. 5.24, |(dm/dt)<sub>2max</sub>| was almost the same for the Raw-form and both impregnated samples in air combustion case. However, the maximum reaction rate profiles of these samples had different trends as we switched to higher oxygen mole fractions. In the case of K-form lignite sample, |(dm/dt)<sub>2max</sub>| increased as the O<sub>2</sub> concentration raised to 30 %

and then continued to drop considerably as the oxygen mole fraction was switched to 35 %. In the case of Fe-based catalyst,  $|(dm/dt)_{2max}|$  increased considerably with increasing oxygen concentrations and experienced considerable increases in comparison with Raw-form combustion in all elevated oxygen mole fractions (6.25 %/min, 8.01 %/min and 13.23 %/min versus 3.72 %/min, 6.72 %/min and 11.34 %/min for original lignite combustion in 25 %, 30 % and 35 % O<sub>2</sub> respectively).

As demonstrated in Fig. 5.24, the K-based catalyst had the best catalytic reactivity in char oxidation and combustion due to its much higher reaction rates in the third region in comparison with Raw- and Fe-form samples.  $|(dm/dt)_{3max}|$  was found to be 5 %/min, 6.62 %/min, 9.36 %/min and 9.02 %/min during the combustion tests in 21 %, 25 %, 30 % and 35 % O<sub>2</sub> respectively. It should be noted that a shoulder was observed in the maximum reaction rates under 30 % O<sub>2</sub> which would suggest that probably there is an optimum oxygen concentration for volatile and char reactivity in K-form sample under O<sub>2</sub>/N<sub>2</sub> ambient conditions. The straight profiles observed in Fig. 5.24 revealed that the elevated oxygen mole fractions did not influence the reaction rates regarding char combustion in the case of Raw- and Fe-form lignite samples.

Table 5.6 Effects of catalysts in air combustion tests of Kangal lignite

<b>Air</b>	<b>Raw-form</b>	<b>Fe-form</b>	<b>K-form</b>
<b>T<sub>in</sub> (°C)</b>	243	246	245
<b>T<sub>ig</sub> (°C)</b>	287	288	274
<b>T<sub>2max</sub> (°C)</b>	332	328	308
<b>T<sub>b</sub> (°C)</b>	751	750	751
<b><math> (dm/dt)_{2max} </math>(%/min)</b>	3.01	3.09	2.88
<b>T<sub>3max</sub> (°C)</b>	608	611	489
<b><math> (dm/dt)_{3max} </math>(%/min)</b>	1.35	1.49	5
<b>Total weight loss up to 980 °C (%)</b>	53.1	50.8	49.9

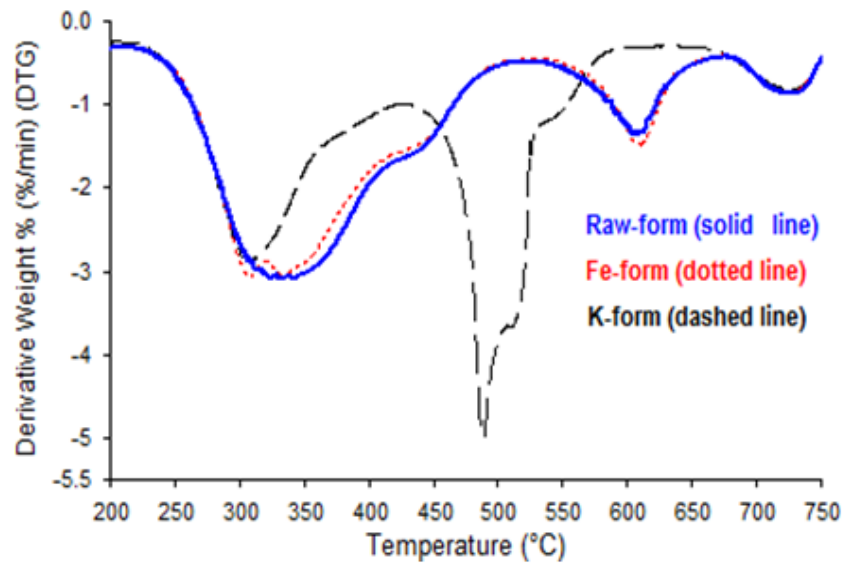


Fig. 5.20 DTG profiles of catalytic combustion tests of Kangal lignite in air

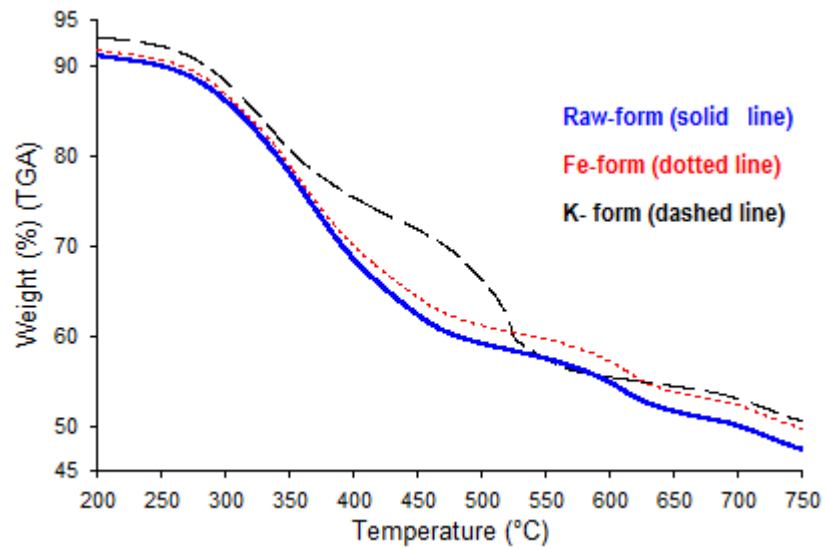


Fig. 5.21 TGA profiles of catalytic combustion tests of Kangal lignite in air

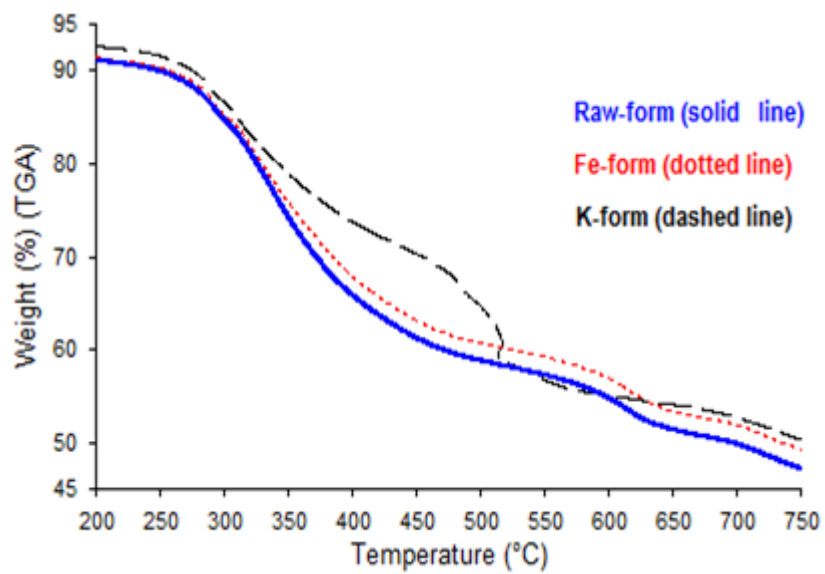


Fig. 5.22 TGA profiles of catalytic combustion tests of Kangal lignite in 30 % O<sub>2</sub> in N<sub>2</sub> ambient

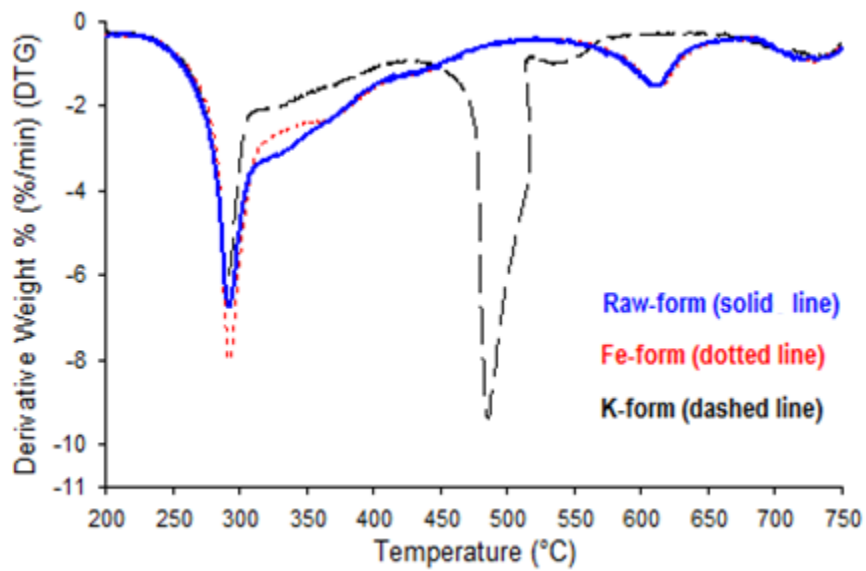


Fig. 5.23 DTG profiles of catalytic combustion tests of Kangal lignite in 30 % O<sub>2</sub> in N<sub>2</sub> ambient

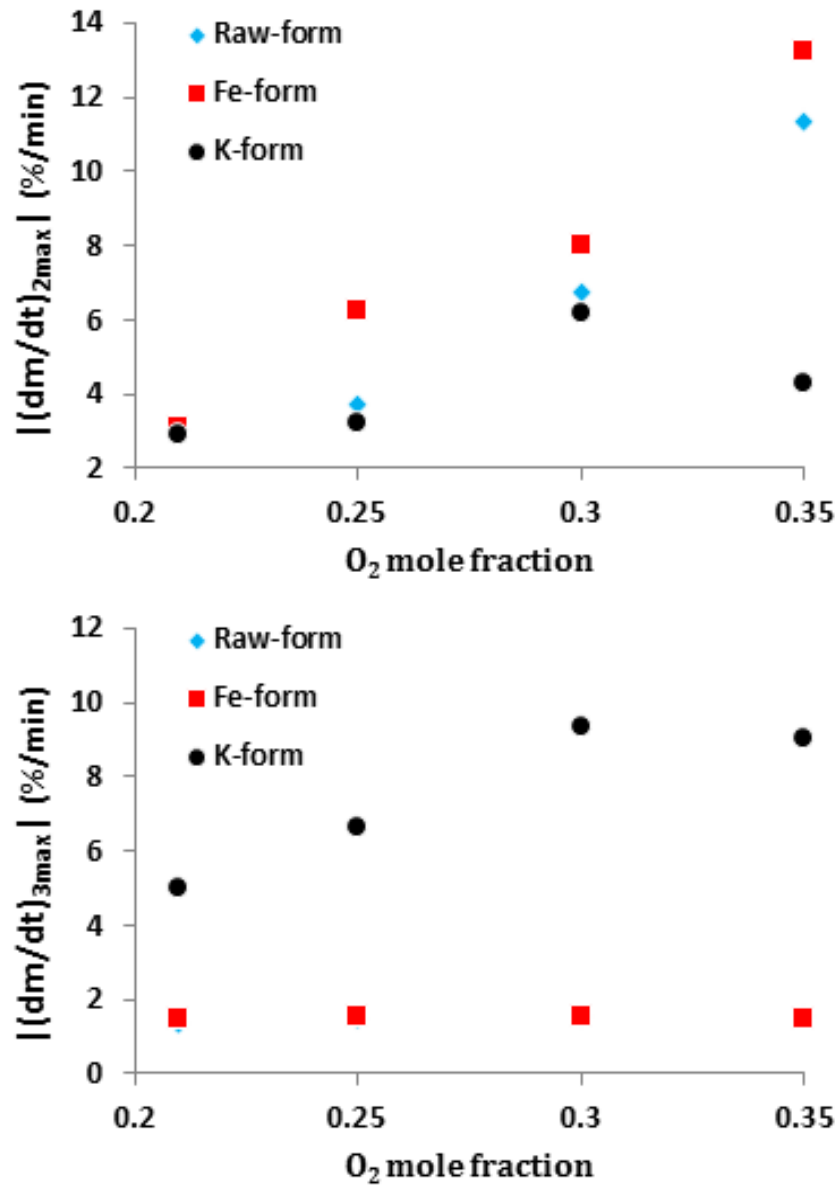


Fig. 5.24 Maximum reaction rates in the second and third regions during Kangal lignite catalytic combustion under various oxygen mole fractions in N<sub>2</sub> ambient

### 5.2.7 Effects of Catalysts on Combustion Tests of Kangal Lignite in N<sub>2</sub> Ambient (FTIR Results)

In order to investigate the effects of catalysts on evolution of combustion gases in N<sub>2</sub> ambient, the FTIR results of combustion tests in air (21 % O<sub>2</sub> in N<sub>2</sub>) and oxygen-enriched air ambient (30 % O<sub>2</sub> in N<sub>2</sub>) with raw and impregnated lignite samples are discussed in this section. Furthermore, the evolution of combustion gases in 25 % O<sub>2</sub> in N<sub>2</sub> and 35 % O<sub>2</sub> in N<sub>2</sub> ambient conditions are referred to Appendix D.

Formation profiles of CO<sub>2</sub> as a dominant product during catalytic combustion tests in air is illustrated in Fig. 5.25. Three main peaks were observed for all the samples. Although K-based catalyst reduced the evolution of CO<sub>2</sub> during devolatilization, it considerably increased the CO<sub>2</sub> emission during char oxidation and combustion. On the other hand, the Fe-based catalyst increased the formation of CO<sub>2</sub> in both second and third regions. As illustrated in Figs. 5.20 and 5.25, a great agreement was observed between the peaks in CO<sub>2</sub> evolution profiles and reaction rates in DTG curves.

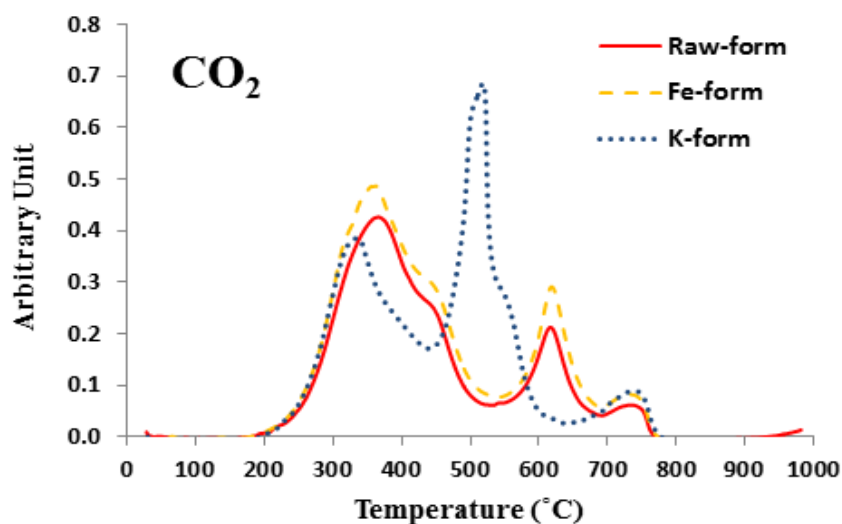


Fig. 5.25 Formation profiles of CO<sub>2</sub> during catalytic combustion tests of Kangal lignite in air

Comparisons of evolution curves of CO, H<sub>2</sub>O, SO<sub>x</sub> and COS in Fig. 5.26 indicated that the K-based catalyst was effective in reducing CO, SO<sub>x</sub> and COS emissions in volatile matter combustion and the peaks occurred in lower temperatures. However, during char combustion in the third region, the evolution profiles of the gases in the case of K-based catalysts had extra peaks at 500 °C which was in accordance with maximum rate of weight loss in the third region. So it can be concluded that char decomposition is the main source for emission release peaks at higher temperatures. Fe-based catalysts did not show any considerable effects with respect to Raw-form combustion in air.

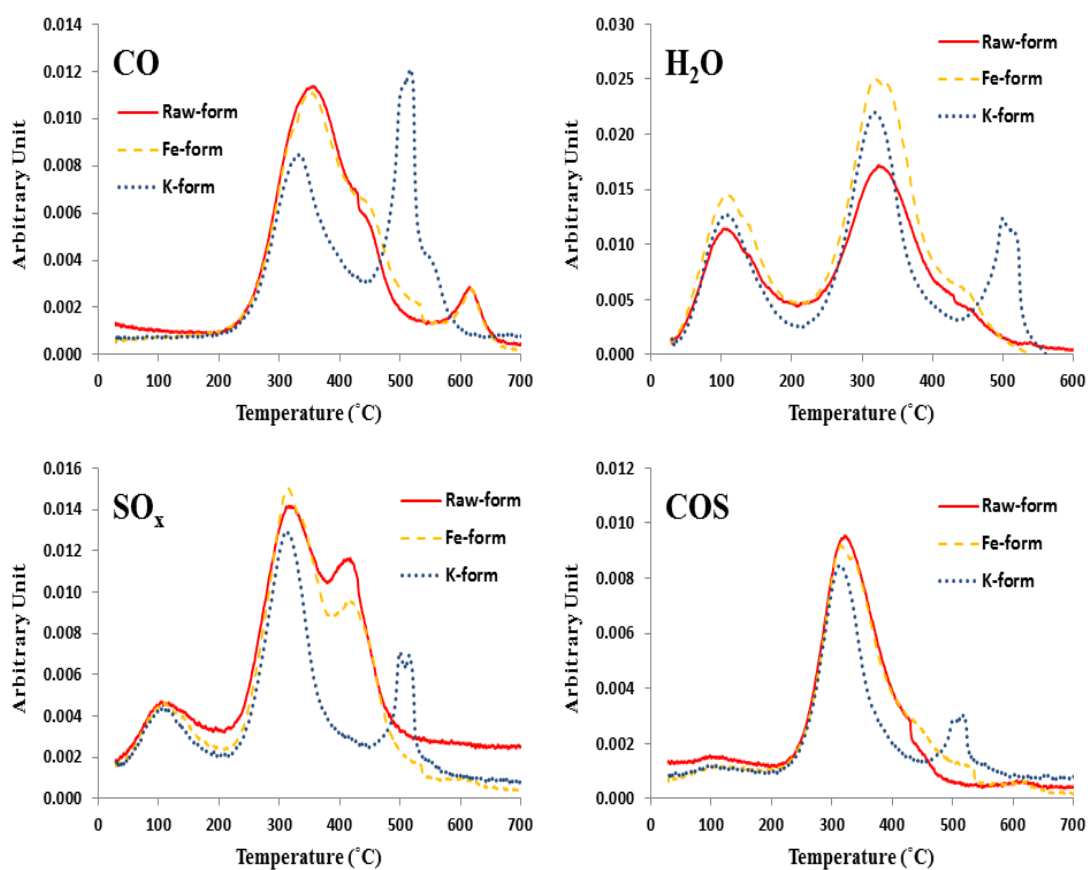


Fig. 5.26 Formation profiles of evolved gases during catalytic combustion tests of Kangal lignite in air

Formation profiles of CO<sub>2</sub> and other evolved gases in 30 % O<sub>2</sub> are illustrated in Figs. 5.27 and 5.28 respectively. The evolution profiles experienced almost similar trends as in air combustion. However, sharper peaks with higher absorbance in FTIR spectra were observed in evolution profiles of the evolved gases.

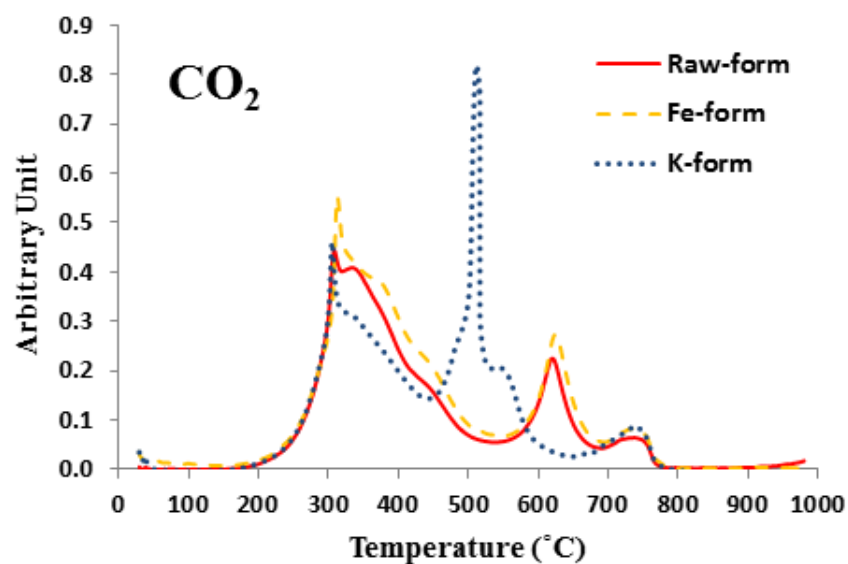


Fig. 5.27 Formation profiles of CO<sub>2</sub> during catalytic combustion tests of Kangal lignite in 30 % O<sub>2</sub> in N<sub>2</sub> ambient

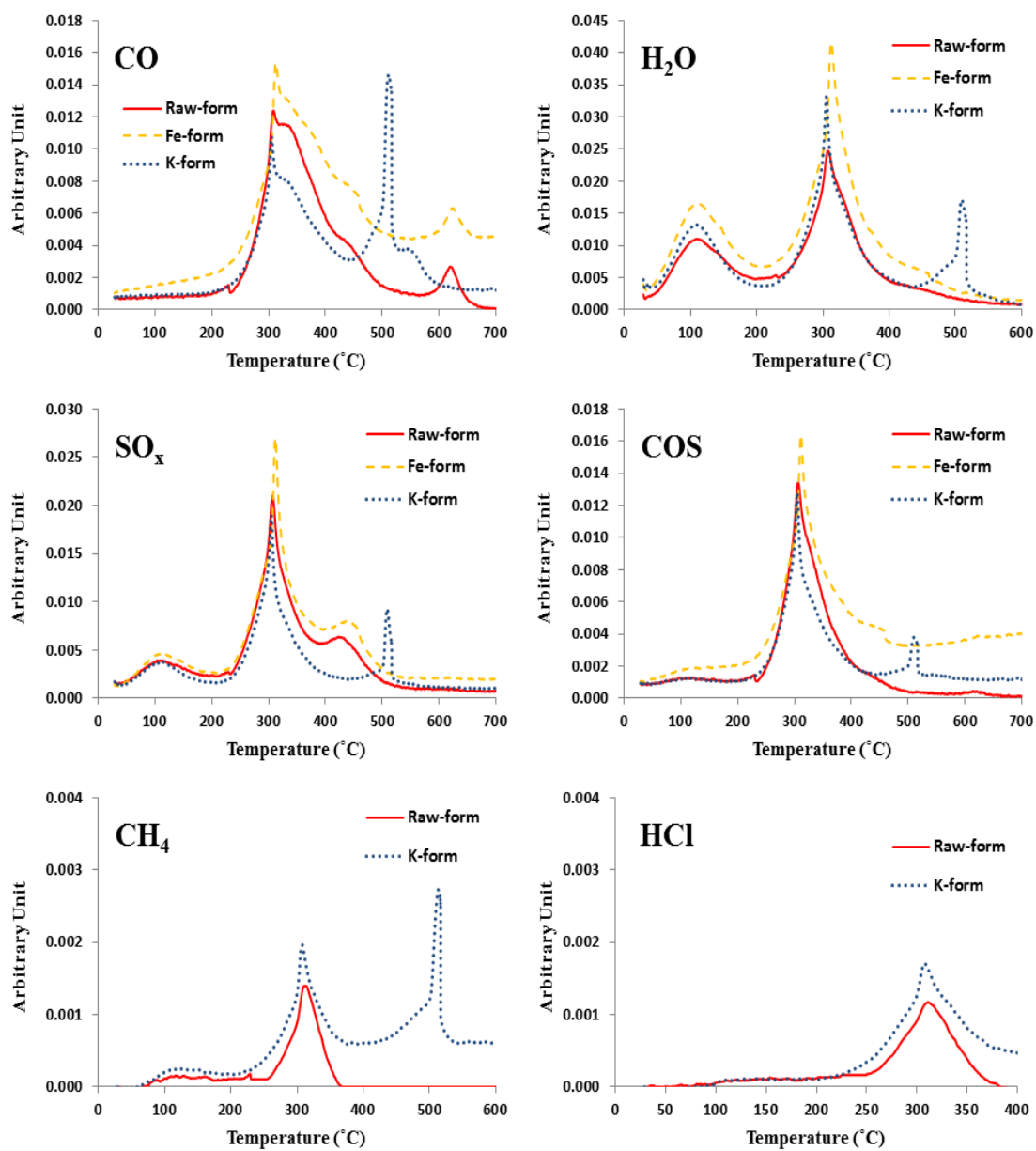


Fig. 5.28 Formation profiles of evolved gases during catalytic combustion tests of Kangal lignite in 30 % O<sub>2</sub> in N<sub>2</sub> ambient

Furthermore, the evolutions of  $\text{CH}_4$ ,  $\text{HCl}$  and nitrogen containing species,  $\text{NH}_3$  (a so-called NO precursor) and  $\text{NO}$ , were also explored during the combustion tests under 30 %  $\text{O}_2$  in  $\text{N}_2$  ambient which were not considered in air combustion due to too low concentration levels in combustion ambient. The K-form sample increased the emission of  $\text{NH}_3$  in the temperature range regarding char oxidation region as illustrated in Fig. 5.29. On the other hand, the evolution of  $\text{NO}$  was decreased considerably in the case of K-based catalyst and occurred at 500 °C which was considerably lower in comparison with Raw-form tests (620 °C). The absorbance peaks at 100 °C and 300 °C were due to water vapor caused by overlapping of the NO absorption bands with the characteristic absorption bands of water.

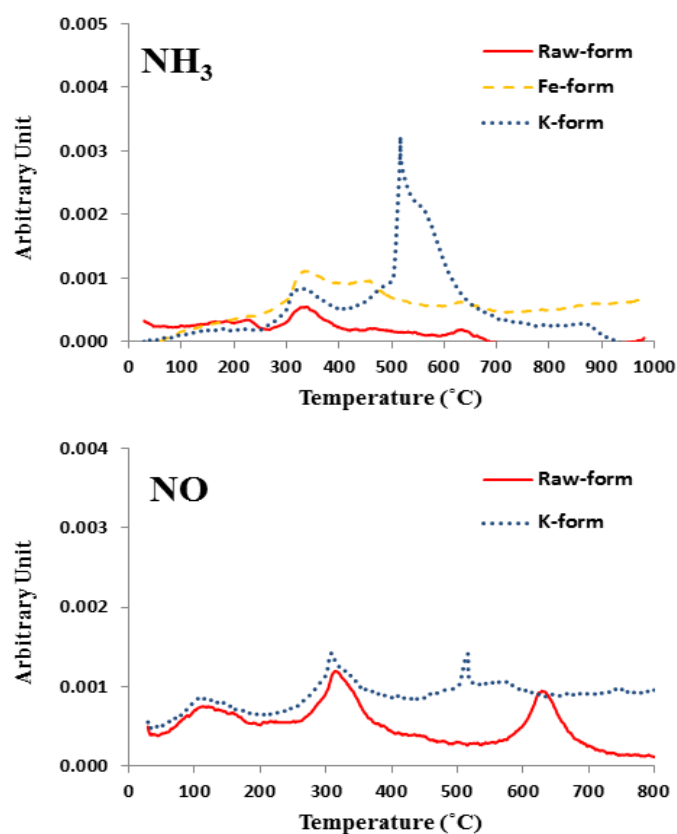


Fig. 5.29 Formation profiles of nitrogen containing species during catalytic combustion tests of Kangal lignite in 30 %  $\text{O}_2$  in  $\text{N}_2$  ambient

## 5.2.8 Effects of Catalysts on Combustion Tests of Kangal Lignite in CO<sub>2</sub> Ambient (TGA/DTG Results)

### 5.2.8.1 Kangal Lignite Combustion in 21 % O<sub>2</sub> in CO<sub>2</sub> Ambient

It has been demonstrated that the catalysts effects mainly manifest in two aspects: firstly, the catalysts promoted the coal decomposition reaction, resulted in the oxidative and transformed reaction of the matter which is difficult to oxidize and transform, accelerate the tar and the crude benzene to be decomposed easily, and increased the release of the coal volatile matter. Secondly, the catalysts to the combustion of lignite may be a carrier of oxygen that impromotes the oxygen transfer to the char, which attributed to the char combustion [54]. The TGA and DTG profiles of Kangal lignite combustion in 21 % O<sub>2</sub> in CO<sub>2</sub> for the raw and impregnated samples are illustrated in Figs. 5.30 and 5.31 and also listed in Table 5.7. Analyzing the effects of these catalysts on characteristic temperatures and reaction rates in both second and third regions of combustion was desired. It is illustrated that T<sub>2max</sub> which is relevant to the first considerable peak after the initial weight loss in DTG curves, was reduced considerably by using all the three catalysts. T<sub>2max</sub> was 319 °C and 297 °C in the combustion tests of Raw-form and K-form lignite samples respectively. The maximum reaction rate of volatile release dropped slightly in the cases of all the catalysts and was around 3 %/min in all the tests. As can be observed in DTG profiles, the reactivity of the catalysts, specially K<sub>2</sub>CO<sub>3</sub>, was more visible in the temperature range above 450 °C where the K-form lignite had a peak at 488 °C with |(dm/dt)<sub>3max</sub>| corresponded 4.73 %/min. While the K-based catalyst did not improve the volatilization, it could prepare char with higher activity. Therefore, among all the catalysts, potassium had the best catalytic reactivity in char combustion due to the formation and dispersion of a liquid–solid interface between K and the carbon surface [45]. High char reactivity is vitally important for achieving high gasification efficiency. Catalytic gasification, particularly using alkali metal (AM) catalysts, has been considered as an important approach to realize high char reactivity [76, 78]. T<sub>b</sub> and T<sub>ig</sub> were 580 °C and 265 °C in the case of K-form sample and were reduced by 9.16 % and 3.6 % with respect to the original lignite. The Ca-based catalyst also had

a higher reaction rate due to the char combustion in the third region. Fe-form lignite did not show any considerable effects in comparison with the original lignite in tests derived in 21 % O<sub>2</sub>. Results obtained from combustion profiles of the raw and impregnated Kangal lignite under various oxygen concentrations in CO<sub>2</sub> ambient are listed in Table 5.8.

Table 5.7 Characteristic parameters of Kangal lignite combustion tests in 21 % O<sub>2</sub> in CO<sub>2</sub> ambient

<b>21 % O<sub>2</sub>-79 % CO<sub>2</sub></b>	<b>Raw-form</b>	<b>Fe-form</b>	<b>Ca-form</b>	<b>K-form</b>
<b>T<sub>in</sub> (°C)</b>	234	237	236	241
<b>T<sub>ig</sub> (°C)</b>	276	275	271	265
<b>T<sub>2max</sub> (°C)</b>	319	303	302	297
<b>T<sub>b</sub> (°C)</b>	639	642	641	580
<b> <math>(\frac{dm}{dt})_{2max}</math> (%/min)</b>	3.28	3	2.96	2.94
<b>T<sub>3max</sub> (°C)</b>	611	614	609	488
<b> <math>(\frac{dm}{dt})_{3max}</math> (%/min)</b>	1.49	1.52	2.19	4.73
<b>Total weight loss up to 980 °C (%)</b>	54.21	51.69	51.41	50.96

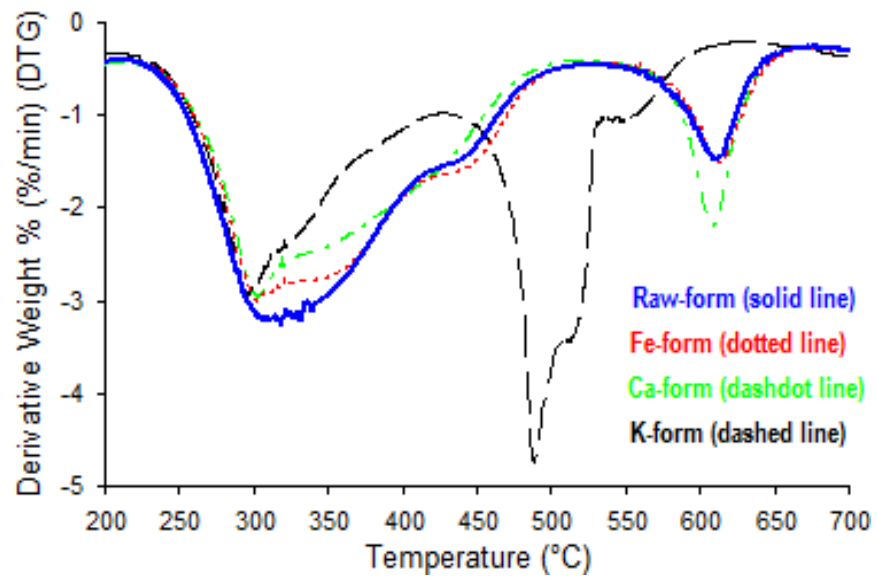


Fig. 5.30 DTG profiles of catalytic combustion tests of Kangal lignite in 21 % O<sub>2</sub> in CO<sub>2</sub> ambient

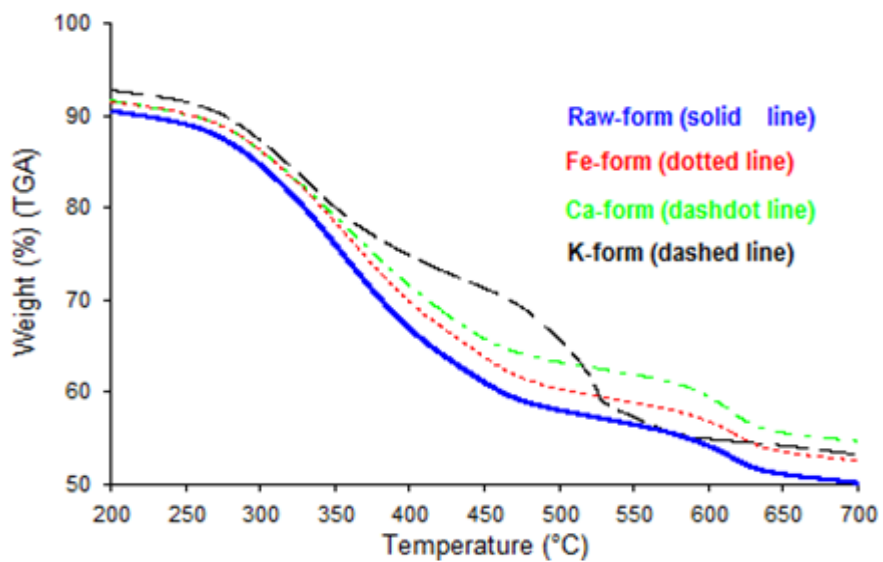


Fig. 5.31 TGA profiles of catalytic combustion tests of Kangal lignite in 21 % O<sub>2</sub> in CO<sub>2</sub> ambient

Table 5.8 Combustion characteristics of raw and impregnated Kangal lignite samples in different O<sub>2</sub>/ CO<sub>2</sub> mixtures

Temperature (°C)	21 % O <sub>2</sub> –79 % CO <sub>2</sub>					25 % O <sub>2</sub> –75 % CO <sub>2</sub>					30 % O <sub>2</sub> –70 % CO <sub>2</sub>					35 % O <sub>2</sub> –65 % CO <sub>2</sub>				
	T <sub>in</sub>	T <sub>ig</sub>	T <sub>2max</sub>	T <sub>3max</sub>	T <sub>b</sub>	T <sub>in</sub>	T <sub>ig</sub>	T <sub>2max</sub>	T <sub>3max</sub>	T <sub>b</sub>	T <sub>in</sub>	T <sub>ig</sub>	T <sub>2max</sub>	T <sub>3max</sub>	T <sub>b</sub>	T <sub>in</sub>	T <sub>ig</sub>	T <sub>2max</sub>	T <sub>3max</sub>	T <sub>b</sub>
<b>Raw-form</b>	234	276	319	611	639	235	271	301	613	642	239	273	304	617	641	233	257	273	615	639
<b>Fe-form</b>	237	275	303	614	642	240	280	310	616	644	238	270	281	617	642	236	266	278	620	645
<b>Ca-form</b>	236	271	302	609	641	232	275	307	613	641	234	276	299	613	642	231	266	281	614	642
<b>K-form</b>	241	265	297	488	580	238	270	295	489	575	238	271	291	488	574	239	268	288	494	573

### 5.2.8.2 Kangal Lignite Combustion in 25 % O<sub>2</sub> in CO<sub>2</sub> Ambient

Results obtained from combustion profiles in 25 % O<sub>2</sub> are illustrated in Figs. 5.32 and 5.33 and listed in Table 5.9. As the combustion ambient was switched to 25 % O<sub>2</sub>, T<sub>2max</sub> increased by around 10 °C and 7 °C to 310 °C and 307 °C in the case of Fe-form and Ca-form respectively with respect to Raw-form in 25 % O<sub>2</sub>. In this oxygen concentration, the relative active sequence of catalysts to the reactivity of char can be described as follows: K > Ca > Fe. Although the same trends as in 21 % O<sub>2</sub> were observed in characteristic temperatures and reaction rates, the elevated oxygen levels shifted the weight loss curves to lower temperature zone which was an expected result.

Table 5.9 Characteristic parameters of Kangal lignite combustion tests in 25 % O<sub>2</sub> in CO<sub>2</sub> ambient

25 % O <sub>2</sub> -75 % CO <sub>2</sub>	Raw-form	Fe-form	Ca-form	K-form
T <sub>in</sub> (°C)	235	240	232	238
T <sub>ig</sub> (°C)	271	280	275	270
T <sub>2max</sub> (°C)	301	310	307	295
T <sub>b</sub> (°C)	642	644	641	575
$(\frac{dm}{dt})_{2max}$  (%/min)	3.54	3.35	3.25	3.07
T <sub>3max</sub> (°C)	613	616	613	489
$(\frac{dm}{dt})_{3max}$  (%/min)	1.55	1.59	2.11	5.14
Total weight loss up to 980 °C (%)	54.13	51.27	52.28	49.93

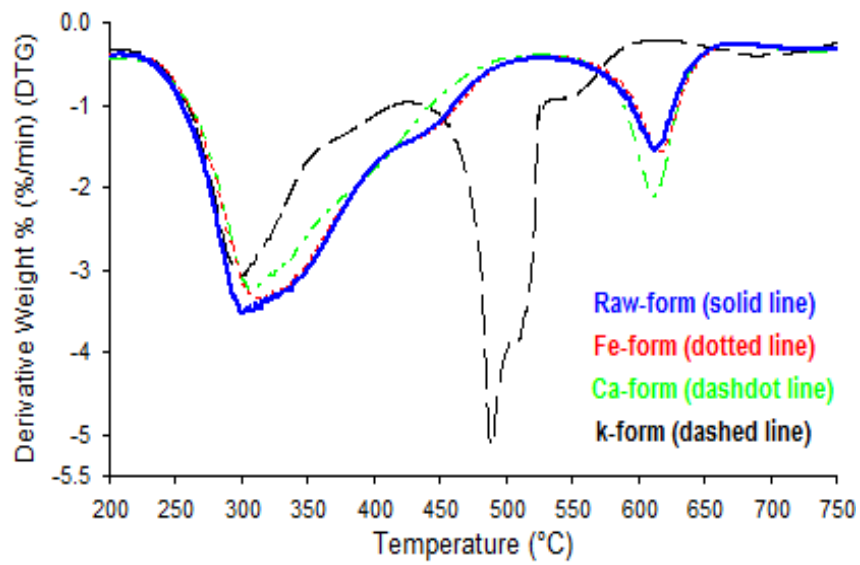


Fig. 5.32 DTG profiles of catalytic combustion tests of Kangal lignite in 25 % O<sub>2</sub> in CO<sub>2</sub> ambient

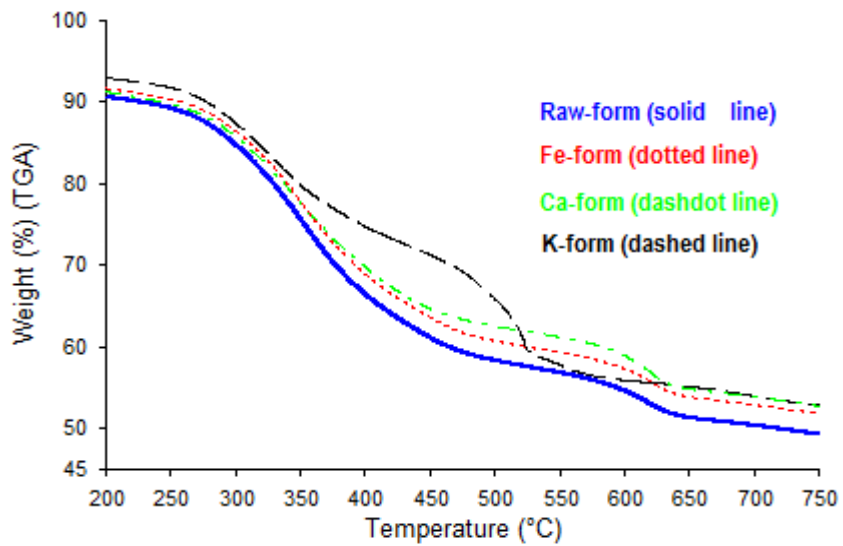


Fig. 5.33 TGA profiles of catalytic combustion tests of Kangal lignite in 25 % O<sub>2</sub> in CO<sub>2</sub> ambient

### 5.2.8.3 Kangal Lignite Combustion in 30 % O<sub>2</sub> in CO<sub>2</sub> Ambient

The results of combustion tests performed in 30 % O<sub>2</sub> are illustrated in Figs. 5.34 and 5.35 and listed in Table 5.10. The most significant result derived from the DTG curves of combustion tests in 30 % O<sub>2</sub> in CO<sub>2</sub> ambient was the improved reactivity of Fe-form, Ca-form and K-form in the temperature interval related to volatile matter release and light hydrocarbon combustion. As summarized in Table 5.8 and illustrated in Fig. 5.34, T<sub>2max</sub> reduced in the order of 281 °C, 299 °C and 291 °C in Fe-form, Ca-form and K-form combustion tests respectively in comparison with 304 °C in Raw-form test in 30 % O<sub>2</sub>. The maximum reaction rates in this region increased significantly to 8.45 %/min, 4.90 %/min and 5.17 %/min in the cases of Fe- Ca- and K-form samples with respect to 4.25 %/min in Raw-form combustion. Therefore, the relative active sequence of catalysts to the reaction rate in volatile and light hydrocarbon combustion can be described as follows: Fe<sub>2</sub>O<sub>3</sub> > K<sub>2</sub>CO<sub>3</sub> > Ca(OH)<sub>2</sub>. These results are thought to be an outcome of temperature dependency in catalytic reactivity of the inorganic catalysts which was more significant in the case of Fe-form and K-form lignite samples.

Table 5.10 Characteristic parameters of Kangal lignite combustion tests in 30 % O<sub>2</sub> in CO<sub>2</sub> ambient

30 % O <sub>2</sub> -70 % CO <sub>2</sub>	Raw-form	Fe-form	Ca-form	K-form
T <sub>in</sub> (°C)	239	238	234	238
T <sub>ig</sub> (°C)	273	270	276	271
T <sub>2max</sub> (°C)	304	281	299	291
T <sub>b</sub> (°C)	641	642	642	574
$(\frac{dm}{dt})_{2max}$  (%/min)	4.25	8.45	4.90	5.17
T <sub>3max</sub> (°C)	617	617	613	488
$(\frac{dm}{dt})_{3max}$  (%/min)	1.60	1.75	2.17	7.87
<b>Total weight loss up to 980 °C (%)</b>	53.85	51.28	51.89	50.82

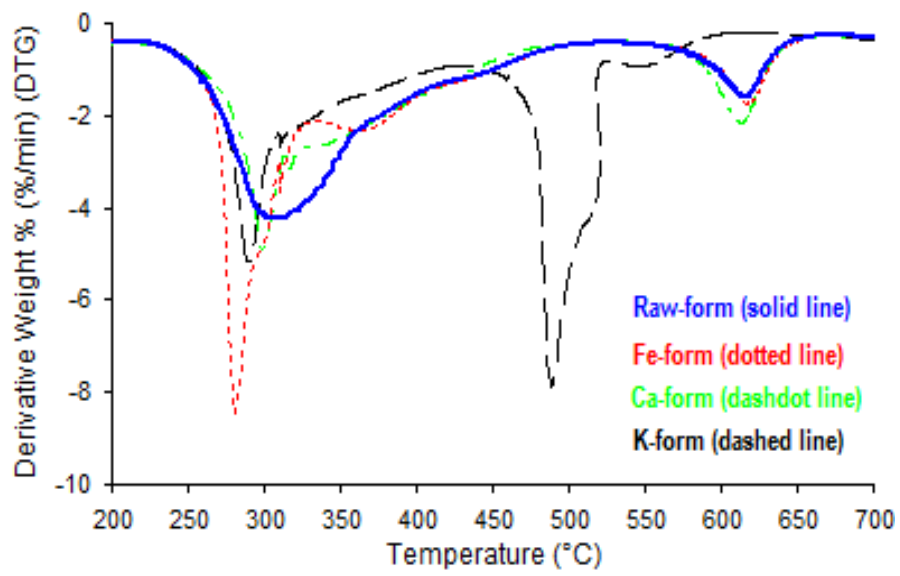


Fig. 5.34 DTG profiles of combustion tests of Kangal lignite in 30 % O<sub>2</sub> in CO<sub>2</sub> ambient

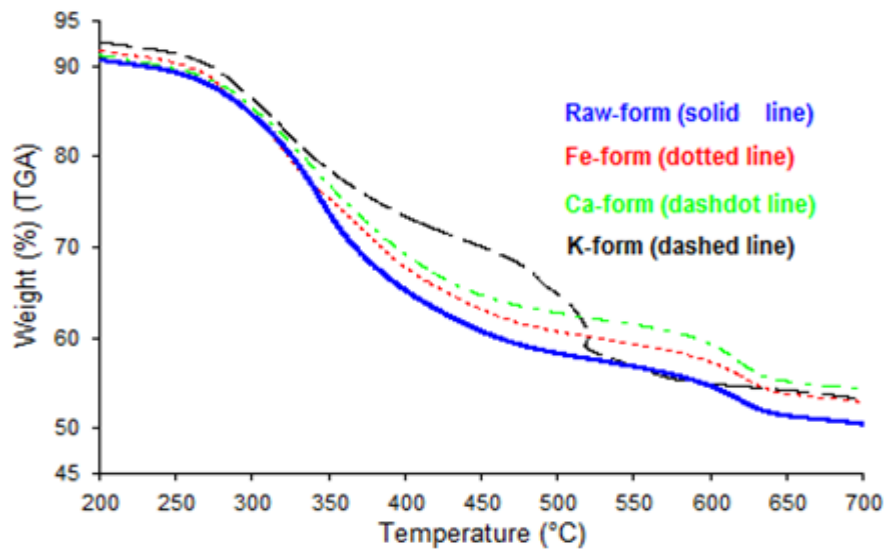


Fig. 5.35 TGA profiles of combustion tests of Kangal lignite in 30 % O<sub>2</sub> in CO<sub>2</sub> ambient

#### 5.2.8.4 Kangal Lignite Combustion in 35 % O<sub>2</sub> in CO<sub>2</sub> Ambient

During combustion tests performed in 35 % O<sub>2</sub> in CO<sub>2</sub> ambient (Figs. 5.36- 5.38 and Table 5.11), the results demonstrated that T<sub>ig</sub> and T<sub>2max</sub> were slightly higher than that in original lignite in all the catalytic cases. Since elevated oxygen levels in combustion ambient of Raw-form lignite shifted the weight loss curves to lower temperature zone dramatically. However, it was observed that the maximum reaction rates were higher in the case of Fe-form and Ca-form samples. Among the entire catalysts, Ca-based sample had the most significant effects as we switched to 35 % O<sub>2</sub>. In the case of K-form lignite, the char reactivity was improved with increasing oxygen concentration. However, the rate of this increase would suggest that probably there was an optimum oxygen concentration for char reactivity in K-form sample.

Table 5.11 Characteristic parameters of Kangal lignite combustion tests in 35 % O<sub>2</sub> in CO<sub>2</sub> ambient

35 % O <sub>2</sub> -65 % CO <sub>2</sub>	Raw-form	Fe-form	Ca-form	K-form
T <sub>in</sub> (°C)	233	236	231	239
T <sub>ig</sub> (°C)	257	266	266	268
T <sub>2max</sub> (°C)	273	278	281	288
T <sub>b</sub> (°C)	639	645	642	573
$(dm/dt)_{2max}$  (%/min)	10.84	12.52	12.35	6.93
T <sub>3max</sub> (°C)	615	620	614	494
$(dm/dt)_{3max}$  (%/min)	1.65	1.61	2.26	9.12
<b>Total weight loss up to 980 °C (%)</b>	53.93	51.72	51.89	49.91

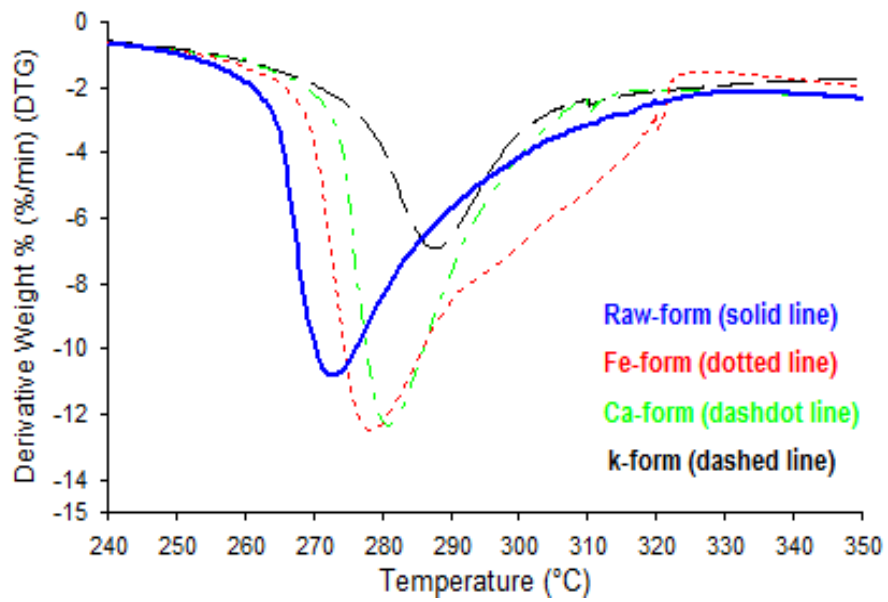


Fig. 5.36 DTG profiles of catalytic combustion tests of Kangal lignite in 35 % O<sub>2</sub> in CO<sub>2</sub> ambient- second region

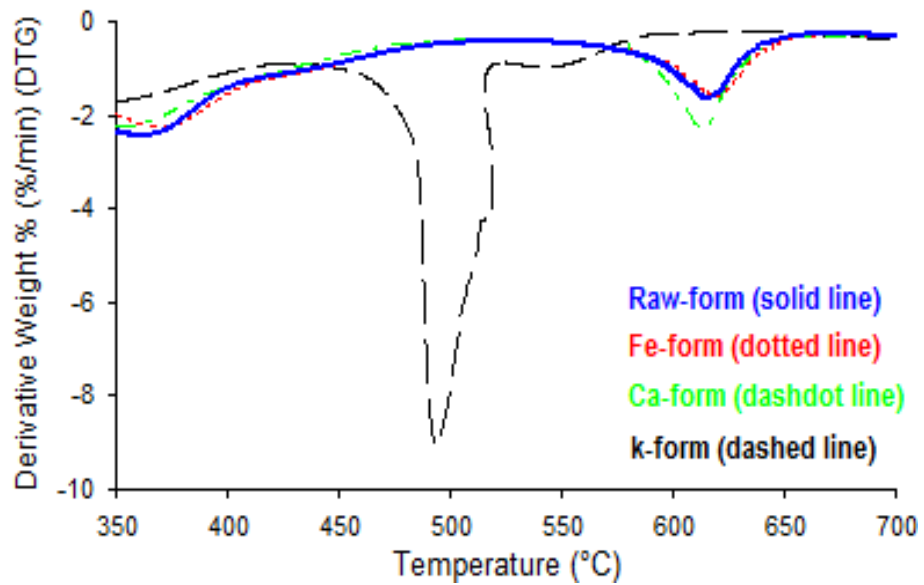


Fig. 5.37 DTG profiles of catalytic combustion tests of Kangal lignite in 35 % O<sub>2</sub> in CO<sub>2</sub> ambient- third region

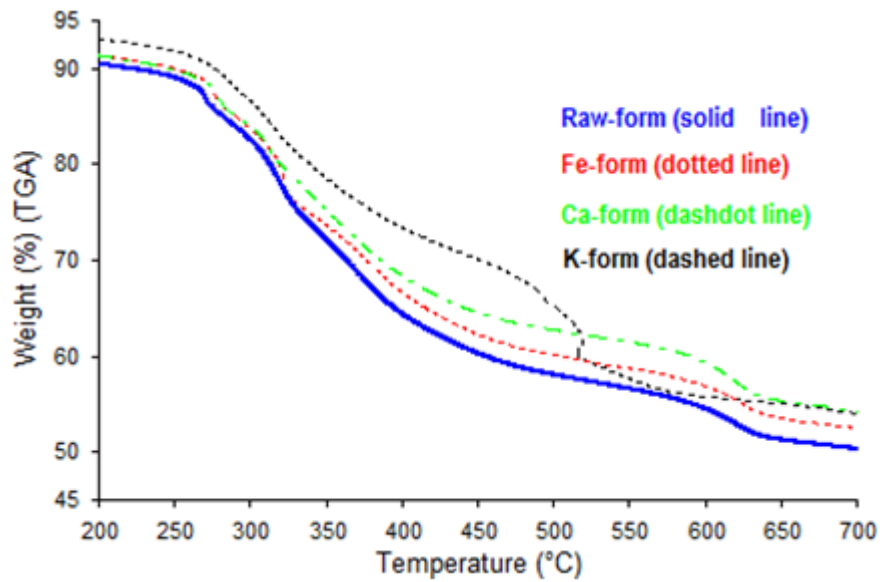


Fig. 5.38 TGA profiles of catalytic combustion tests of Kangal lignite in 35 % O<sub>2</sub> in CO<sub>2</sub> ambient

## 5.2.9 Effects of Catalysts on Reaction Rates of Kangal Lignite Combustion

The effects of catalysts on maximum reaction rates during combustion processes in the second and third regions under different O<sub>2</sub> mole fractions in CO<sub>2</sub> ambient were investigated and the results are illustrated in Figs. 5.39.

### 5.2.9.1 Effects of Catalysts in the Devolatilization Region

As illustrated in Fig. 5.39 and listed in Table 5.8, elevated oxygen levels shifted the weight loss curves to lower temperature zone (lower  $T_{2max}$ ) accompanied with much higher reaction rates ( $|(dm/dt)_{2max}|$ ) in both Raw-form and impregnated lignite samples. However, these increasing  $|(dm/dt)_{2max}|$  profiles had different trends as we switched to higher oxygen mole fractions. In all the samples,  $|(dm/dt)_{2max}|$  increased slightly as the O<sub>2</sub> concentration increased to 25 %. However, beyond this oxygen

mole fraction, Fe-based catalyst had significant increase and the maximum reaction rate reached 8.45 %/min and 12.52 %/min in 30 % and 35 % O<sub>2</sub> respectively. A considerable rise during combustion tests of the Raw- and Ca-form samples, however, was observed after 30 % O<sub>2</sub> and the maximum reaction rates for these two samples reached 10.84 %/min and 12.35 %/min in 35 % O<sub>2</sub> respectively. Although the catalysts did not show considerable effects in lower oxygen conditions (up to 25 % O<sub>2</sub>), they seemed to be very effective in oxygen concentrations beyond 25 %. As the relative active sequence of catalysts to the reaction rate in the volatile and light hydrocarbon combustion in 30 % and in 35 % O<sub>2</sub> can be described as Fe>> K> Ca> Raw-form and Fe> Ca> Raw-form>> K respectively.

#### **5.2.9.2 Effects of Catalysts in the Char Combustion Region**

As demonstrated in Fig. 5.39, the K-based catalyst had the best catalytic reactivity in char oxidation and combustion due to its much higher reaction rates in the third region.  $|(dm/dt)_{3max}|$  was 4.73 %/min, 5.14 %/min, 7.87 %/min and 9.12 %/min during the combustion tests in 21 %, 25 %, 30 % and 35 % O<sub>2</sub> respectively. The straight profiles observed in Fig. 5.39 (third region) revealed that the elevated oxygen mole fractions did not influence the reaction rates regarding char combustion in the case of Raw- Ca- and Fe-form lignite samples. However, the Char combustion maximum rates were higher in the case of Ca-based catalyst in comparison with Raw- and Fe-form samples in all the oxygen mole fractions.

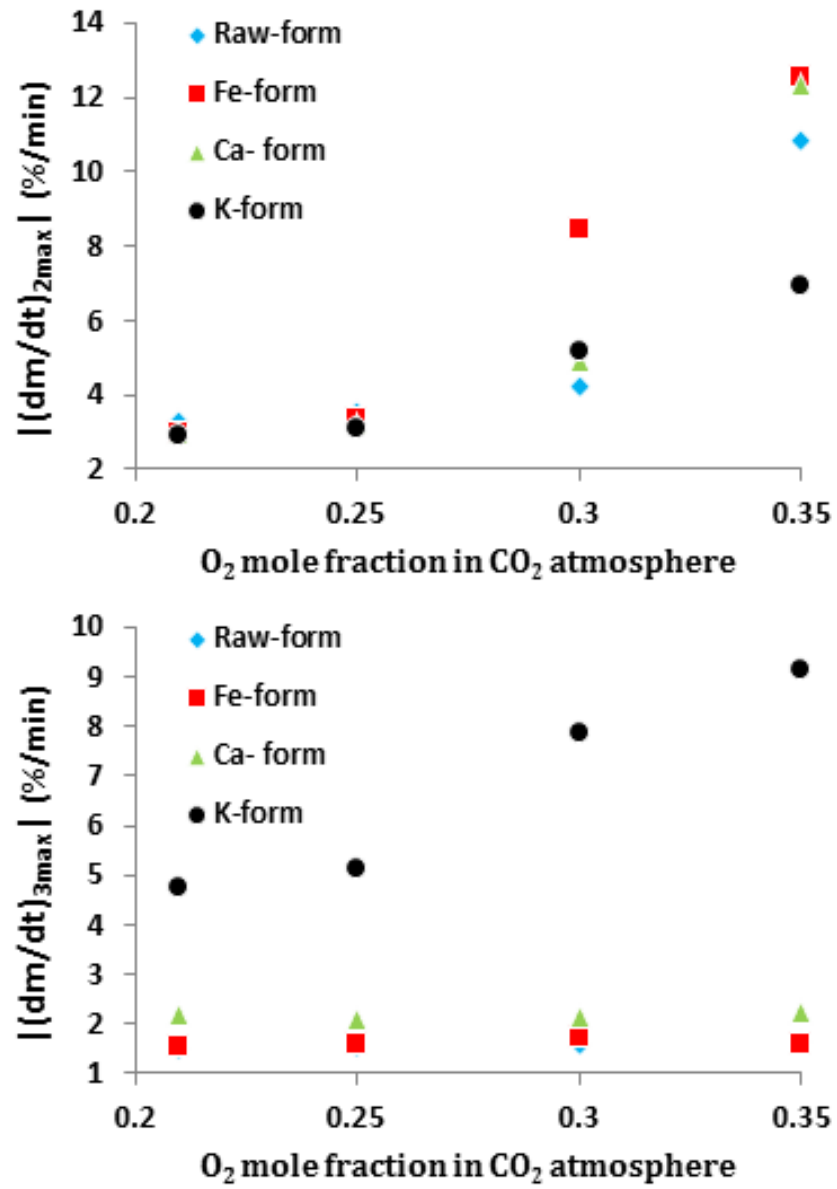


Fig. 5.39 Maximum reaction rates in the second and third regions of combustion during Kangal lignite catalytic combustion under various oxygen mole fractions in CO<sub>2</sub> ambient

### 5.2.10 Effects of Catalysts on Combustion Tests of Kangal Lignite in CO<sub>2</sub> Ambient (FTIR Results)

The effects of catalysts on evolution of combustion gases in CO<sub>2</sub> ambient were investigated and the FTIR results of combustion tests in 21 % O<sub>2</sub> in CO<sub>2</sub> and 30 % O<sub>2</sub> in CO<sub>2</sub> ambient conditions with raw and impregnated lignite samples are indicated in Figs. 5.40- 5.43. Furthermore, the emission characteristics of the evolved gases in 25 % O<sub>2</sub> in CO<sub>2</sub> and 35 % O<sub>2</sub> in CO<sub>2</sub> ambient conditions are referred to Appendix D.

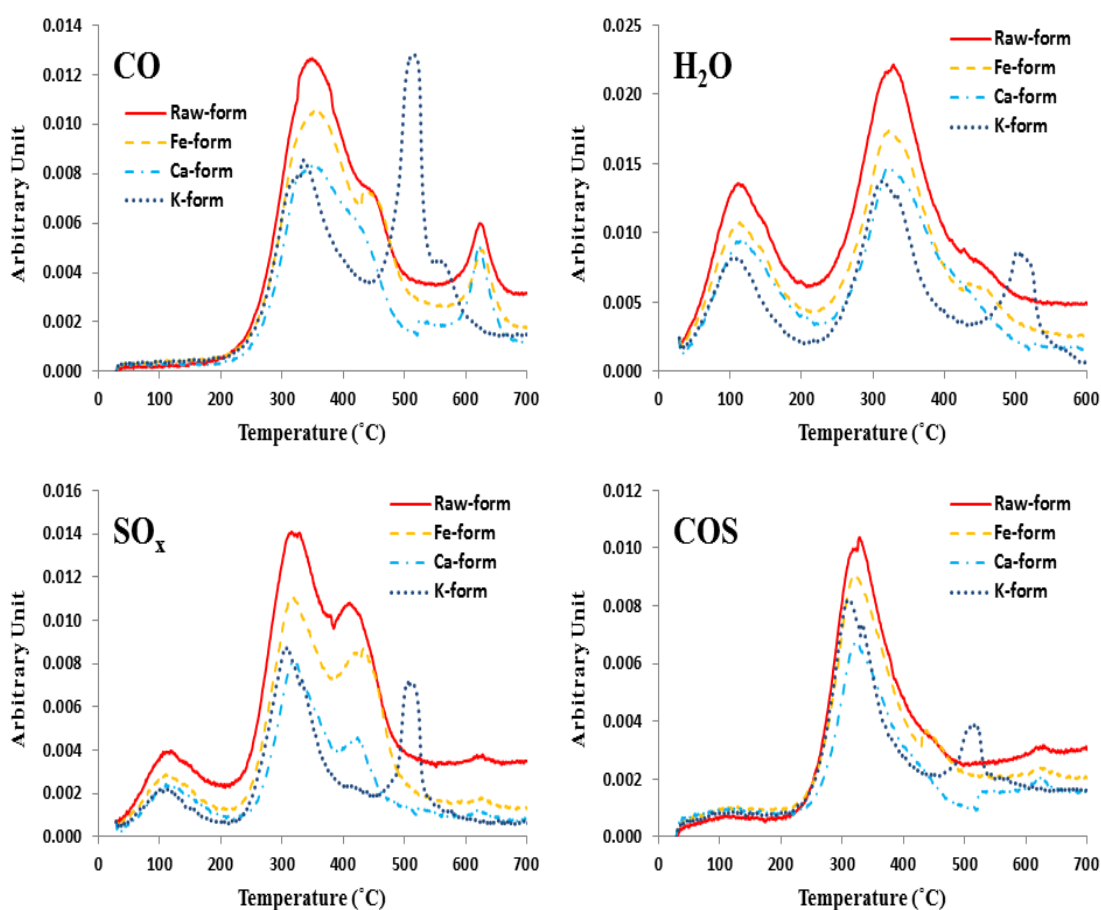


Fig. 5.40 Formation profiles of evolved gases during catalytic combustion tests in 21 % O<sub>2</sub> in CO<sub>2</sub> ambient

The evolution of evolved gases was influenced by the use of Fe, Ca and K catalysts as indicated in Figs. 5.40 and 5.41. While Fe-based catalyst increased the evolution of  $\text{SO}_x$  and COS in 30 %  $\text{O}_2$ , K-based catalyst reduced the formation of CO,  $\text{H}_2\text{O}$ ,  $\text{SO}_x$  and COS in both 21 % and 30 %  $\text{O}_2$  in the temperature interval below 400 °C. It is well known that the sulphur containing species increase a risk of corrosion throughout the plant and transport pipelines [79]. Adding absorbents such as limestone or dolomite to the combustion process is a familiar way to reduce  $\text{SO}_x$  emissions [8, 42]. During these experiments Ca-based catalyst had the best catalytic activity in reducing sulphur containing species through formation of mainly  $\text{CaSO}_4$  to result in sulphur retention as solid compounds in the ash. The related mechanisms can be found elsewhere [8]. In the  $\text{Ca}(\text{OH})_2$  catalytic run under 30 %  $\text{O}_2$ , the  $T_{\text{FG-max}}$  values of CO,  $\text{H}_2\text{O}$ ,  $\text{SO}_x$  and COS shifted to lower temperatures which was more considerable in CO emission. This result was in agreement with Wang et al. [40]. Combustion tests performed with K-form lignite sample experienced extra peaks in accordance with the maximum rate of weight loss due to char oxidation and combustion in DTG curve (temperature interval 450-550 °C) which was generally related to the secondary cracking of the char, residue of the primary combustion process.

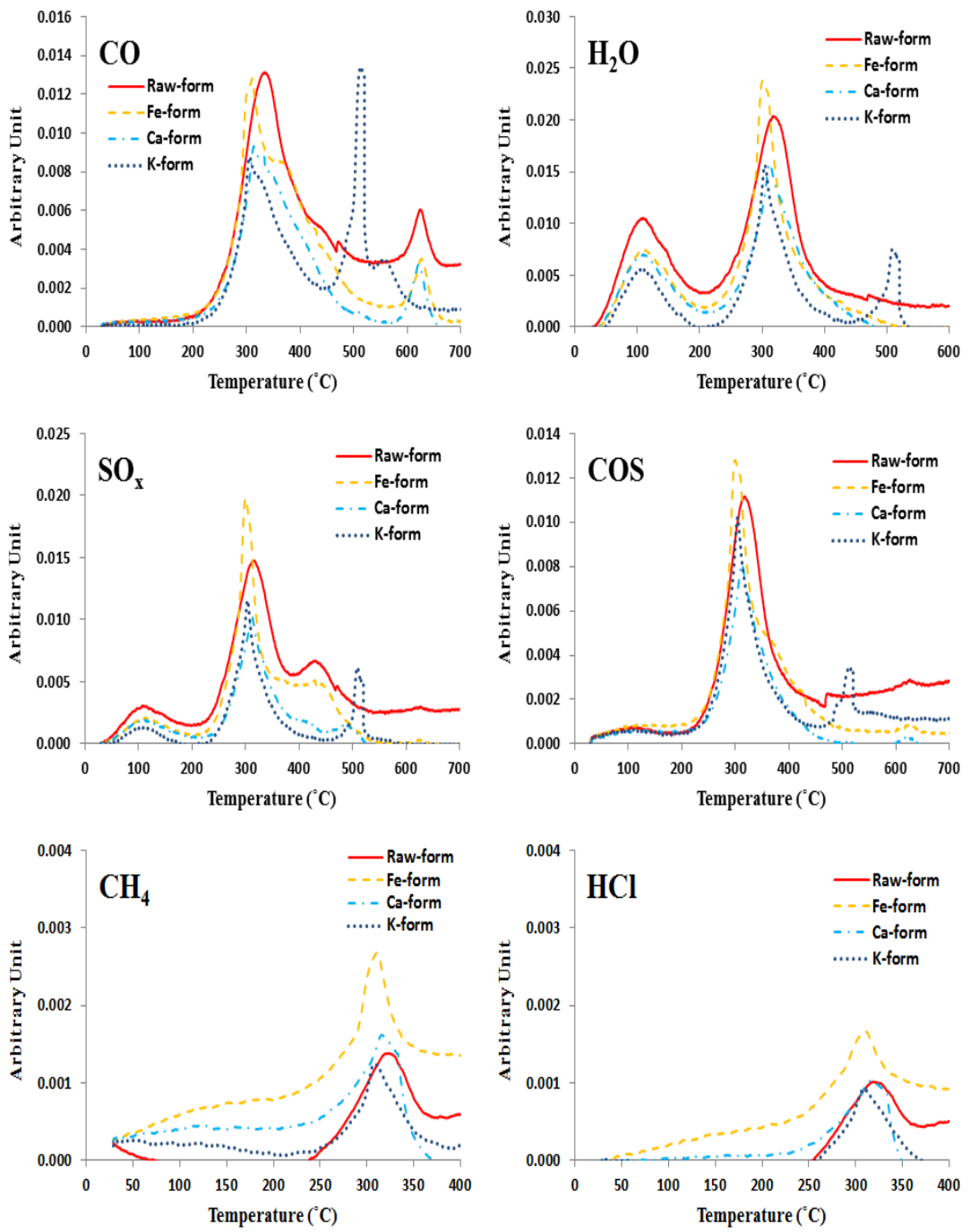


Fig. 5.41 Formation profiles of evolved gases during catalytic combustion tests in 30 % O<sub>2</sub> in CO<sub>2</sub> ambient

The evolution of CH<sub>4</sub> and HCl was also explored during combustion tests in 30 % O<sub>2</sub> in CO<sub>2</sub> ambient and the results are illustrated in Fig. 5.41 for the second region. In this region, Fe and Ca catalysts increased CH<sub>4</sub> emission as was confirmed by Zhu et al. [38]. The evolution profile of CH<sub>4</sub> during the combustion test performed with K-form lignite experienced another peak at 500 °C (Fig. 5.42) which was due to the char combustion in this temperature interval. During combustion tests, most of the organic chlorine is converted into HCl and a little chlorine is converted into Cl<sub>2</sub> directly that both will cause high temperature corrosion in furnace surface and heat transfer surface during the combustion process [41]. CaO is reported to be very effective in deacidification by Wang et al. [40] which was not confirmed by using Ca(OH)<sub>2</sub> in this study. Although Fe catalyst increased the HCl emission in 30 % O<sub>2</sub> in CO<sub>2</sub> ambient, the high content of potassium in K-form lignite was likely to contribute in reduction of HCl emission ( $K_2O + 2HCl \rightarrow 2KCl + H_2O$ ).

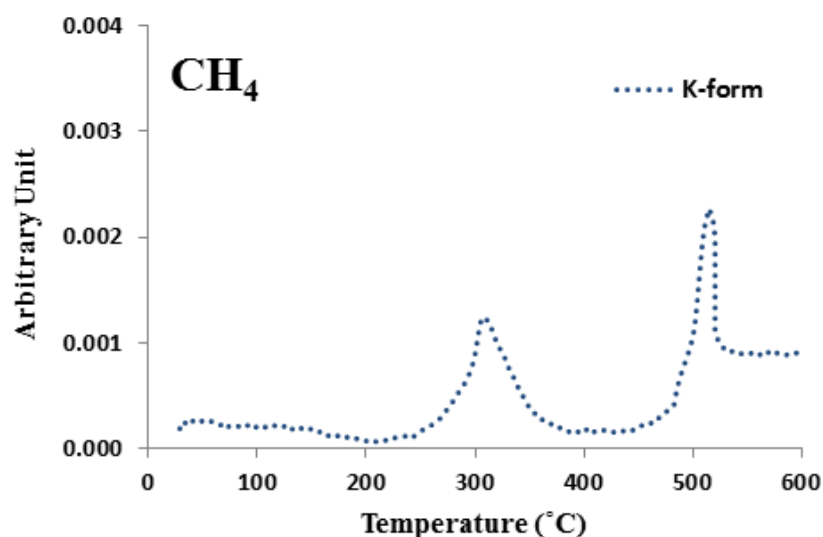


Fig. 5.42 Formation profiles of CH<sub>4</sub> during K-form sample combustion test in 30 % O<sub>2</sub> in CO<sub>2</sub> ambient

Exploring the effects of catalysts on  $\text{NH}_3$  and  $\text{NO}$  emissions (Fig. 5.43) indicated that K catalyst considerably increased the emission of  $\text{NH}_3$  in the temperature region regarding char oxidation. However, in the second region, the highest absorbance was attributed to the Fe-form lignite sample. Moreover, a considerable reduction was observed in  $\text{NO}$  formation in the case K-based catalyst in comparison with Fe- and Ca-based catalysts. The absorbance peaks at around 100 °C and 300 °C were due to water vapor caused by overlapping of the  $\text{NO}$  absorption bands with the characteristic absorption bands of water.

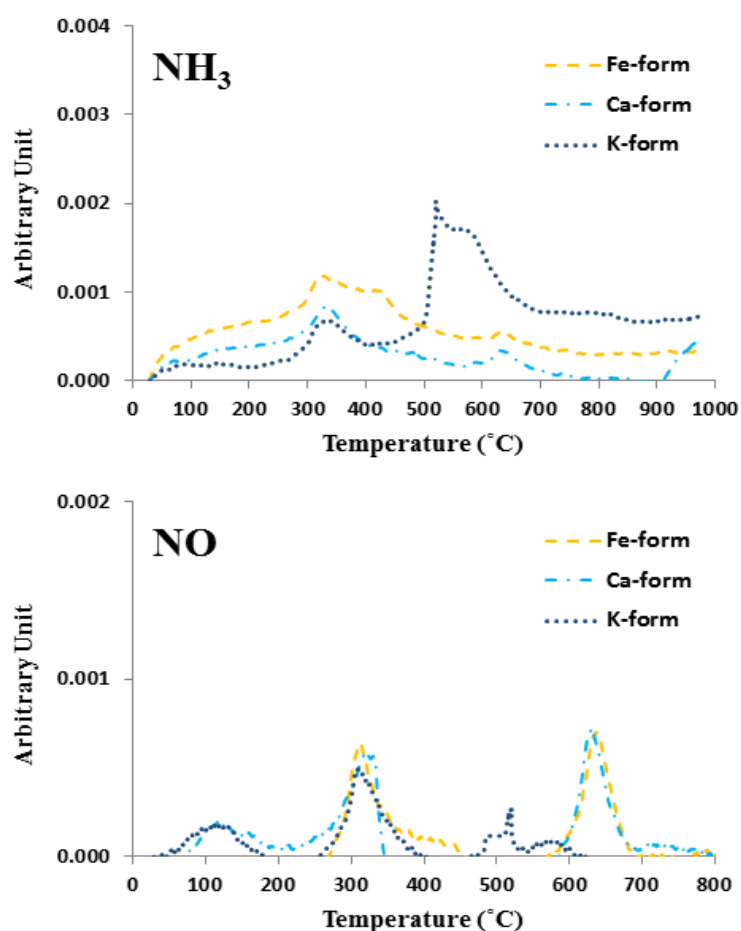


Fig. 5.43 Formation profiles of  $\text{NH}_3$  and  $\text{NO}$  during catalytic combustion tests in 30 %  $\text{O}_2$  in  $\text{CO}_2$  ambient

The correlations between the maximum rate of weight loss in DTG curves ( $|(\text{dm}/\text{dt})_{2\text{max}}|$ ) and the peak absorbance of the emissions and also between  $T_{2\text{max}}$  and  $T_{\text{FG-max}}$  for different catalysts in  $\text{O}_2/\text{CO}_2$  ambient are plotted in Fig. 5.44. A considerable delay observed in  $T_{\text{FG-max}}$  with respect to  $T_{2\text{max}}$  was more evident in CO emission during Raw- and Fe-form combustion tests. However, almost the same trend was observed in  $T_{2\text{max}}$  and  $T_{\text{FG-max}}$  profiles of different emissions for raw and impregnated lignite samples (Fig. 5.44 (a)). Furthermore, as illustrated in Fig. 5.44 (b), the maximum absorbance of the evolved gases was nearly consistent with the maximum rate of weight loss due to volatile matter combustion for raw and impregnated lignite samples. This correlation was better observed in the sulphur containing species,  $\text{SO}_x$  and COS.

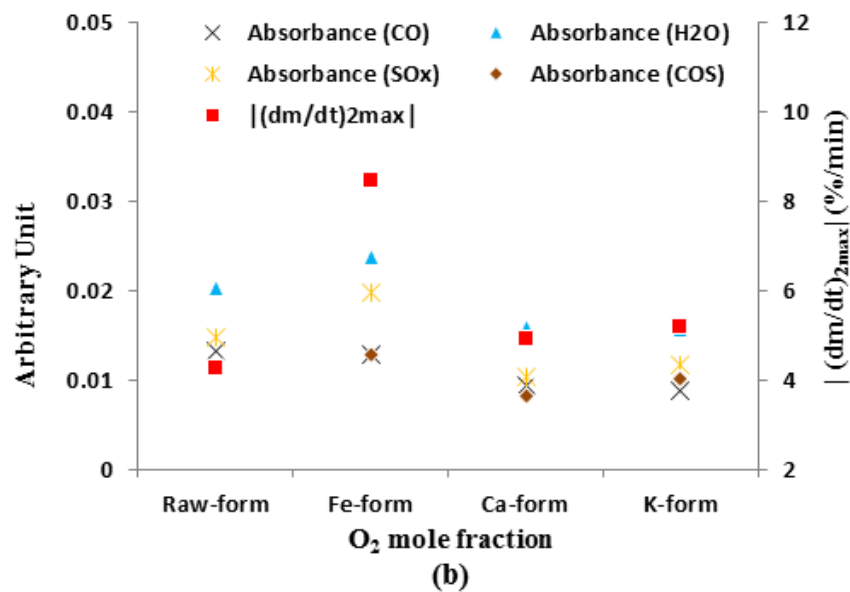
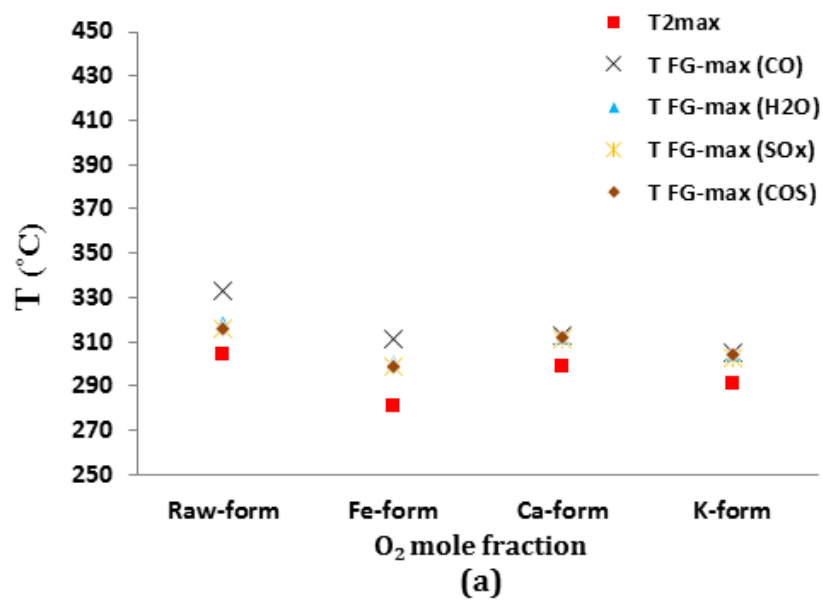


Fig. 5.44 Characteristic parameters of the catalytic combustion tests in 30 % O<sub>2</sub> in CO<sub>2</sub> ambient: correlations between: a) T<sub>2max</sub> and T<sub>FG-max</sub>, b) |(dm/dt)<sub>2max</sub>| and maximum absorbance of the evolved gases in FTIR spectra

### 5.2.11 Effects of Ambient on Catalytic Reactivity in Kangal Lignite Combustion Tests

In this part of the study a special attention is focused on the effects of ambient ( $N_2$  and  $CO_2$  which are the main diluting gases in normal air and oxy-fuel combustion) on catalytic reactivity of Fe-based and K-based catalysts.

#### 5.2.11.1 Fe-based Catalyst

A comparison was made between the combustion processes of impregnated Kangal lignite under the same oxygen concentration but different ambient conditions and the results are indicated in Figs. 5.45- 5.47 and the detailed data is referred to Appendix D. During the combustion tests performed in 21 %  $O_2$ , no considerable influence of ambient on the reactivity of Fe-based catalyst was observed. In 25 %  $O_2$  in  $N_2$  ambient, the combustion process was improved as the DTG curve was pushed toward the lower temperature zone corresponded with much higher reaction rate.

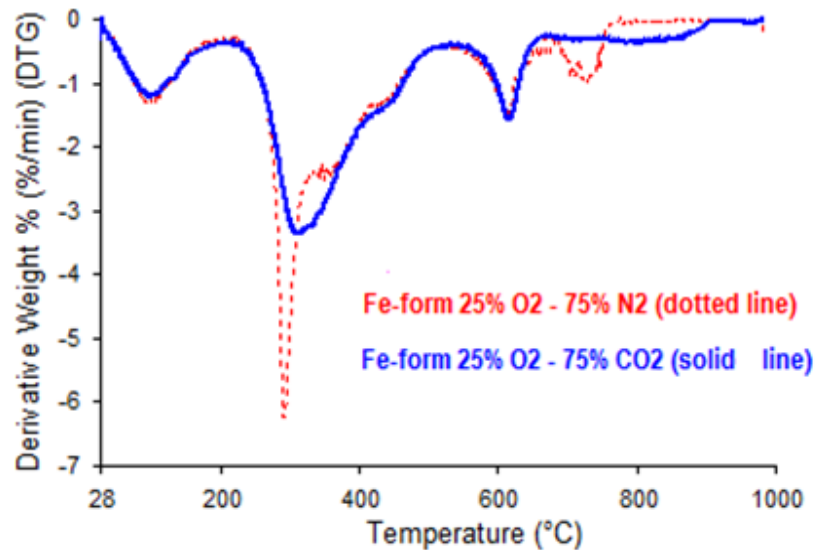


Fig. 5.45 DTG profiles of Fe-form Kangal lignite combustion in 25 %  $O_2$

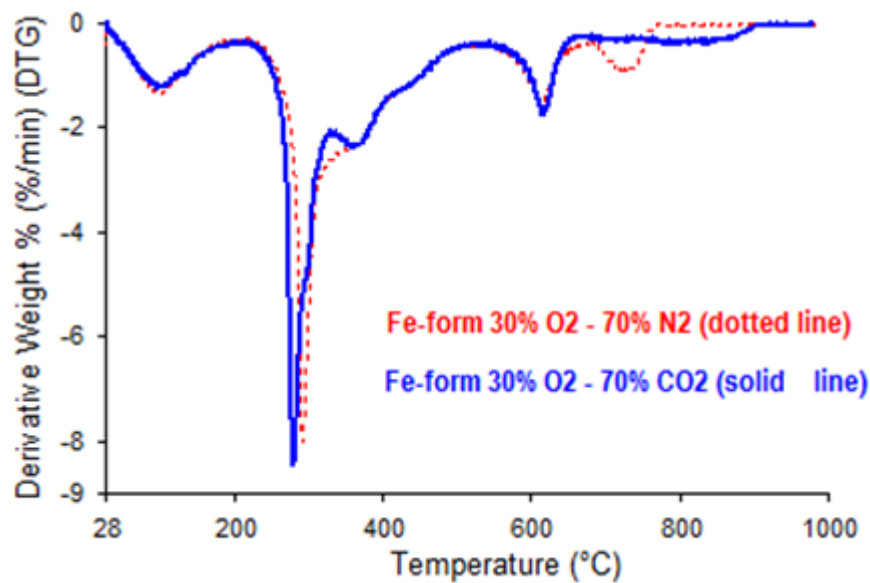


Fig. 5.46 DTG profiles of Fe-form Kangal lignite combustion in 30 % O<sub>2</sub>

On the contrary to 25 % O<sub>2</sub>, during the tests in 30 % O<sub>2</sub>, it was observed that the Fe catalyst was slightly more reactive in CO<sub>2</sub> than in N<sub>2</sub> ambient conditions. This result can be confirmed by the fact that in N<sub>2</sub> ambient, T<sub>ig</sub> and T<sub>max</sub> were slightly higher and the maximum reaction rate was lower with respect to Fe-form sample combustion in CO<sub>2</sub>.

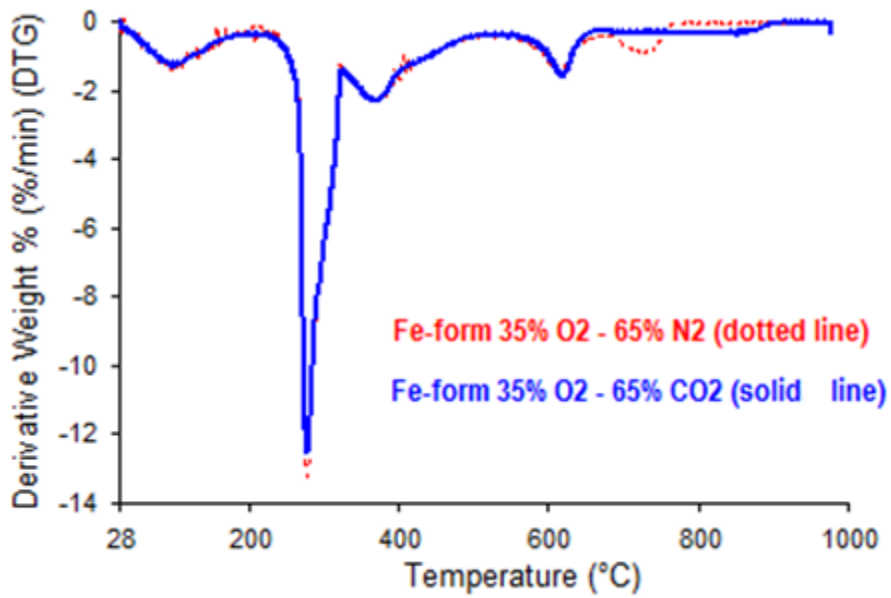


Fig. 5.47 DTG profiles of Fe-form Kangal lignite combustion in 35 % O<sub>2</sub>

In the case of 35 % O<sub>2</sub> and Fe-based catalyst, it was illustrated that the N<sub>2</sub> and CO<sub>2</sub> ambient conditions have almost the same influence in catalyst reactivity.

#### 5.2.11.2 K-based Catalyst

According to the DTG profiles in Figs. 5.48- 5.50, the effects of ambient conditions (N<sub>2</sub> and CO<sub>2</sub>) on the reactivity of K-based catalyst are investigated and the detailed data is referred to Appendix D. In 25 % O<sub>2</sub>, it was observed that the influence of different ambient conditions was observed in the 440-580 °C temperature interval which coincided with the considerable peak observed in combustion tests of K-based catalyst. However, the peak in N<sub>2</sub> ambient was more considerable than in CO<sub>2</sub> in this temperature range which can be an indication of higher char reactivity in N<sub>2</sub> while performing tests with K-based catalyst.

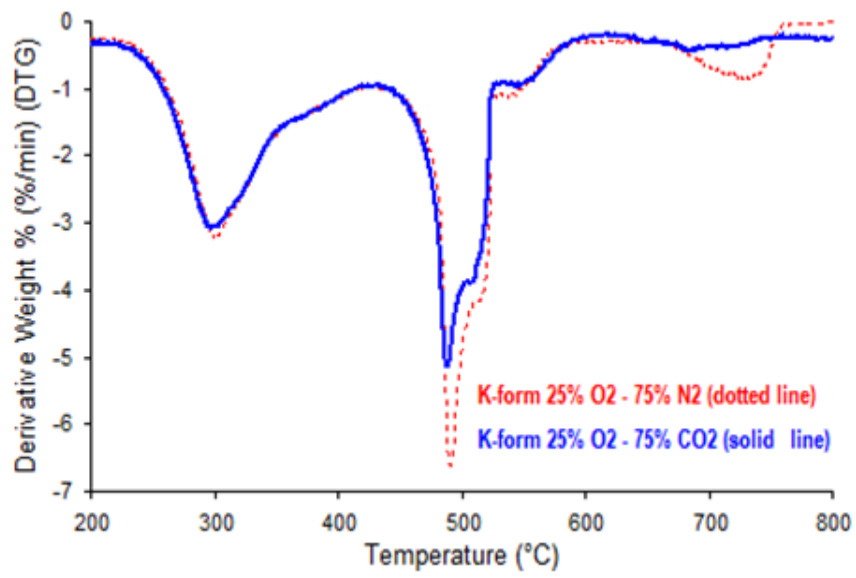


Fig. 5.48 DTG profiles of K-form Kangal lignite combustion in 25 % O<sub>2</sub>

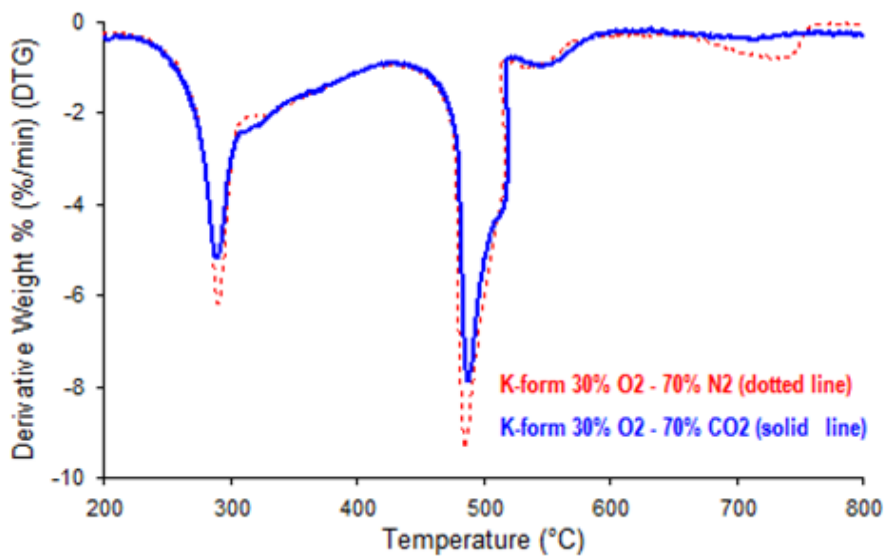


Fig. 5.49 DTG profiles of K-form Kangal lignite combustion in 30 % O<sub>2</sub>

In 30 % O<sub>2</sub>, the better reactivity of Fe-form sample was confirmed by higher reaction rates in both second and third regions.

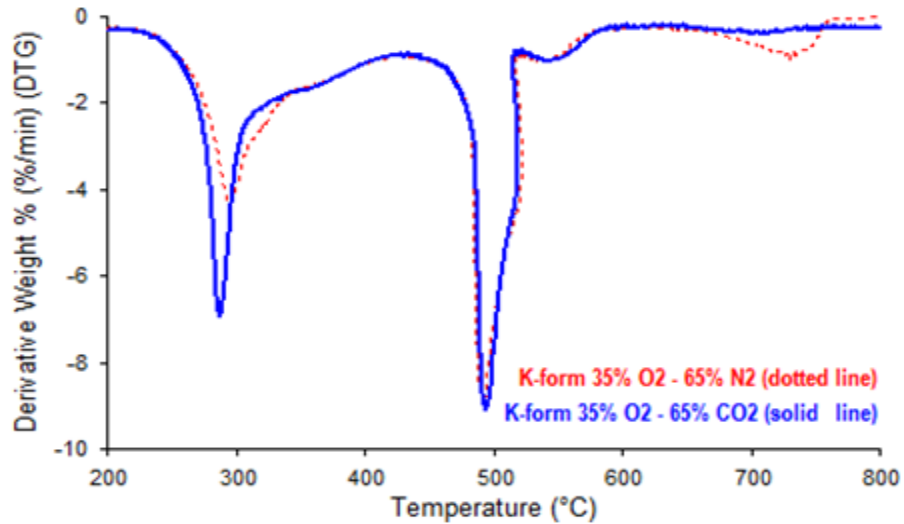


Fig. 5.50 DTG profiles of K-form Kangal lignite combustion in 35 % O<sub>2</sub>

In exploring the effects of ambient conditions on catalytic activities of K catalyst in 35 % O<sub>2</sub>, the only difference was observed in temperature interval related to the volatile release and combustion. In this region, the better reactivity of K-based catalyst was observed in CO<sub>2</sub> ambient.

### 5.3 Combustion Tests of Tunçbilek Sub-Bituminous Coal Sample

#### 5.3.1 Effects of N<sub>2</sub> and CO<sub>2</sub> Ambient Conditions (TGA/DTG Results)

The TGA/DTG curves illustrated in Fig. 5.51 are profiles to investigate the effects of different ambient conditions on combustion characteristics of Tunçbilek sub-

bituminous coal in 30 % O<sub>2</sub>. As is obvious from the DTG profiles, no considerable difference was observed in combustion characteristics of this coal sample in the low temperature region (< 550 °C). However, slight differences were observed at 600 °C due to the remaining char oxidation.

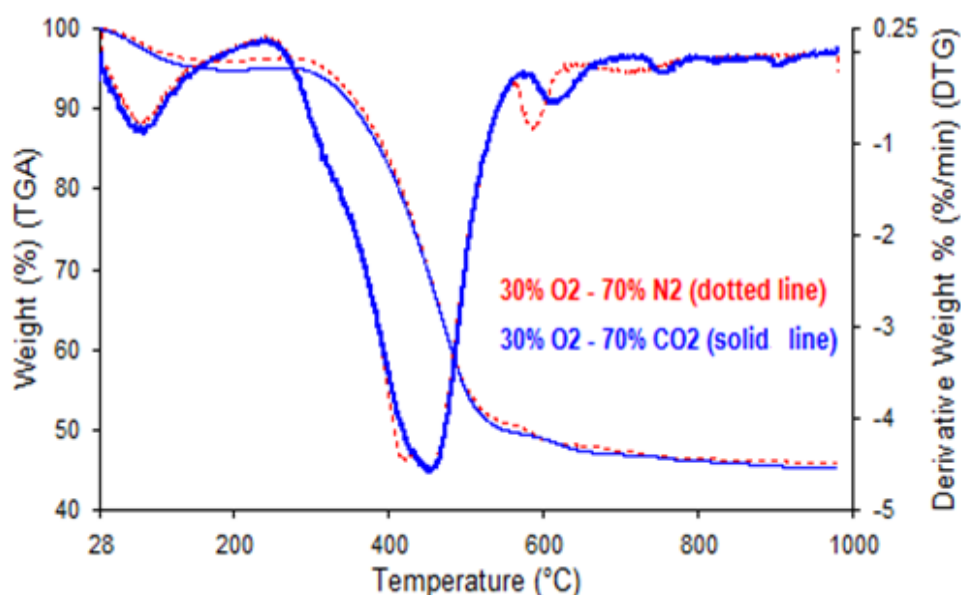


Fig. 5.51 TGA and DTG profiles of Tunçbilek coal combustion during 30 % O<sub>2</sub> in N<sub>2</sub> and 30 % O<sub>2</sub> in CO<sub>2</sub> ambient conditions

### 5.3.2 Effects of N<sub>2</sub> and CO<sub>2</sub> Ambient Conditions (FTIR Results)

The evolution profiles of CO, H<sub>2</sub>O and sulphur containing species, SO<sub>x</sub> and COS, were monitored in 30 % O<sub>2</sub> for both N<sub>2</sub> and CO<sub>2</sub> ambient conditions and the results are indicated in Fig. 5.52. According to these results, in both ambient conditions a main peak and a shoulder were detected at 460 °C and 330 °C respectively in CO evolution profiles. H<sub>2</sub>O emission profiles had two peaks at 100 °C and 325 °C in both

ambient conditions for which the first one was due to the primary moisture release.  $\text{SO}_x$  and COS profiles peaked at 430 °C and 450 °C respectively. However, a shoulder was observed at 330 °C in COS emission profiles. The first peaks at 100 °C and 325 °C in  $\text{SO}_x$  formation profiles were more likely to be related to the water vapor emissions. Furthermore, the emission of  $\text{SO}_x$  was slightly higher in  $\text{N}_2$  with respect to  $\text{CO}_2$  ambient while in the case of COS emissions, the inverse behavior was observed.

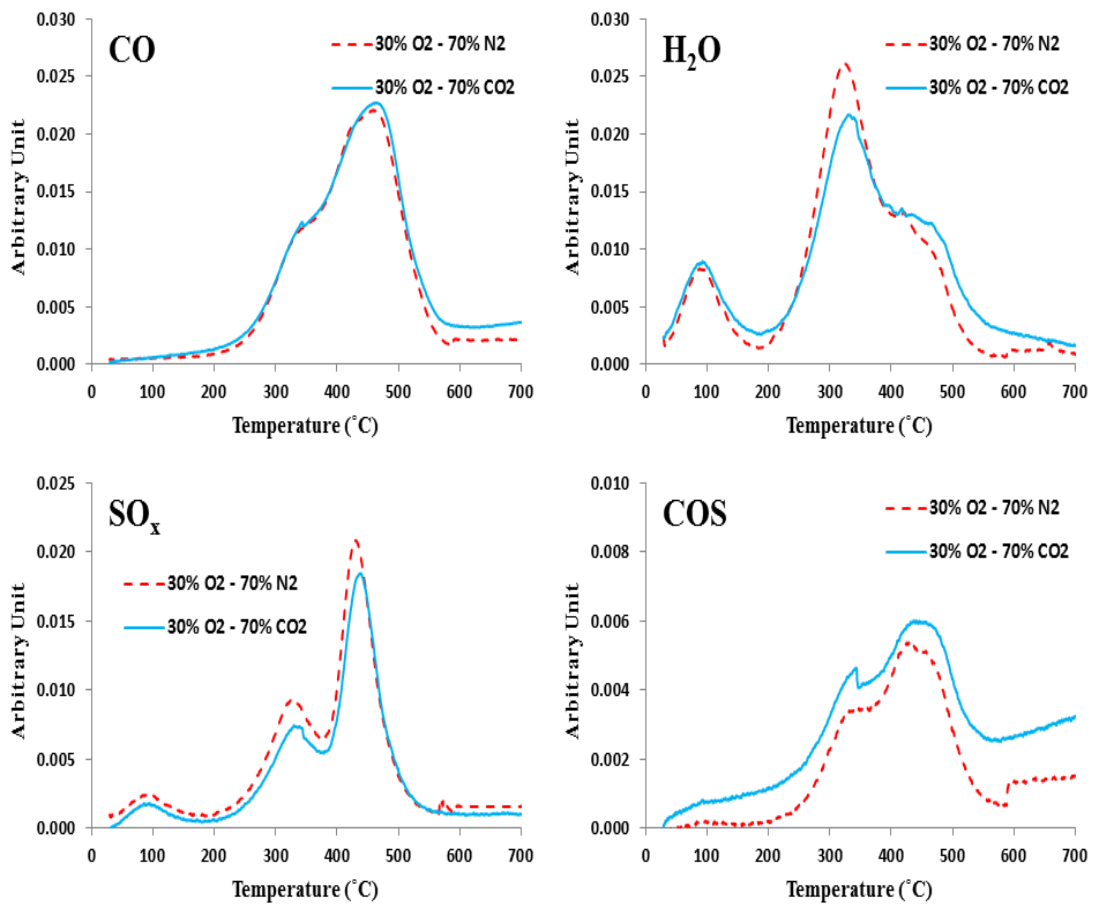


Fig. 5.52 Formation profiles of evolved gases during combustion tests under 30 % O<sub>2</sub> in N<sub>2</sub> and 30 % O<sub>2</sub> in CO<sub>2</sub> ambient conditions

### 5.3.3 Effects of Different Oxygen Mole Fractions (TGA/DTG Results)

The effects of different oxygen mole fractions on combustion characteristics of Tunçbilek coal sample were analyzed through TGA and DTG profiles (Fig. 5.53) of combustion tests under 21 % and 30 % O<sub>2</sub> in N<sub>2</sub> ambient conditions. As illustrated in Fig. 5.53, the TGA and DTG profiles were pushed to lower temperature zone as the oxygen concentration was switched to 30 %. However, the maximum rate of weight loss was not improved in the case of higher oxygen concentration which was not an expected result.

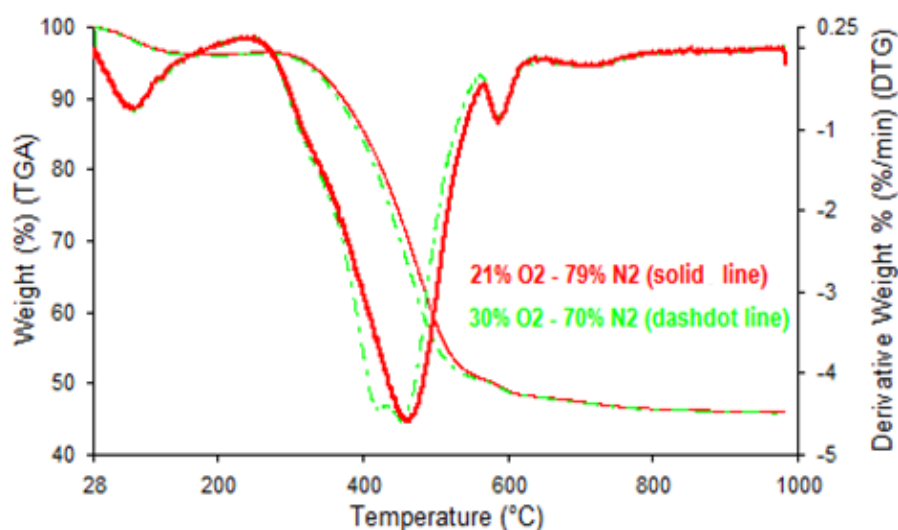


Fig. 5.53 Combustion profiles of Tunçbilek sample under 21 % O<sub>2</sub> in N<sub>2</sub> and 30 % O<sub>2</sub> in N<sub>2</sub> ambient conditions

### 5.3.4 Effects of Different Oxygen Mole Fractions (FTIR Results)

The FTIR results of Tunçbilek combustion tests are indicated in Figs. 5.54 and 5.55. As illustrated in these figures, the evolution profiles of the gases were pushed

slightly to the lower temperature zone. However, no considerable effect was observed in these profiles.

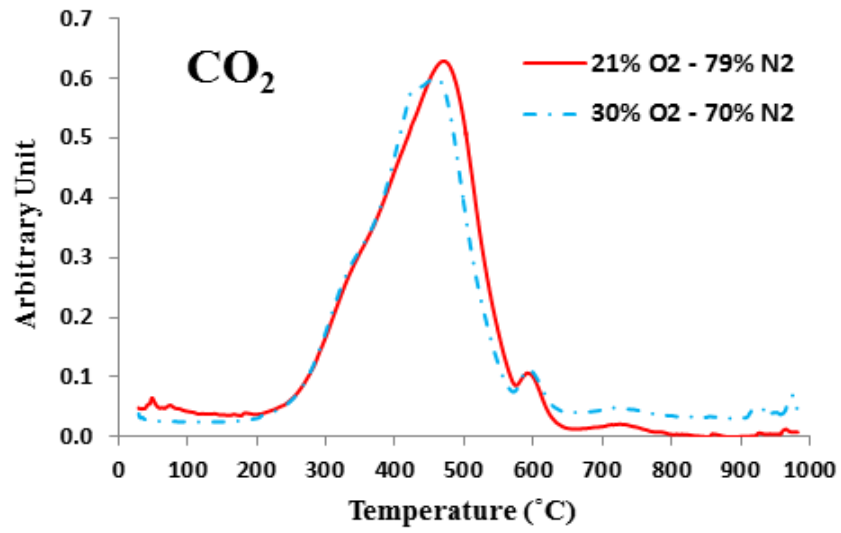


Fig. 5.54 Formation profiles of CO<sub>2</sub> during Tunçbilek combustion tests in N<sub>2</sub> ambient

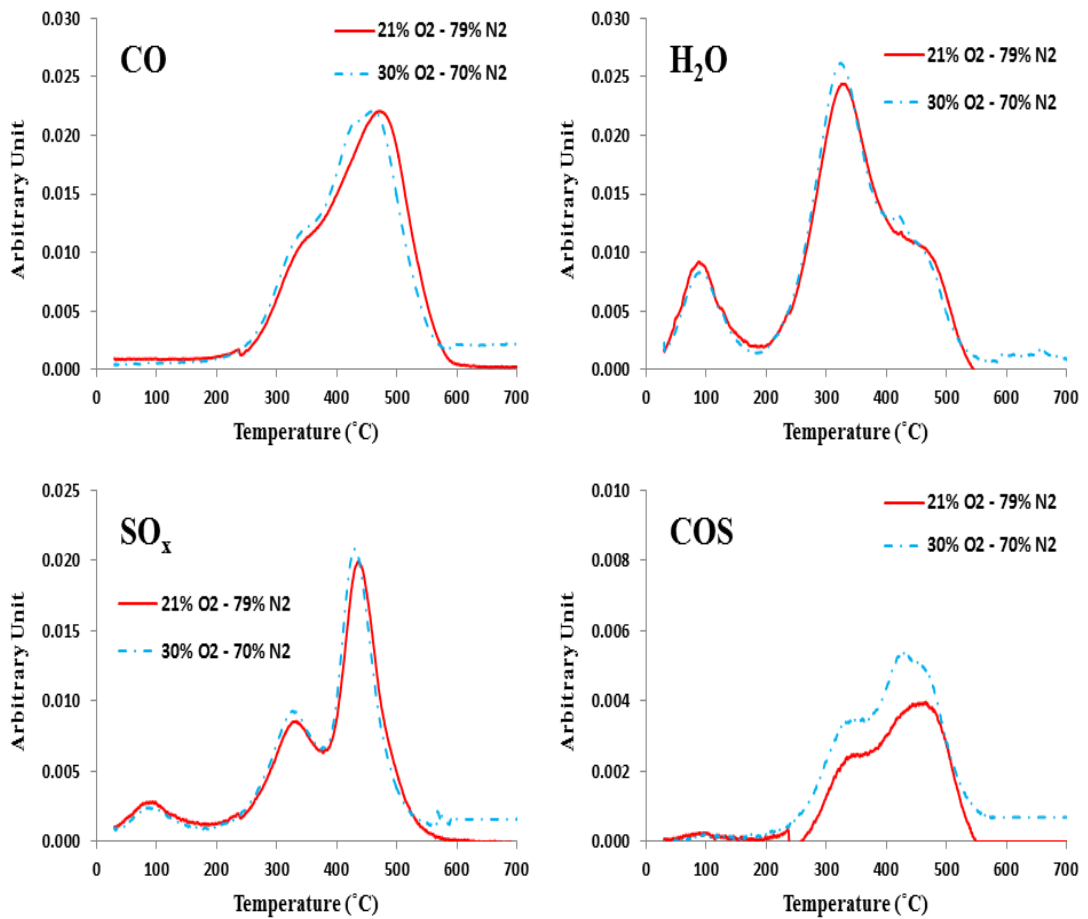


Fig. 5.55 Formation profiles of evolved gases during Tunçbilek combustion tests in N<sub>2</sub> ambient

### 5.3.5 Effects of Catalysts on Combustion Tests of Tunçbilek Sub-Bituminous Coal Sample in N<sub>2</sub> Ambient (TGA/DTG Results)

The TGA and DTG profiles of Tunçbilek combustion in 30 % O<sub>2</sub> in N<sub>2</sub> for the raw and impregnated samples with Fe catalyst is illustrated in Fig. 5.56. Analyzing the effects of Fe-based catalyst on combustion characteristics demonstrated that addition of Fe improved the reactivity of the Tunçbilek sample. This was confirmed by much higher reaction rates in the temperature interval of 350- 450 °C and lower

$T_{ig}$  and  $T_{max}$ . Furthermore, it was observed that during the combustion tests carried out with Fe-form coal sample, the process of combustion varied from a single stage to double stages in this temperature interval.

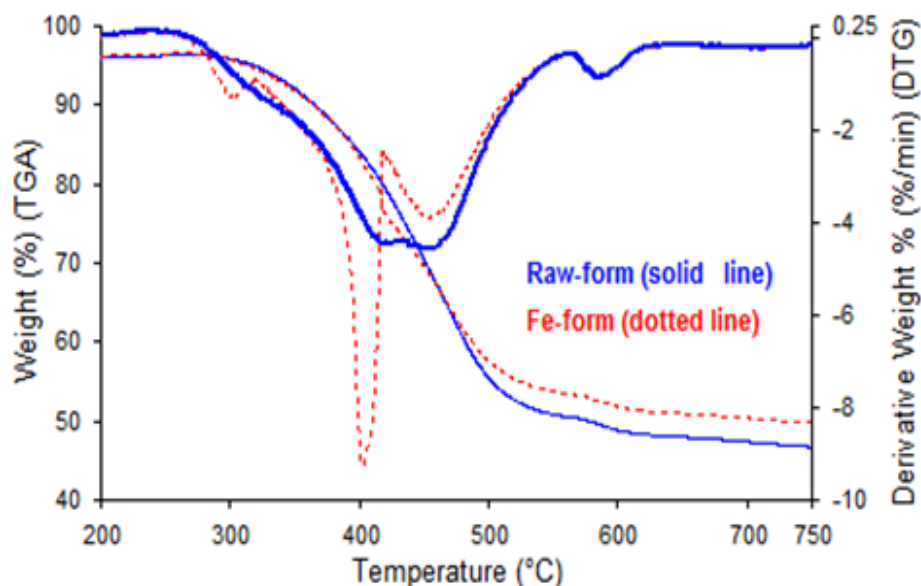


Fig. 5.56 Combustion profiles of catalytic Tunçbilek combustion tests in 30 %  $O_2$  in  $N_2$  ambient

### 5.3.6 Effects of Catalysts on Combustion Tests of Tunçbilek Sub-Bituminous Coal Sample in $N_2$ Ambient (FTIR Results)

Comparisons of evolution profiles of  $CO$ ,  $H_2O$ ,  $SO_x$  and  $COS$  in Fig. 5.57 indicated that the evolution of these gases experienced sharper peaks corresponded with lower  $T_{FG-max}$  in the case Fe-based catalyst in comparison with the Raw-form combustion. These sharp peaks occurred in correlation with the peak observed at around  $400\text{ }^\circ C$  in DTG curves due to volatile matter release and combustion.

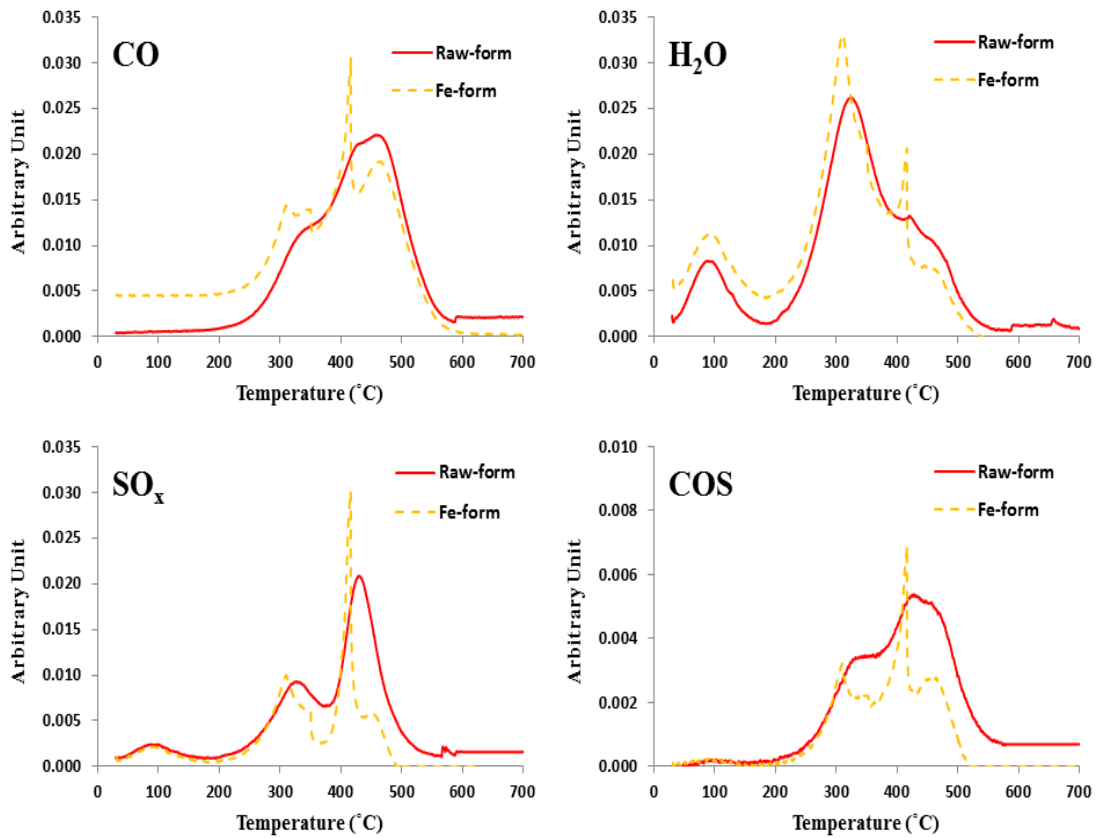


Fig. 5.57 Formation profiles of evolved gases during catalytic Tunçbilek combustion tests in 30 % O<sub>2</sub> in N<sub>2</sub> ambient

### 5.3.7 Effects of Catalysts on Combustion Tests of Tunçbilek Sub-Bituminous Coal Sample in CO<sub>2</sub> Ambient (TGA/DTG Results)

The catalytic combustion characteristics of Tunçbilek sample under 30 % O<sub>2</sub> in CO<sub>2</sub> ambient are indicated in Figs. 5.58 and 5.59. The most significant effects of catalysts were observed in the temperature region of 250-550 °C which was more significant in the case of K-based catalyst. During the catalytic combustion tests, it was observed that the process of combustion varied from a single stage to double stages within the temperature interval of 350-500 °C which was clear in K-form

combustion case. The maximum rate of weight loss was lower in Ca- and Fe-form tests with respect to original coal combustion while the K-form showed the highest. Furthermore, a slight peak was observed at 280 °C in K-form combustion which was thought to be due to the further moisture release as was confirmed by FTIR tests.

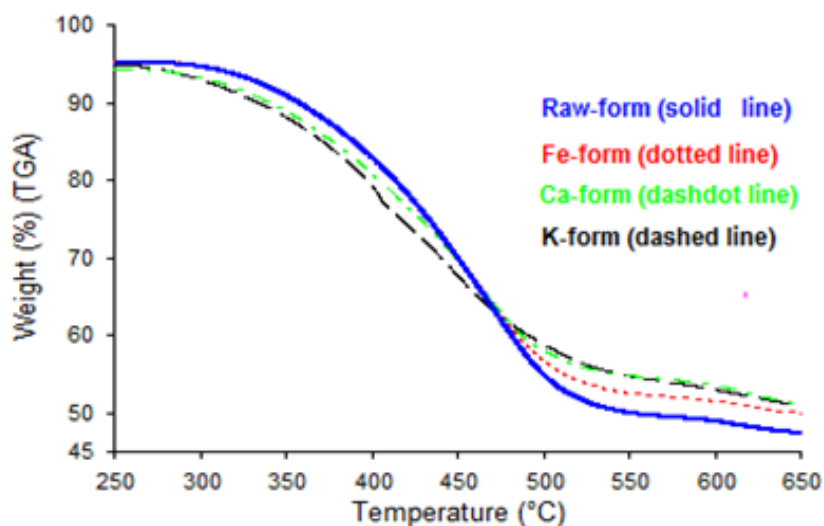


Fig. 5.58 TGA profiles of catalytic Tunçbilek combustion tests in 30 % O<sub>2</sub> in CO<sub>2</sub> ambient

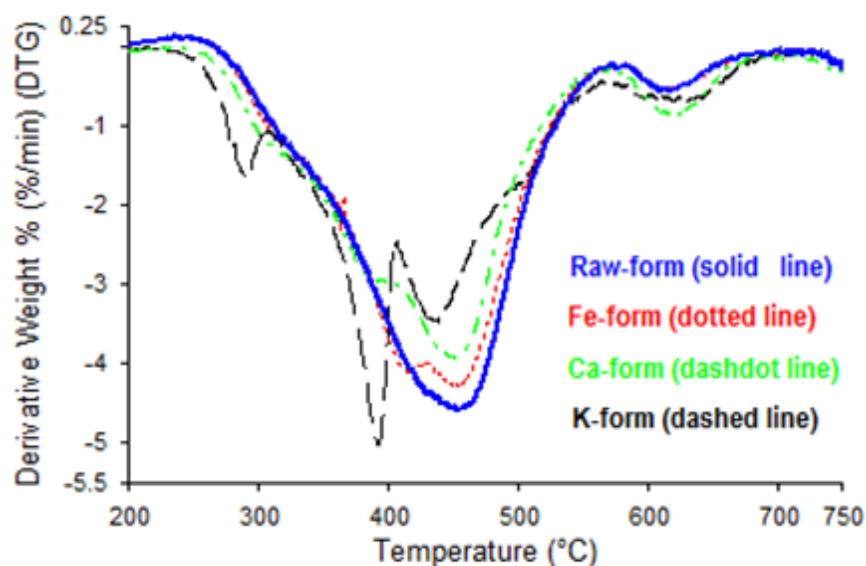


Fig. 5.59 DTG profiles of Tunçbilek catalytic combustion tests in 30 % O<sub>2</sub> in CO<sub>2</sub> ambient

### 5.3.8 Effects of Catalysts on Combustion Tests of Tunçbilek Sub-Bituminous Coal Sample in CO<sub>2</sub> Ambient (FTIR Results)

The evolution of evolved gases was influenced by the use of catalysts as illustrated in Fig. 5.60. While the Fe-based catalyst did not show any considerable effects on evolution of sulphur containing species (SO<sub>x</sub> and COS), Ca- and K-based catalysts had remarkable effects in reduction of these emissions. The main peaks of SO<sub>x</sub> and COS were considerably lower in the case of these catalysts. Moreover, CO emissions were reduced in combustion tests carried out with Ca- and K-based catalysts.

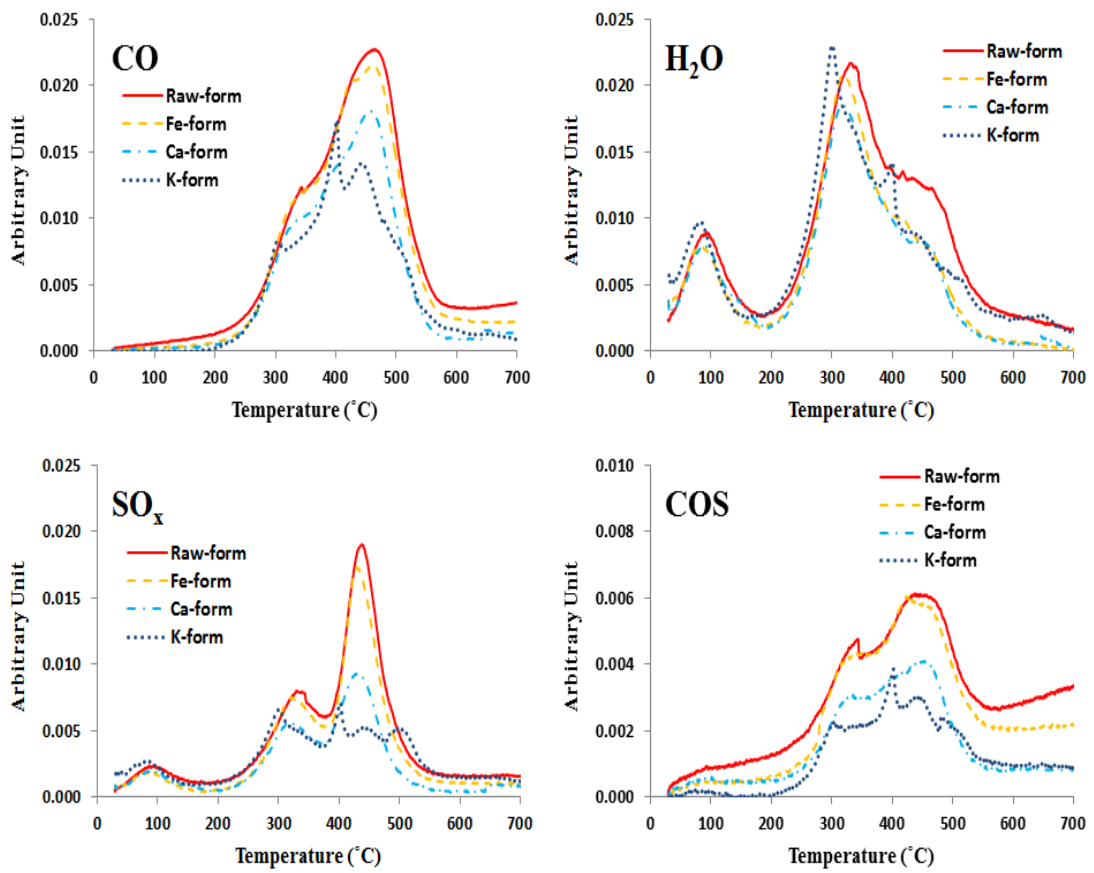


Fig. 5.60 Formation profiles of evolved gases during catalytic Tunçbilek combustion tests in 30 % O<sub>2</sub> in CO<sub>2</sub> ambient

#### 5.4 Co-processing Combustion Tests of Lignite and the Ash Contents of Turkish Biomass Fuels

In this section, the possible way of using Turkish biomass fuels as a potential source of inexpensive catalysts in the co-processing of lignite and biomass ash in O<sub>2</sub>/N<sub>2</sub> and O<sub>2</sub>/CO<sub>2</sub> (oxy-fuel conditions) ambient conditions was investigated using TGA-FTIR method. Throughout this part of the study, various types of biomass including walnut shell (WSh), hazelnut shell (HSh), wheat straw (WS), Limba wood saw dust (SD) and cattle manure (CM) from the domestic sources were used. The

biomass ash contents were applied as the precursors of catalysts to form WSh-form, HSh-form, WS-form, CM-form and SD-form lignite samples and the results compared with the results obtained from the utilization of potassium (K) and calcium (Ca) inorganic catalysts. The same impregnation method and procedure was used as described in Chapter 3. The biomass ash addition to the raw lignite by impregnation corresponded 15 % in terms of mass ratio of biomass ash to coal (dry basis). Kangal lignite ( $< 106 \mu\text{m}$ ) was used in these experiments. Characteristic temperatures and parameters defined in Chapter 3.2.1.3 were used to analyze and compare the results.

#### **5.4.1 Biomass Ash Analyses**

The XRF method was used to analyze the ash contents of the biomass fuels and the results are listed in Table 5.12. Moreover, the major contributions of alkali and alkaline earth metals in the ash contents of the evolved biomass are illustrated in Fig. 5.61.

Table 5.12 Ash analyses of the Turkish biomass fuels

<b>Element-based Oxides (% By weight)</b>	<b>Si</b>	<b>Al</b>	<b>Ca</b>	<b>Mg</b>	<b>K</b>	<b>Na</b>	<b>Fe</b>	<b>Ti</b>	<b>P</b>	<b>S</b>
<b>Walnut shell</b>	5.287	2.099	29.04	5.854	35.52	< 0.11	0.7726	0.0421	2.565	0.9244
<b>Hazelnut shell</b>	10.29	5.349	24.89	6.049	33.82	< 0.11	0.7089	0.0568	3.140	2.071
<b>Wheat straw</b>	77.01	0.717	4.520	2.464	11.58	< 0.11	0.6049	0.0371	2.749	2.723
<b>Cattle manure</b>	66.46	0.752	4.373	4.140	6.771	10,77	0.6151	0.0342	6.272	1.492
<b>Saw dust</b>	1.965	0.1846	65.02	8.419	16.276	< 0.11	1.012	0.601	2.192	1.740

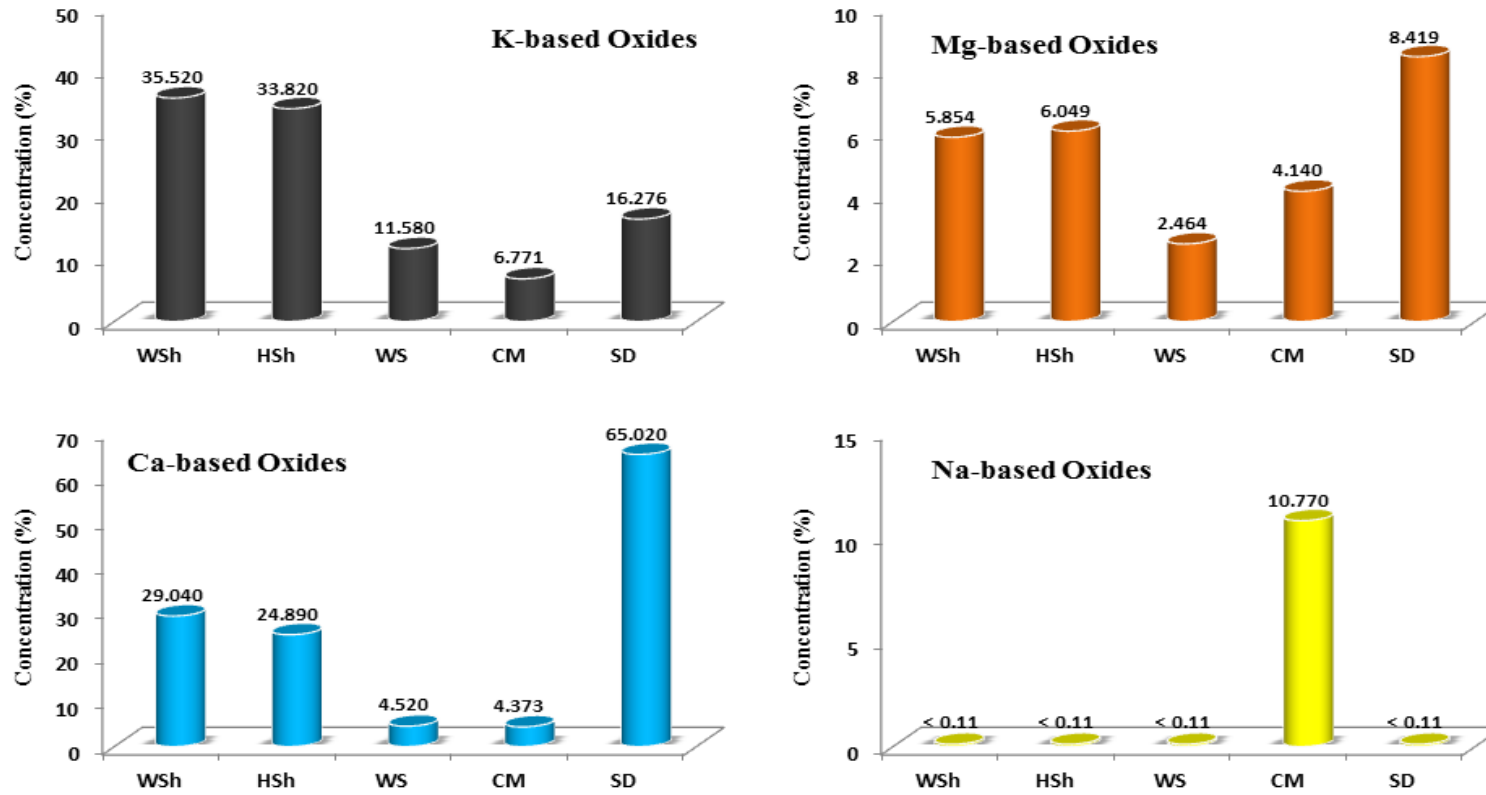


Fig. 5.61 Major contributions of alkali and alkaline earth metals in the ash contents of Turkish biomass fuels

As listed in Table 5.12 and indicated in Fig. 5.61, a considerably high amount of Si-based oxides were observed in the ash contents of indigenous wheat straw and cattle manure which correspond 77 % and 66 % respectively. However, the amount of Ca-based oxides were observed to be the lowest (~ 4 %) in wheat straw and cattle manure while the XRF results indicated that this contribution was significantly high (~ 65 %) in the ash content of Limba wood saw dust. Furthermore, The XRF results revealed that K-based oxides were the major contributors of the ash in walnut and hazelnut shell biomass fuels for which these contributions corresponded 35.52 % and 33.82 % respectively. The amount of Na-based oxides traced in the ash contents was considerably higher in the case of cattle manure (10.77 %) in comparison with other biomass fuels evolved in this study. No considerable contribution of Fe-based oxides was observed in the ash contents of the evolved biomass fuels.

#### **5.4.2 Combustion Test Results**

Combustion tests carried out in air, 30 % O<sub>2</sub> in N<sub>2</sub>, 21 % O<sub>2</sub> in CO<sub>2</sub> and 30 % O<sub>2</sub> in CO<sub>2</sub> ambient conditions. However, analyses in this part of the study will cover the combustion tests in air and in 30 % O<sub>2</sub> in CO<sub>2</sub> ambient.

##### **5.4.2.1 Combustion Tests Carried Out in Air**

The combustion test results of the impregnated lignite samples in air are listed in Table 5.13. Comparisons are made between the combustion processes of original Kangal lignite and the impregnated lignite samples with biomass ash contents using DTG curves (Fig. 5.62).

Table 5.13 Characteristic temperatures and parameters of original and impregnated Kangal lignite combustion tests in air

<b>Air</b>	<b>Original Kangal lignite</b>	<b>Fe-form</b>	<b>K-form</b>	<b>HSh-form</b>	<b>WSh-form</b>	<b>WS-form</b>	<b>CM-form</b>	<b>SD-form</b>
<b>T<sub>in</sub> (°C)</b>	243	246	245	248	248	250	247	252
<b>T<sub>ig</sub> (°C)</b>	287	288	274	286	281	283	283	280
<b>T<sub>2max</sub> (°C)</b>	332	328	308	319	318	302	306	312
<b>T<sub>b</sub> (°C)</b>	751	750	751	750	766	740	731	770
<b> <math>(\frac{dm}{dt})_{2max}</math>  (%/min)</b>	3.01	3.09	2.88	2.57	2.33	6.20	4.15	2.91
<b>T<sub>3max</sub> (°C)</b>	608	611	489	495	496	606	602	590
<b> <math>(\frac{dm}{dt})_{3max}</math>  (%/min)</b>	1.35	1.49	5	3.92	3.16	1.78	1.76	1.92

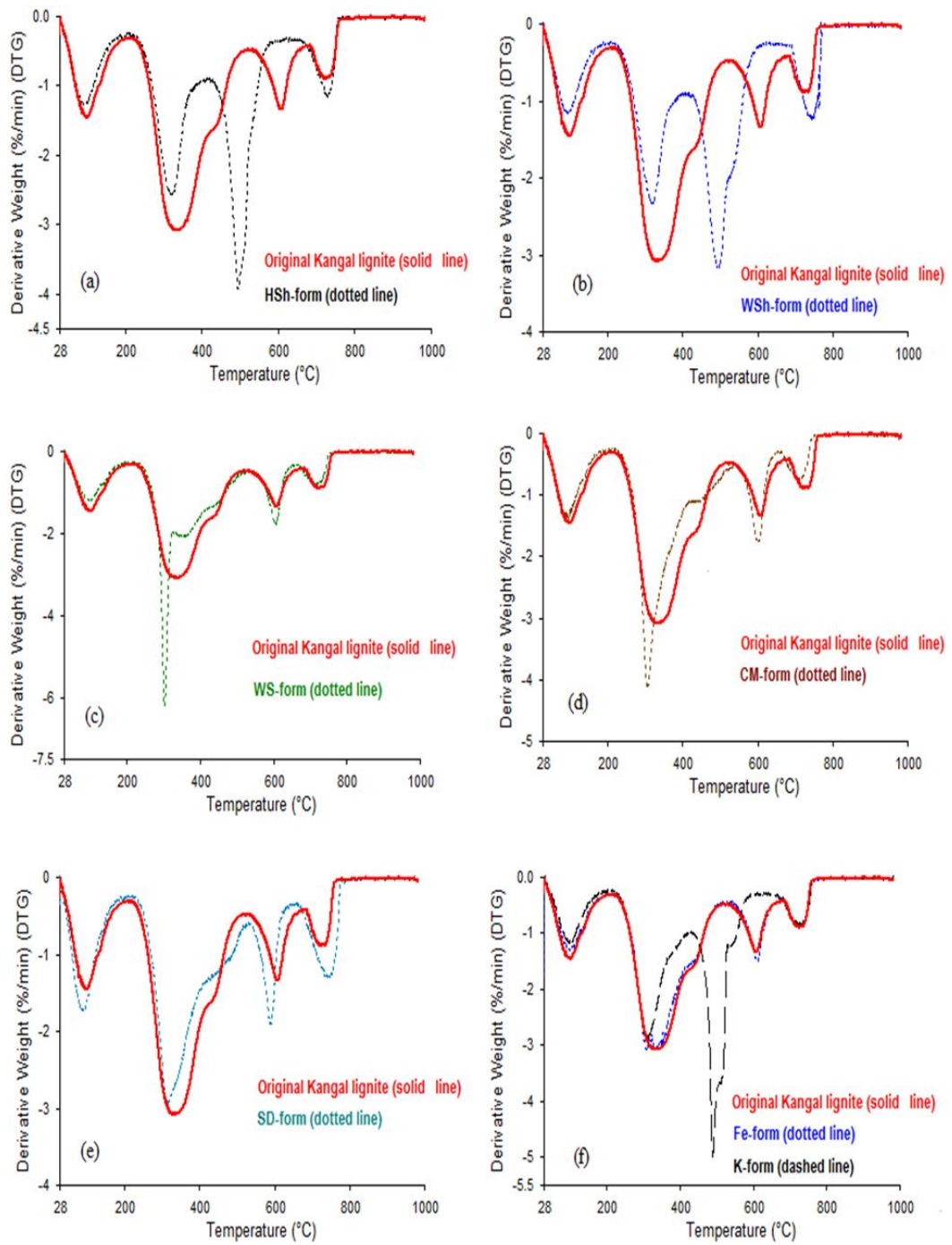


Fig. 5.62 DTG combustion curves of original and impregnated Kangal lignite with biomass ash contents in air

During air combustion tests and in the case of HSh-form sample (Fig. 5.62 (a)), it was illustrated that  $T_{2\max}$  was reduced by 13 °C and  $|(dm/dt)_{2\max}|$  was also decreased from 3.01 %/min to 2.57 %/min. Furthermore, a considerable peak was observed at 495 °C (3.92 %/min) which was not seen in the tests carried out with Raw-form samples. WSh (Fig. 5.62 (b)) decreased  $T_{2\max}$  and the reaction rates were lower in the second region. However, a considerable peak in the third region was observed for WSh-form sample in comparison with Raw-form combustion which corresponded 3.16 %/min. These peaks regarding char combustion in the third region during the tests carried out with HSh and WSh lignite samples indicated that char reactivity was much higher due to high concentration of potassium in the ash contents of the impregnated samples (with the HSh and WSh) with respect to Raw-form sample. The catalytic activity of WS and CM ash contents (Fig. 5.62 (c and d)), was confirmed by higher maximum reaction rates which occurred in considerably lower temperatures in the second region of combustion regarding volatile matter release and combustion.  $T_{2\max}$  and  $|(dm/dt)_{2\max}|$  were 302 °C and 306 °C and 6.20 %/min and 4.15 %/min in the cases of WS and CM respectively. These results might be due to the high concentrations of alkali and alkaline earth metals existed in the impregnated lignite samples and especially Na-based oxides in the CM-form. No significant difference was observed in the combustion tests of impregnated lignite sample with SD ash (Fig. 5.62 (e)). However, the maximum reaction rate in the second region occurred in the lower temperature zone and the char combustion was improved slightly.

The combustion tests carried out in air revealed that the HSh-form lignite sample showed the best catalytic reactivity in the third region regarding char combustion. Furthermore, it was indicated that the best catalytic reactivity in the second region was related with WS-form lignite sample. The DTG curve comparisons of Raw- Fe- and K-form samples are illustrated in Fig. 5.62 (f).

The catalytic effects of HSh and WSh ash, containing considerably high amounts of K-based oxides, were compared with catalytic reactivity of potassium applied using  $K_2CO_3$  precursor in air (Fig. 5.63). As listed in Table 5.14, the original Kangal lignite was impregnated with 5 % (by weight) of  $K_2CO_3$  precursor while the impregnation with biomass ash contents corresponded 15 % (by weight). However,

almost the same concentrations of K-based oxides (~ 8.5 %) were traced in the ash contents of impregnated lignite samples. As indicated in Fig. 5.63, although the reactivity of lignite char in the third region was higher in the case of K-form sample with respect to HSh- and WSh-form lignite samples, these results revealed that the ash contents of walnut and hazelnut shell biomass fuels can be used as a potential source of inexpensive K-based catalysts in the co-processing of coal and biomass ash.

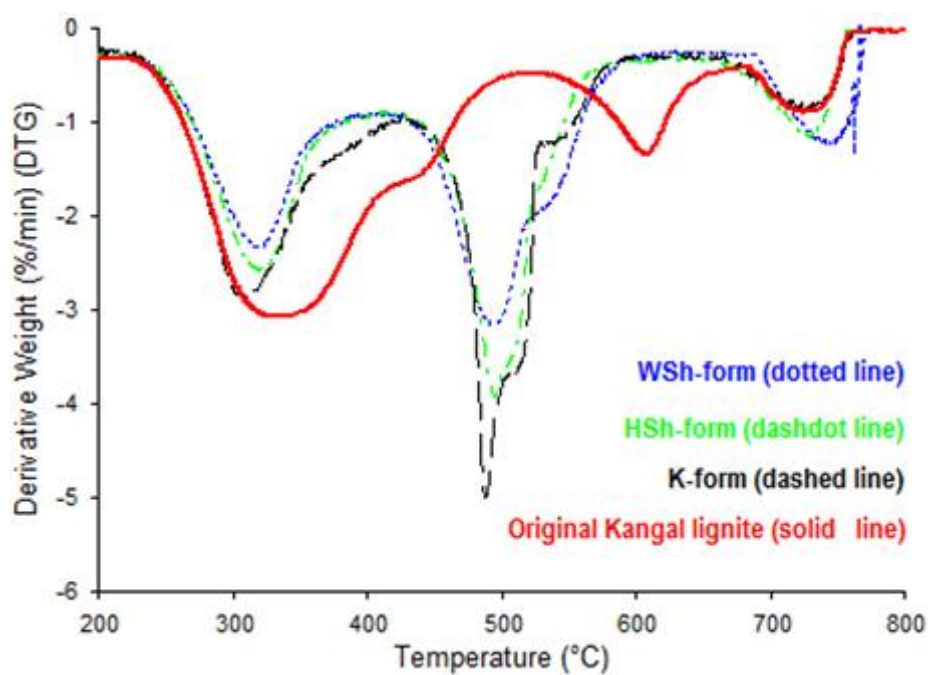


Fig. 5.63 DTG profile comparisons of K-form lignite and the catalytic effects of HSh and WSh ash contents in air

Table 5.14 Concentrations of K-based oxides in the ash contents of impregnated Kangal lignite

Impregnated Kangal lignite sample	Impregnation (% by weight)	Concentration of K-based oxides in ash (XRF test) (%)	Concentration of K-based oxides in ash (calculated) (%)
K-form (K <sub>2</sub> CO <sub>3</sub> precursor)	5 %	8.574	-
WSh-form	15 %	-	8.734
HSh-form	15 %	-	8.358

#### 5.4.2.2 Combustion Tests Carried Out in 30 % O<sub>2</sub> in CO<sub>2</sub> Ambient

The effects of biomass ash as the precursors of inorganic catalysts were also explored under 30 % O<sub>2</sub> in CO<sub>2</sub> ambient. These results are listed in Table 5.15 and also indicated in Fig. 5.64. The combustion tests carried out with WSh- and HSh-form lignite samples (Fig. 5.64 (a and b)) demonstrated that the char oxidation reactivity was improved considerably in the third region while devolatilization reactivity was dropped in comparison with Raw-form lignite combustion tests. T<sub>b</sub> decreased significantly in tests carried out with WSh- and HSh-form samples with respect to Raw-form combustion. These results are thought to be caused by high concentration of K-based oxides in the ash content of the impregnated samples as was observed in the K-form combustion experiments. Furthermore, the char combustion process in the third region and in the case of WSh-form sample was observed to be a two-stage process, since two peaks were observed in the temperature interval of 400-600 °C. The volatile matter release and combustion was improved in the combustion tests carried out by WS- and CM-form samples due to high concentrations of inorganic matters. However, this improvement was more considerable in the case of CM-form sample due to its significantly high |(dm/dt)<sub>2max</sub>| of 13.09 %/min. A possible reason for this behavior can be the high concentration of Na-based oxides (10.77 %) in the ash content of this biomass. Finally, in the case of

SD-form combustion test with considerably high concentration of Ca-based oxides in the ash, it was observed that the impregnated lignite sample was more reactive in the second region and  $|(dm/dt)_{2max}|$  was 9.03 %/min. Furthermore,  $T_b$  was reduced in comparison with Kangal lignite combustion.

Table 5.15 Characteristic temperatures and parameters of original and impregnated Kangal lignite combustion tests in 30 % O<sub>2</sub> in CO<sub>2</sub> ambient

<b>30 % O<sub>2</sub>-70 % CO<sub>2</sub></b>	<b>Original Kangal lignite</b>	<b>Fe-form</b>	<b>Ca-form</b>	<b>K-form</b>	<b>HSh-form</b>	<b>WSh-form</b>	<b>WS-form</b>	<b>CM-form</b>	<b>SD-form</b>
<b>T<sub>in</sub> (°C)</b>	239	238	234	238	239	239	243	240	243
<b>T<sub>ig</sub> (°C)</b>	273	270	276	271	272	272	278	265	277
<b>T<sub>2max</sub> (°C)</b>	304	281	299	291	302	308	303	278	290
<b>T<sub>b</sub> (°C)</b>	641	642	642	574	560	583	632	631	615
<b> <math>(\frac{dm}{dt})_{2max}</math>  (%/min)</b>	4.25	8.45	4.90	5.17	3.30	2.78	5.88	13.09	9.03
<b>T<sub>3max</sub> (°C)</b>	617.05	617	613	488	490	490	614	608	596
<b> <math>(\frac{dm}{dt})_{3max}</math>  (%/min)</b>	1.60	1.75	2.17	7.87	6.96	3.86	2.02	1.89	2.13

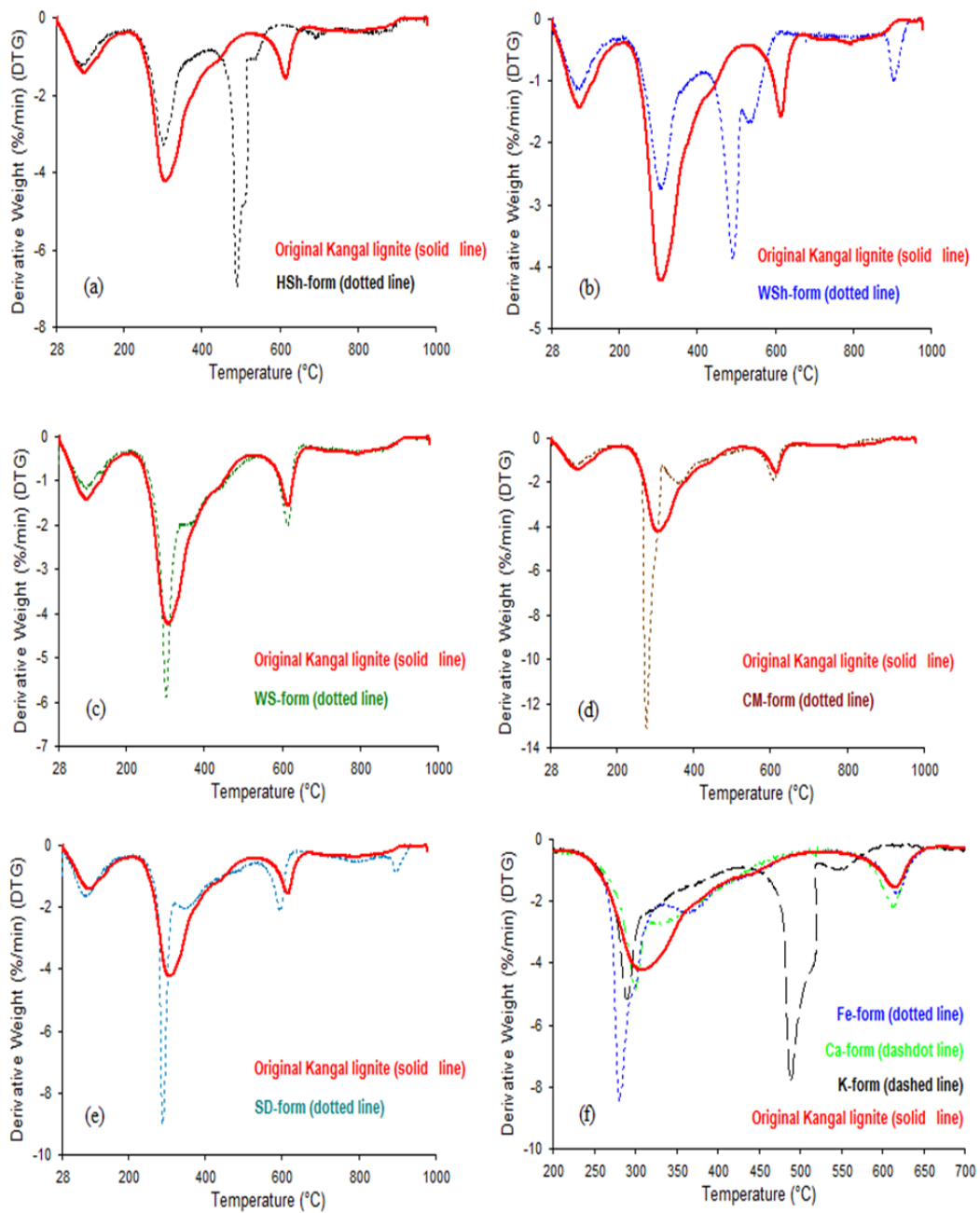


Fig. 5.64 DTG combustion curves of original and impregnated Kangal lignite with biomass ash contents in 30 % O<sub>2</sub> in CO<sub>2</sub> ambient

The catalytic effects of HSh and WSh were compared with the catalytic reactivity of potassium applied using  $K_2CO_3$  precursor in 30 %  $O_2$  in  $CO_2$  ambient and the results are illustrated in Fig. 5.65. The concentration of K-based oxides in the ash content of the K-form and the samples impregnated with biomass ash contents are listed in Table 5.14.

As illustrated in Fig. 5.65, the reactivity of K-form sample was higher in the second region in comparison with WSh- and HSh-form lignite samples. However, the reactivity of all these three impregnated samples was considerably higher in the third region regarding char combustion with respect to Raw-form combustion. These results confirm similarities in combustion behavior of K-form sample and the lignite samples impregnated with the ash contents of WSh and HSh biomass fuels.

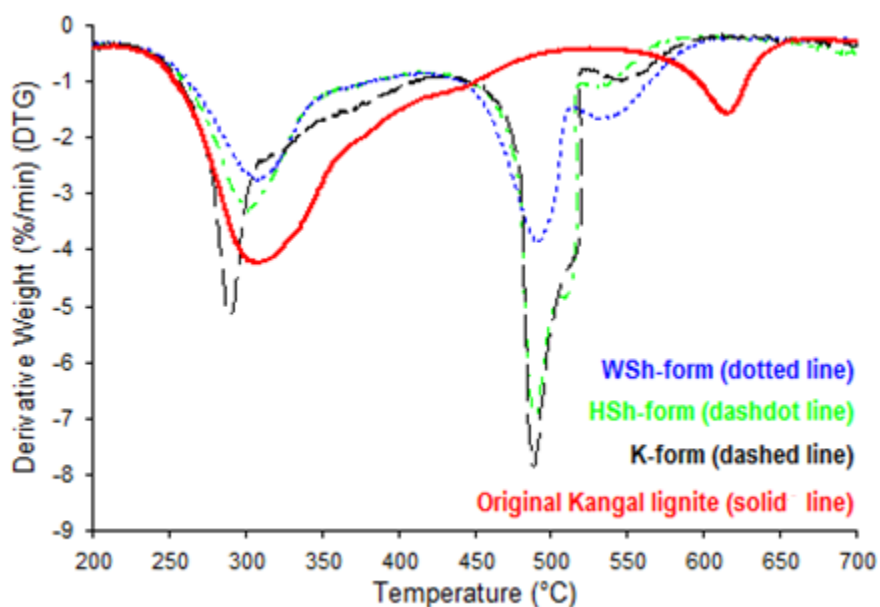


Fig. 5.65 DTG profile comparisons of K-form lignite and the catalytic effects of HSh and WSh ash contents in 30 %  $O_2$  in  $CO_2$  ambient

The combustion behavior of Ca-form sample and the impregnated lignite with Limba wood saw dust ash as a Ca catalyst precursor was compared (Fig. 5.66). The concentration of Ca-based oxides in the ash content of the impregnated samples was analyzed experimentally for Ca-form sample and was calculated for SD-form sample (Table 5.16). This concentration corresponded 30.71 % and 33.39 % for Ca-form and SD-form samples respectively. As indicated in 5.66,  $|(dm/dt)_{2max}|$  was considerably higher and  $T_{3max}$  was lower in the case of SD-form with respect to Ca-form lignite sample. The higher reactivity of SD-form sample in comparison with Raw-form lignite in the second region and with considering the behavior of Ca-form sample in this region (higher  $|(dm/dt)_{2max}|$  with respect to Raw-form), might be due to the high concentration of Ca-based oxides in the ash content of SD-form sample. Furthermore, the higher reactivity of SD-form with respect to Ca-form in the second region can be caused by considerably high amounts of Mg- and K-based oxides in the ash content of SD-form sample in comparison with Ca-form sample. These concentrations corresponded 8.42 % and 16.28 % for Mg- and K-based oxides in the ash content of SD-form sample with respect to 3.86 % and 0.99 % for Mg- and K-based oxides in the case of Ca-form sample respectively.

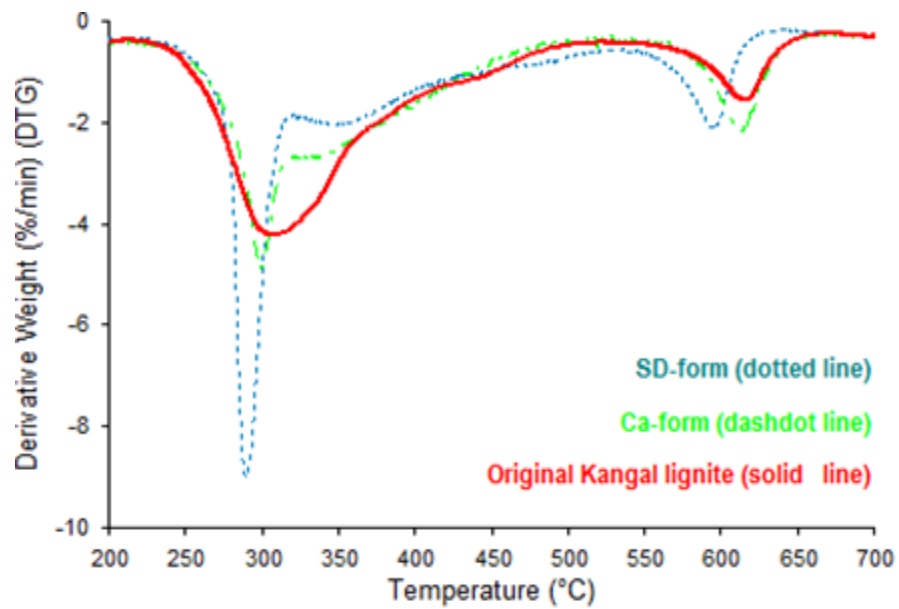


Fig. 5.66 DTG profile comparisons of Ca-form lignite and the catalytic effect of SD ash content in 30 % O<sub>2</sub> in CO<sub>2</sub> ambient

Table 5.16 Concentrations of Ca-based oxides in the ash contents of impregnated Kangal lignite

Impregnated Kangal lignite sample	Impregnation (% by weight)	Concentration of Ca-based oxides in ash (XRF test) (%)	Concentration of Ca-based oxides in ash (calculated) (%)
Ca-form (Ca(OH) <sub>2</sub> precursor)	5 %	30.71	-
SD-form	15 %	-	33.391

## CHAPTER 6

### CONCLUSIONS

In this study an attempt was done to profoundly explore the pyrolysis and combustion behaviors and emission characteristics of Turkish coal samples in O<sub>2</sub>/N<sub>2</sub> and O<sub>2</sub>/CO<sub>2</sub> (oxy-fuel conditions) ambient conditions. In this study, an especial focus was allocated to the effects of three inorganic materials, potassium (K), calcium (Ca) and iron (Fe) on combustion characteristics of Turkish lignite using non-isothermal Thermogravimetric Analysis (TGA) technique combined with Fourier Transform Infrared (FTIR) spectroscopy and the effects of ambient gases and various oxygen mole fractions were considered. Furthermore, the effects of these catalysts on calorimetric tests of Turkish coal samples were also investigated. Eventually, the co-processing combustion tests of lignite and the ash contents of Turkish biomass fuels were investigated and the possible way of using Turkish biomass as a potential source of inexpensive catalysts in combustion processes were discussed. The following conclusions can be summarized:

#### 6.1 Calorimetric Tests

Calorimetric tests indicated that the influences of the evolved catalysts might be described as follows:

- Although there were some slight differences in the calorific values of the impregnated samples, these fluctuations can be the result of the experimental and sample impregnation errors. Therefore, within the experimental uncertainty, calorific values were same and no significant

catalytic effects were observed in the calorimetric tests. However, further studies using more accurate calorimetric methods are required to have clear idea about the effects of catalysts on calorimetric values.

## 6.2 TGA-FTIR Tests

### 6.2.1 Pyrolysis Tests of Kangal Lignite

- Pyrolysis behavior of Kangal lignite sample in  $N_2$  and  $CO_2$  ambient conditions was observed to be very similar until  $720\text{ }^\circ\text{C}$ . In the temperature range beyond  $720\text{ }^\circ\text{C}$ , the major difference was observed with the separation of TGA profiles and a sharp peak in 100 %  $CO_2$  DTG curve. These results can be attributed to the char- $CO_2$  gasification reaction which may increase the reactivity of char in  $O_2/CO_2$  ambient due to the high concentrations of  $CO_2$ .
- $K_2CO_3$  found to be the most effective catalyst in char gasification of Kangal lignite during  $CO_2$  pyrolysis tests. Since it increased the maximum rate of weight loss by almost 14 % in comparison with the tests carried out with the Raw-form sample in this region.
- FTIR results of Kangal lignite pyrolysis tests in 100 %  $CO_2$  revealed that significant amount of CO was evolved in high temperature zone from char- $CO_2$  gasification reaction. Furthermore, evolution of  $SO_x$  occurred in high temperature zone, as the emission started at  $900\text{ }^\circ\text{C}$ . In the case of pyrolysis tests in 100 %  $N_2$ ,  $SO_x$  evolution occurred between  $250\text{ }^\circ\text{C}$  and  $600\text{ }^\circ\text{C}$ . COS formation increased significantly with the initiation of gasification reaction in 100 %  $CO_2$ .
- The FTIR results of Kangal lignite pyrolysis tests revealed that the evolution of CO and COS decreased in the cases of all the three catalysts and the main peaks were at  $800\text{ }^\circ\text{C}$ .

## 6.2.2 Combustion Tests

- TGA and DTG profiles of combustion tests performed with Kangal lignite and Tunçbilek sub-bituminous samples in air and in 30 % O<sub>2</sub> in CO<sub>2</sub> ambient revealed that oxidation and removal of volatile matters occurred in considerably lower temperature zone in the case of lignite in comparison with sub-bituminous sample. Furthermore, during Tunçbilek sub-bituminous combustion, devolatilization and char burning steps were not discretely separated.
- Combustion tests of Kangal lignite derived in air and in 21 % O<sub>2</sub> in CO<sub>2</sub> ambient revealed that the reactivity of the lignite sample in 21 % O<sub>2</sub> in CO<sub>2</sub> was higher than that in air. Accordingly, the higher reactivity of the sample in 30 % O<sub>2</sub> in N<sub>2</sub> ambient was confirmed in comparison with CO<sub>2</sub> ambient by the lower T<sub>ig</sub> and T<sub>2max</sub> in addition with higher |(dm/dt)<sub>2max</sub>|. However, these results did not agree with the expected delay in oxy-fuel combustion in most of the oxygen concentrations. One possible reason might be due to the fact that in TGA technique, combustion temperature of the sample is controlled by electrical heating and sample temperature is not affected by the combustion ambient completely. Furthermore, during Kangal lignite combustion tests derived in O<sub>2</sub>/CO<sub>2</sub> and O<sub>2</sub>/N<sub>2</sub> ambient conditions, T<sub>b</sub> was independent from oxygen concentration and was considerably lower in O<sub>2</sub>/CO<sub>2</sub> ambient.
- Comparisons of DTG curves of Kangal lignite combustion tests indicated that the effect of oxygen concentration was more significant than that of the diluting gases (N<sub>2</sub> or CO<sub>2</sub>) on the combustion profiles. The effects of elevated oxygen levels in both N<sub>2</sub> and CO<sub>2</sub> ambient conditions were observed in the second region of combustion and shifted the weight loss curves to the lower temperature zone accompanied with much higher reaction rates (|(dm/dt)<sub>2max</sub>|) in the second region of combustion. T<sub>in</sub> and T<sub>ig</sub> also decreased when we switched to higher oxygen mole fractions.

- During catalytic Kangal lignite combustion tests derived in  $N_2$  ambient, the relative active sequence of catalysts to the reaction rate in the second and third regions in air and elevated oxygen mole fractions can be described as  $Fe > \text{Raw-form} > K$  and  $K \gg \text{Raw-form} \sim Fe$  respectively.
- Investigating the effects of catalysts in the second region during Kangal lignite combustion tests in  $CO_2$  ambient revealed that in 30 %  $O_2$  and 35 %  $O_2$ , the relative active sequence of catalysts to the reaction rate in the volatile and light hydrocarbon combustion can be described as  $Fe \gg K > Ca > \text{Raw-form}$  and  $Fe > Ca > \text{Raw-form} \gg K$  respectively. No significant effect was observed in the cases of 21 %  $O_2$  and 25 %  $O_2$  in this region rather than a considerable reduction in  $T_{2max}$  by using all the three catalysts in 21 %  $O_2$ .
- In the third region of combustion, K-based catalyst had the best catalytic reactivity in char oxidation and combustion of the Kangal lignite due to its much higher reaction rates in all the oxygen concentrations. Furthermore,  $T_b$  also had a significant drop in the case of K-based catalyst in comparison with the Raw- Ca- and Fe-form lignite samples. Therefore, the relative active sequence of catalysts to the reactivity of char can be described as follows:  $K \gg Ca > Fe \sim \text{Raw-form}$ . However, the rate of increase in the reaction rate of K-based catalyst with increasing oxygen mole fraction would suggest that probably there is an optimum oxygen concentration for char reactivity in K-form sample.
- In combustion tests performed with the raw and impregnated Kangal lignite samples, it was observed that the main emission of combustion gases occurred in the second region of combustion due to the volatile matter release and light hydrocarbon combustion with an exception of combustion tests derived with K-based catalyst. During K-form tests, it was illustrated that a main part of  $CO_2$  and CO emissions was attributed to the char combustion

region.

- During the combustion tests carried out with raw Kangal lignite sample, three main peaks were detected in CO<sub>2</sub> and two in CO and H<sub>2</sub>O formation profiles for which the most remarkable peak was observed in the second region. However, the information profiles of sulphur containing species, SO<sub>x</sub> and COS, had only a main peak in the second region.
- The evolution profiles of CO, H<sub>2</sub>O, SO<sub>x</sub> and COS gases during Kangal lignite combustion tests in 21 % O<sub>2</sub> revealed that the formation of these gases was slightly higher in O<sub>2</sub>/CO<sub>2</sub> ambient with respect to normal air combustion as |(dm/dt)<sub>2max</sub>| also had an increasing trend. On the contrary, the evolution profiles of H<sub>2</sub>O, SO<sub>x</sub> and COS experienced sharper peaks with higher maximum absorbance and in lower corresponding temperatures in N<sub>2</sub> in comparison with CO<sub>2</sub> ambient in 30 % O<sub>2</sub>. The CO formation still showed higher amounts in CO<sub>2</sub> ambient.
- Comparisons of the flue gas emission curves indicated that the effects of oxygen mole fractions on Kangal lignite combustion tests were more evident in the second region during which the peaks shifted to lower temperatures and higher absorbance as oxygen concentration increased from 21 % to 35 %. Moreover, a good correlation was observed between the maximum rate of weight loss in DTG curves (|(dm/dt)<sub>2max</sub>|) and the peak absorbance of the emissions and also between T<sub>2max</sub> and T<sub>FG-max</sub> in both N<sub>2</sub> and CO<sub>2</sub> ambient conditions while increasing oxygen concentrations were tested.
- K<sub>2</sub>CO<sub>3</sub> was the most effective catalyst in char gasification and combustion of Kangal lignite during the tests in both O<sub>2</sub>/N<sub>2</sub> and O<sub>2</sub>/CO<sub>2</sub> ambient conditions. Furthermore, burnout temperature (T<sub>b</sub>) also experienced a significant drop in the case of K-based catalyst in comparison with the Raw- Ca- and Fe-form lignite samples.

- During catalytic Kangal lignite combustion tests derived in air, it was observed that Fe catalyst increased the CO<sub>2</sub> formation in both second and third regions. Moreover, the K-based catalyst was effective in reducing CO, SO<sub>x</sub> and COS emissions during devolatilization. However, during char combustion in the third region, the evolution profiles of the evolved gases in the case of K-based catalysts had extra peaks at 500 °C which was in accordance with the maximum rate of weight loss in the third region.
- Investigating the effects of catalysts on combustion characteristics of Kangal lignite in O<sub>2</sub>/CO<sub>2</sub> ambient revealed that the Ca-based catalyst had the best catalytic activity in reducing sulphur containing species, SO<sub>x</sub> and COS. Although K-based catalyst reduced the formation of CO, H<sub>2</sub>O, SO<sub>x</sub> and COS in the second region of combustion, however, extra peaks were observed in 450-550 °C temperature interval which was in accordance with the maximum rate of weight loss due to char oxidation and combustion in DTG curve. While Fe and Ca catalysts increased CH<sub>4</sub> emission in the second region, K-form sample profile had another peak at 500 °C. Furthermore, the maximum absorbance of the evolved gases in O<sub>2</sub>/CO<sub>2</sub> ambient was nearly consistent with the maximum rate of weight loss due to volatile matter combustion for raw and impregnated lignite samples.
- The TGA and DTG profiles of raw and impregnated Tunçbilek combustion tests revealed that the addition of Fe improved the reactivity of the Tunçbilek sample confirmed by much higher reaction rates in 30 % O<sub>2</sub> in N<sub>2</sub> ambient. In 30 % O<sub>2</sub> in CO<sub>2</sub> ambient, the most significant effects of catalysts were observed in the case of K-based catalyst during which the process of combustion varied from a single stage to double stages in 350-500 °C temperature interval. Furthermore, Fe-based catalyst increased the emissions of CO and SO<sub>x</sub> while Ca- and K-based catalysts showed considerable effects in reducing the sulphur based emissions.

- Co-processing combustion tests of lignite and biomass ash contents indicated that the hazelnut shell and walnut shell ash contents were significantly effective in increasing the char reactivity of Kangal lignite due to high concentration of potassium-based oxides during combustion tests carried out in both air and 30 % O<sub>2</sub> in CO<sub>2</sub> ambient conditions. Furthermore, the catalytic reactivity of wheat straw and cattle manure ash contents were observed in the second region of combustion regarding volatile matter release and combustion in both air and 30 % O<sub>2</sub> in CO<sub>2</sub> ambient conditions. These results are thought to be due to high concentrations of alkali and alkaline earth metals existed in the impregnated lignite samples with WS and CM ash contents and especially Na-based oxides in the CM-form. Finally, in the case of lignite sample impregnated with saw dust ash content, it was observed that the impregnated lignite was significantly more reactive in devolatilization process in 30 % O<sub>2</sub> in CO<sub>2</sub> ambient. This result might be due to the high concentrations of Ca- Mg and K-based oxides in the ash content of SD-form sample in comparison with Raw-form lignite. In conclusion, these results revealed that the ash contents of walnut and hazelnut shell biomass fuels can be used as a potential source of inexpensive K-based catalysts in the co-processing of coal and biomass ash. Furthermore, high concentrations of alkali and alkaline earth metals existed in the ash contents of biomass fuels like wheat straw, cattle manure and saw dust can make them suitable sources of inexpensive catalysts and develop a step forward in economic aspects of catalytic coal combustion.

### **6.3 Future Work**

According to the conclusions obtained throughout this study and the wide literature survey carried out to cover the general view point of the topic, further research needs are realized. Therefore, the effects of catalysts on pyrolysis, combustion and gasification characteristics of coal, biomass and non-biomass fuels and their co-processing effects, can be further investigated through these research

topics suggested by the author:

- Investigating the effects of catalyst loading in TGA-FTIR experiments
- Using fast heating rates in TGA-FTIR experiments
- Steam gasification of Turkish lignite, biomass fuels and their blends in TGA-FTIR
- Co-processing of coal and non-biomass wastes like MSW and waste tire
- Exploring the effects of biomass fuels on pyrolysis and combustion characteristics of Turkish lignite both as fuel blends and as catalysts in Fluidized Bed Combustion systems

## REFERENCES

- [1] International Energy Agency, IEA Statistics, CO<sub>2</sub> Emissions from Fuel Combustion, 2009 Edition.
- [2] J. Davison, K. Thambimuthu, Technologies for capture Of carbon dioxide, *Greenhouse Gas Control Technologies*, 1 (2005) 3-13.
- [3] H. Sis, Evaluation of combustion characteristics of different size elbistan lignite by using TG/DTG and DTA, *Journal of Thermal Analysis and Calorimetry*, 88 (2007) 863–870.
- [4] BP Statistical Review of World Energy. September 2010. [Online]. Available: [www.bp.com](http://www.bp.com).
- [5] J. Deutch, J. Moniz, The Future of Coal: Options for a Carbon-Constrained World, Massachusetts Institute of Technology Interdisciplinary Study (2007).
- [6] B. Arias, C. Pevida, F. Rubiera, J. J. Pis, Effect of biomass blending on coal ignition and burnout during oxy-fuel combustion, *Fuel* 87 (2008) 2753–2759.
- [7] M. F. Irfan, M. R. Usman, K. Kusakabe, Coal gasification in CO<sub>2</sub> atmosphere and its kinetics since 1948: A brief review, *Energy* 36 (2011) 12-40.
- [8] Y. Liu, D. Che, T. Xu, Catalytic reduction of SO<sub>2</sub> during combustion of typical Chinese coals, *Fuel Processing Technology* 79 (2002) 157– 169.
- [9] M. Kozłowski, I. I. Maes, H. Wachowska, J. Yperman, D. V. Franco, J. Mullens, et al., Reduction of high-sulphur coal in the potassium–liquid ammonia system, *Fuel* 78 (1999) 769-774.
- [10] T. Wall, Y. Liu, C. Spero, L. Elliott, S. Khare, R. Rathnam, et al., An overview on oxyfuel coal combustion—State of the art research and technology development, *Chemical Engineering Research and Design*, 87 (2009) 1103-1016.

- [11] J. Gibbins, H. Chalmers, Carbon capture and storage, *Energy Policy*, 36 (2008) 4317–4322.
- [12] M. T. Toftegaard, J. Brix, P. A. Jensen, P. Glarborg, A. D. Jensen, Oxy-fuel combustion of solid fuels, *Progress in Energy and Combustion Science* 36 (2010) 581-625; 2010.
- [13] A. Franco, A. R. Diaz, The future challenges for “clean coal technologies”: Joining efficiency increase and pollutant emission control, *Energy*, 34 (2009) 348–354.
- [14] R. K. Rathnam, L. K. Elliott, T. F. Wall, Y. Liu, B. Moghtaderi, Differences in reactivity of pulverised coal in air ( $O_2/N_2$ ) and oxy-fuel ( $O_2/CO_2$ ) conditions, *Fuel Processing Technology* 90 (2009) 797–802.
- [15] H. Liu, Combustion of Coal Chars in  $O_2/CO_2$  and  $O_2/N_2$  Mixtures: A Comparative Study with Non-isothermal Thermogravimetric Analyzer (TGA) Tests, *Energy Fuels* 23 (2009) 4278–4285.
- [16] R. Tan, S. Santos, H. Spliethoff, G23/y/2, IFRF Report (2006).
- [17] B. J. P. Buhre, L. K. Elliott, C. D. Sheng, R. P. Gupta, T.F. Wall, Oxy-fuel combustion technology for coal-fired power generation, *Progress in Energy and Combustion Science* 31 (2005) 283–307.
- [18] P. A. Bejarano, Y. A. Levendis, Single-coal-particle combustion in  $O_2/N_2$  and  $O_2/CO_2$  environments, *Combustion and Flame* 153 (2008) 270–287.
- [19] N. Selcuk, N. S. Yuzbasi, Combustion behaviour of Turkish lignite in  $O_2/N_2$  and  $O_2/CO_2$  mixtures by using TGA–FTIR, *Journal of Analytical and Applied Pyrolysis* 90 (2011) 133–139.
- [20] N. Kimura, K. Omata, T. Kiga, S. Takano, S. Shikisima, The characteristics of pulverized coal combustion in  $O_2/CO_2$  mixtures for  $CO_2$  recovery, *Energy Conversion and Management* 36 (1995) 805-808.
- [21] T. Kiga, S. Takano, N. Kimura, K. Omata, M. Okawa, T. Mori, M. Kato, Characteristics of pulverized-coal combustion in the system of oxygen/recycled flue gas combustion, *Energy Conversion and Management* 38 (1997) 129-134.

- [22] H. Liu, R. Zailani, B. M. Gibbs, Comparisons of pulverized coal combustion in air and in mixtures of O<sub>2</sub>/CO<sub>2</sub>, *Fuel* 84 (2005) 833-840.
- [23] H. Liu, R. Zailani, B. M. Gibbs, Pulverized coal combustion in air and in O<sub>2</sub>/CO<sub>2</sub> mixtures with NO<sub>x</sub> recycle, *Fuel* 84 (2005) 2109-2115.
- [24] K. Andersson, F. Johnsson, Flame and radiation characteristics of gas-fired O<sub>2</sub>/CO<sub>2</sub> combustion, *Fuel* 86 (2007) 656-668.
- [25] Y. Tan, E. Croiset, M. A. Douglas, K. V. Thambimuthu, Combustion characteristics of coal in a mixture of oxygen and recycled flue gas, *Fuel* 85 (2006) 507- 512.
- [26] D. Singh, E. Croiset, P. L. Douglas, M. A. Douglas, Techno-economic study of CO<sub>2</sub> capture from an existing coal-fired power plant: MEA scrubbing vs. O<sub>2</sub>/CO<sub>2</sub> recycle combustion, *Energy Conversion and Management* 44 (2003) 3073-3091.
- [27] X. Gong, Z. Guo, Z. Wang, Reactivity of pulverized coals during combustion catalyzed by CeO<sub>2</sub> and Fe<sub>2</sub>O<sub>3</sub>, *Combustion and Flame* 157(2010) 351–356.
- [28] N. A. Öztaş, Y. Yürüm, Pyrolysis of Turkish Zonguldak bituminous coal. Part 1. Effect of mineral matter, *Fuel* 79 (2000) 1221–1227.
- [29] H. D. Franklin, W. A. Peters, J. B. Howard, Mineral matter effects on the rapid pyrolysis and hydrolysis of a bituminous coal. 1. Effects on yields of char, tar and light gaseous volatiles, *Fuel* 61 (1982) 155-160.
- [30] H. D. Franklin, W. A. Peters, J. B. Howard, Mineral matter effects on the rapid pyrolysis and hydrolysis of a bituminous coal: 2. Effects of yields of C3-C8 hydrocarbons, *Fuel* 61 (1982) 1213-1217.
- [31] J. Yang, N. A. Cai, TG-FTIR study on catalytic pyrolysis of coal, *Journal of Fuel Chemistry and Technology* 34 (2006) 650– 654.
- [32] L. Lemaigen, Y. Zhuo, G. P. Reed, D. R. Dugwell, R. Kandiyoti, Factors governing reactivity in low temperature coal gasification. Part II. An attempt to correlate conversions with inorganic and mineral constituents, *Fuel* 81(2002) 315–326.

- [33] Q. Liu, H. Hu, Q. Zhou, S. Zhu, G. Chen, Effect of inorganic matter on reactivity and kinetics of coal pyrolysis, *Fuel* 83 (2004) 713–718.
- [34] X. Shenqi, Z. Zhijie, X. Jie, Y. Guangsu, W. Fuchen, Effects of alkaline metal on coal gasification at pyrolysis and gasification phases, *Fuel* 90 (2011) 1723–1730.
- [35] J. Wang, M. Jiang, Y. Yao, Y. Zhang, J. Cao, Steam gasification of coal char catalyzed by  $K_2CO_3$  for enhanced production of hydrogen without formation of methane, *Fuel* 88 (2009) 1572–1579.
- [36] J. Yu, F. Tian, m. C. Chow, L. J. McKenzie, C. Li, Effect of iron on the gasification of Victorian brown coal with steam: enhancement of hydrogen production, *Fuel* 85 (2006) 127–133.
- [37] Y. Huang, X. Yin, C. Wu, C. Wang, J. Xie, Z. Zhou, et al., Effects of metal catalysts on  $CO_2$  gasification reactivity of biomass char, *Biotechnology Advances* 27 (2009): 568 - 572.
- [38] T. Zhu, L. liu, Y. Wang, J. Huang, Study on coal mild gasification with CaO catalyst., *Journal of Fuel Chemistry and Technology* 28 (2000) 36–39.
- [39] C. Wang, Y. Wu, Q. Liu, H. Yang, F. Wang, Analysis of the behaviour of pollutant gas emissions during wheat straw/coal cofiring by TG–FTIR, *Fuel Processing Technology* 92 (2011) 1037–1041.
- [40] D. Wang, R. Xiao, H. Zhang, G. He, Comparison of catalytic pyrolysis of biomass with MCM-41 and CaO catalysts by using TGA–FTIR analysis, *Journal of Analytical and Applied Pyrolysis* 89 (2010) 171–177.
- [41] Q. Ren, C. Zhao, X. Wua, C. Liang, X. Chen, J. Shen, TG–FTIR study on copyrolysis of municipal solid waste with biomass, *Bioresource Technology* 100 (2009) 4054–4057.
- [42] R. Guan, W. Li, B. Li, Effects of Ca-based additives on desulfurization during coal pyrolysis, *Fuel* 82 (2003) 1961–1966.
- [43] N. Tsubouchi, Y. Ohtsuka, Nitrogen release during high temperature pyrolysis of coals and catalytic role of calcium in  $N_2$  formation, *Fuel* 81 (2002) 2335–2342.

- [44] H. Liu, Y. Liu, Y. Liu, D. Che, Experimental investigation on the conversion of nitrogenous gas products during coal pyrolysis, *JOURNAL OF FUEL CHEMISTRY AND TECHNOLOGY* 36 (2008) 134-138.
- [45] W. Zhu, W. Song, W. Lin, Catalytic gasification of char from co-pyrolysis of coal and biomass, *Fuel Processing Technology* 89 (2008) 890-896.
- [46] C. Bakisgan, A. Gümrah Dumanli, Y. Yürüm, Trace elements in Turkish biomass fuels: Ashes of wheat straw, olive bagasse and hazelnut shell, *Fuel* 88 (2009) 1842–1851.
- [47] World Coal Institute, *THE COAL RESOURCE: A COMPREHENSIVE OVERVIEW OF COAL*, [www.worldcoal.org](http://www.worldcoal.org).
- [48] International Energy Agency, [www.iea.org](http://www.iea.org), 2009.
- [49] S. R. Turns, *An Introduction to Combustion: concepts and application*, 2<sup>nd</sup> ed., McGraw- Hill series in Mechanical engineering, International Editions 2000.
- [50] Y. Q. Hu, N. Kobayashi, M. Hasatani, Effects of coal properties on recycled-NO<sub>x</sub> reduction in coal combustion with O<sub>2</sub>/recycled flue gas, *Energy Conversion and Management* 44 (2003) 2331-2340.
- [51] Y. Q. Hu, N. Kobayashi, M. Hasatani, The reduction of recycled-NO<sub>x</sub> in coal combustion with O<sub>2</sub>/recycled flue gas under low recycling ratio, *Fuel* 80 (2001) 1851-1855.
- [52] K. Okazaki, T. Ando, NO<sub>x</sub> reduction mechanism in coal combustion with recycled CO<sub>2</sub>, *Energy* 22 (1997) 207–215.
- [53] R. Strube, G. Manfrida, CO<sub>2</sub> capture in coal-fired power plants—Impact on plant performance 5 (2011) 710- 726.
- [54] B. Ma, X. Li, L. Xu, K. Wang, X. Wang, Investigation on catalyzed combustion of high ash coal by thermogravimetric analysis, *Thermochimica Acta* 445 (2006) 19–22.

- [55] M. X. Fang, D. K. Shen, Y. X. Li, C. J. Yu, Z. Y. Luo, K. F. Cen, Kinetic study on pyrolysis and combustion of wood under different oxygen concentrations by using TG-FTIR analysis," *Journal of Analytical and Applied Pyrolysis* 77 (2006) 22-27.
- [56] Q. Li, C. Zhao, X. Chen, W. Wu, Y. Li, Comparison of pulverized coal combustion in air and in O<sub>2</sub>/CO<sub>2</sub> mixtures by thermo-gravimetric analysis, *Journal of Analytical and Applied Pyrolysis* 85 (2009) 521–528.
- [57] M. Balat, Turkey's Major Lignite Fields and Significance of Lignite for Energy Nec essity, *Energy Sources*, 3 (2008) 13-25.
- [58] M. Z. Duz, Y. Tonbul, A. Baysal, O. Akba, A. Saydut, C. Hamamci, Pyrolysis kinetics and chemical composition of hazro coal according to the particle size, *Journal of Thermal Analysis and Calorimetry* 81 (2005) 395–398.
- [59] A. Küçük, Y. Kadioğlu, M. Ş. Gülaboğlu, A study of spontaneous combustion characteristics of a Turkish lignite: particle size, moisture of coal, humidity of air, *Combustion and Flame* 133 (2003) 255–261.
- [60] P. R. Griffiths, J. A. de Haseth, *Fourier Transform Infrared Spectrometry*. 2<sup>nd</sup> ed., Hoboken, New Jersey, John Wiley& Sons, 2007.
- [61] J. Heland, K. Schäfer, Determination of major combustion products in aircraft exhausts by FTIR emission spectroscopy, *Atmospheric Environment*, 32 (1998) 3067-3072.
- [62] A. A. Stec, P. Fardell, P. Blomqvist, L. Bustamante-Valencia, L. Saragoza, E. Guillaume, Quantification of fire gases by FTIR: Experimental characterisation of calibration systems, *Fire Safety Journal* 46 (2011) 225-233.
- [63] W. O. George, P. S. McIntyre, *Infrared Spectroscopy*, London, John Wiley& Sons, 1987.
- [64] E. G. Brame, Jr. Grasselli, J. Grasselli, *Infrared and Raman Spectroscopy Part A*, New York and Basel, Marcel Dekker, 1976.
- [65] B. Stuart, *Infrared Spectroscopy: Fundamentals and Applications*, chichester, John Wiley & Sons, 2004.

- [66] L. Jia, E. J. Anthony, I. Lau, J. Wang, Study of coal and coke ignition in fluidized beds, *Fuel* 85 (2006) 635-642.
- [67] J. G. Speight, *Handbook of Coal Analysis*, Hoboken, New Jersey, John Wiley & Sons, 2005.
- [68] Z. Tingyu, Z. Shouyu, H. Jiejie, W. Yang, Effect of calcium oxide on pyrolysis of coal in a fluidized bed, *Fuel Processing Technology* 64 (2000) 271–284.
- [69] J. Yu, J. A. Lucas, T. F. Wall, Formation of the structure of chars during devolatilization of pulverized coal and its thermoproperties: A review, *Progress in Energy and Combustion Science* 33 (2007) 135-170.
- [70] D. Vamvuka, E. Kakaras, E. Kastanaki, P. Grammelis, Pyrolysis characteristics and kinetics of biomass residuals mixtures with lignite, *Fuel* 82 (2003) 1949-1960.
- [71] G. Ö. Çakal, H. Yücel, A. G. Gürüz, Physical and chemical properties of selected Turkish lignites and their pyrolysis and gasification rates determined by thermogravimetric analysis, *Journal of Analytical and Applied Pyrolysis* 80 (2007) 262–268.
- [72] T. Kwon, S. D. Kim, D. P. C. Fung, Reaction kinetics of char-CO<sub>2</sub> gasification, *Fuel* 67 (1988) 530-535.
- [73] A. Arenillas, F. Rubiera, J. J. Pis, Simultaneous thermogravimetric–mass spectrometric study on the pyrolysis behaviour of different rank coals, *Journal of Analytical and Applied Pyrolysis* 50 (1999) 31–46.
- [74] G. H. Liu, X. Q. Ma, Z. Yu, Experimental and kinetic modeling of oxygen-enriched air combustion of municipal solid waste, *Waste Management* 29 (2009) 792-796.
- [75] J. W. Cumming, A DTG combustion study on anthracitic and other coal chars, *Thermochimica Acta* 155 (1989) 151-161.
- [76] Y. Zhang, S. Hara, S. Kajitani, M. Ashizawa, Modeling of catalytic gasification kinetics of coal char and carbon, *Fuel* 89 (2010) 152-157.

- [77] Q. Sun, W. Li, H. Chen, B. Li, The CO<sub>2</sub>-gasification and kinetics of Shenmu maceral chars with and without catalyst, *Fuel* 83 (2004) 1787-1793.
- [78] C.-Z. Li, C. Sathe, J. R. Kershaw, Y. Pang, Fates and roles of alkali and alkaline earth metals during the pyrolysis of a Victorian brown coal, *Fuel* 79 (2000) 427-438.
- [79] R. Stanger, T. Wall, Sulphur impacts during pulverised coal combustion in oxy-fuel technology for carbon capture and storage, *Progress in Energy and Combustion Science* 37 (2011) 69-88.
- [80] I. Yuksel, K. Kaygusuz, Renewable energy sources for clean and sustainable energy policies in Turkey, *Renewable and Sustainable Energy Reviews* 15 (2011) 4132– 4144.

## APPENDIX A

### SAMPLES AND EXPERIMENTAL METHODS

Table A.1 Original humidity content analyses of Kangal and Seyitömer lignite samples  
(as received) (%)

Temperature=  $107 \pm 4$  °C

Time interval (min)	Kangal		Seyitömer	
	Petri plate* + sample weight (g)	Sample weight (g)	Petri plate + sample weight (g)	Sample weight (g)
30	68.479	6.103	71.496	7.805
45	68.345	5.969	71.455	7.764
60	68.309	5.933	71.451	7.76
75	68.296	5.920	71.440	7.749
90	68.292	5.916	71.441	7.75
105	<b>68.291</b>	<b>5.915</b>	<b>71.436</b>	<b>7.745</b>
120	-	-	71.436	7.745
Sample weight (g) at 0 min	10		10	
Petri plate weight (g)	62.376		63.691	
Original Humidity (as received) (%)	40.85		22.55	

\*Glass container

Table A.2 Original humidity content analyses of Tunçbilek and Zonguldak coal samples  
(as received) (%)

Temperature=  $107 \pm 4$  °C

Time interval (min)	Tunçbilek		Zonguldak	
	Petri plate* + sample weight (g)	Sample weight (g)	Petri plate + sample weight (g)	Sample weight (g)
30	71.580	9.243	72.502	8.857
45	71.574	9.237	72.492	8.847
60	71.582	9.245	<b>72.491</b>	<b>8.846</b>
75	<b>71.570</b>	<b>9.233</b>	-	-
90	71.571	9.234	-	-
105	-	-	-	-
Sample weight (g) at 0 min	10		10	
Petri plate weight (g)	62.337		63.645	
Original Humidity (as received) (%)	7.67		11.54	

\*Glass container

Table A.3 Humidity content analyses of Kangal and Seyitömer lignite samples as used in the tests (after milling) (%)

Temperature=  $107 \pm 4$  °C

Time interval (min)	Kangal		Seyitömer	
	Petri plate* + sample weight (g)	Sample weight (g)	Petri plate + sample weight (g)	Sample weight (g)
15	56.660	2.216	40.900	2.56
30	56.637	2.193	40.878	2.538
45	56.625	2.181	40.872	2.532
60	56.625	2.181	40.860	2.52
75	56.618	2.174	40.862	2.522
90	56.616	2.172	40.858	2.518
105	<b>56.615</b>	<b>2.171</b>	<b>40.860</b>	<b>2.52</b>
Sample weight (g) at 0 min	3		3	
Petri plate weight (g)	54.444		38.340	
Humidity as tested (after milling) (%)	27.63		16.00	

\*Glass container

Table A.4 Humidity content analyses of Tunçbilek and Zonguldak coal samples as used in the tests (after milling) (%)

Temperature=  $107 \pm 4$  °C

Time interval (min)	Tunçbilek		Zonguldak	
	Petri plate* + sample weight (g)	Sample weight (g)	Petri plate + sample weight (g)	Sample weight (g)
15	41.666	2.889	48.560	2.93
30	41.663	2.886	48.556	2.926
45	41.654	2.877	48.558	2.928
60	41.652	2.875	<b>48.549</b>	<b>2.919</b>
75	41.650	2.873	48.555	2.925
90	<b>41.646</b>	<b>2.869</b>	48.553	2.923
105	41.648	2.871	-	-
Sample weight (g) at 0 min	3		2.997	
Petri plate weight (g)	38.777		45.630	
Humidity as tested (after milling) (%)	4.37		2.60	

\*Glass container

Table A.5 Humidity content analyses of the impregnated coal samples

Time (min)	S + 5 % $K_2CO_3$ *	T + 10 % $Ca(OH)_2$ *	T + 10 % $K_2CO_3$ *
	Sample weight (g)	Sample weight (g)	Sample weight (g)
45	4.740	6.347	6.235
60	4.737	6.356	6.241
Sample weight (g) at 0 time	5.065	6.707	6.530
Humidity (after impregnation) (%)	6.48	5.37	4.52

\*Random sample selection for humidity content tests after impregnation

## Biomass Energy Potential in Turkey

Table A.6 Production of crop residues in Turkey [80]

Crop/animal	Residue	Theoretical production (tons/year)	Actual production (tons/year)	Available residue manure (tons/year)
<b>Crop residues</b>				
Wheat	Straw	29,270,775	23,439,910	3,520,384
Barley	Straw	9,986,879	8,954,014	1,342,460
Rye	Straw	420,214	365,08	56,712
Oats	Straw	421,658	322,238	48,216
Maize	Stalk	5,924,860	4,964,254	2,984,164
	Cob	598,574	1,908,324	1,146,394
Rice	Straw	584,545	209,544	126,716
	Husk	88,530	78,064	62,214
Tobacco	Stalk	384,762	362,643	248,685
Cotton	Stalk	6,320,186	2,534,286	1,543,24
	Ginning	484,586	424,43	435,686
Sunflower	Stalk	2,354,687	2,260,321	1,356,643
Groundnut	Shell	28,213	28,424	23,687
Soybean	Straw	62,468	21,896	13,225
<b>Fruit and fruit tree residues</b>				
Apricots	Shell		156,687	
	Tree pruning	1,336,646	87,212	70,242
Olive	Cake	674,686	638,926	596,876
	Tree pruning		424,464	226,432
Walnut	Shell	174,634	76,864	61,246
Hazelnut	Shell	698,246	562,642	453,224
	Tree pruning		2,065,462	1,642,245
	Tree pruning	234,742	86,642	69,664
Orange	Tree pruning	3,420,460	236,489	189,984
Mandarin	Tree pruning	978,970	996,876	82,364
<b>Animal wastes, available dry manure and biogas</b>				
Cow	Waste	15,864,056	10,024,123	10,024,172
Sheep	Waste	5,865,784	736,465	736,465
Poultry	Waste	1,875,543	1,864,768	1,864,768

Table A.7 Specifications of the Perkin Elmer Pyris STA 6000 TGA

<b>Sensor</b>	Pure platinum pan holder and reference ring		Corrosion-resistant, making the instrument suitable for a wide variety of samples and applications
<b>Furnace design</b>	Vertical		Optimized for performance, user exchangeable SaTurnA sensor. Ensures even purge gas flow.
<b>Balance design</b>	Top loading, single beam		Easy loading and unloading in manual and automated mode
<b>Balance resolution</b>	0.1 ug		
<b>Balance measurement range</b>	Up to 1500 mg		
<b>Temperature range</b>	15 °C to 1000 °C		Start experiments below room temperature to capture complete moisture and solvent evaporation
<b>Heating rate</b>	Ambient to 1000 °C	0.1 to 100 °C/min	
<b>Cooling rates</b>	From 1000 °C to 30 °C	Under 10 minutes	Forced air and chiller to achieve fastest cool down for higher productivity
<b>Temperature calibration</b>	Metal standards such as Indium and Silver		
<b>Temperature accuracy</b>	< ±0.5 °C		
<b>Temperature reproducibility</b>	< ±0.5 °C		
<b>Calorimetric data</b>	Accuracy/precision	±2% based on metal standards	
<b>Thermocouples</b>	PT-PT/Rh (Type R)		
<b>Sample pans</b>	Alumina 180 µl		
<b>Dimensions</b>	(HxWxD) 17 / 38 / 41 cm 6.7 / 15 / 16.5 in		Small footprint allows for the best use of your laboratory space
<b>Weight</b>	12-16 kg		
<b>Instrument control</b>	Pyris software		Benchmark software in Thermal Analysis
<b>Accessories</b>	Mass flow control and switch	Included	Integrated mass flow gas control and switching for accurate environmental control and high precision analysis
	Autosampler	Optional, 45-position	For unattended operation 24/7
	Transparent cover	Included in autosampler configurations Optional for standard configurations	Best protection for your samples
<b>Hyphenated techniques</b>	Combine with MS or IR analyzers		MS or IR connectivity capabilities allow the analysis of evolved gases
<b>Certificates/Compliance/Quality Assurance</b>	Developed under ISO 9001. Designed and tested to be in compliance with the legal requirements for laboratory analytical instruments		

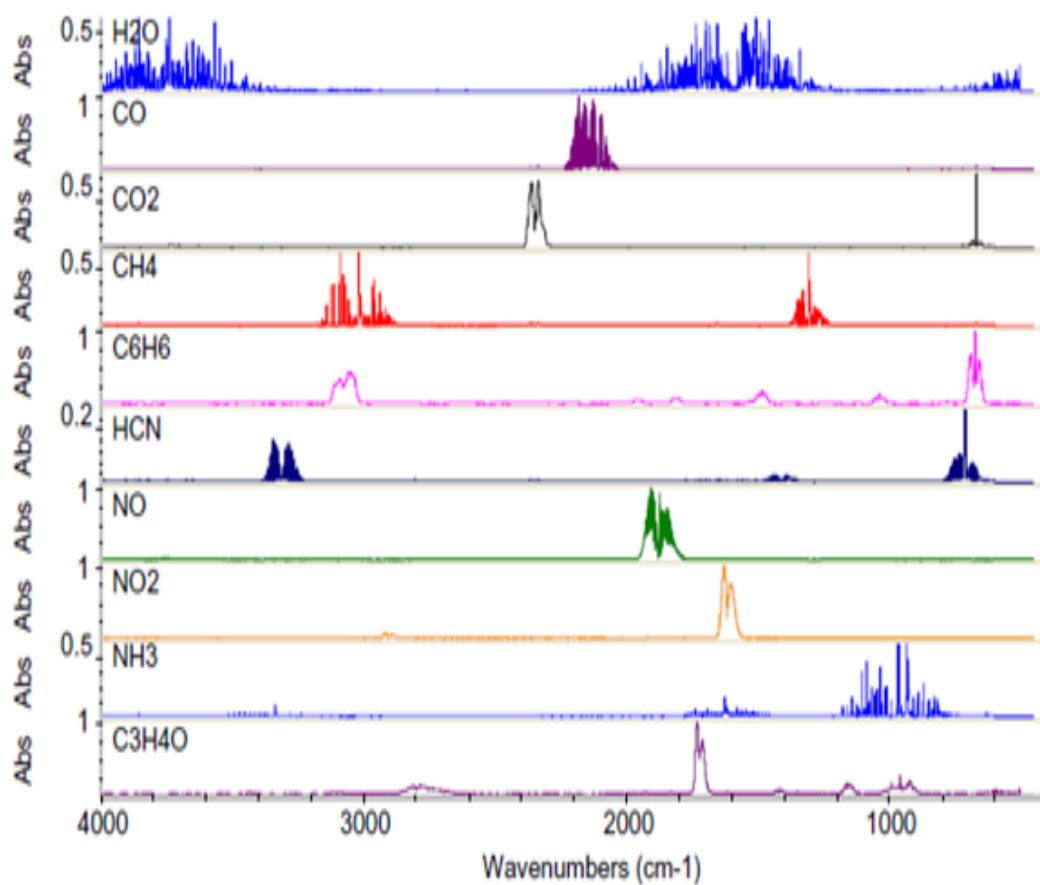


Fig. A.1 Typical FTIR spectra of important species for being used in identification and calibration [62]

Table A.8 Specifications of the Perkin Elmer Spectrum 1 FTIR spectrometer

**Optical performance**

	FR-DTGS Detector	LiTaO <sub>3</sub> Detector
Wavelength range	7,800 – 350 cm <sup>-1</sup> with KBr beamsplitter	7,800 – 350 cm <sup>-1</sup> with KBr beamsplitter 7,800 – 225 cm <sup>-1</sup> with CsI beamsplitter
Resolution	0.5 cm <sup>-1</sup> to 64 cm <sup>-1</sup>	0.5 cm <sup>-1</sup> to 64 cm <sup>-1</sup>
Wavelength accuracy	0.1 cm <sup>-1</sup> at 1,600 cm <sup>-1</sup>	0.1 cm <sup>-1</sup> at 1,600 cm <sup>-1</sup>
Signal to noise ratio – for KBr optics	30,000/1 rms, 6,000/1 p-p for a 5 second measurement and 100,000/1 rms, 20,000/1 p-p for a 1 minute measurement	7,500/1 rms, 1,500/1 p-p for a 5 second measurement and 26,000/1 rms, 5,000/1 p-p for a 1 minute measurement
Available OPD velocities	0.1, 0.2, 0.5, 1 and 2 cms <sup>-1</sup>	0.1, 0.2, 0.5, 1 and 2 cms <sup>-1</sup>

### **Cole-Parmer EW-03229-03 variable area flow meter**

Correlated flow meters with high-resolution valves - Cole-Parmer 150-mm correlated flow meter; 316 SS with 316 SS float; for liquids and gases with high-resolution valve:

- Longer 150-mm scale makes these flow meters perfect for applications demanding high resolution
- Clear polycarbonate front shield magnifies scale 16 %
- Hairline accuracy in reading float position is ensured by a vertical tangential locator line.
- Each flow meter consists of a heavy-walled glass flow tube mounted in an anodized aluminum frame with white acrylic back plate (1/8" thick).
- To determine the minimum flow value, take one tenth of the maximum flow value.
- Select a flow meter with a high-precision valve for superior flow rate control; ideal for low-flow applications or for any application where you need precise flow control
- The 16-turn high-precision valve features a nonrising stem to more accurately hit your desired set point

All flow meters come with correlation data sheets for water and air at standard temperature and pressure (STP).

Table A.9 Specifications of Cole-Parmer EW-03229-03 variable area flow meter

<b>Specifications</b>	
Product Type	Correlated Flowmeter
Description	Variable Area, Correlated Flowmeter
Flow rate (CO <sub>2</sub> )	87 mL/min
Flow rate (O <sub>2</sub> )	65 mL/min
Flow rate (N <sub>2</sub> )	79 (mL/min)
Flow rate (Ar)	59 mL/min
Flow rate (H <sub>2</sub> )	160 (mL/min)
Accuracy	±2% full-scale
Material (fitting)	316 Stainless Steel
Material (Valve)	316 Stainless Steel
Material (o-ring)	Viton®
Material (Flow Tube)	Borosilicate Glass
Material (Housing)	316 Stainless Steel
Material (float)	316 Stainless Steel
Max operating temperature (° F)	250
Max operating temperature (° C)	121
Max pressure	200 psi
Process connection	1/8" NPT(F)
Repeatability	±0.25%
Brand	Cole-Parmer
Manufacturer number	P21/1-N042-15ST

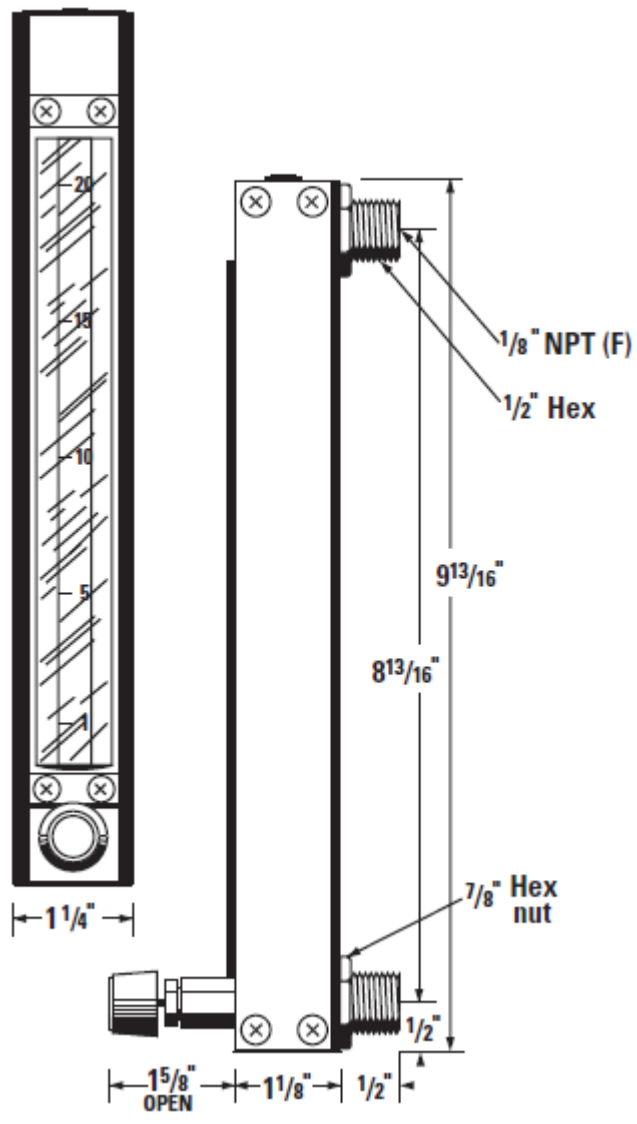


Fig. A.2 EW-03229-03 Cole-Parmer variable area flow meter drawing sketch

Table A.10 Flow meter calibration data for different gases

Scale Reading (mm)	N <sub>2</sub>	CO <sub>2</sub>	O <sub>2</sub>	Air
Scale Reading (mm)	Std. ml/min	Std. ml/min	Std. ml/min	Std. ml/min
150	62.5	72	54.2	60.6
145	59.4	68.7	51.45	57.55
140	56.3	65.4	48.7	54.5
135	53.65	62.5	46.4	51.95
130	51	59.6	44.1	49.4
125	47.85	56.15	41.35	46.35
120	44.7	52.7	38.6	43.3
115	42	49.7	36.3	40.7
110	39.3	46.7	34	38.1
105	37.45	44.6	32.35	36.3
100	35.6	42.5	30.7	34.5
95	33.6	40.2	28.95	32.55
90	31.6	37.9	27.2	30.6
85	29.1	35.05	25.05	28.2
80	26.6	32.2	22.9	25.8
75	24.65	29.9	21.2	23.85
70	22.7	27.6	19.5	21.9
65	21.35	26	18.35	20.65
60	20	24.4	17.2	19.4
55	18.3	22.35	15.7	17.7
50	16.6	20.3	14.2	16
45	14.95	18.3	12.8	14.45
40	13.3	16.3	11.4	12.9
35	11.95	14.65	10.245	11.55
30	10.6	13	9.09	10.2
25	9.485	11.65	8.145	9.15
20	8.37	10.3	7.2	8.1
15	7.2	8.85	6.2	6.97
10	6.03	7.4	5.2	5.84

## XRF results

Table A.11 XRF ash analyses of Kangal lignite and impregnated lignite samples

Sample Name	Kangal lignite	Dilution Material	M-HWC
Description	Sample Mass (g)	6,2500	
Method press	Dilution Mass (g)	1,4000	
Job Number	Collective Job	Dilution Factor	0,8170
Sample State	Pressed tablet, 40 mm	Sample rotation	Yes
Sample Type	Pellet_40	Date of Receipt	12/15/2011
Sample Status	AAXXXX	Date of Evaluation	12/15/2011

### Results

The error is the statistical error with 1 sigma confidence interval

Z	Symbol	Element	Concentration	Abs. Error
11	Na2O	Sodiumoxide	< 0,11 %	(0,0) %
12	MgO	Magnesiumoxide	4,107 %	0,035 %
13	Al2O3	Aluminumoxide	15,96 %	0,02 %
14	SiO2	Siliconoxide	34,00 %	0,03 %
15	P2O5	Phosphorusoxide	0,1361 %	0,0033 %
16	SO3	Sulfurtrioxide	14,84 %	0,01 %
17	Cl	Chlorine	0,03487 %	0,00055 %
19	K2O	Potassiumoxide	1,120 %	0,011 %
20	CaO	Calciumoxide	24,40 %	0,03 %
22	TiO2	Titaniumdioxide	0,6774 %	0,0060 %
23	V2O5	Vanadiumoxide	0,0429 %	0,0014 %
24	Cr2O3	Chromiumoxide	0,1459 %	0,0058 %
25	MnO	Manganesoxide	< 0,00066%	(0,0) %
26	Fe2O3	Ironoxide	6,037 %	0,011 %
27	CoO	Cobaltoxide	< 0,00038	%(0,0) %
28	NiO	Nickeloxide	0,0542 %	0,0011 %
29	CuO	Copperoxide	0,0191 %	0,0013 %
30	ZnO	Zincoxide	0,0589 %	0,0036 %
31	Ga	Gallium	< 0,00010 %	(0,0) %
32	Ge	Germanium	< 0,00010	%(0,0) %
33	As2O3	Arsenicoxide	0,01769 %	0,00042 %
34	Se	Selenium	0,00183 %	0,00016 %
35	Br	Bromine	0,00311 %	0,00021 %
37	Rb2O	Rubidiumoxide	0,00794 %	0,00022 %
38	SrO	Strontiumoxide	0,1154 %	0,0005 %
39	Y	Yttrium	0,00350 %	0,00021 %
40	ZrO2	Zirconiumoxide	< 0,068 %	(0,018) %
41	Nb2O5	Niobiumoxide	0,00248 %	0,00015 %
42	Mo	Molybdenum	0,00316 %	0,00005 %
47	Ag	Silver	0,00045 %	0,00025 %
48	Cd	Cadmium	< 0,00051 %	(0,0) %
49	In	Indium	< 0,00051 %	(0,0) %
50	SnO2	Tinoxide	0,0042 %	0,0035 %
51	Sb2O5	Antimonyoxide	0,00094 %	0,00021 %
52	Te	Tellurium	0,0148 %	0,0024 %
53	I	Iodine	0,00075 %	0,00075 %
55	Cs	Cesium	0,00436 %	0,00033 %
56	Ba	Barium	0,137 %	0,012 %
57	La	Lanthanum	< 0,0010	%(0,0) %
58	Ce	Cerium	< 0,0012 %	(0,0) %
72	Hf	Hafnium	< 0,00020 %	(0,0) %
73	Ta2O5	Tantalumoxide	0,0681 %	0,0029 %
74	WO3	Tungstenoxide	0,00283 %	0,00035 %
80	Hg	Mercury	< 0,00020 %	(0,0) %
81	Tl	Thallium	0,00398 %	0,00036 %
82	PbO	Leadoxide	< 0,00022	%(0,0) %
83	Bi	Bismuth	< 0,00020	%(0,0) %
90	Th	Thorium	0,00589 %	0,00036 %
92	U	Uranium	0,00629 %	0,00036 %

Sample Name Kangal lignite +5 %Fe2O3(silica) Dilution Material  
 Description Sample Mass (g) 6,2500  
 Method press Dilution Mass (g) 1,4000  
 Job Number Collective Job Dilution Factor 0,8170  
 Sample State Pressed tablet, 40 mm Sample rotation Yes  
 Sample Type Pellet\_40 Date of Receipt 12/15/2011  
 Sample Status AAXXXX Date of Evaluation 12/15/2011

Results

The error is the statistical error with 1 sigma confidence interval

Z	Symbol	Element	Concentration	Abs. Error
11	Na2O	Sodiumoxide	< 0,11 %	(0,0) %
12	MgO	Magnesiumoxide	3,707 %	0,035 %
13	Al2O3	Aluminumoxide	14,03 %	0,02 %
14	SiO2	Siliconoxide	29,84 %	0,02 %
15	P2O5	Phosphorusoxide	0,1145 %	0,0031 %
16	SO3	Sulfurtrioxide	13,49 %	0,01 %
17	Cl	Chlorine	0,04460 %	0,00054 %
19	K2O	Potassiumoxide	< 0,0012	%(0,0) %
20	CaO	Calciumoxide	21,58 %	0,03 %
22	TiO2	Titaniumdioxide	0,4486 %	0,0056 %
23	V2O5	Vanadiumoxide	0,0262 %	0,0014 %
24	Cr2O3	Chromiumoxide	0,1703 %	0,0057 %
25	MnO	Manganeseoxide	< 0,00066	%(0,0) %
26	Fe2O3	Ironoxide	16,70 %	0,02 %
27	CoO	Cobaltoxide	< 0,00038	%(0,0) %
28	NiO	Nickeloxide	0,0616 %	0,0017 %
29	CuO	Copperoxide	0,0125 %	0,0015 %
30	ZnO	Zincoxide	0,0573 %	0,0032 %
31	Ga	Gallium	< 0,00010 %	(0,0) %
32	Ge	Germanium	< 0,00010	%(0,0) %
33	As2O3	Arsenicoxide	0,00880 %	0,00052 %
34	Se	Selenium	0,00074 %	0,00019 %
35	Br	Bromine	0,00359 %	0,00023 %
37	Rb2O	Rubidiumoxide	0,00477 %	0,00026 %
38	SrO	Strontiumoxide	0,1040 %	0,0005 %
39	Y	Yttrium	0,00330 %	0,00020 %
40	ZrO2	Zirconiumoxide	< 0,068 %	(0,015) %
41	Nb2O5	Niobiumoxide	0,00192 %	0,00014 %
42	Mo	Molybdenum	0,00272 %	0,00005 %
47	Ag	Silver	0,00032 %	0,00029 %
48	Cd	Cadmium	< 0,00051 %	(0,0) %
49	In	Indium	< 0,00051 %	(0,0) %
50	SnO2	Tinoxide	0,00181 %	0,00007 %
51	Sb2O5	Antimonyoxide	< 0,00081	%(0,0) %
52	Te	Tellurium	0,0028 %	0,0017 %
53	I	Iodine	0,00019 %	0,00019 %
55	Cs	Cesium	0,0017 %	0,0013 %
56	Ba	Barium	0,1160 %	0,0031 %
57	La	Lanthanum	< 0,0010	%(0,0) %
58	Ce	Cerium	< 0,0012 %	(0,0) %
72	Hf	Hafnium	< 0,00020 %	(0,0) %
73	Ta2O5	Tantalumoxide	0,1020 %	0,0042 %
74	WO3	Tungstenoxide	0,0229 %	0,0020 %
80	Hg	Mercury	< 0,00020 %	(0,0) %
81	Tl	Thallium	< 0,00020	%(0,0) %
82	PbO	Leadoxide	0,00677 %	0,00042 %
83	Bi	Bismuth	< 0,00020 %	(0,0) %
90	Th	Thorium	< 0,00020 %	(0,0) %
92	U	Uranium	0,00825 %	0,00039 %

Sample Name Kangal lignite+5%Ca(OH)2 Dilution Material M-HWC  
 Description Sample Mass (g) 6,2500  
 Method press Dilution Mass (g) 1,4000  
 Job Number Collective Job Dilution Factor 0,8170  
 Sample State Pressed tablet, 40 mm Sample rotation Yes  
 Sample Type Pellet\_40 Date of Receipt 10/22/2011  
 Sample Status AAXXXX Date of Evaluation 10/22/2011

Results

The error is the statistical error with 1 sigma confidence interval

Z	Symbol	Element	Concentration	Abs. Error
11	Na2O	Sodiumoxide	< 0,11 %	(0,0) %
12	MgO	Magnesiumoxide	3,864 %	0,034 %
13	Al2O3	Aluminumoxide	14,73 %	0,02 %
14	SiO2	Siliconoxide	31,64 %	0,03 %
15	P2O5	Phosphorusoxide	0,0955 %	0,0031 %
16	SO3	Sulfurtrioxide	13,88 %	0,01 %
17	Cl	Chlorine	0,04923 %	0,00054 %
19	K2O	Potassiumoxide	0,986 %	0,011 %
20	CaO	Calciumoxide	30,71 %	0,03 %
22	TiO2	Titaniumdioxide	0,5784 %	0,0060 %
23	V2O5	Vanadiumoxide	0,0388 %	0,0014 %
24	Cr2O3	Chromiumoxide	0,1367 %	0,0065 %
25	MnO	Manganeseoxide	< 0,00066 %	%(0,0) %
26	Fe2O3	Ironoxide	5,391 %	0,011 %
27	CoO	Cobaltoxide	< 0,00038 %	%(0,0) %
28	NiO	Nickeloxide	0,0469 %	0,0011 %
29	CuO	Copperoxide	0,00890 %	0,00096 %
30	ZnO	Zincoxide	0,0575 %	0,0033 %
31	Ga	Gallium	< 0,00010 %	(0,0) %
32	Ge	Germanium	< 0,00010 %	%(0,0) %
33	As2O3	Arsenicoxide	0,01333 %	0,00044 %
34	Se	Selenium	0,00160 %	0,00016 %
35	Br	Bromine	0,00498 %	0,00022 %
37	Rb2O	Rubidiumoxide	0,00727 %	0,00022 %
38	SrO	Strontiumoxide	0,1068 %	0,0005 %
39	Y	Yttrium	0,00306 %	0,00015 %
40	ZrO2	Zirconiumoxide	< 0,068 %	(0,016) %
41	Nb2O5	Niobiumoxide	0,00233 %	0,00015 %
42	Mo	Molybdenum	0,00264 %	0,00004 %
47	Ag	Silver	0,00027 %	0,00026 %
48	Cd	Cadmium	< 0,00051 %	(0,0) %
49	In	Indium	< 0,00051 %	(0,0) %
50	SnO2	Tinoxide	0,0031 %	0,0031 %
51	Sb2O5	Antimonyoxide	0,00157 %	0,00030 %
52	Te	Tellurium	0,0145 %	0,0023 %
53	I	Iodine	0,00021 %	0,00021 %
55	Cs	Cesium	0,00449 %	0,00047 %
56	Ba	Barium	0,124 %	0,015 %
57	La	Lanthanum	0,00092 %	0,00051 %
58	Ce	Cerium	< 0,0012 %	(0,0) %
72	Hf	Hafnium	< 0,00020 %	(0,0) %
73	Ta2O5	Tantalumoxide	0,0901 %	0,0030 %
74	WO3	Tungstenoxide	< 0,00025 %	%(0,0) %
80	Hg	Mercury	< 0,00020 %	(0,0) %
81	Tl	Thallium	0,00372 %	0,00032 %
82	PbO	Leadoxide	< 0,00022 %	%(0,0) %
83	Bi	Bismuth	< 0,00020 %	(0,0) %
90	Th	Thorium	0,00209 %	0,00028 %
92	U	Uranium	0,00492 %	0,00031 %

Sample Name Kangal lignite+5%K2CO3 Dilution Material M-HWC  
 Description Sample Mass (g) 6,2500  
 Method press Dilution Mass (g) 1,4000  
 Job Number Collective Job Dilution Factor 0,8170  
 Sample State Pressed tablet, 40 mm Sample rotation Yes  
 Sample Type Pellet\_40 Date of Receipt 12/15/2011  
 Sample Status AAXXXX Date of Evaluation 12/15/2011

Results

The error is the statistical error with 1 sigma confidence interval

Z	Symbol	Element	Concentration	Abs. Error
11	Na2O	Sodiumoxide	< 0,11 %	(0,0) %
12	MgO	Magnesiumoxide	3,155 %	0,034 %
13	Al2O3	Aluminumoxide	12,85 %	0,02 %
14	SiO2	Siliconoxide	30,60 %	0,02 %
15	P2O5	Phosphorusoxide	0,1392 %	0,0032 %
16	SO3	Sulfurtrioxide	15,06 %	0,01 %
17	Cl	Chlorine	0,03290 %	0,00055 %
19	K2O	Potassiumoxide	8,574 %	0,020 %
20	CaO	Calciumoxide	23,53 %	0,03 %
22	TiO2	Titaniumdioxide	0,6116 %	0,0065 %
23	V2O5	Vanadiumoxide	0,0424 %	0,0015 %
24	Cr2O3	Chromiumoxide	0,1189 %	0,0062 %
25	MnO	Manganeseoxide	< 0,00066 %	%(0,0) %
26	Fe2O3	Ironoxide	5,775 %	0,011 %
27	CoO	Cobaltoxide	< 0,00038 %	%(0,0) %
28	NiO	Nickeloxide	0,0451 %	0,0011 %
29	CuO	Copperoxide	0,00583 %	0,00078 %
30	ZnO	Zincoxide	0,0510 %	0,0029 %
31	Ga	Gallium	< 0,00010 %	(0,0) %
32	Ge	Germanium	< 0,00010 %	%(0,0) %
33	As2O3	Arsenicoxide	0,01261 %	0,00046 %
34	Se	Selenium	0,00022 %	0,00017 %
35	Br	Bromine	0,00362 %	0,00023 %
37	Rb2O	Rubidiumoxide	0,00714 %	0,00023 %
38	SrO	Strontiumoxide	0,1087 %	0,0005 %
39	Y	Yttrium	0,00262 %	0,00017 %
40	ZrO2	Zirconiumoxide	0,017 %	0,017 %
41	Nb2O5	Niobiumoxide	0,00165 %	0,00013 %
42	Mo	Molybdenum	0,00299 %	0,00005 %
47	Ag	Silver	0,00043 %	0,00027 %
48	Cd	Cadmium	< 0,00051 %	(0,0) %
49	In	Indium	< 0,00051 %	(0,0) %
50	SnO2	Tinoxide	0,00495 %	0,00017 %
51	Sb2O5	Antimonyoxide	0,00098 %	0,00011 %
52	Te	Tellurium	0,0285 %	0,0034 %
53	I	Iodine	< 0,00071 %	(0,0) %
55	Cs	Cesium	0,00659 %	0,00096 %
56	Ba	Barium	0,134 %	0,028 %
57	La	Lanthanum	< 0,0010 %	%(0,0) %
58	Ce	Cerium	< 0,0012 %	(0,0) %
72	Hf	Hafnium	< 0,00020 %	(0,0) %
73	Ta2O5	Tantalumoxide	0,0978 %	0,0032 %
74	WO3	Tungstenoxide	< 0,00025 %	%(0,0) %
80	Hg	Mercury	< 0,00020 %	(0,0) %
81	Tl	Thallium	< 0,00020 %	%(0,0) %
82	PbO	Leadoxide	0,00122 %	0,00006 %
83	Bi	Bismuth	< 0,00020 %	(0,0) %
90	Th	Thorium	< 0,00020 %	(0,0) %
92	U	Uranium	0,00400 %	0,00029 %

Sample Name Kangal lignite+5%FeCl3 Dilution Material M-HWC  
 Description Sample Mass (g) 6,2500  
 Method press Dilution Mass (g) 1,4000  
 Job Number Collective Job Dilution Factor 0,8170  
 Sample State Pressed tablet, 40 mm Sample rotation Yes  
 Sample Type Pellet\_40 Date of Receipt 12/15/2011  
 Sample Status AAXXXX Date of Evaluation 12/15/2011

Results

The error is the statistical error with 1 sigma confidence interval

Z	Symbol	Element	Concentration	Abs. Error
11	Na2O	Sodiumoxide	< 0,11 %	(0,0) %
12	MgO	Magnesiumoxide	3,413 %	0,035 %
13	Al2O3	Aluminumoxide	13,10 %	0,02 %
14	SiO2	Siliconoxide	29,18 %	0,02 %
15	P2O5	Phosphorusoxide	< 0,00069 %	%(0,0) %
16	SO3	Sulfurtrioxide	12,34 %	0,01 %
17	Cl	Chlorine	1,055 %	0,001 %
19	K2O	Potassiumoxide	0,905 %	0,011 %
20	CaO	Calciumoxide	21,12 %	0,03 %
22	TiO2	Titaniumdioxide	0,5042 %	0,0059 %
23	V2O5	Vanadiumoxide	0,0212 %	0,0017 %
24	Cr2O3	Chromiumoxide	0,1565 %	0,0059 %
25	MnO	Manganeseoxide	0,0037 %	0,0037 %
26	Fe2O3	Ironoxide	11,55 %	0,02 %
27	CoO	Cobaltoxide	< 0,00038 %	%(0,0) %
28	NiO	Nickeloxide	0,0591 %	0,0014 %
29	CuO	Copperoxide	0,0260 %	0,0017 %
30	ZnO	Zincoxide	0,0508 %	0,0026 %
31	Ga	Gallium	< 0,00010 %	(0,0) %
32	Ge	Germanium	< 0,00010 %	%(0,0) %
33	As2O3	Arsenicoxide	0,01102 %	0,00048 %
34	Se	Selenium	0,00079 %	0,00017 %
35	Br	Bromine	0,00189 %	0,00021 %
37	Rb2O	Rubidiumoxide	0,00555 %	0,00024 %
38	SrO	Strontiumoxide	0,1073 %	0,0005 %
39	Y	Yttrium	0,00290 %	0,00013 %
40	ZrO2	Zirconiumoxide	< 0,068 %	(0,017) %
41	Nb2O5	Niobiumoxide	0,00207 %	0,00014 %
42	Mo	Molybdenum	0,00275 %	0,00004 %
47	Ag	Silver	0,00030 %	0,00026 %
48	Cd	Cadmium	< 0,00051 %	(0,0) %
49	In	Indium	< 0,00051 %	(0,0) %
50	SnO2	Tinoxide	0,0040 %	0,0040 %
51	Sb2O5	Antimonyoxide	0,00053 %	0,00053 %
52	Te	Tellurium	0,014 %	0,014 %
53	I	Iodine	< 0,00071 %	(0,0) %
55	Cs	Cesium	0,0034 %	0,0012 %
56	Ba	Barium	0,1138 %	0,0048 %
57	La	Lanthanum	0,0070 %	0,0020 %
58	Ce	Cerium	< 0,0012 %	(0,0) %
72	Hf	Hafnium	< 0,00020 %	(0,0) %
73	Ta2O5	Tantalumoxide	0,0796 %	0,0035 %
74	WO3	Tungstenoxide	0,0102 %	0,0011 %
80	Hg	Mercury	< 0,00020 %	(0,0) %
81	Tl	Thallium	< 0,00020 %	%(0,0) %
82	PbO	Leadoxide	0,00530 %	0,00027 %
83	Bi	Bismuth	< 0,00020 %	(0,0) %
90	Th	Thorium	< 0,00020 %	(0,0) %
92	U	Uranium	0,00710 %	0,00035 %

Table A.12 XRF ash analysis of hazelnut shell (HSh) biomass

Sample Name	Hazelnut Shell Ash	Dilution Material	M-HWC
Description	Sample Mass (g)	6,2500	
Method	press	Dilution Mass (g)	1,4000
Job Number	0	Dilution Factor	0,8170
Sample State	Pressed tablet, 40 mm	Sample rotation	Yes
Sample Type	Pellet_40	Date of Receipt	06/12/2012
Sample Status	AAXXXX	Date of Evaluation	06/12/2012

Results

The error is the statistical error with 1 sigma confidence interval

Z	Symbol	Element	Concentration	Abs. Error
11	Na2O	Sodiumoxide	< 0,11 %	(0,0) %
12	MgO	Magnesiumoxide	6,049 %	0,026 %
13	Al2O3	Aluminumoxide	5,349 %	0,013 %
14	SiO2	Siliconoxide	10,29 %	0,01 %
15	P2O5	Phosphorusoxide	3,140 %	0,004 %
16	SO3	Sulfurtrioxide	2,071 %	0,002 %
17	Cl	Chlorine	0,1995 %	0,0004 %
19	K2O	Potassiumoxide	33,82 %	0,04 %
20	CaO	Calciumoxide	24,89 %	0,04 %
22	TiO2	Titaniumdioxide	0,0568 %	0,0036 %
23	V2O5	Vanadiumoxide	0,0043 %	0,0014 %
24	Cr2O3	Chromiumoxide	0,0076 %	0,0054 %
25	MnO	Manganeseoxide	0,3518 %	0,0059 %
26	Fe2O3	Ironoxide	0,7089 %	0,0047 %
27	CoO	Cobaltoxide	< 0,00038 %	%(0,0) %
28	NiO	Nickeloxide	0,01079 %	0,00055 %
29	CuO	Copperoxide	0,1241 %	0,0022 %
30	ZnO	Zincoxide	0,060 %	0,014 %
31	Ga	Gallium	0,00004 %	0,00004 %
32	Ge	Germanium	< 0,00010 %	%(0,0) %
33	As2O3	Arsenicoxide	< 0,00013 %	%(0,0) %
34	Se	Selenium	< 0,00010 %	%(0,0) %
35	Br	Bromine	0,00104 %	0,00021 %
37	Rb2O	Rubidiumoxide	0,04193 %	0,00037 %
38	SrO	Strontiumoxide	0,1467 %	0,0006 %
39	Y	Yttrium	< 0,00071 %	(0,0) %
40	ZrO2	Zirconiumoxide	< 0,068 %	(0,0) %
41	Nb2O5	Niobiumoxide	< 0,0014 %	(0,0) %
42	Mo	Molybdenum	< 0,0010 %	(0,00042) %
47	Ag	Silver	0,00035 %	0,00025 %
48	Cd	Cadmium	< 0,00051 %	(0,0) %
49	In	Indium	< 0,00051 %	(0,0) %
50	SnO2	Tinoxide	0,00358 %	0,00096 %
51	Sb2O5	Antimonyoxide	< 0,00081 %	%(0,0) %
52	Te	Tellurium	0,0117 %	0,0020 %
53	I	Iodine	0,0170 %	0,0026 %
55	Cs	Cesium	< 0,00081 %	(0,0) %
56	Ba	Barium	0,0712 %	0,0027 %
57	La	Lanthanum	< 0,0010 %	%(0,0) %
58	Ce	Cerium	< 0,0012 %	%(0,0) %
72	Hf	Hafnium	< 0,00020 %	(0,0) %
73	Ta2O5	Tantalumoxide	0,0687 %	0,0035 %
74	WO3	Tungstenoxide	< 0,00025 %	%(0,0) %
80	Hg	Mercury	< 0,00020 %	%(0,0) %
81	Tl	Thallium	< 0,00020 %	%(0,0) %
82	PbO	Leadoxide	< 0,00022 %	%(0,0) %
83	Bi	Bismuth	< 0,00020 %	%(0,0) %
90	Th	Thorium	0,00032 %	0,00020 %
92	U	Uranium	< 0,00030 %	(0,0) %

**APPENDIX B**

**CALORIMETRIC TEST RESULTS**

Table B.1 Calorimetric test results of Tunçbilek sub- bituminous samples

Sample Definition	Sample Number	Sample Weight (g)	Modified Weight (Theoretical) (g)	Amb. Temp. (°C)	Lower Temp. (T <sub>1</sub> °C)	Higher Temp. (T <sub>2</sub> °C)	(GCV) or (HHV) (Kcal/Kg)	Ave. (Kcal/Kg)	Difference (%)	Ash (g)	Wire Length (cm)
T (Amb. Temp. ≈ 17 °C)	1st	1.447	1.447	≈17	30.62	32.685	3440.38	3433.84	-	0.644	5.3
"	2nd	1.497	1.497	"	30.32	32.45	3427.30	"	-	0.668	3.3
T + 2 % Ca(OH) <sub>2</sub>	1st	1.518	1.4863	≈17	28.52	30.62	3402.59	3397.59	-1.06	0.584	2.9
"	2nd	1.474	1.4432	"	28.845	30.873	3392.60	"	"	0.632	8.5
T + 5 % Ca(OH) <sub>2</sub>	1st	1.532	1.4519	≈17	30.935	32.88	3230.04	3276.71	-4.58	0.702	5.9
"	2nd	1.567	1.4851	"	29.10	31.15	3323.38	"	"	0.718	2.5
T+ 10 % Ca(OH) <sub>2</sub>	1st	1.502	1.3449	≈17	28.30	30.145	3312.68	3303.66	-3.79	0.682	9
"	2nd	1.503	1.3458	"	28.24	30.08	3294.65	"	"	0.693	5
T + 2 % K <sub>2</sub> CO <sub>3</sub>	1st	1.460	1.4295	≈17	30.585	32.525	3272.20	3303.61	-3.79	0.680	5.9
"	2nd	1.499	1.4677	"	29.39	31.42	3335.03	"	"	0.698	5.8
T + 5 % K <sub>2</sub> CO <sub>3</sub>	1st	1.494	1.4159	≈17	29.51	31.38	3178.83	3205.20	-6.66	0.690	2.6
"	2nd	1.462	1.3856	"	29.60	31.46	3231.57	"	"	0.687	3
T + 10 % K <sub>2</sub> CO <sub>3</sub>	1st	1.400	1.2536	≈17	29.66	31.32	3191.34	3206.02	-6.63	0.681	5.7
"	2nd	1.435	1.2849	"	28.74	30.46	3220.69	"	"	0.700	2.5
T + 2 % FeCl <sub>3</sub>	1st	1.439	1.4089	18-19	28.22	30.27	3507.20	3512.66	2.30	0.642	5
"	2nd	1.489	1.4579	"	27.955	30.085	3518.12	"	"	0.667(T)	2.6
T + 5 % FeCl <sub>3</sub>	1st	1.546	1.4652	19-20	27.615	29.735	3483.94	3456.79	0.67	0.698	2.5
"	2nd	1.448	1.3723	"	27.437	29.39	3429.63	"	"	0.654	4.8
T + 10 % FeCl <sub>3</sub>	1st	1.436	1.2858	17	28.245	30.11	3491.79	3487.62	1.57	0.645	3
"	2nd	1.461	1.3082	"	27.955	29.845	3483.44	"	"	0.652	6
T + 2 % Fe <sub>2</sub> O <sub>3</sub>	1st	1.475	1.4442	20	29.14	31.14	3334.17	3311.26	-3.57	0.682	2.7
"	2nd	1.531	1.4990	"	29.565	31.61	3288.34	"	"	0.725	5
T + 5 % Fe <sub>2</sub> O <sub>3</sub>	1st	1.497	1.4187	20-21	28.863	30.73	3172.96	3201.13	-6.78	0.731	6
"	2nd	1.510	1.4311	"	28.79	30.71	3229.31	"	"	0.749	2.5
T + 10 % Fe <sub>2</sub> O <sub>3</sub>	1st	1.467	1.3136	19-20	30.015	31.79	3262.87	3307.95	-3.67	0.725	9
"	2nd	1.503	1.3458	"	29.61	31.485	3353.04	"	"	0.739	2.4

Table B.2 Calorimetric test results of Seyitömer lignite samples

Sample Definition	Sample Number	Sample Weight (g)	Modified Weight (Theoretical) (g)	Amb. Temp. (°C)	Lower Temp. (T <sub>1</sub> °C)	Higher Temp. (T <sub>2</sub> °C)	(GCV) or (HHV) (Kcal/ Kg)	Ave. (Kcal/ Kg)	Difference (%)	Ash (g)	Wire Length (cm)
S	1st	1.453	1.453	18- 19	27.875	29.20	2190.98	2192.48	-	0.816	2.3
"	2nd	1.554	1.554	"	27.605	29.02	2193.98	"	-	0.876	6
S + 2 % Ca(OH) <sub>2</sub>	1st	1.529	1.4926	≈ 17	28.19	29.59	2259.64	2243.03	2.31	0.824	5.8
"	2nd	1.562	1.5251	"	27.91	29.32	2226.42	"	"	-	5.2
S + 5 % Ca(OH) <sub>2</sub>	1st	1.516	1.4258	≈ 17	29.60	30.89	2179.44	2115.21	-3.52	0.828	6
"	2nd	1.011	0.9508	"	28.295	29.13	2102.88	"	"	0.564	2.2
"	3rd	1.486	1.3976	"	27.575	28.77	2063.30	"	"	0.832	8.5
S +10 %Ca(OH) <sub>2</sub>	1st	1.438	1.2668	≈ 17	30.23	31.34	2113.87	2161.83	-1.40	0.783	8.3
"	2nd	1.484	1.3073	"	29.29	30.49	2209.78	"	"	0.813	5.5
S + 2 % K <sub>2</sub> CO <sub>3</sub>	1st	1.426	1.3920	≈ 17	28.665	29.96	2240.21	2261.56	3.15	0.783	5.5
"	2nd	1.423	1.3891	"	27.895	29.215	2282.90	"	"	0.800	2.2
S + 5 % K <sub>2</sub> CO <sub>3</sub>	1st	-	-	-	-	-	-	-	-	-	-
"	2nd	-	-	-	-	-	-	-	-	-	-
S + 10 % K <sub>2</sub> CO <sub>3</sub>	1st	1.524	1.3556	≈ 17	28.155	29.39	2194.11	2197.24	0.22	0.898	5.9(Av)
"	2nd	1.471	1.2959	"	29.94	31.125	2200.37	"	"	0.871	5
S + 2 % FeCl <sub>3</sub>	1st	1.470	1.4350	19	30.763	31.99	2060.04	2074.21	-5.39	0.836	6.4
"	2nd	1.534	1.4975	"	29.825	31.12	2088.37	"	"	0.877	9.4
S + 5 % FeCl <sub>3</sub>	1st	1.552	1.4596	19-20	27.627	28.89	2088.21	2082.34	-5.02	0.886	8.5
"	2nd	1.517	1.4267	"	28.24	29.47	2076.46	"	"	0.871	6
S + 10 % FeCl <sub>3</sub>	1st	1.488	1.3109	19	29.315	30.547	2263.57	2229.69	1.70	0.817	6
"	2nd	1.514	1.3338	"	29.747	30.96	2195.81	"	"	0.829	9.2
S + 2 % Fe <sub>2</sub> O <sub>3</sub>	1st	1.562	1.5248	20	27.745	28.96	1918.80	1936.11	-11.69	0.963	5.8
"	2nd	1.486	1.4506	"	27.275	28.455	1953.42	"	"	0.917	2.5
S+ 5 % Fe <sub>2</sub> O <sub>3</sub>	1st	1.564	1.4709	20-21	28.927	30.11	1940.61	1930.13	-11.97	0.969	8.4
"	2nd	1.512	1.4220	"	29.33	30.465	1919.65	"	"	0.992	4.6
S + 10 % Fe <sub>2</sub> O <sub>3</sub>	1st	1.492	1.3144	19-20	28.525	29.53	1840.64	1874.36	-14.51	0.956	6.2
"	2nd	1.453	1.2800	"	27.915	28.93	1908.09	"	"	0.945	5.7

Table B. 3 Calorimetric test results of Kangal lignite samples

Sample Definition	Sample Number	Sample Weight (g)	modified weight (Theoretical) (g)	Amb. Temp. (°C)	Lower Temp. (T <sub>1</sub> °C)	Higher Temp. (T <sub>2</sub> °C)	(GCV) or (HHV) (Kcal/ Kg)	Ave. (Kcal/ Kg)	Difference (%)	Ash (g)	Wire Length (cm)
<b>K (Temp. ≈ 17 °C)</b>	<b>1st</b>	<b>1.498</b>	<b>1.498</b>	<b>17-18</b>	<b>28.18</b>	<b>29.643</b>	<b>2358.17</b>	<b>2374.80</b>	<b>-</b>	<b>0.665</b>	<b>9.1</b>
"	<b>2nd</b>	<b>1.540</b>	<b>1.540</b>	"	<b>27.705</b>	<b>29.23</b>	<b>2391.42</b>	"	<b>-</b>	<b>-</b>	<b>9.3</b>
K + 2 % Ca(OH) <sub>2</sub>	1st	1.556	1.5130	≈ 17	30.775	32.215	2295.78	2264.20	-4.66	0.699	7.6
"	2nd	1.309	1.2728	"	28.255	29.435	2232.62	"	"	0.585	6
K + 5 % Ca(OH) <sub>2</sub>	1st	1.512	1.4075	17-18	27.965	29.215	2144.83	2166.28	-8.78	0.658	9.5
"	2nd	1.550	1.4429	"	28.955	30.265	2187.73	"	"		6.4(Av)
K + 10 % Ca(OH) <sub>2</sub>	1st	1.515	1.3057	≈ 17	27.045	28.27	2258.40	2229.92	-6.10	0.716	5.3
"	2nd	1.438	1.2393	"	27.40	28.53	2201.44	"	"	0.667	9.2
K + 2 % K <sub>2</sub> CO <sub>3</sub>	1st	1.376	1.3380	≈ 17	31.835	33.08	2239.13	2325.78	-2.06	0.620	4.8
"	2nd	1.503	1.4615	"	29.34	30.80	2412.42	"	"	-	9.3
K + 5 % K <sub>2</sub> CO <sub>3</sub>	1st	1.314	1.2232	18-19	27.68	28.795	2199.84	2195.11	-7.57	0.631	8.7
"	2nd	1.340	1.2474	"	30.21	31.345	2190.37	"	"	0.642	5.7
K + 10 % K <sub>2</sub> CO <sub>3</sub>	1st	1.594	1.3737	18-19	29.40	30.785	2426.83	2431.57	2.39	0.768	4.6
"	2nd	1.508	1.2996	"	27.59	28.905	2436.31	"	"	0.740	5.3
K + 2 % FeCl <sub>3</sub>	1st	1.560	1.5169	18-19	31.34	32.885	2458.33	2471.53	4.07	0.692	8.4
"	2nd	1.513	1.4712	"	28.285	29.805	2484.73	"	"	0.669	2.7
K + 5 % FeCl <sub>3</sub>	1st	1.578	1.4690	18-19	28.145	29.69	2533.48	2489.62	4.83	0.707	5.2
"	2nd	1.486	1.3833	"	30.85	32.255	2445.75	"	"	0.669	5.1
K + 10 % FeCl <sub>3</sub>	1st	1.566	1.3496	18-19	28.98	30.435	2598.38	2602.40	9.58	0.703	6.3
"	2nd	1.471	1.2677	"	28.973	30.345	2606.43	"	"	0.664	5.4
K + 2 % Fe <sub>2</sub> O <sub>3</sub>	1st	1.493	1.4517	19-20	27.22	28.62	2322.83	2351.34	-0.99	0.664	5.5
"	2nd	1.414	1.3749	"	27.145	28.50	2379.86	"	"	0.629	9.3
K+ 5 % Fe <sub>2</sub> O <sub>3</sub>	1st	1.524	1.4187	20-21	27.793	29.175	2346.69	2371.52	-0.14	0.720	5.8
"	2nd	1.411	1.3135	"	28.51	29.817	2396.34	"	"	0.670	5.6
K + 10 % Fe <sub>2</sub> O <sub>3</sub>	1st	1.567	1.3505	19-20	29.627	30.94	2336.48	2334.03	-1.72	0.772	2.7
"	2nd	1.543	1.3298	"	28.79	30.08	2331.58	"	"	0.748	3

Table B. 4 Calorimetric test results of Zonguldak bituminous samples

Sample Definition	Sample Number	Sample Weight (g)	modified weight (Theoretical) (g)	Amb. Temp. (°C)	Lower Temp. (T <sub>1</sub> °C)	Higher Temp. (T <sub>2</sub> °C)	(GCV) or (HHV) (Kcal/Kg)	Ave. (Kcal/Kg)	Difference (%)	Ash (g)	Wire Length (cm)
Z (45min drying)	1st	1.448	1.448	17-18	30.235	32.77	4218.23	"	-	0.587	2.8
"	2 <sup>nd</sup>	1.406	1.406	"	27.785	30.28	4275.18	"	-	0.568	2.6
Z + 2 % Ca(OH) <sub>2</sub>	1st	1.442	1.4124	17-18	28.23	30.69	4200.17	4169.87	-1.34	0.592	5.2
"	2nd	1.505	1.4741	"	28.48	31.01	4139.56	"	"	0.604	5.5
Z + 5 % Ca(OH) <sub>2</sub>	1st	1.492	1.4154	17-18	27.675	30.125	4170.95	4182.65	-1.03	0.648	3.2(Av)
"	2nd	1.547	1.4676	"	28.785	31.34	4194.35	"	"	0.666	2.5
Z + 10 % Ca(OH) <sub>2</sub>	1st	1.448	1.2993	17-18	27.275	29.66	4422.43	4353.34	3.00	0.616	3
"	2nd	1.541	1.3828	"	27.985	30.445	4284.26	"	"	0.661	1.7
Z + 2 % K <sub>2</sub> CO <sub>3</sub>	1st	1.445	1.4153	17-18	28.655	31.12	4195.71	4239.39	0.31	0.596	2.5
"	2nd	1.506	1.4751	"	28.265	30.885	4283.07	"	"	0.619	4.8
Z + 5 % K <sub>2</sub> CO <sub>3</sub>	1st	1.492	1.4154	17-18	28.65	31.085	4144.37	4114.59	-2.65	0.645	2.6
"	2nd	1.554	1.4742	17	26.89	29.39	4084.81	"	"	0.653	2.1
Z + 10 % K <sub>2</sub> CO <sub>3</sub>	1st	1.478	1.3263	17-18	28.89	31.175	4149.89	4183.14	-1.02	0.646	2.8
"	2nd	1.429	1.2823	"	28.06	30.305	4216.38	"	"	-	2.5
Z + 2 % FeCl <sub>3</sub>	1st	1.489	1.4584	17	27.735	30.205	4080.79	4186.84	-0.94	0.634(T)	3
"	2nd	1.510	1.4790	"	27.545	30.155	4252.02	"	"	0.643	2.6
Z + 5 % FeCl <sub>3</sub>	1st	1.464	1.3889	19-20	29.35	31.785	4223.44	4182.20	-1.05	0.622	2.6
"	2nd	1.527	1.4486	"	29.09	31.58	4140.96	"	"	0.651	2.5
Z + 10 % FeCl <sub>3</sub>	1st	1.498	1.3442	19-20	29.985	32.445	4408.31	4420.15	4.58	0.621	2.3
"	2nd	1.559	1.3989	"	28.50	31.07	4432.00	"	"	0.680	6
Z + 2 % Fe <sub>2</sub> O <sub>3</sub>	1st	1.441	1.4114	20	28.167	30.565	4092.62	4122.02	-2.47	0.667	2.5
"	2nd	1.584	1.5515	"	28.437	31.11	4151.43	"	"	0.694	2.6
Z + 5 % Fe <sub>2</sub> O <sub>3</sub>	1st	1.443	1.3689	20-21	27.395	29.79	4219.76	4220.86	-0.13	0.646	5.7
"	2nd	1.474	1.3983	"	28.07	30.52	4221.96	"	"	0.664	3.2(Av)
Z + 10 % Fe <sub>2</sub> O <sub>3</sub>	1st	1.464	1.3137	20	27.453	29.78	4272.01	4248.60	0.53	0.687	5.7
"	2nd	1.459	1.3092	"	28.313	30.61	4225.18	"	"	0.679	2.2

Table B.5 Sample weight definition (Tunçbilek sub-bituminous)

Sample Definition	Sample Number	Sample Weight (g)	Catalyst in Raw Sample (%)	Catalyst after Drying (with regard to Humidity Error Factor) (%)	Modified sample mass (g)
T (Amb.Temp. $\approx 27$ °C)	1st	1.518	-	-	1.518
"	2nd	1.494	-	-	1.494
<b>T (Amb.Temp. <math>\approx 17</math> °C)</b>	<b>1st</b>	<b>1.447</b>	-	-	<b>1.447</b>
"	<b>2nd</b>	<b>1.497</b>	-	-	<b>1.497</b>
T + 2 % Ca(OH) <sub>2</sub>	1st	1.518	2	2.091	1.4863
"	2nd	1.474	2	2.091	1.4432
T + 5 % Ca(OH) <sub>2</sub>	1st	1.532	5	5.228	1.4519
"	2nd	1.567	5	5.228	1.4851
T + 10 % Ca(OH) <sub>2</sub>	1st	1.502	10	10.457	1.3449
"	2nd	1.503	10	10.457	1.3458
T + 2 % K <sub>2</sub> CO <sub>3</sub>	1st	1.460	2	2.091	1.4295
"	2nd	1.499	2	2.091	1.4677
T + 5 % K <sub>2</sub> CO <sub>3</sub>	1st	1.494	5	5.228	1.4159
"	2nd	1.462	5	5.228	1.3856
T + 10 % K <sub>2</sub> CO <sub>3</sub>	1st	1.400	10	10.457	1.2536
"	2nd	1.435	10	10.457	1.2849
T + 2 % FeCl <sub>3</sub>	1st	1.439	2	2.091	1.4089
"	2nd	1.489	2	2.091	1.4579
T + 5 % FeCl <sub>3</sub>	1st	1.546	5	5.228	1.4652
"	2nd	1.448	5	5.228	1.3723
T + 10 % FeCl <sub>3</sub>	1st	1.436	10	10.457	1.2858
"	2nd	1.461	10	10.457	1.3082
T + 2 % Fe <sub>2</sub> O <sub>3</sub>	1st	1.475	2	2.091	1.4442
"	2nd	1.531	2	2.091	1.4990
T + 5 % Fe <sub>2</sub> O <sub>3</sub>	1st	1.497	5	5.228	1.4187
"	2nd	1.510	5	5.228	1.4311
T + 10 % Fe <sub>2</sub> O <sub>3</sub>	1st	1.467	10	10.457	1.3136
"	2nd	1.503	10	10.457	1.3458

Table B.6 Sample weight definition (Kangal lignite)

Sample Definition	Sample Number	Sample Weight (g)	Catalyst in Raw Sample (%)	Catalyst after Drying (with regard to Humidity Error Factor) (%)	Modified sample mass (g)
K (Amb.Temp. $\approx 27$ °C)	1st	1.505	-	-	1.505
"	2nd	1.521	-	-	1.521
<b>K (Amb.Temp. <math>\approx 17</math> °C)</b>	<b>1st</b>	<b>1.498</b>	-	-	<b>1.498</b>
"	<b>2nd</b>	<b>1.540</b>	-	-	<b>1.540</b>
K + 2 % Ca(OH) <sub>2</sub>	1st	1.556	2	2.764	1.5130
"	2nd	1.309	2	2.764	1.2728
K + 5 % Ca(OH) <sub>2</sub>	1st	1.512	5	6.909	1.4075
"	2nd	1.550	5	6.909	1.4429
K + 10 % Ca(OH) <sub>2</sub>	1st	1.515	10	13.818	1.3057
"	2nd	1.438	10	13.818	1.2393
K + 2 % K <sub>2</sub> CO <sub>3</sub>	1st	1.376	2	2.764	1.3380
"	2nd	1.503	2	2.764	1.4615
K + 5 % K <sub>2</sub> CO <sub>3</sub>	1st	1.314	5	6.909	1.2232
"	2nd	1.340	5	6.909	1.2474
K + 10 % K <sub>2</sub> CO <sub>3</sub>	1st	1.594	10	13.818	1.3737
"	2nd	1.508	10	13.818	1.2996
K + 2 % FeCl <sub>3</sub>	1st	1.560	2	2.764	1.5169
"	2nd	1.513	2	2.764	1.4712
K + 5 % FeCl <sub>3</sub>	1st	1.578	5	6.909	1.4690
"	2nd	1.486	5	6.909	1.3833
K + 10 % FeCl <sub>3</sub>	1st	1.566	10	13.818	1.3496
"	2nd	1.471	10	13.818	1.2677
K + 2 % Fe <sub>2</sub> O <sub>3</sub>	1st	1.493	2	2.764	1.4517
"	2nd	1.414	2	2.764	1.3749
K + 5 % Fe <sub>2</sub> O <sub>3</sub>	1st	1.524	5	6.909	1.4187
"	2nd	1.411	5	6.909	1.3135
K + 10 % Fe <sub>2</sub> O <sub>3</sub>	1st	1.567	10	13.818	1.3505
"	2nd	1.543	10	13.818	1.3298

Table B.7 Sample weight definition (Seyitömer lignite)

Sample Definition	Sample Number	Sample Weight (g)	Catalyst in Raw Sample (%)	Catalyst after Drying (with regard to Humidity Error Factor) (%)	Modified sample mass (g)
S (Amb.Temp.≈27°C)	1st	1.534	-	-	1.534
"	2nd	1.513	-	-	1.513
<b>S (Amb.Temp.≈17°C)</b>	<b>1st</b>	<b>1.453</b>	-	-	<b>1.453</b>
"	<b>2nd</b>	<b>1.554</b>	-	-	<b>1.554</b>
S + 2 % Ca(OH) <sub>2</sub>	1st	1.529	2	2.381	1.4926
"	2nd	1.562	2	2.381	1.5251
S + 5 % Ca(OH) <sub>2</sub>	1st	1.516	5	5.952	1.4258
"	2nd	1.011	5	5.952	0.9508
"	3rd	1.486	5	5.952	1.3976
S + 10 % Ca(OH) <sub>2</sub>	1st	1.438	10	11.905	1.2668
"	2nd	1.484	10	11.905	1.3073
S + 2 % K <sub>2</sub> CO <sub>3</sub>	1st	1.426	2	2.381	1.3920
"	2nd	1.423	2	2.381	1.3891
S + 5 % K <sub>2</sub> CO <sub>3</sub>	1st	-	5	5.952	-
"	2nd	-	5	5.952	-
S + 10 % K <sub>2</sub> CO <sub>3</sub>	1st	1.524	10	11.905	1.3556
"	2nd	1.471	10	11.905	1.2959
S + 2 % FeCl <sub>3</sub>	1st	1.470	2	2.381	1.4350
"	2nd	1.534	2	2.381	1.4975
S + 5 % FeCl <sub>3</sub>	1st	1.552	5	5.952	1.4596
"	2nd	1.517	5	5.952	1.4267
S + 10 % FeCl <sub>3</sub>	1st	1.488	10	11.905	1.3109
"	2nd	1.514	10	11.905	1.3338
S + 2 % Fe <sub>2</sub> O <sub>3</sub>	1st	1.562	2	2.381	1.5248
"	2nd	1.486	2	2.381	1.4506
S + 5 % Fe <sub>2</sub> O <sub>3</sub>	1st	1.564	5	5.952	1.4709
"	2nd	1.512	5	5.952	1.4220
S + 10 % Fe <sub>2</sub> O <sub>3</sub>	1st	1.492	10	11.905	1.3144
"	2nd	1.453	10	11.905	1.2800

Table B.8 Sample weight definition (Zonguldak bituminous)

Sample Definition	Sample Number	Sample Weight (g)	Catalyst in Raw Sample (%)	Catalyst after Drying (with regard to Humidity Error Factor) (%)	Modified sample mass (g)
Z (Amb.Temp.≈27°C)	1st	1.507	-	-	1.507
"	2nd	1.518	-	-	1.518
<b>Z (60min drying)</b>	<b>1st</b>	<b>1.524</b>	-	-	<b>1.524</b>
"	<b>2nd</b>	<b>1.461</b>	-	-	<b>1.461</b>
<b>Z (45min drying)</b>	<b>1st</b>	<b>1.448</b>	-	-	<b>1.448</b>
"	<b>2nd</b>	<b>1.406</b>	-	-	<b>1.406</b>
Z + 2 % Ca(OH) <sub>2</sub>	1st	1.442	2	2.053	1.4124
"	2nd	1.505	2	2.053	1.4741
Z + 5 % Ca(OH) <sub>2</sub>	1st	1.492	5	5.133	1.4154
"	2nd	1.547	5	5.133	1.4676
Z + 10 % Ca(OH) <sub>2</sub>	1st	1.448	10	10.267	1.2993
"	2nd	1.541	10	10.267	1.3828
Z + 2 % K <sub>2</sub> CO <sub>3</sub>	1st	1.445	2	2.053	1.4153
"	2nd	1.506	2	2.053	1.4751
Z + 5 % K <sub>2</sub> CO <sub>3</sub>	1st	1.492	5	5.133	1.4154
"	2nd	1.554	5	5.133	1.4742
Z + 10 % K <sub>2</sub> CO <sub>3</sub>	1st	1.478	10	10.267	1.3263
"	2nd	1.429	10	10.267	1.2823
Z + 2 % FeCl <sub>3</sub>	1st	1.489	2	2.053	1.4584
"	2nd	1.510	2	2.053	1.4790
"	3rd	1.411	2	2.053	1.3820
Z + 5 % FeCl <sub>3</sub>	1st	1.464	5	5.133	1.3889
"	2nd	1.527	5	5.133	1.4486
Z + 10 % FeCl <sub>3</sub>	1st	1.498	10	10.267	1.3442
"	2nd	1.559	10	10.267	1.3989
Z + 2 % Fe <sub>2</sub> O <sub>3</sub>	1st	1.441	2	2.053	1.4114
"	2nd	1.584	2	2.053	1.5515
Z + 5 % Fe <sub>2</sub> O <sub>3</sub>	1st	1.443	5	5.133	1.3689
"	2nd	1.474	5	5.133	1.3983
Z + 10 % Fe <sub>2</sub> O <sub>3</sub>	1st	1.464	10	10.267	1.3137
"	2nd	1.459	10	10.267	1.3092

Table B.9 Repeatability in calorific value tests of impregnated Kangal lignite with K<sub>2</sub>CO<sub>3</sub> catalyst

Sample Definition	Sample Number	Sample Weight (g)	modified weight (Theoretical) (g)	Amb. Temp. (°C)	Lower Temp. (T <sub>1</sub> °C)	Higher Temp. (T <sub>2</sub> °C)	(GCV) or (HHV) (Kcal/ Kg)	Ave. (Kcal/ Kg)	Difference (%)	Wire Length (cm)
<b>K (Temp. ≈ 17 °C)</b>	<b>1st</b>	<b>1.498</b>	<b>1.498</b>	<b>17-18</b>	<b>28.18</b>	<b>29.643</b>	<b>2358.17</b>	<b>2374.80</b>	-	<b>9.1</b>
"	<b>2nd</b>	<b>1.540</b>	<b>1.540</b>	"	<b>27.705</b>	<b>29.23</b>	<b>2391.42</b>	"	-	<b>9.3</b>
K+2 % K <sub>2</sub> CO <sub>3</sub>	1st	1.502	1.4605	19-20	28.21	29.665	2400.60	2402.83	1.18	6
"	2nd	1.497	1.4556	"	26.967	28.42	2405.05	"	"	5.8
K+5 % K <sub>2</sub> CO <sub>3</sub>	1st	1.508	1.4038	"	28.06	29.48	2436.18	2426.20	2.16	5.3
"	2nd	1.501	1.3973	"	27.083	28.485	2416.23	"	"	5.2
K+10 % K <sub>2</sub> CO <sub>3</sub>	1st	1.444	1.2445	"	29.02	30.31	2498.79	2491.74	4.92	7
"	2nd	1.552	1.3375	"	27.085	28.465	2484.69	"	"	5.3

Table B.10 Repeatability in calorific value tests of Tunçbilek sub-bituminous samples impregnated with 5 % catalysts

Sample Definition	Sample Number	Sample Weight (g)	modified weight (Theoretical) (g)	Amb. Temp. (°C)	Lower Temp. (T <sub>1</sub> °C)	Higher Temp. (T <sub>2</sub> °C)	(GCV) or (HHV) (Kcal/ Kg)	Ave. (Kcal/ Kg)	Difference (%)	Ash (g)	Wire Length (cm)
<b>T (Temp. ≈ 17 °C)</b>	<b>1st</b>	<b>1.447</b>	1.447	≈17	<b>30.62</b>	<b>32.685</b>	<b>3440.38</b>	<b>3433.84</b>	-	<b>0.644</b>	<b>5.3</b>
"	<b>2nd</b>	<b>1.497</b>	<b>1.497</b>	"	<b>30.32</b>	<b>32.45</b>	<b>3427.30</b>	"	-	<b>0.668</b>	<b>3.3</b>
T+5 % Ca(OH) <sub>2</sub>	1st	1.497	1.4187	19	28.395	30.23	3124.95	3138.79	-8.59	0.717	2.2
"	2nd	1.504	1.4254	18	27.595	29.455	3152.63	"	"	0.717	6.1
T +5 % K <sub>2</sub> CO <sub>3</sub>	1st	1.535	1.4548	19	28.90	30.84	3221.78	3150.15	-8.26	0.747	2.5
"	2nd	1.416	1.3420	18	27.29	29.0	3078.51	"	"	0.695	5.1
T + 5 % FeCl <sub>3</sub>	1st	1.577	1.4946	19	28.605	30.60	3224.89	3227.35	-6.01	0.731	3.6
"	2nd	1.405	1.3315	18	28.20	29.98	3229.80	"	"	0.647	2.2

## APPENDIX C

### TGA-FTIR (EXPERIMENTAL)

Table C.1 Flow fluctuations during TGA-FTIR combustion tests

**At 300 °C and System Purge Gas of 30 ml<sub>n</sub>/min 30**

Sample	Environment	O <sub>2</sub> flow (mm)	N <sub>2</sub> flow (mm)	CO <sub>2</sub> flow (mm)
Kangal lignite	21 % O <sub>2</sub> /N <sub>2</sub>	51	140-144	-
Kangal lignite	25 % O <sub>2</sub> /N <sub>2</sub>	68	139-142	-
Kangal lignite	30 % O <sub>2</sub> /N <sub>2</sub>	83	142-143	-
Kangal lignite	35 % O <sub>2</sub> /N <sub>2</sub>	97-99	139-140	-
Kangal lignite	21 % O <sub>2</sub> / CO <sub>2</sub>	55-56	-	133-134
Kangal+5 % Fe <sub>2</sub> O <sub>3</sub>	21 % O <sub>2</sub> / CO <sub>2</sub>	57	-	135
Kangal+5 % Ca(OH) <sub>2</sub>	21 % O <sub>2</sub> / CO <sub>2</sub>	57	-	135
Kangal+5 % K <sub>2</sub> CO <sub>3</sub>	21 % O <sub>2</sub> / CO <sub>2</sub>	57-58	-	135
Kangal lignite	25 % O <sub>2</sub> / CO <sub>2</sub>	72-73	-	134-135
Kangal+5 % Fe <sub>2</sub> O <sub>3</sub>	25 % O <sub>2</sub> / CO <sub>2</sub>	75	-	134-135
Kangal+5 % Ca(OH) <sub>2</sub>	25 % O <sub>2</sub> / CO <sub>2</sub>	75	-	135
Kangal+5 % K <sub>2</sub> CO <sub>3</sub>	25 % O <sub>2</sub> / CO <sub>2</sub>	74-75	-	134-135
Kangal lignite	30 % O <sub>2</sub> / CO <sub>2</sub>	88-89	-	135
Kangal+5 % Fe <sub>2</sub> O <sub>3</sub>	30 % O <sub>2</sub> / CO <sub>2</sub>	88-89	-	135
Kangal+5 % Ca(OH) <sub>2</sub>	30 % O <sub>2</sub> / CO <sub>2</sub>	88-89	-	135
Kangal+5 % K <sub>2</sub> CO <sub>3</sub>	30 % O <sub>2</sub> / CO <sub>2</sub>	88-89	-	135
Kangal lignite	35 % O <sub>2</sub> / CO <sub>2</sub>	104	-	130
"	35 % O <sub>2</sub> / CO <sub>2</sub>	104	-	129
Kangal+5 % Fe <sub>2</sub> O <sub>3</sub>	35 % O <sub>2</sub> / CO <sub>2</sub>	104	-	130
Kangal+5 % Ca(OH) <sub>2</sub>	35 % O <sub>2</sub> / CO <sub>2</sub>	104	-	129
Kangal+5 % K <sub>2</sub> CO <sub>3</sub>	35 % O <sub>2</sub> / CO <sub>2</sub>	103-104	-	129-130
Tunçbilek sub- bituminous	30 % O <sub>2</sub> / CO <sub>2</sub>	88-89	-	135
Tunçbilek +5 % Fe <sub>2</sub> O <sub>3</sub>	30 % O <sub>2</sub> / CO <sub>2</sub>	89	-	135-136
Tunçbilek +5 % Ca(OH) <sub>2</sub>	30 % O <sub>2</sub> / CO <sub>2</sub>	89-90	-	135
Tunçbilek +5 % K <sub>2</sub> CO <sub>3</sub>	30 % O <sub>2</sub> / CO <sub>2</sub>	90	-	135
Tunçbilek sub- bituminous	21 % O <sub>2</sub> /N <sub>2</sub>	52-53	139	-
Kangal+5 % Fe <sub>2</sub> O <sub>3</sub>	21 % O <sub>2</sub> / CO <sub>2</sub>	52-53	140	-
Kangal+5 % K <sub>2</sub> CO <sub>3</sub>	21 % O <sub>2</sub> / CO <sub>2</sub>	53	140	-
Kangal+5 % Fe <sub>2</sub> O <sub>3</sub>	30 % O <sub>2</sub> /N <sub>2</sub>	83	140-141	-
Kangal+5 % K <sub>2</sub> CO <sub>3</sub>	30 % O <sub>2</sub> /N <sub>2</sub>	82-83	140	-
Tunçbilek sub- bituminous	30 % O <sub>2</sub> /N <sub>2</sub>	82-83	139-140	-
Tunçbilek +5 % Fe <sub>2</sub> O <sub>3</sub>	30 % O <sub>2</sub> /N <sub>2</sub>	82-83	140-141	-
Kangal+5 % Fe <sub>2</sub> O <sub>3</sub>	25 % O <sub>2</sub> /N <sub>2</sub>	65-66	142-143	-
Kangal+5 % K <sub>2</sub> CO <sub>3</sub>	25 % O <sub>2</sub> /N <sub>2</sub>	-	-	-
Kangal+5 % Fe <sub>2</sub> O <sub>3</sub>	35 % O <sub>2</sub> /N <sub>2</sub>	97-98	136-137	-
Kangal+5 % K <sub>2</sub> CO <sub>3</sub>	35 % O <sub>2</sub> /N <sub>2</sub>	97-98	137	-
Kangal lignite	25 % O <sub>2</sub> / CO <sub>2</sub>	71-72	-	130-131

Table C.2 Flow fluctuations during TGA-FTIR pyrolysis tests

**At 300 °C and System Purge Gas 40 ml<sub>n</sub>/min**

<b>Sample</b>	<b>Environment</b>	<b>N<sub>2</sub> flow (mm)</b>	<b>CO<sub>2</sub> flow (mm)</b>
Kangal lignite	CO <sub>2</sub>	-	2*150
Kangal+5 % Fe <sub>2</sub> O <sub>3</sub>	CO <sub>2</sub>	-	2*150
Kangal+5 % Ca(OH) <sub>2</sub>	CO <sub>2</sub>	-	2*150
Kangal+5 % K <sub>2</sub> CO <sub>3</sub>	CO <sub>2</sub>	-	2*150

## APPENDIX D

### TGA-FTIR (RESULTS)

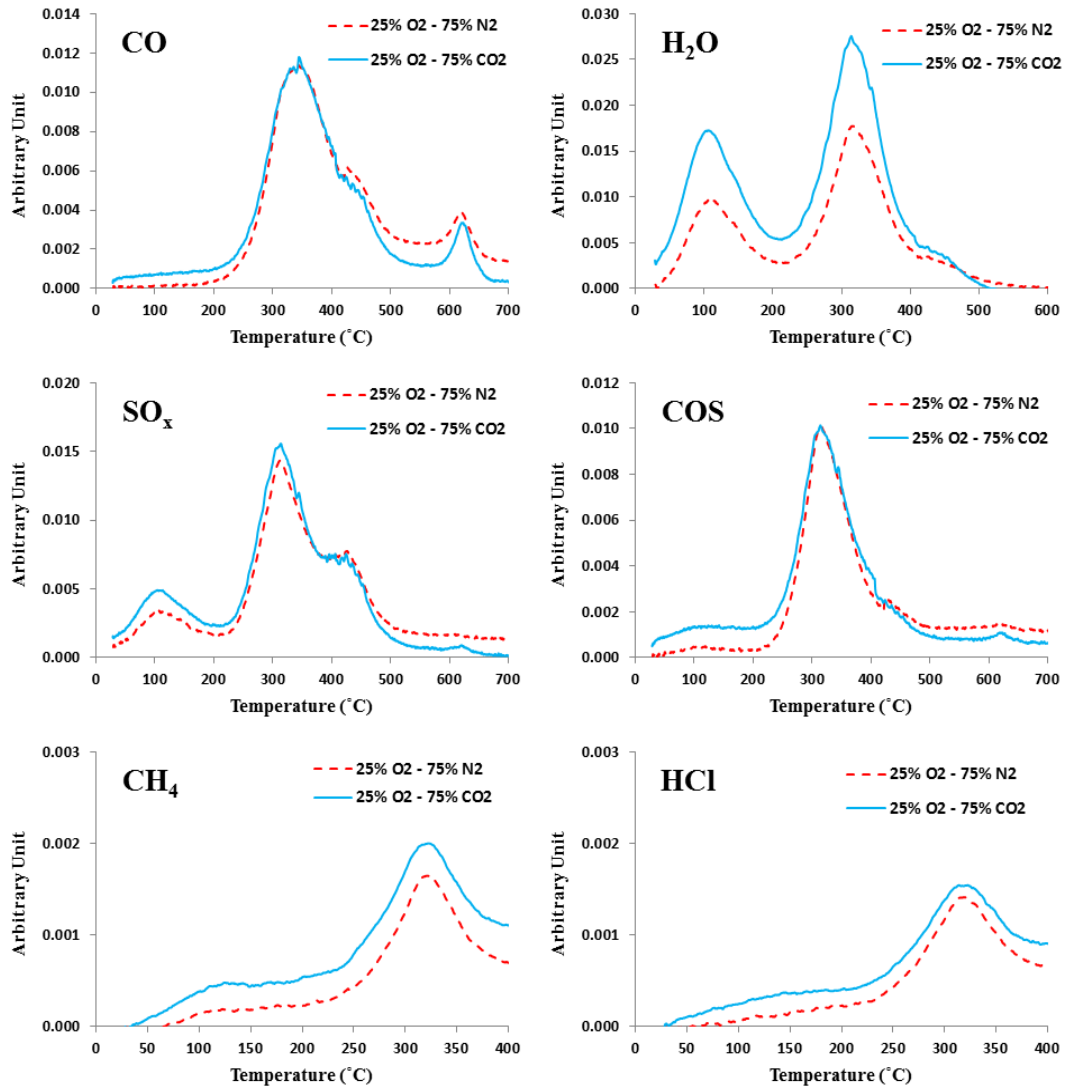


Fig. D.1 Formation profiles of evolved gases during combustion tests in 25 % O<sub>2</sub> in N<sub>2</sub> and 25 % O<sub>2</sub> in CO<sub>2</sub> ambient conditions

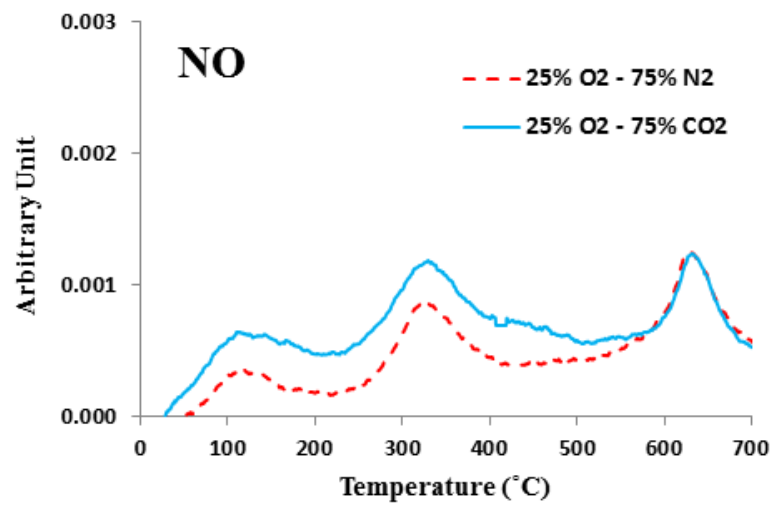


Fig. D.2 Formation profiles of NO during combustion tests in 25 % O<sub>2</sub> in N<sub>2</sub> and 25 % O<sub>2</sub> in CO<sub>2</sub> ambient conditions

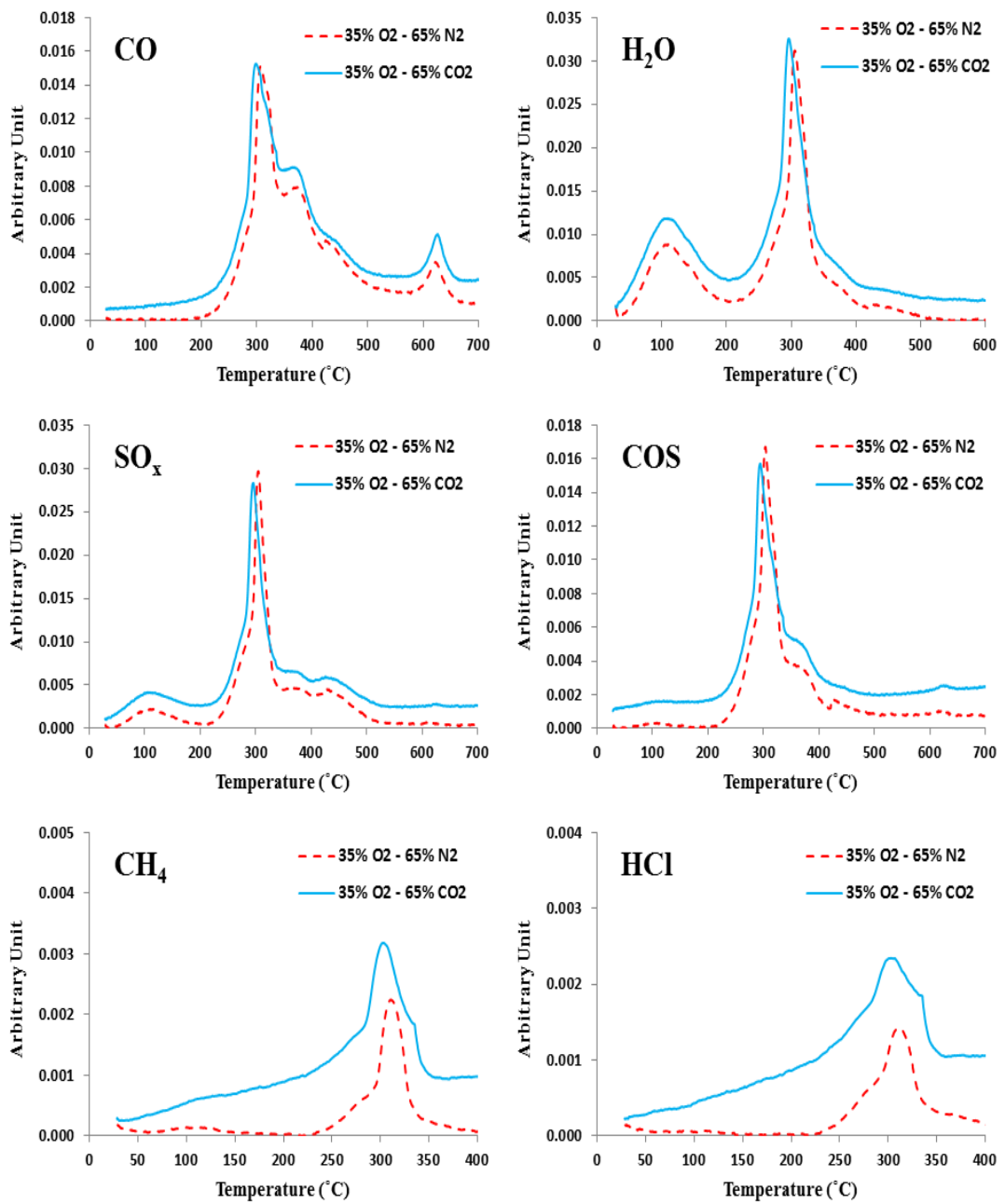


Fig. D.3 Formation profiles of evolved gases during combustion tests in 35 % O<sub>2</sub> in N<sub>2</sub> and 35 % O<sub>2</sub> in CO<sub>2</sub> ambient conditions

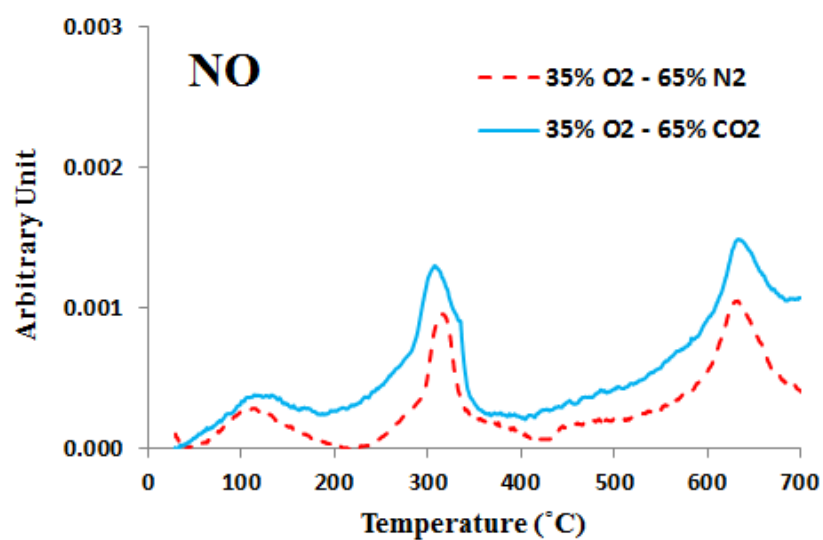


Fig. D.4 Formation profiles of NO during combustion tests in 35 % O<sub>2</sub> in N<sub>2</sub> and 35 % O<sub>2</sub> in CO<sub>2</sub> ambient conditions

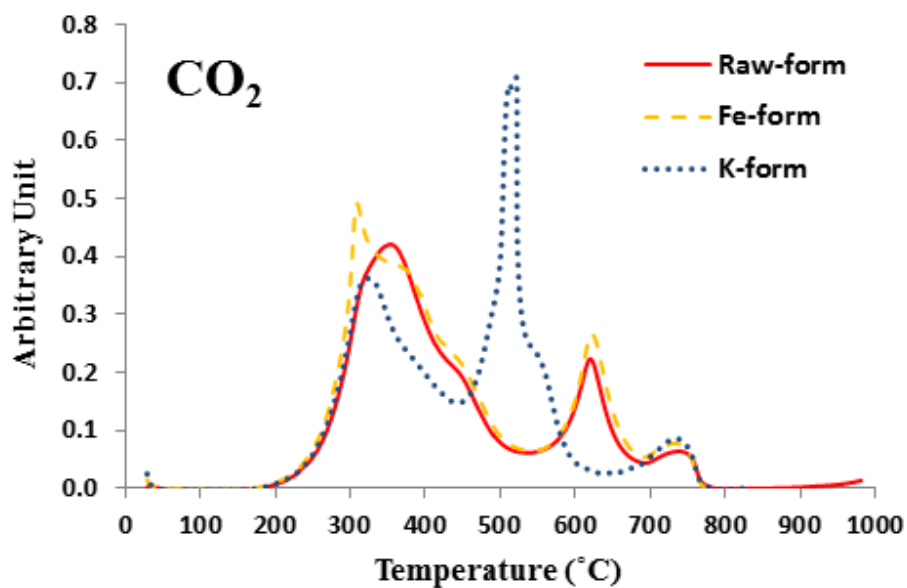


Fig. D.5 Formation profiles of CO<sub>2</sub> during catalytic combustion tests in 25 % O<sub>2</sub> in N<sub>2</sub> ambient

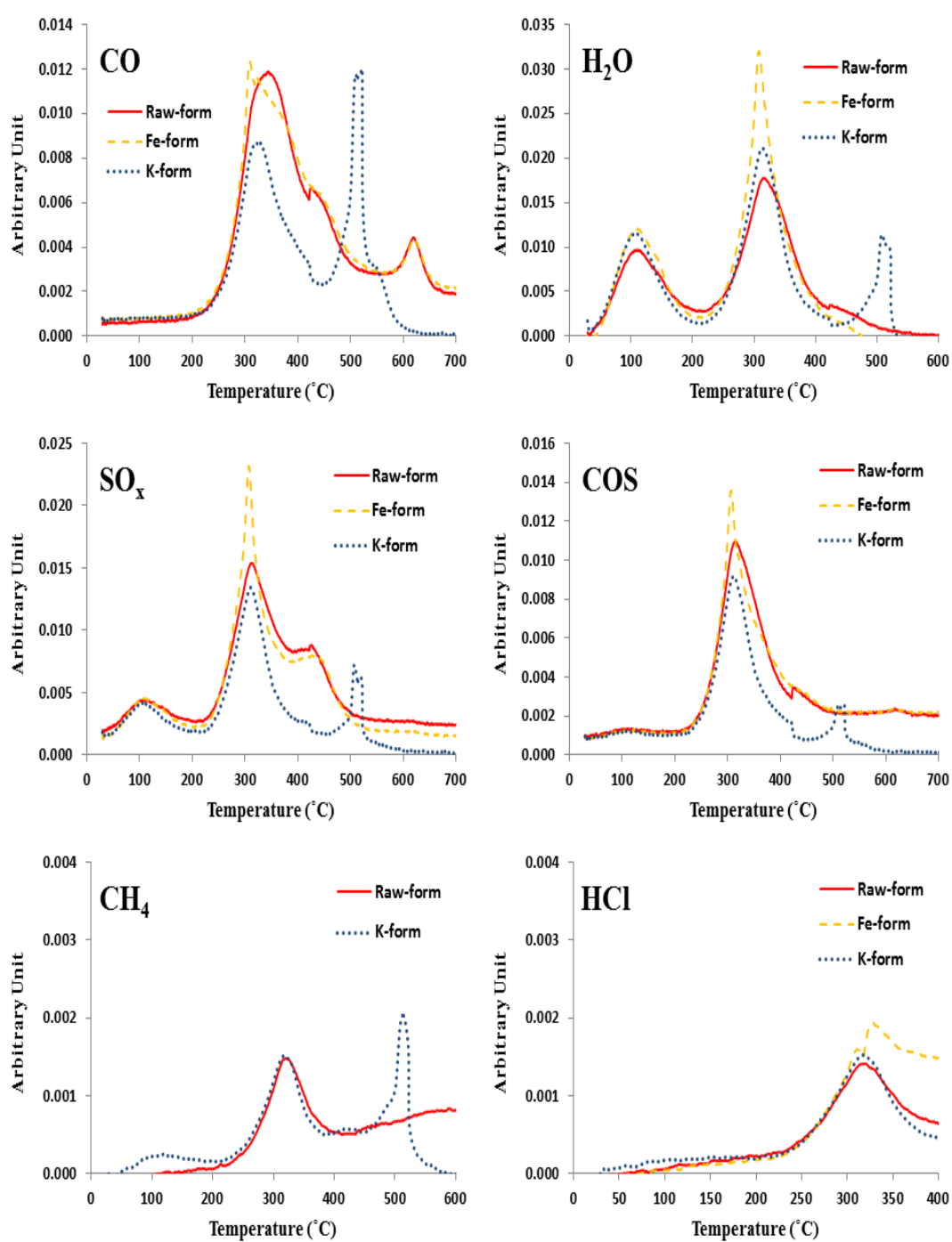


Fig. D.6 Formation profiles of evolved gases during catalytic combustion tests in 25 % O<sub>2</sub> in N<sub>2</sub> ambient

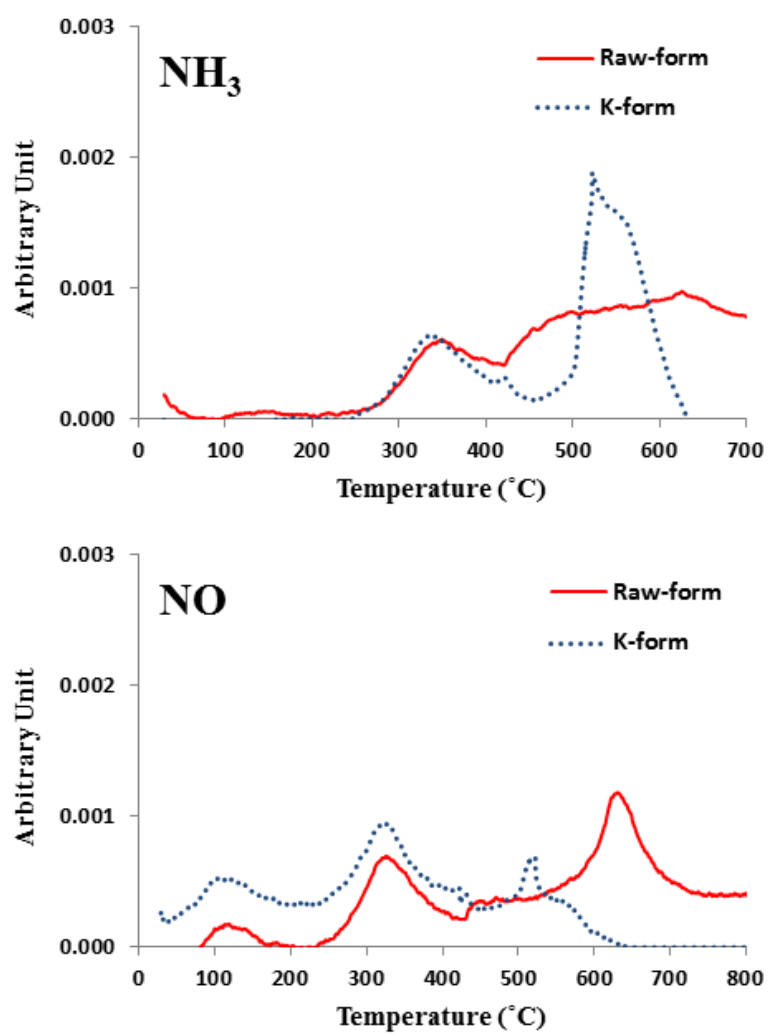


Fig. D.7 Formation profiles of nitrogen containing species during catalytic combustion tests in 25 %  $\text{O}_2$  in  $\text{N}_2$  ambient

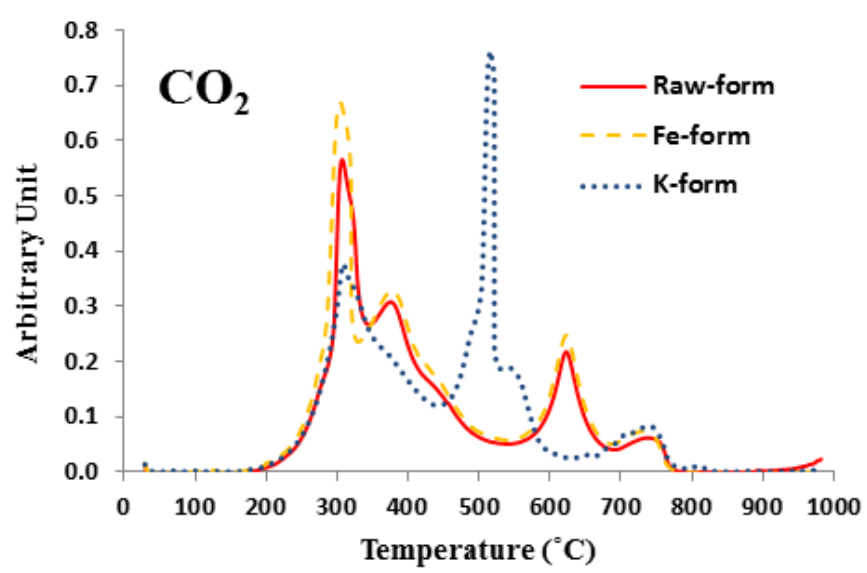


Fig. D.8 Formation profiles of CO<sub>2</sub> during catalytic combustion tests in 35 % O<sub>2</sub> in N<sub>2</sub> ambient

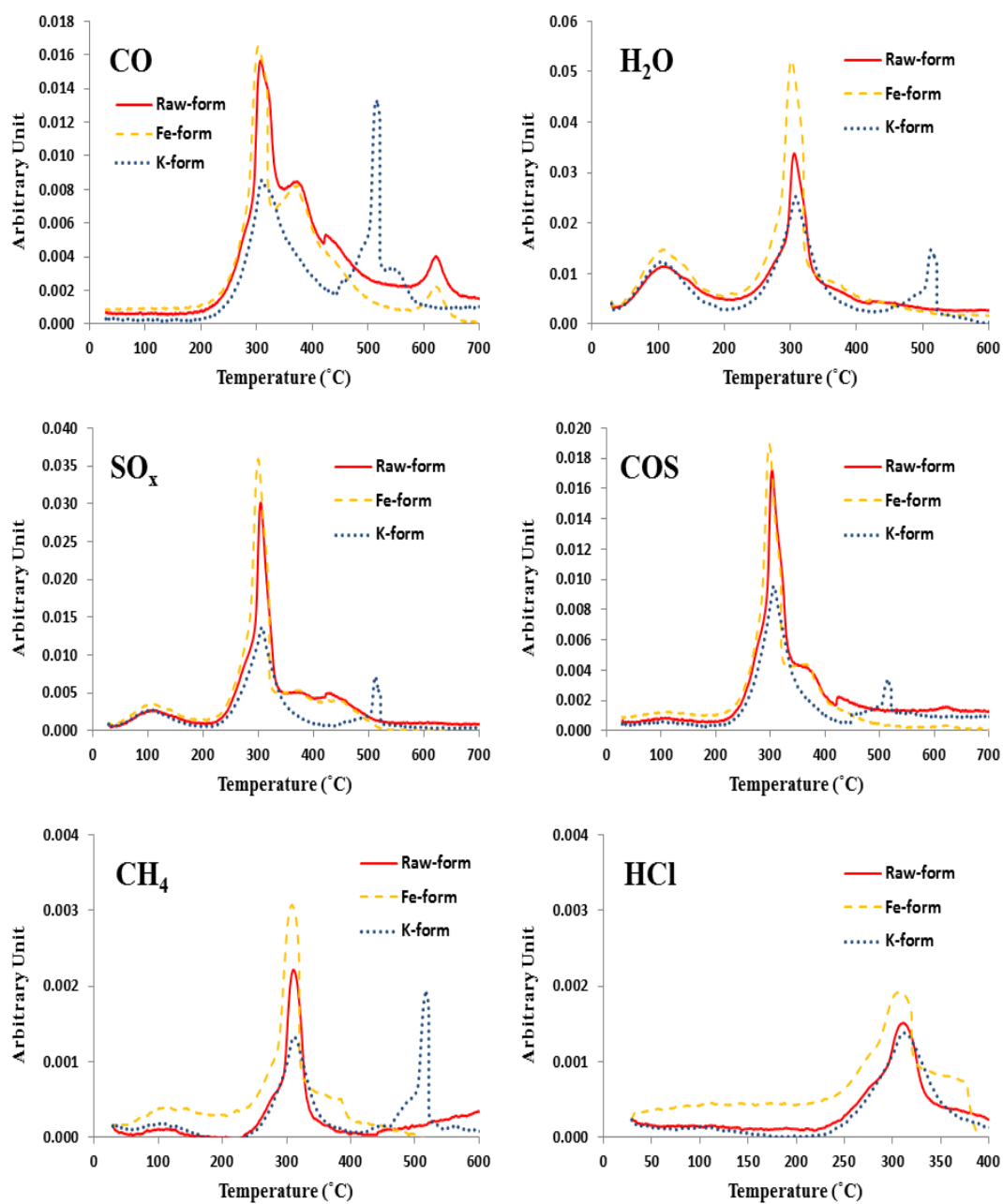


Fig. D.9 Formation profiles of evolved gases during catalytic combustion tests in 35 % O<sub>2</sub> in N<sub>2</sub> ambient

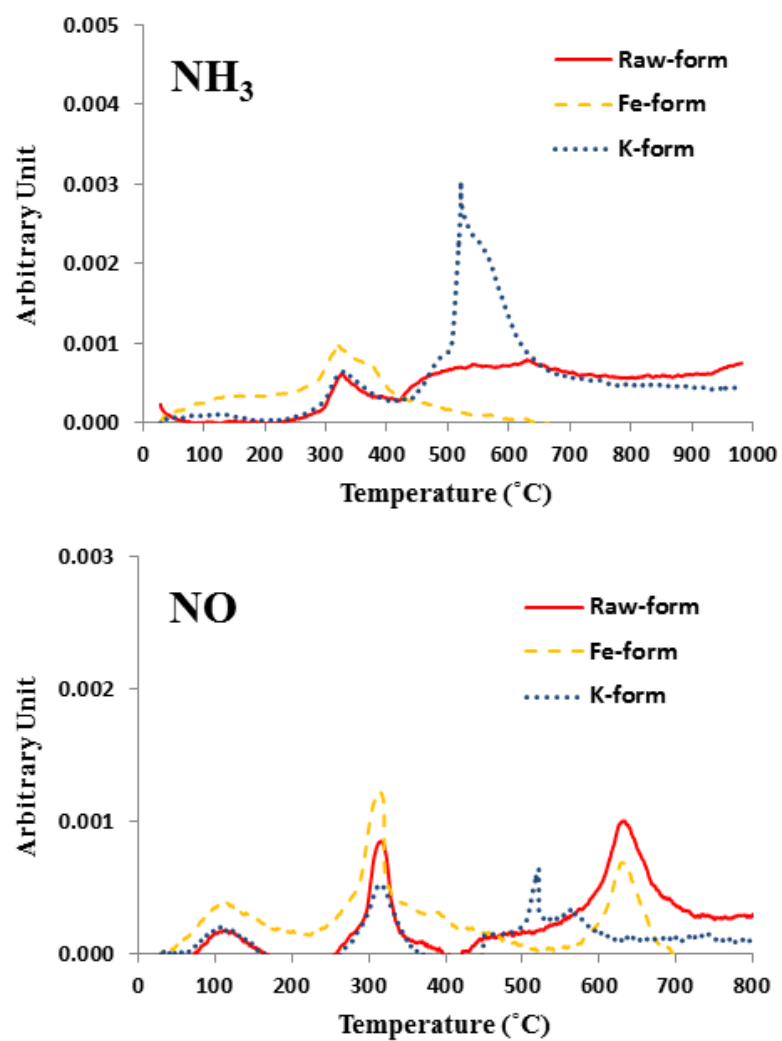


Fig. D.10 Formation profiles of nitrogen containing species during catalytic combustion tests in 35 %  $\text{O}_2$  in  $\text{N}_2$  ambient

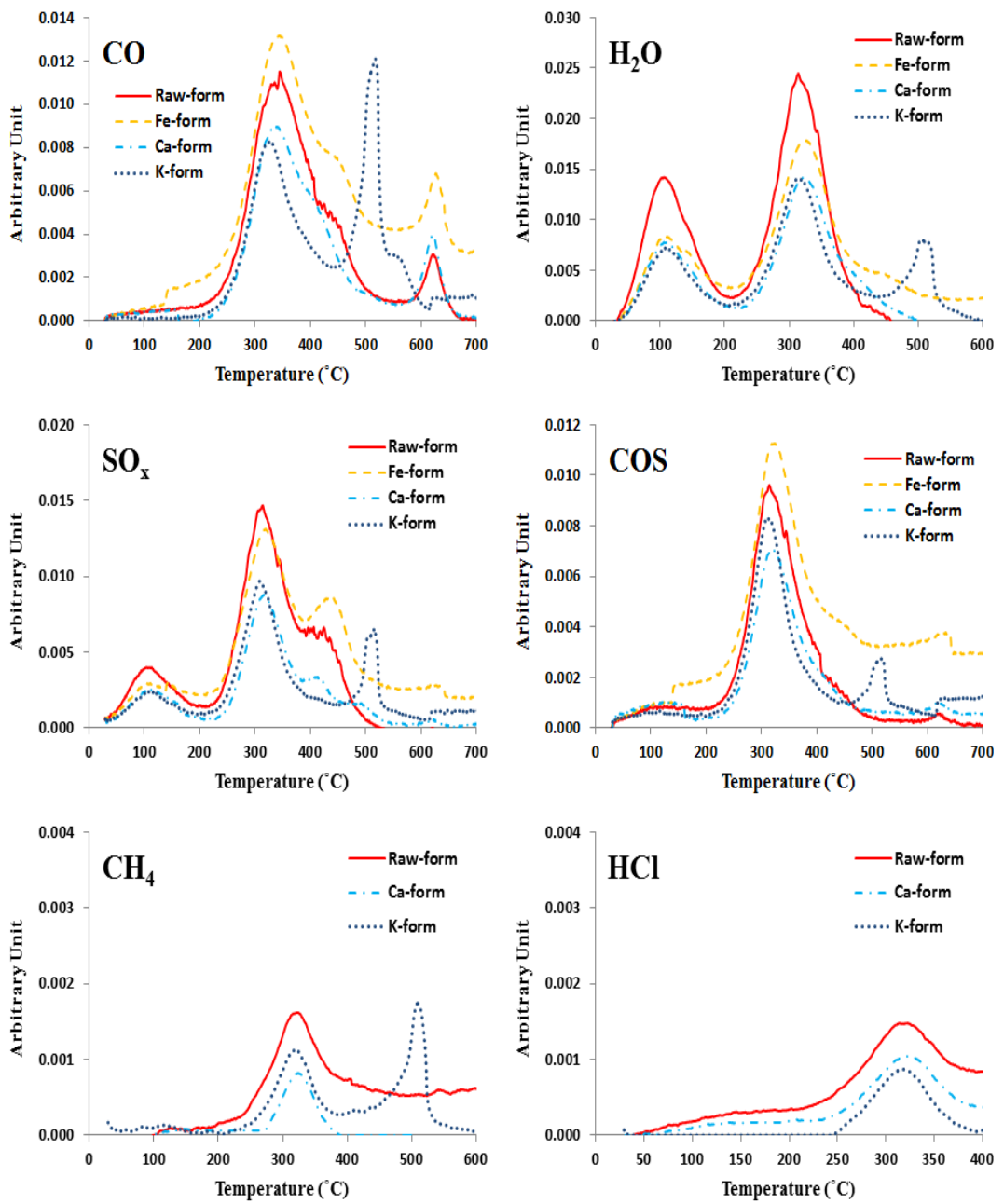


Fig. D.11 Formation profiles of evolved gases during catalytic combustion tests in 25 % O<sub>2</sub> in CO<sub>2</sub> ambient

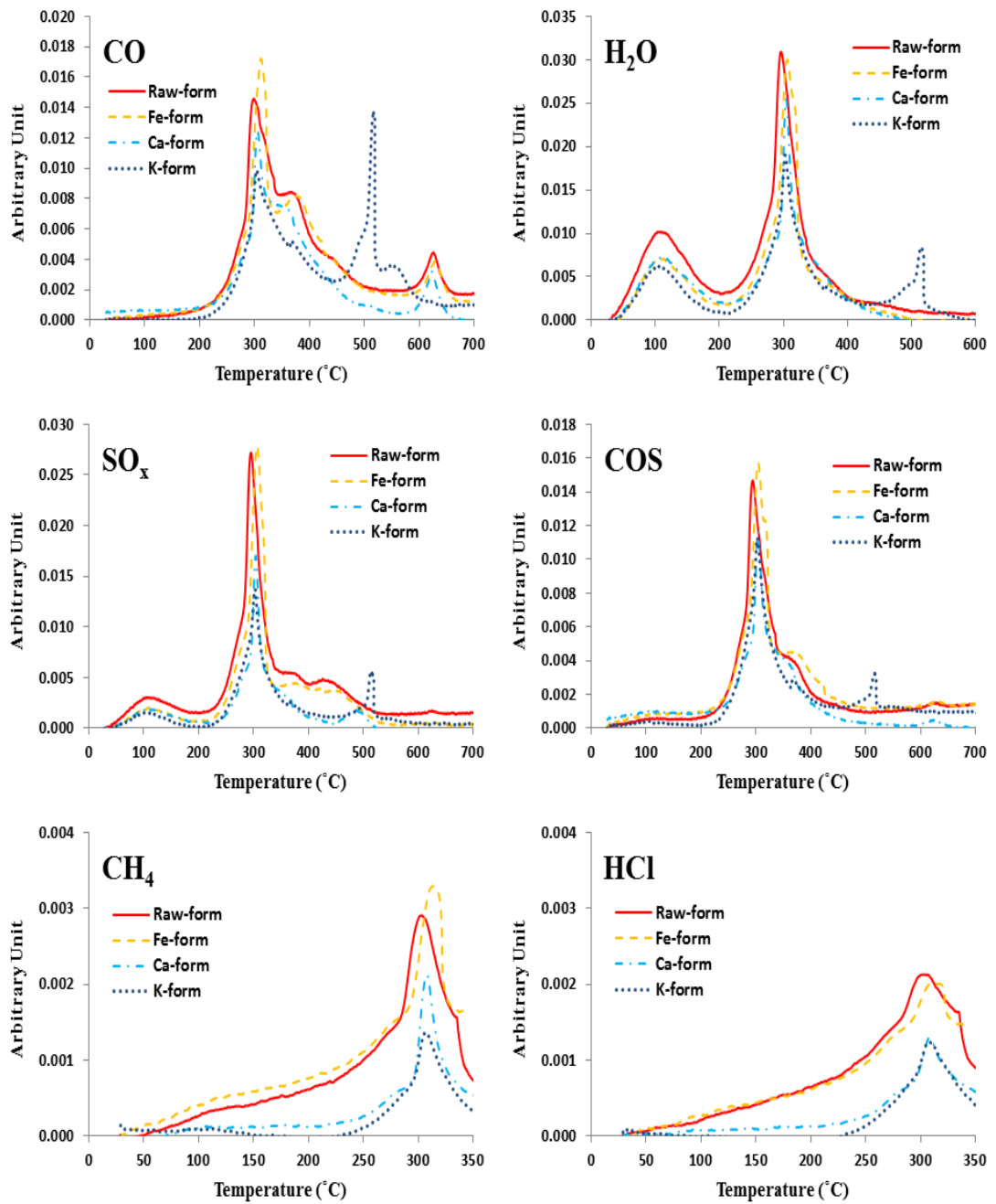


Fig. D.12 Formation profiles of evolved gases during catalytic combustion tests in 35 % O<sub>2</sub> in CO<sub>2</sub> ambient

Table D.1 Characteristic temperatures and parameters of Fe-form Kangal lignite combustion in O<sub>2</sub>/N<sub>2</sub> ambient

O <sub>2</sub> /N <sub>2</sub>	21% O <sub>2</sub> -79% N <sub>2</sub>	25% O <sub>2</sub> -75% N <sub>2</sub>	30% O <sub>2</sub> -70% N <sub>2</sub>	35% O <sub>2</sub> -65% N <sub>2</sub>
	Fe-form	Fe-form	Fe-form	Fe-form
T <sub>in</sub> (°C)	246	242	243	241
T <sub>ig</sub> (°C)	288	272	275	265
T <sub>2max</sub> (°C)	328	292	293	278
T <sub>b</sub> (°C)	750	746	750	750
<b>(dm/dt)</b> <sub>2max</sub> (%/min)	3.09	6.25	8.01	13.23

Table D.2 Characteristic temperatures and parameters of Fe-form Kangal lignite combustion in O<sub>2</sub>/CO<sub>2</sub> ambient

O <sub>2</sub> /CO <sub>2</sub>	21% O <sub>2</sub> -79% CO <sub>2</sub>	25% O <sub>2</sub> -75% CO <sub>2</sub>	30% O <sub>2</sub> -70% CO <sub>2</sub>	35% O <sub>2</sub> -65% CO <sub>2</sub>
	Fe-form	Fe-form	Fe-form	Fe-form
T <sub>in</sub> (°C)	237	240	238	236
T <sub>ig</sub> (°C)	275	280	270	266
T <sub>2max</sub> (°C)	303	310	281	278
T <sub>b</sub> (°C)	642	644	642	645
<b>(dm/dt)</b> <sub>2max</sub> (%/min)	3	3.35	8.45	12.52

Table D.3 Characteristic temperatures and parameters of K-form Kangal lignite combustion in O<sub>2</sub>/N<sub>2</sub> ambient

O <sub>2</sub> /N <sub>2</sub>	21% O <sub>2</sub> -79% N <sub>2</sub>	25% O <sub>2</sub> -75% N <sub>2</sub>	30% O <sub>2</sub> -70% N <sub>2</sub>	35% O <sub>2</sub> -65% N <sub>2</sub>
	K-form	K-form	K-form	K-form
T <sub>in</sub> (°C)	245	244	242	241
T <sub>ig</sub> (°C)	274	273	271	270
T <sub>2max</sub> (°C)	308	301	291	295
T <sub>b</sub> (°C)	751	749	750	752
<b>(dm/dt)</b> <sub>2max</sub> (%/min)	2.88	3.22	6.17	4.31
T <sub>3max</sub> (°C)	489	491	486	491
<b>(dm/dt)</b> <sub>3max</sub> (%/min)	5	6.62	9.36	9.02

Table D.4 Characteristic temperatures and parameters of K-form Kangal lignite combustion in O<sub>2</sub>/CO<sub>2</sub> ambient

O <sub>2</sub> /CO <sub>2</sub>	21% O <sub>2</sub> -79% CO <sub>2</sub>	25% O <sub>2</sub> -75% CO <sub>2</sub>	30% O <sub>2</sub> -70% CO <sub>2</sub>	35% O <sub>2</sub> -65% CO <sub>2</sub>
	K-form	K-form	K-form	K-form
T <sub>in</sub> (°C)	241	238	238	239
T <sub>ig</sub> (°C)	265	270	271	268
T <sub>2max</sub> (°C)	297	295	291	288
T <sub>b</sub> (°C)	580	575	574	573
<b>(dm/dt)</b> <sub>2max</sub> (%/min)	2.94	3.07	5.17	6.93
T <sub>3max</sub> (°C)	488	489	488	494
<b>(dm/dt)</b> <sub>3max</sub> (%/min)	4.73	5.14	7.87	9.12

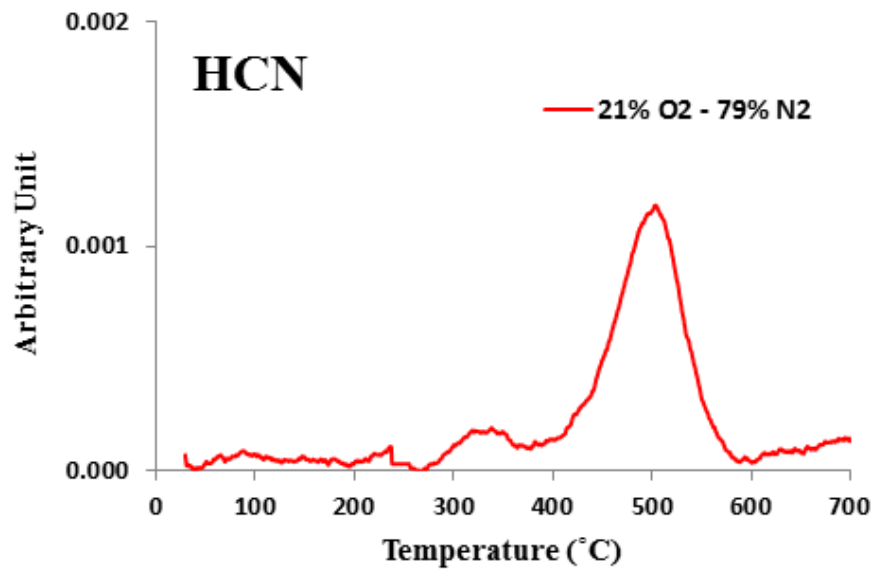


Fig. D.13 Formation profile of HCN during combustion test of Tunçbilek coal sample in air

## APPENDIX E

### CURRICULUM VITAE

#### PERSONAL INFORMATION

Surname, Name: Abbasi Atibeh, Ehsan  
Nationality: Iran  
Date and Place of Birth: 31 May 1986, Tehran  
Marital Status: Married  
Phone: +90 312 210 2581, +90 554 889 7018  
Email: e.abbasi.am@gmail.com, e170553@metu.edu.tr

#### EDUCATION

Degree	Institution	Year of Graduation
MS	METU Mechanical Engineering	2012
BS	Urmia University Mechanical Engineering	2009
High school	National Organization for Development of Exceptional Talents	2005

#### WORK EXPERIENCE

Year	Place	Enrollment
2010-present	METU Department of Mechanical Engineering	Research Assistant

## **FOREIGN LANGUAGES**

- English: Fluent
- Persian: Native Language
- Turkish: Fluent
- Azerbaijani: Fluent
- French: Basic
- Arabic: Basic

## **PUBLICATIONS**

1. Yozgatligil A, Abbasi Atibeh E. Methane (CH<sub>4</sub>) combustion behavior in O<sub>2</sub>/CO<sub>2</sub> versus O<sub>2</sub>/N<sub>2</sub> environments. "11<sup>th</sup> International Combustion Symposium, Sarajevo, Bosnia and Herzegovina ", June 24-27, 2010.
2. Abbasi Atibeh E, Yozgatligil A. A study on the effects of catalysts on pyrolysis and combustion characteristics of Turkish lignite under oxy-fuel conditions. "12<sup>th</sup> International Combustion Symposium, Kocaeli, Turkey ", May 24-26, 2012.
3. Abbasi Atibeh E, Yozgatligil A. A study on the effects of catalysts on pyrolysis and combustion characteristics of Turkish lignite in oxy-fuel conditions. Submitted to the Journal of Fuel (Ref: JFUE-D-12-01222), 2012.
4. Abbasi Atibeh E, Yozgatligil A. A study on combustion gas emissions of Turkish lignite in oxy-fuel conditions and the effects of catalysts. In preparation to be submitted to the Journal of Fuel processing Technology, 2012.
5. Abbasi Atibeh E, Yozgatligil A. Co-processing combustion tests of Turkish lignite and biomass fuels in O<sub>2</sub>/N<sub>2</sub> and O<sub>2</sub>/CO<sub>2</sub> ambient conditions: the catalytic effects of the ash contents of Turkish biomass fuels. In preparation to be submitted to the Journal of Fuel processing Technology, 2012.
6. Abbasi Atibeh E, Yozgatligil A. A study on catalytic pyrolysis and combustion characteristics of Turkish lignite and co-processing effects with biomass under oxy-fuel conditions. Work in progress poster presented in "34<sup>th</sup> International Symposium on Combustion, Warsaw University of Technology ", Warsaw, Poland, July 29 – August 3, 2012.

## **HOBBIES**

Tennis, Fitness, Nature, Off-roading, Camping, Sport cars and motorcycles, Experimental approach to scientific issues, Social relations